

Dissertation

submitted to the
Combined Faculty of Natural Sciences and Mathematics
of the Ruperto Carola University Heidelberg, Germany

for the degree of
Doctor of Natural Sciences

Presented by
Philipp Darius Konstantin Walch, M.Sc.

Born in: Buchen (Odenwald), Germany

Date of birth: January 19, 1992

Oral Examination: May 17, 2021

Dissecting the host-pathogen interface during *Salmonella* infection

Referees:

Dr. Mikhail Savitski
Prof. Dr. Michael Boutros

Supervisor:

Dr. Athanasios Typas

Summary

Facultatively intracellular pathogens adapt to and rewire host defenses to induce infection and promote survival and proliferation. *Salmonella enterica* serovar Typhimurium (STm) injects effector proteins *via* two Type 3 secretion systems into the host cytoplasm to usurp host cell machineries. Hence, investigating protein-protein interactions at the host-pathogen interface is essential for gaining a deeper insight into the interdependency between *Salmonella* and their host during infection. While more than 30 translocated effectors have been described, knowledge about their function during infection remains incomplete, and the number of proteins that are secreted during infection is likely underestimated.

In this work, I demonstrate the identification of interaction partners of known translocated effectors, maintaining the infection context and without relying on ectopic expression. The Affinity Purification Quantitative Mass Spectrometry (AP/QMS) workflow that I describe in this thesis bridges the gap between large-scale proteomics and high physiological relevance. In the process, I highlight, validate and characterize interactions occurring at endogenous levels of effector secretion. Many bacterial effector proteins displayed promiscuity and multifunctionality by targeting different host processes. Additionally, I assess effector convergence on distinct host processes, as well as effector cooperation and physical effector-effector interaction. These concepts are of groundbreaking importance to better understanding the reprogramming of host pathways in different host backgrounds.

I identify cholesterol transport as a convergence point for multiple effector proteins and assess the impact of the involved effectors and targeted host proteins on cholesterol accumulation at the *Salmonella*-containing vacuole. In addition, I demonstrate that the *Salmonella* effector SteC is able to directly bind and phosphorylate formin-like proteins, thereby providing a missing link regarding the method by which *Salmonella* induces cytoskeletal rearrangements during infection. Furthermore, I describe an arrayed STm knockout screen in an infection context, relying on high-throughput microscopy and unbiased image feature extraction. This is used to showcase bacterial processes that are essential for infection and to predict a novel secreted effector protein, YebF, based on its feature fingerprint.

In conclusion, the work presented in this thesis provides the infection biology research community with a rich dataset of novel effector-target interactions, an adaptable and validated AP/QMS workflow, and a well-characterized strain collection for the identification of protein-protein interactions at the pathogen-host interface. Additionally, a database of unbiased phenotypic fingerprints obtained from high-throughput microscopy will be invaluable for the prediction of novel effector proteins and the dissection of host-pathogen interconnectivity. The multifaceted systems biology approach to *Salmonella* infection presented in this study will fuel hypothesis-driven research and provides a decisive step towards a holistic understanding of the host-pathogen interface.

Zusammenfassung

Fakultativ intrazelluläre Pathogene passen sich den Verteidigungsmechanismen ihres Wirtes an und vernetzen diese neu, um eine Infektion auszulösen und ihr Überleben und ihre Vermehrung zu begünstigen. *Salmonella enterica* serovar Typhimurium (STm) injiziert mittels zweier Typ 3 Sekretionsapparate Effektorproteine in das Zytoplasma des Wirtes, um dort Proteinkomplexe neu zu verschalten. Daher ist die Untersuchung der Protein-Protein Interaktionen an der Schnittstelle zwischen Wirt und Pathogen essentiell, um ein genaueres Bild der Wechselbeziehungen zwischen Salmonellen und ihrem Wirt zu erlangen. Obwohl mehr als 30 sekretierte Effektorproteine beschrieben wurden, bleibt das Wissen über ihre Funktion im Verlauf der Infektion unvollständig. Außerdem ist die Anzahl der während der Infektion sekretierten Proteine höchstwahrscheinlich unterschätzt.

In dieser Arbeit stelle ich die Identifizierung von Interaktionspartnern bekannter, sekretierter Effektorproteine im Infektionskontext und ohne ektopische Expression dar. Die Methodik aus Affinitätsreinigung, gekoppelt an quantitative Massenspektrometrie (AP/QMS), die ich hier beschreibe, schlägt eine Brücke zwischen großskaliger Proteomik und hoher physiologischer Relevanz. Im Zuge dessen identifiziere, validiere und charakterisiere ich Protein-Protein Interaktionen, die bei endogenen Mengen an sekretiertem Effektorprotein auftreten. Viele der bakteriellen Effektoren zeigten ein promiskuitives Bindeverhalten und Multifunktionalität, da sie verschiedene Wirtsprozesse beeinflussten. Außerdem beleuchte ich die Konvergenz von Effektoren auf bestimmte Wirtsprozesse, sowie Effektor-Kooperation und Interaktionen zwischen Effektorproteinen. Diese Konzepte sind von grundlegender Wichtigkeit für ein besseres Verständnis der Umprogrammierung von Signalwegen des Wirtes in verschiedenen Wirtssystemen.

Ich identifiziere den Transport von Cholesterin als Konvergenzpunkt mehrerer Effektorproteine und untersuche die Rolle der involvierten Effektoren und Wirtsproteine in der Ansammlung von Cholesterin in der Replikationsnische der Salmonellen. Außerdem zeige ich, dass das Effektorprotein SteC Proteine der „Formin-like“ Familie direkt binden und phosphorylieren kann. Dadurch schließe ich ein fehlendes Bindeglied im Verständnis, wie Salmonellen das Zytoskelett ihres Wirtes verändern. Darüber hinaus beschreibe ich ein Deletionsmutanten-Screening im Infektionskontext, das auf Hochdurchsatzmikroskopie und unverzerrter Extraktion von Bildmerkmalen beruht. Im Zuge dessen beleuchte ich Prozesse im Bakterium, die essentiell für die Infektion sind und identifiziere ein neues sekretiertes Effektorprotein, YebF, auf Grund der Ähnlichkeit der Bildmerkmale zu bekannten Effektoren.

Zusammenfassend stellt die hier präsentierte Arbeit der infektionsbiologischen Forschungsgemeinschaft einen reichhaltigen Datensatz neuer Protein-Protein Interaktionen zwischen bakteriellen Effektoren und den Zielproteinen des Wirtes, eine vielseitige und validierte AP/QMS Methodik, sowie eine gut charakterisierte Sammlung an Salmonellenstämmen für die Identifikation von Protein-Protein Interaktionen an der Schnittstelle zwischen Wirt und Pathogen zur Verfügung. Außerdem ist die vorgestellte Datenbank aus unverzerrten, phänotypischen Merkmalen von unschätzbarem Wert für die Bestimmung neuer Effektorproteine und die Entschlüsselung der Vernetzung zwischen Wirt und Pathogen. Der facettenreiche, systembiologische Ansatz, mit dem die Salmonelleninfektion in dieser Arbeit beleuchtet wurde, wird die hypothesengetriebene Forschung vorantreiben und stellt einen maßgebenden Schritt hin zu einem holistischeren Verständnis der Schnittstelle zwischen Wirt und Pathogen dar.

Acknowledgements

The work presented in this thesis would not have been possible without the support of several people who should be named and thanked for here. I would like to thank **Dr. Nassos Typas** for letting me join his research group. During the four productive years of my PhD, I could acquire new knowledge, both theoretically and practically. Thank you for vivid discussions, a very open-minded, creative research environment and constructive feedback throughout the entire project. You gave me a lot of freedom to grow and always strongly encouraged personal development. Furthermore, my Thesis Advisory Committee: **Dr. Pedro Beltrao**, **Prof. Dr. Michael Boutros** and **Dr. Mikhail Savitski** for their feedback, scientific input and valuable advice during and outside of the TAC meetings. I would also like to thank the **EMBL International PhD Programme** for excellent training and providing the funding for my position.

My gratitude goes to the entire Typas Lab and all external collaborators, here first and foremost **Dr. Joel Selkrig** for great mentorship and personal support during the entire project. Working with you has always been a pleasure and I highly cherish our discussions. I also want to thank **Dr. Bachir El Debs** for introducing me to the world of high-throughput screening and for giving me the chance to join his very exciting project. Furthermore, **Dr. Cristina Viéitez**, **Dr. Clément Potel**, **Karoline Scholzen**, **Keith Fernandez**, **Mandy Rettel**, **Dr. Frank Stein**, **Dr. Leigh Knodler**, **Dr. Matthias Geyer**, **Dr. Klemens Rottner**, **Dr. Olivia Steele-Mortimer** and **Prof. Dr. David Holden** for joining forces on identifying the mysteries behind protein-protein interactions at the host pathogen interface. I am thankful for all other collaborators who provided material or scientific input to the various parts of the project and who are acknowledged specifically in the respective chapters.

I would like to thank **Dr. Nassos Typas**, **Dr. Karin Mitošch**, **Dr. Joel Selkrig**, **Dr. Milka Hammarén**, **Stefan Bassler**, **Dr. André Mateus** and **Alex Lederer** for investing their precious time and giving me valuable feedback on the structuring and writing of this thesis.

My PhD time would not have been the same without the incredible people at EMBL, many of whom I am now privileged to call my friends: former and current members of the Typas Lab, the Predocs in my year, and all others I grew close to during my time here. I would like to thank you for all happy memories ranging from Bollywood dancing to coffee break hydration control and quarantine zoom sessions.

Finally, I am and will forever be thankful to my parents, my brother and his family, Alex and his family, and my friends for their never-ending support and love.

Chapter I: Introduction	1
1. The host-pathogen interface during infection	3
2. <i>Salmonella</i> biology and relevance	5
3. Biology and dynamics of <i>Salmonella</i> infection	6
3.1. Systemic infection dynamics and persistence	6
3.2. Molecular mechanisms of the intracellular lifestyle	7
4. Current approaches at probing the host-pathogen interface	10
4.1. Mechanistic approaches to probe the <i>Salmonella</i> -host interface	10
4.2. 3D-cell culture and co-culture systems in infection	11
4.3. High-throughput proteomics and genomics	11
4.4. <i>In silico</i> approaches to predict interaction points	12
4.5. Shortcomings and unknowns of current approaches	12
5. Bibliography of this chapter	14
Chapter II: Establishing AP/QMS to map the STm infection interactome	25
1. Summary	27
2. Contributions	28
3. Library construction of tagged-effector strains and large-scale infection	28
4. Optimization of the AP/QMS workflow	30
4.1. Label-free proteomics vs multiplexing with TMT-labeling	31
4.2. Use of the crosslinker DSP vs native pulldown	32
4.3. Immunoprecipitation <i>via</i> Strep-tag vs FLAG-tag	33
4.4. Final experimental set-up for the large-scale AP/QMS study	34
5. Large-scale proteomics and quality control	35
6. Calculating enrichments and thresholding	38
6.1. Calculation of the enrichment values	38
6.2. Calculation of the statistical reliability	39
6.3. Determination of thresholds to distinguish hits from background	40
7. Appendix	42
7.1. Tagged effector strain library	42
7.2. Volcano Plots of AP/QMS study	43
8. Bibliography of this chapter	47
Chapter III: Large-scale identification of novel effector-target interactions	49
1. Summary	51
2. Contributions	51
3. Large-scale AP/MS identifies hundreds of novel effector-target PPIs	52
4. Network construction and analysis	53
4.1. STm effector PPIs converge on biologically relevant cellular processes	53
4.2. Connectivity of the networks	56
4.3. GO-term enrichment analysis	56
4.4. Bacterial-bacterial interactions	58
5. Cell line- and condition-specificity	59
6. Validation	62
6.1. Validation <i>via</i> reciprocal immunoprecipitation	62
6.2. Validation in primary bone marrow derived macrophages (pBMDMs)	64
7. Comparison to previous AP/MS studies mapping <i>Salmonella</i> effector PPIs	66
8. Appendix	68
9. Bibliography of this chapter	69

Chapter IV: Biological implications of identified effector-target interactions	75
1. Summary	77
2. Contributions	77
3. SseL and SseJ influence cholesterol trafficking	78
3.1. Effector-effector interactions and functional cooperation are prominent around host intracellular cholesterol trafficking	79
3.2. NPC1 localizes to the SCV during STm infection in SifA-dependent manner	80
3.3. The presence of cholesterol at the SCV depends on SifA, SseJ and SseL	83
3.4. The OSPB-inhibitor OSW-1 reduces cholesterol accumulation at the SCV	85
3.5. Hypothesis on biological action	86
4. SteC modulates actin rearrangements <i>via</i> formin-like proteins	88
4.1. SteC and FMNL1 interact <i>in vitro</i>	88
4.2. In vitro phosphorylation of FMNL1 by SteC and phosphosite identification <i>via</i> phosphoproteomics	89
4.3. Quantification of SteC-dependent actin bundling during infection	90
4.4. Concluding hypothesis on the biological function	92
5. Appendix	93
6. Bibliography of this chapter	94
Chapter V: Screening a genome-wide STm knockout library during infection	99
1. Summary	101
2. Contributions	101
3. Background and significance	101
4. Genome-wide knockout screen of <i>Salmonella</i> mutants during infection	102
4.1. High-throughput screening and microscopy	102
4.2. Data analysis and overview of screening results	103
4.3. Small-scale validation reveals high accuracy and specificity	105
4.4. YebF: a secreted protein with a feature fingerprint similar to SseJ	106
4.5. Conclusion and wider potential of the workflow	108
5. Bibliography of this chapter	110
Chapter VI: Discussion and Outlook	113
1. Effector-target PPIs at the host-pathogen interface	115
1.1. Brief recap of results	115
1.2. Connectivity and specificity within the STm effector interaction network	115
1.3. New insights into STm host-pathogen interactions	116
1.3.1. SseJ, SseL and other effectors are involved in cholesterol trafficking	116
1.3.2. SteC interacts with FMNLs to trigger actin polymerization	118
1.3.3. Other protein families and biological processes targeted by effector PPIs	119
1.3.4. Bacterial-bacterial PPIs in the host cytoplasm	121
1.4. Outlook on the global mapping of the STm-host interplay	121
1.5. Shortcomings and potential pitfalls	123
1.6. Conclusion and outlook	124
2. Host-pathogen interface beyond effector PPIs	125
2.1. Unbiased approaches and their advantages	125
2.2. New insights into interdependency	125
2.3. Next developments in the field of host-pathogen interactions	126
2.4. Conclusion and further outlook	127
3. Bibliography of this chapter	129

Chapter VII: Experimental Procedures	141
1. List of antibodies	143
2. List of primers and plasmids	143
3. List of stains and cell lines used in this work	154
4. Bacterial growth conditions	156
5. Electroporation of bacterial strains	156
6. P22 phage transduction	156
7. Generation of STm tagged-effector library	157
8. STm gene deletion mutants	158
9. Cell culture conditions	158
10. Infection and gentamicin protection assay	159
10.1. Infection of RAW264.7 macrophages and pBMDMs	159
10.2. Infection of HeLa and 3T3 cells	159
11. Harvesting of protein lysates	160
11.1. Native harvest	160
11.2. Harvest after crosslinking	160
12. Immunoprecipitation using anti-FLAG affinity gel	160
13. SDS-PAGE and Immunoblotting	161
14. Mass spectrometry and data analysis	162
14.1. Preparation for TMT-labeling and Mass Spectrometry	162
14.2. Mass Spectrometry Data acquisition	163
14.3. AP-QMS Data Analysis	163
15. Network building and GO-term analysis	165
16. Reciprocal pulldown validation	165
17. Sample preparation for microscopy	166
17.1. Staining of unesterified cholesterol with filipin	166
17.2. Staining of F-actin with phalloidin	167
17.3. Immunostaining for NPC1 or LAMP1	167
18. Fluorescence microscopy	167
18.1. Widefield fluorescence microscopy	167
18.2. Confocal fluorescence microscopy	168
19. Image analysis and quantification of infection rate and intracellular growth	168
20. Colocalization quantification	169
21. Protein purification and size exclusion chromatography	169
22. <i>In vitro</i> kinase assay using radiolabeled γ - ³² P ATP	170
23. <i>In vitro</i> kinase assay coupled with phosphoproteomics	171
24. High-throughput infection of RAW264.7 cells and microscopy	172
25. Validation of a subset of mutants	173
26. Bibliography of this chapter	174

List of Figures

Chapter I: Introduction	1
Figure I.1.	Intracellular niches used for replication of bacterial pathogens..... 4
Figure I.2.	Overview over secretion systems in Gram-negative bacteria, their mode of transport and their use..... 5
Figure I.3.	Partial phylogenetic tree of serovars belonging to <i>Salmonella enterica subsp. enterica</i> 6
Figure I.4.	Intracellular persistence leads to lower susceptibility towards antibiotic treatment and host immune defense..... 7
Figure I.5.	Schematic of <i>Salmonella</i> effectors reprogramming host processes..... 8
Figure I.6.	Overview over model systems with respect to their controllability, biological complexity and physiological relevance..... 10
Chapter II: Establishing AP/QMS to map the STm infection interactome	25
Figure II.1.	Graphical abstract..... 27
Figure II.2.	Cloning strategy for introducing the chromosomal STF-tag..... 28
Figure II.3.	Time-course infection, expression and translocation at 20 hpi..... 30
Figure II.4.	Quantification in label-free MS and comparison to TMT-multiplexing..... 31
Figure II.5.	Use of the crosslinker DSP prior to cell lysis and comparing Strep- and FLAG-IP..... 33
Figure II.6.	Correlations between technical and biological replicates, and between native vs crosslinked harvest..... 35
Figure II.7.	Overlap between replicates in the different conditions and cell lines..... 36
Figure II.8.	Batch effect removal and signal normalization reduces variability between replicates..... 37
Figure II.9.	Distribution of p-values across both cell lines and conditions..... 38
Figure II.10.	Comparison of FC-calculation with respect to median and wildtype control..... 39
Figure II.11.	Comparing limma and fdrtool for fdr-calculation..... 40
Figure II.12.	Increasing the FC-threshold reduces diversity in effectors with enriched targets..... 41
Figure II.13.	Enrichments after native IP in HeLa cells..... 43
Figure II.14.	Enrichments after IP under crosslinking conditions in HeLa cells..... 44
Figure II.15.	Enrichments after native IP in RAW264.7..... 45
Figure II.16.	Enrichments after IP under crosslinking conditions in RAW264.7..... 46
Chapter III: Large-scale identification of novel effector-target interactions	49
Figure III.1.	Number of PPIs detected for each bait..... 53
Figure III.2.	<i>Salmonella</i> -host PPI networks in RAW264.7 and HeLa..... 55
Figure III.3.	Connectivity of the interaction networks as indicated by the number of effectors binding to a given host protein..... 56
Figure III.4.	GO-term enrichments (Biological Process) across both cell lines..... 57
Figure III.5.	GroEL and STM14_3767, but not other highly abundant bacterial proteins (RecA), are present in the host cytoplasm during infection..... 59
Figure III.6.	Overlap between native and crosslinked samples as well as across cell lines reveals several conserved PPIs..... 60
Figure III.7.	Comparison of background proteome determined in AP/QMS of RAW264.7 and HeLa..... 61
Figure III.8.	Validation <i>via</i> reciprocal co-IP using specific antibodies against a panel of novel target proteins..... 64
Figure III.9.	Validation of successful effector translocation and capture of previously identified PPIs in pBDMDs..... 66

Chapter IV: Biological implications of identified effector-target interactions	75
Figure IV.1. Graphical abstract of the chapter.....	77
Figure IV.2. Increased resolution of the SseJ-interactome during infection of HeLa cells.....	80
Figure IV.3. Confocal immunofluorescence microscopy images (60x magnification) to assess the recruitment of NPC1 to the SCV in various STm mutant conditions at 12 hpi.....	81
Figure IV.4. Widefield immunofluorescence images and quantification of colocalization between NPC1 and the SCV.....	82
Figure IV.5. Microscopy images of WT and NPC1-KO HeLa cells infected with different STm mutants and stained with filipin 12 hpi.....	84
Figure IV.6. Quantification of colocalization between STm and cholesterol after treatment with the OSBP- inhibitor OSW-1.....	86
Figure IV.7. The complex interplay of STm effectors and host cell targets.....	87
Figure IV.8. SteC directly binds and phosphorylates FMNL1 <i>in vitro</i>	89
Figure IV.9. Identification of phosphosites in the N-terminal domains of FMNL1 and FMNL2 after incubation with SteC <i>in vitro</i>	90
Figure IV.10. SteC induces actin bundles in 3T3 fibroblasts through FMNL2/3.....	91
Figure IV.11. Abundance of FMNL proteins across the various cell lines used in experimentation.....	92
Figure IV.12. Model of the molecular interplay between SteC and host factors to induce actin bundling at the SCV.....	92
Chapter V: Screening a genome-wide STm knockout library during infection	99
Figure V.1. Experimental workflow and high-throughput microscopy data analysis.....	103
Figure V.2. Cell entry and intracellular proliferation of all tested STm single gene knockout mutants in HeLa cells and RAW264.7.....	104
Figure V.3. Small-scale validation of high-throughput screening data.....	106
Figure V.4. Characterization of YebF, a <i>Salmonella</i> protein which is secreted during infection.....	107
Figure V.5. YebF interaction partners during infection after native and crosslinked IP.....	108
Figure V.6. Layout of a gene-gene interaction screening study in the context of infection.....	109
List of Tables	
Table II.1. STF-tagged effector library.....	42
Table III.1. List of previously described protein-protein interactions recapitulated in this study.....	68
Table IV.1. Phosphosites identified in SteC, FMNL1 ₁₋₃₈₅ and FMNL2 ₂₋₄₇₈ after co-incubation.....	93
Table VII.1. Antibodies used in the study.....	143
Table VII.2. All plasmids used in the study.....	143
Table VII.3. All oligos / primers used in the study.....	144
Table VII.4. All cell lines and bacterial strains used in this work.....	154

List of Abbreviations

aa	amino acid
ALMF	Advanced Light Microscopy Facility
AP/MS	affinity purification / mass spectrometry
AP/QMS	affinity purification / quantitative mass spectrometry
ATP	adenosine triphosphate
BSA	bovine serum albumin
CRISPR	Clustered Regularly Interspaced Short Palindromic Repeats
D	aspartic acid
DMEM	Dulbecco's Modified Eagle's Medium
DMSO	dimethyl sulfoxide
DSP	dithiobis(succinimidyl propionate)
DTT	dithiothreitol
EDTA	ethylenediaminetetraacetic acid
EIAV	equine infectious anemia virus
FBS	fetal bovine serum
FC	fold change
fdr	false discovery rate
fwd	forward
FITC	fluorescein isothiocyanate
FMNL	formin-like protein
FPLC	fast protein liquid chromatography
GAPDH	glyceraldehyde 3-phosphate dehydrogenase
GO	gene ontology
GTP	guanidine triphosphate
HEPES	4-(2-hydroxyethyl)-1-piperazineethanesulfonic acid
HIV	human immunodeficiency virus
hpi	hours post infection
I	isoleucine
iBAQ	intensity-based absolute quantification
IF	immunofluorescence
IP	immunoprecipitation
Kan	kanamycin (resistance cassette)
kDa	kilo Dalton
LAMP1	Lysosome-associated membrane protein 1
LB	lysogeny broth
LC/MS	liquid chromatography / mass spectrometry
M cells	microfold cells
M-CSF	macrophage colony-stimulating factor
MOI	multiplicity of infection
mRNA	messenger ribonucleic acid
MS	mass spectrometry
MW	molecular weight
NPC1	Niemann-Pick C1 protein
OSBP	oxysterol-binding protein
pBMDM	primary bone marrow-derived macrophage
PBS	phosphate buffer saline
PCF	Proteomics Core Facility

PCR	polymerase chain reaction
PFA	paraformaldehyde
PI4P	phosphatidylinositol 4-phosphate
PPI	protein-protein interaction
PVDF	polyvinylidene fluoride
R ²	squared correlation
RAB	Ras-associated binding
rev	reverse
RNAi	RNA-interference
rpm	rotations per minute
RS	recipient strain
S	serine
SCV	<i>Salmonella</i> Containing Vacuole
SDS	dodecyl-sulfate
SDS-PAGE	SDS-polyacrylamide gel electrophoresis
SEC	size exclusion chromatography
SIF	<i>Salmonella</i> -induced filament
SLC	solute carrier protein
SLM	short linear motif
SNARE	SNAP receptor
SPI	<i>Salmonella</i> Pathogenicity Islands
STF	2xStrep-TEV-3xFLAG
STm	<i>Salmonella enterica</i> serovar Typhimurium
T	threonine
T3SS	Type III secretion system
Tat	Twin Arginine Translocon
TBST	Tris-buffered saline with Tween-20
TMT	Tandem Mass Tag
TPP	Thermal Proteome Profiling
Tx-100	Triton-X-100
VPS	Vacuolar Sorting Protein
WB	Western blot
WHO	World Health Organization
WT	wildtype
Y	tyrosine

Chapter I

Introduction

Chapter I: Introduction

1. The host-pathogen interface during infection

Interdependency, adaptation and co-evolution of pathogens and their hosts are fundamental principles of infection biology. Several types of pathogens, with varying degrees of host specificity, exist and continuously evolve in an arms race of adaptation with their host. Pathogens of various origins can infect eukaryotic hosts, which are at the focus of this thesis. Human and mouse pathogens comprise viruses, bacteria, fungi, parasites and helminths. Within each of these groups, various lifestyles during the infection cycle and outside of it exist.

Intracellular pathogens display a very high degree of interdependency with their host and therefore represent one of the most complex forms of pathogenicity. Viruses are almost exclusively intracellular, while several bacterial (e.g. *Salmonella*, *Mycobacterium*, *Legionella*, *Shigella*) and eukaryotic (e.g. *Plasmodium*, *Toxoplasma*) intracellular pathogens exist (Thakur, Mikkelsen, and Jungersen 2019). A common feature of these pathogens is their bypassing of the humoral host immune defense (e.g. the complement system) by residing inside cells of their host. There, they need to subvert intracellular host defenses and hijack host pathways in order to survive in their niche (Diacovich and Gorvel 2010).

Intracellular bacterial pathogens employ distinct strategies to avoid host cell defenses and promote their proliferation (Figure I.1). Upon entry into the host cell, which is caused by phagocytosis, macropinocytosis or endocytosis, many intracellular bacteria reside in the generated vacuolar compartment and usurp various cellular processes, such as vesicular trafficking, actin cytoskeleton organization, metabolic processes and lysosomal degradation (Toledo and Benach 2015; Colonne, Winchell, and Voth 2016; Eisenreich et al. 2019).

The compartments used by bacterial pathogens for intracellular replication also differ. *Salmonella* impedes the host endocytic process at the stage of late endosomes, preventing them from fusing to lysosomes and thereby undergoing degradation (Holden 2002). *Mycobacterium* resides in intracellular replication vacuoles, which are derived from early endosomes and modify the functionality of Rab-proteins to stimulate their survival (Seto, Tsujimura, and Koide 2011). *Coxiella*, upon cell entry, forms a lysosome-like parasitophorous vacuole through fusion of their phagocytic compartment with host endocytic vacuoles (Mulye et al. 2017). In addition, the vacuolar compartment of some intracellular pathogens, such as *Brucella* and *Legionella*, fuses with the endoplasmic reticulum, which from then on serves as their replication niche (Gorvel and Moreno 2002; Oliva, Sahr, and Buchrieser 2018). Some species, such as *Shigella* and *Listeria*, only transiently reside in a vacuolar niche, before escaping into the host cytoplasm (Figure I.1), where they can replicate and use the actin cytoskeleton for motility (Monack and Theriot 2001; Killackey, Sorbara, and Girardin 2016).

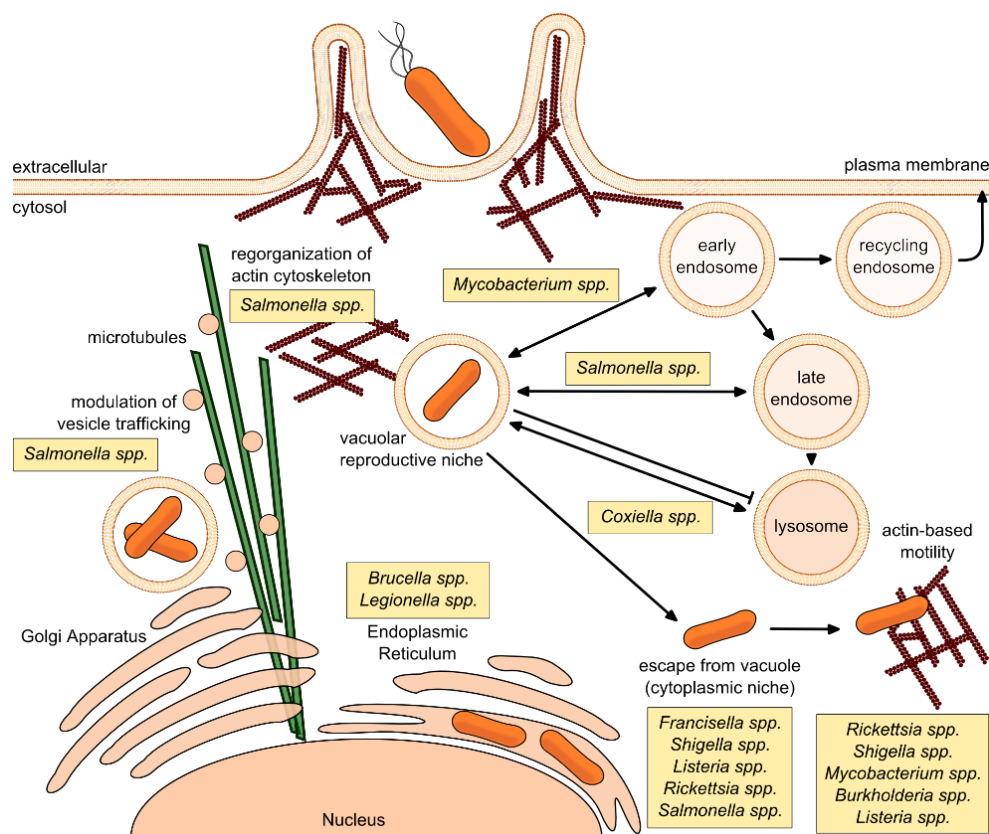


Figure I.1 Intracellular niches used for replication of bacterial pathogens. Upon entry into host cells via endocytosis, intracellular bacterial pathogens reside in different niches. Several species stay within a vacuolar replication niche, which is derived from various stages of the host endocytic pathway (indicated for each species). From there, *Salmonella* spp. modify various host processes (as indicated). Other pathogens facultatively or obligately escape from their vacuolar compartment and reside within the host cytoplasm (species indicated in yellow boxes). This graphic was adapted from: (Diacovich and Gorvel 2010).

To interact with their surroundings, other bacteria or their host, pathogens produce and secrete or translocate an arsenal of proteins, called effectors. While *Legionella pneumophila* secretes more than 300 different effectors (Ninio and Roy 2007; Burstein et al. 2009; Schroeder 2017), there are only about 30 effectors described in *Salmonella enterica* serovar Typhimurium (STm) (Schleker, Sun, et al. 2012; Ramos-Morales 2012; D. L. LaRock, Chaudhary, and Miller 2015), and 6 in *Yersinia pestis* (Navarro, Alto, and Dixon 2005; Matsumoto and Young 2009). These are exported from the bacterial cytosol *via* specialized secretion systems which are categorized according to their molecular structure and composition, as well as their function. Apart from the Twin Arginine Translocon (Tat) and the Sec translocon proteins, there are 7 secretion systems described in Gram-negative bacteria (Type I, II, III, IV, V, VI and IX; Figure I.2), and the Type VII secretion system in Gram-positive bacteria and *Mycobacterium* (Leo, Grin, and Linke 2012; T. R. D. Costa et al. 2015; Lasica et al. 2017; Famelis et al. 2019).

In Gram-negative bacteria, types I, II, V and IX serve various means of transport from the bacterial cytoplasm or periplasmic space to the cell surface or exterior, and types III, IV and VI are essential for different forms of inter-organismal interaction (Figure I.2).

Type III secretion systems (T3SS) are responsible for the translocation of effector proteins to the host cytoplasm in various bacterial pathogens, such as *Salmonella*, *Shigella*, *Yersinia*, or *Vibrio* (Coburn, Sekirov, and Finlay 2007; Wagner et al. 2018). The T4SS is best known from *Agrobacterium* and *Helicobacter*, where it translocates part of the tumor-inducing Ti-plasmid or CagA protein, respectively, to host cells (Aguilar et al. 2010; Yuan, Wang, and Wang 2018), thereby causing tumorous growth. Lastly, the T6SS is most prominently used for the injection of toxins from one bacterial species to another or into a eukaryotic prey (Hood et al. 2010; Ho, Dong, and Mekalanos 2014; Joshi et al. 2017; Logan et al. 2018; Navarro-Garcia et al. 2019) (Figure I.2).

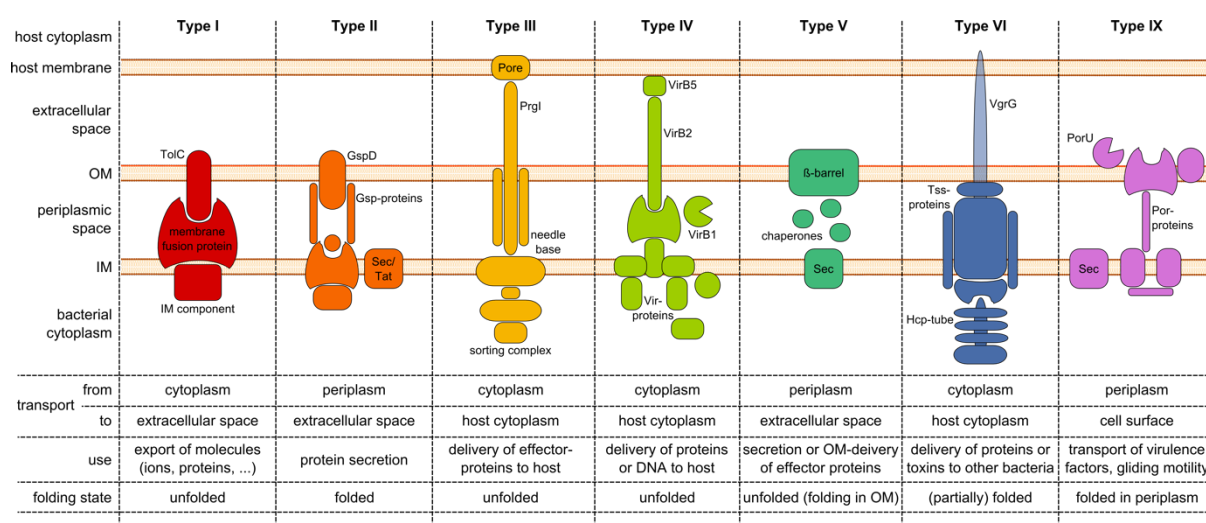


Figure I.2 Overview over secretion systems in Gram-negative bacteria, their mode of transport and their use. Bacterial secretion systems come in many shapes and purposes. Some (Types I, II, V and IX) are required for transport of a variety of molecules to the extracellular space or the cell surface (as indicated) and can do this either autonomously (Type I) or in a transport chain with the Sec or Tat translocon. Others (Types III, IV and VI) are capable of reaching across the extracellular space and transport molecules into the cytoplasm of a host or a neighboring bacterium. Main components of the transport systems and their reach, as well as their biological use, is indicated in the table. *This figure was adapted from: (Leo, Grin, and Linke 2012; T. R. D. Costa et al. 2015; Green and Meccas 2016; Lasica et al. 2017; Lauber et al. 2018).*

2. *Salmonella* biology and relevance

The rod-shaped, Gram-negative and facultative intracellular pathogen *Salmonella enterica* is among the most prominent causing agents for many food-borne intestinal diseases, such as typhoid fever, gastroenteritis or bacteremia (Zhang et al. 2003). These diseases are endemic in many developing countries (Okeke et al. 2005) and account for 35% of foodborne hospitalizations (28% of deaths) in the United States (Scallan et al. 2011). In addition, multi-drug resistant strains are currently emerging (Threlfall 2002; Nishino, Latifi, and Groisman 2006), posing an enormous threat to immunocompromised people and children (Jacobs et al. 1985). Consequently, they were included on the list of higher risk pathogens by the WHO in early 2017 (Organization and Others 2017). The *Salmonella enterica subsp. enterica* comprises typhoidal serovars (*S. typhi* and *S. paratyphi* A, B and C), causing systemic enteric fever, as well as non-typhoidal serovars of varying genomic relatedness (Figure I.3),

causing gastroenteritis or, rarely, invasive non-typhoidal salmonellosis (Gal-Mor, Boyle, and Grassl 2014).

Salmonella enterica serovar Typhimurium (STm) is a non-typhoidal serovar which, in addition to its clinical relevance, has been used as a model organism for intracellular pathogens (Garai, Gnanadhas, and Chakravorty 2012). This is mainly due to the deep understanding of basic biology and infection, as STm was one of the first organisms with established genetic tools (Ohl and Miller 2001). Complete sequencing of *Salmonella* serovars (Strauss and Falkow 1997; McClelland et al. 2001) and investigation of genomic variation has further deepened the knowledge. Signature tagged mutagenesis (Hensel et al. 1995) has been developed in *Salmonella* and a broad panel of tools for genetic manipulation continues to be established and improved, including comprehensive mutant libraries (Porwollik et al. 2014). STm strain 14028S, as well as mutants derived from 14028S wildtype, is used in this work. Other STm strains which are frequently used in the literature are indicated in Figure I.3.

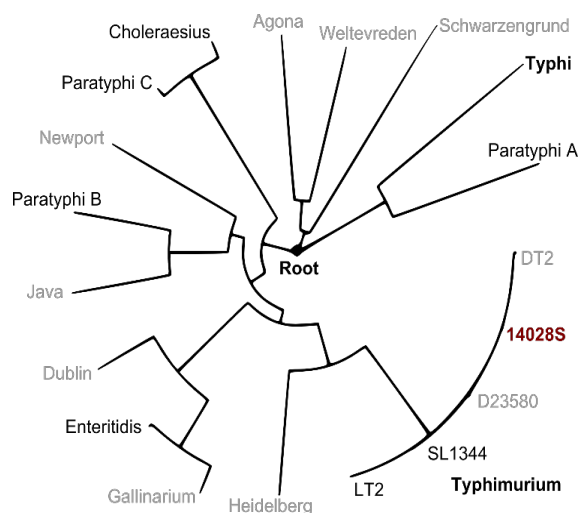


Figure I.3 Partial phylogenetic tree of serovars belonging to *Salmonella enterica* subsp. *enterica*. Typhoidal and non-typhoidal serovars of *Salmonella enterica* subsp. *enterica* are shown according to their genetic distance. S. Typhimurium 14028S, the strain used in this work, is indicated in red. *This figure was adapted from: (Branchu, Bawn, and Kingsley 2018).*

3. Biology and dynamics of *Salmonella* infection

3.1. Systemic infection dynamics and persistence

During their infection cycle, *Salmonella* can invade a variety of host cell types: enterocytes, microfold cells (M cells, epithelial cells in the intestinal tract), as well as dendritic cells and macrophages (Haraga, Ohlson, and Miller 2008; D. L. LaRock, Chaudhary, and Miller 2015). Infection of epithelial cells leads to apoptosis and inflammation. Subsequent recruitment of cells of the immune system allows some *Salmonella* serovars to spread systemically. Similarly, the passage through M cells serves as a gateway to systemic spread.

In addition to maintained systemic infection, *S. typhi* and *S. paratyphi* A have been shown to cause chronic, asymptomatic infection through persistence in a biofilm formed on gallstones (Di Domenico et al. 2017). Intermittently, these biofilm-forming persisters can shed and cause either infection or transmission. Furthermore, *Salmonella* can persist intracellularly by turning off their metabolic activity and proliferation. These persisting *Salmonella* cannot easily be targeted by the immune system or by antibiotic treatment, due to their metabolic state, as they are non-growing, yet still expressing and translocating effector proteins that modulate host cell response (Figure I.4, (Stapels et al. 2018)).

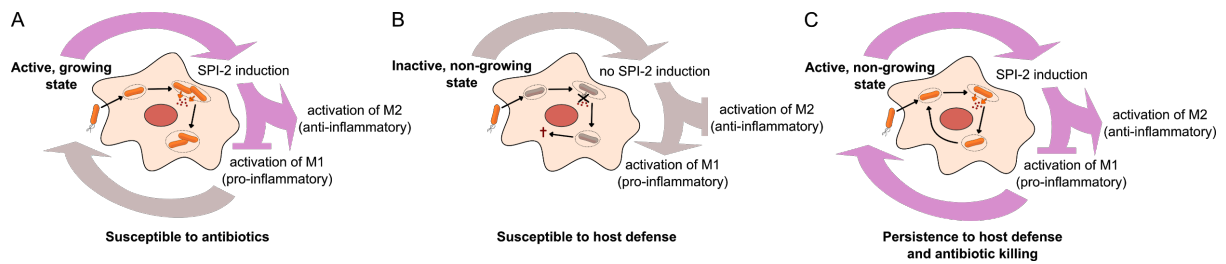


Figure I.4 Intracellular persistence leads to lower susceptibility towards antibiotic treatment and host immune defense. Upon infection, *Salmonella* form reservoirs, either extracellularly, e.g. on gallstones, or intracellularly. The latter is mediated by switching their metabolic state. A) In an active, growing state, where translocation of effector protein occurs, bacteria are susceptible to antibiotics due to their active growth metabolism. B) In an inactive non-growing state, without induction of effector translocation, *Salmonella* get cleared by host immune cells. C) By switching to an active, yet non-growing state, where translocation of effector proteins is induced, *Salmonella* can become persistent to both host defenses (due to protection via effectors) and antibiotic treatment (due to their non-growing state). *This figure was adapted from: (Stapels et al. 2018).*

3.2. Molecular mechanisms of the intracellular lifestyle

The *Salmonella* genome contains two *Salmonella* Pathogenicity Islands (SPI) -1 and -2 that are essential for the initiation and maintenance of infection. Within these regions, components of T3SS, alongside several secreted effectors, are encoded (Hansen-Wester and Hensel 2001). During infection, the bacteria need to enter host cells – a process which is mainly mediated by SPI-1 encoded T3SS, which translocates effectors into the host cytosol (Ramos-Morales 2012; D. L. LaRock, Chaudhary, and Miller 2015). Depending on the cell type, the entry into the host occurs differently: macrophages will easily take up *Salmonella* cells by phagocytosis (Jennings, Thurston, and Holden 2017), while gut epithelial cells require pathogen-induced, SPI-1-driven actin rewiring and changes in lipid composition of the cell membrane at the entry site (Figure I.5) (Brooks et al. 2017). SPI-1-activation during the infection of macrophages plays an essential role in triggering the non-apoptotic cell death pyroptosis (Fink and Cookson 2007; C. N. LaRock and Cookson 2013).

Upon host entry, *Salmonella* resides in the *Salmonella* Containing Vacuole (SCV) – a specialized compartment, derived from late endosomes. The SCV is further modified at the surface by the recruitment of LAMP1 and vATPases and loss of mannose-6-phosphate receptors (Kumar and Valdivia 2009). Subsequently, the SCV is transported to the perinuclear region along the host cytoskeleton using host transport

machineries (Knuff and Finlay 2017). The SPI-2 T3SS plays a major role in these processes, which are part of the maturation of the SCV (Pucciarelli and García-Del Portillo 2017). The effectors secreted by the SPI-2 T3SS reprogram many host defense pathways, such as the fusion of the SCV with lysosomes (Wasylnka et al. 2008; Namakchian et al. 2018). Furthermore, the microtubules and actin fibers of the cytoskeleton alongside the respective motor proteins are hijacked to facilitate migration and later expansion of the SCV (Krieger et al. 2014; D. L. LaRock, Chaudhary, and Miller 2015). In the latest stages of infection, the SCV is known to elongate along the microtubule network, recruiting endosomal vesicles, thereby forming *Salmonella*-induced filaments (SIFs, Figure I.5, (Liss et al. 2017)). This rewiring of the host endocytosis and vesicular trafficking is linked to several SPI-2 T3SS effectors and serves the supplying of intracellular *Salmonella* with nutrients (Drecktrah et al. 2008; Perrett and Zhou 2013; Knuff and Finlay 2017).

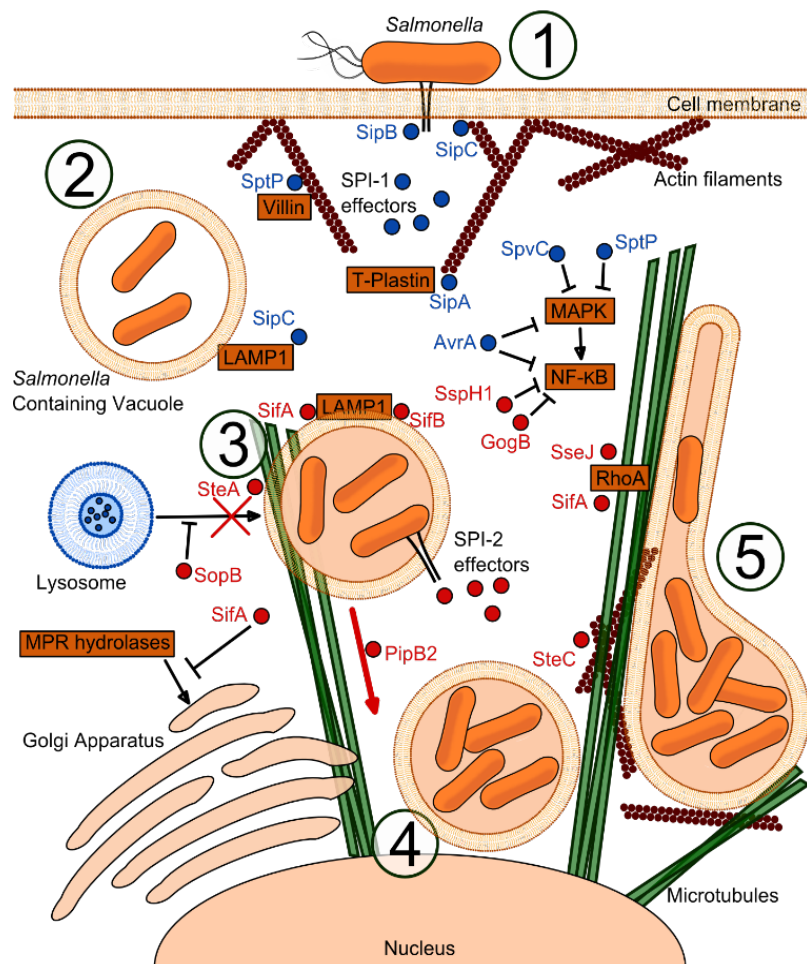


Figure I.5 Schematic of *Salmonella* effectors reprogramming host processes. SPI-1 effectors (in blue) play a major role in cell entry and the early stages of infection (1 and 2), especially in epithelial cells. The main processes that are influenced are actin remodeling, membrane ruffling at the entry site and the recruitment of Phosphatidylinositol-3-Phosphate. Upon formation of the SCV, *Salmonella* translocates SPI-2 effectors (red) into the host cytoplasm. These mediate the maturation of the SCV and protect it from the host defense systems (3). Furthermore, they induce movement of the SCV in a juxtannuclear position (3 and 4). In the late stages of infection, several effectors mediate the expansion along microtubules and other cytoskeletal components (5). Furthermore, several SPI-1 and SPI-2 effectors modulate cell survival and inflammation at different time points of the infection. Figure adapted from (D. L. LaRock, Chaudhary, and Miller 2015).

SPI-1 and SPI-2 effectors are also required to change the infection environment on a more global scale – by inducing and mediating inflammation. Upon STm infection, macrophages initiate pyroptosis (C. N. LaRock and Cookson 2013), which is dependent on Caspase-1 activity and through which inflammatory cytokines such as IL-18 are activated (Tait, Ichim, and Green 2014). This causes the recruitment of additional macrophages and other monocytes, which is highly relevant for the propagation of *Salmonella* infection *in vivo*. On the other hand, *Salmonella* secretes effectors that decrease NF- κ B signaling and thereby TNF α dependent necroptotic cell death (Günster et al. 2017). This balance of promoting inflammation and cell-protection allows *Salmonella* to further proliferate within macrophages (Figure 1.5).

Furthermore, autophagy is differentially influenced by *Salmonella* throughout the infection (Casanova 2017). While the autophagic response is induced and highly upregulated when SPI-1 effectors are expressed and translocated, it gets suppressed to baseline by SPI-2 effectors as early as 3 hours post infection (hpi) (Tattoli et al. 2012). In line with these dynamics, suppression of host autophagy proteins through siRNA causes a decreased intracellular STm proliferation (H. B. Yu et al. 2014).

Several effector proteins have been associated with alterations in lipid trafficking (Kolodziejek et al. 2019; Arena et al. 2011; Azimi et al. 2020). In early stages of infection, *Salmonella* induces membrane ruffling, and influences the growth and stability of the SCV by interfering with host lipid transport (Deleu et al. 2006; D. L. LaRock, Chaudhary, and Miller 2015). Throughout infection, the recruitment of specific lipids, lipid-anchored proteins or host vesicles is essential for the maintenance and protection of the SCV (Jennings, Thurston, and Holden 2017; Kolodziejek et al. 2019), and is modulated by several SPI-1 and SPI-2 effector proteins.

Recent reports demonstrate that these dependencies between effectors do not only occur indirectly (e.g. functional redundancy described in (Zhou, Chen, and Hernandez 2001; Figueira et al. 2013)), but can also occur through physical interactions (X.-J. Yu, Liu, and Holden 2016; Kolodziejek et al. 2019). These effector-effector interactions, whether direct or *via* a common target, are shifting more and more into focus of scientific research.

In addition to altering intracellular host responses, STm triggers a competition with other microbes for iron, e.g. through accumulation of lipocalin-2 in the lumen. Lipocalin-2 sequesters enterochelin, which is required for iron acquisition by microbiota, but not salmochelin, the *Salmonella* siderophore (Nairz et al. 2010; D. L. LaRock, Chaudhary, and Miller 2015). This does not only affect *Salmonella*'s ability to colonize the intestine and gain advantage over gut microbes but also affects host immune response (Nedialkova et al. 2014; D. L. LaRock, Chaudhary, and Miller 2015; L. F. Costa et al. 2016). Furthermore, triggering inflammation provides *Salmonella* with a competitive advantage over commensal gut microbes. The reactive oxygen species generated by inflammation can react with thiosulfate to form tetrathionate, which can

be utilized by *Salmonella* as an electron acceptor (Winter et al. 2010) to anaerobically grow on ethanolamine (Thiennimitr et al. 2011). Gut microbes lack this ability and are hence at a growth disadvantage during acute gut inflammation.

4. Current approaches at probing the host-pathogen interface

In order to probe the interface between *Salmonella* and their host cells, a diverse panel of model systems has been applied in the past and continues to be broadened and further developed. In general, model systems can be ordered alongside two anti-correlated axes: on the one hand biological complexity and physiological relevance, and on the other hand accessibility and controllability (Figure I.6).

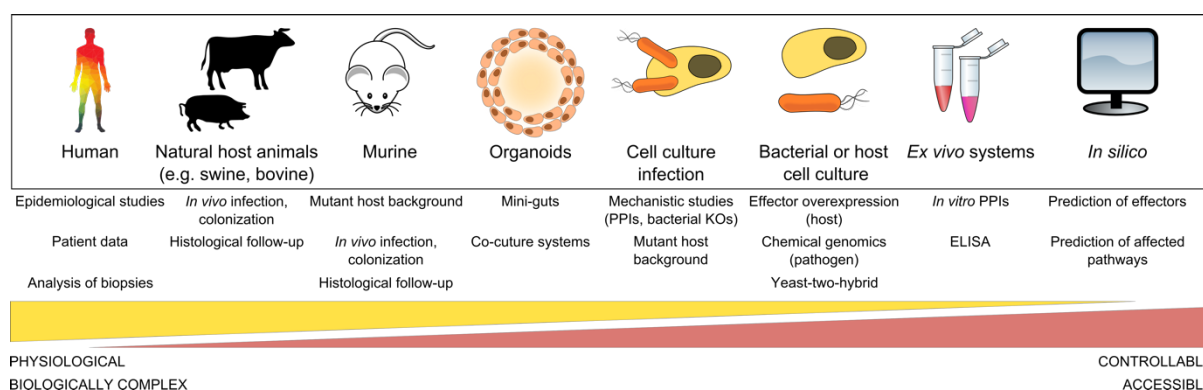


Figure I.6 Overview over model systems with respect to their controllability, biological complexity and physiological relevance. A vast panel of different model systems has been applied in *Salmonella* research, and host-pathogen interactions more generally. While systems of high biological complexity (such as patient studies or *in vivo* host systems) offer high physiological relevance, they are very difficult to control and manipulate due to their complexity. *Ex vivo* systems or *in silico* approaches allow for a higher degree of manipulation and provide accessibility, yet they often operate outside of the physiological context. Recent advances at the interface between simplified systems and physiological models include organoids, as well as improved cell culture infection, which can more readily be upscaled. Current high-throughput approaches are limited to *ex vivo* or more easily accessible cell culture systems.

4.1. Mechanistic approaches to probe the *Salmonella*-host interface

Targeted approaches have been employed for decades to decipher host-pathogen interactions. These studies have been conducted for a wide panel of pathogens and continue to play an essential role in deepening the understanding of the interconnectivity between pathogen and host. In *Salmonella* pathogenesis specifically, the aforementioned rewiring of host cell pathways is mediated entirely by secretion of SPI-1 and SPI-2 effectors. Identifying and understanding the mechanism of infection, as well as the key players and mediators involved in both, the host and the pathogen side, are therefore the main goals of *Salmonella* infection research. Many studies have used mechanistic elucidation of effector-host interaction pairs in cell culture (Ruiz-Albert et al. 2002; Knodler et al. 2003; Lossi et al. 2008) and then validated the physiological role of these interactions in mouse models (Barthel et al. 2003; Maier et al. 2014). From such studies, a panel of well-characterized interaction pairs (gold-standard) has emerged (Ramos-Morales 2012; D. L. LaRock, Chaudhary, and Miller 2015; Jennings, Thurston, and Holden 2017; Azimi et al. 2020).

In addition to understanding effector biochemistry and biology, other relevant concepts for infection dynamics and *Salmonella*-host interactions have been studied mechanistically. Various routes have been taken to assess heterogeneity within the bacterial population (K. M. Davis and Isberg 2016), such as reporter plasmids for persistence (Helaine et al. 2014; Claudi et al. 2014). Investigating heterogeneity and its underlying factors is highly relevant for understanding tolerance or resistance to antibiotics.

4.2. 3D-cell culture and co-culture systems in infection

Novel approaches try bridging controllability of the system with physiological relevance by using organoids (Nickerson et al. 2018; Lees et al. 2019; Verma et al. 2020). This spans infection in organoid or minigut systems, as well as setting up co-culture systems which, in addition to intestinal cells, contain either commensal bacteria (Lu et al. 2020) or immune cells (Karve et al. 2017). By introducing a higher complexity than feasible in 2D-monoculture, the protection of the intestinal mucosa by *Lactobacillus* (Lu et al. 2020) as well as the invasion of neutrophils into the site of infection (Karve et al. 2017) have been studied. While current studies focus on a proof-of-concept and lack mechanistic depth, these co-culture systems have the potential to provide a more physiological, yet controllable model for *Salmonella* infection.

4.3. High-throughput proteomics and genomics

With the rise of large-scale proteomics and high-throughput genomics, the global profiling of protein-protein interactions (PPIs), as well as the genome-wide mapping of genotype-phenotype relationships became accessible for host-pathogen interaction studies (Shah et al. 2015). Affinity-tag purification/mass spectrometry (AP/MS) studies, spanning from viral to bacterial pathogens (Jäger, Cimermancic, et al. 2011; Penn et al. 2018; Sontag et al. 2016; D'Costa et al. 2019), global yeast two-hybrid approaches (Joung, Ramm, and Pabo 2000; Uetz et al. 2006; Brückner et al. 2009; Fossum et al. 2009), and screening of knock-out libraries on either host- or pathogen-side have proven instrumental in previous efforts to understand the role of effectors in the pathogenesis of diverse pathogens.

Early global PPI studies suffered from a large number of false positives, which caused skepticism and doubt regarding their reliability and applicability (Stynen et al. 2012; Rajagopala, Hughes, and Uetz 2009). In recent years, due to significant advancements in both experimental and data analysis approaches, systematic mapping of host-pathogen PPIs has become increasingly important for driving research. A powerful example is HIV research, where relevant *bona fide* physical interactions were identified through systematic AP/MS (Jäger, Cimermancic, et al. 2011), thereby resolving uncertainty about thousands of reported PPIs for very few viral proteins (Jäger, Gulbahce, et al. 2011) and sparking a vast panel of mechanistic hypotheses in HIV biology (Chou et al. 2013; Jäger, Kim, et al. 2011). Since then, similar host-pathogen PPI mapping approaches have been extended to several important human pathogens, e.g. Kaposi's sarcoma-associated herpesvirus, dengue virus, Zika virus, Ebola virus,

Chlamydia, *Mycobacterium*, or SARS-CoV2 (Jäger, Cimermancic, et al. 2011; Mirrashidi et al. 2015; Penn et al. 2018; Shah et al. 2018; Z. H. Davis et al. 2015; Batra et al. 2018; Jean Beltran et al. 2017; Selkrig et al. 2020). Systemic approaches have also been used in *Salmonella* research to elucidate effector-target PPIs (Auweter et al. 2011; Sontag et al. 2016; D’Costa et al. 2019). These large-scale datasets continue to fuel a deeper understanding of host-pathogen infection mechanisms.

Besides proteomics-based approaches, recent studies of the host-pathogen interface have seen an increase in genomics-based studies. These address the interdependency, redundancy and heterogeneity during infection from various different angles. While the number of studies is ever increasing, their principles can be exemplified in the following vignettes: 1) Capitalizing on the improvements in RNAseq sensitivity, a dual-seq methodology has been developed to distinguish host- and pathogen-transcriptomics throughout the course of infection (Westermann et al. 2016; Westermann, Barquist, and Vogel 2017). 2) Using genetic modification of the host background using RNAi or CRISPR-based methods (Québatte and Dehio 2017), cellular processes that are essential for pathogenicity (Chang et al. 2019), detrimental for intracellular growth or part of the host-pathogen interface have been identified (Yeung et al. 2019). 3) Several similar strategies on the pathogen side, such as Signature tagged mutagenesis (Hensel et al. 1995; Tsolis et al. 1999; Cummins and Gahan 2012) or transposon-libraries (Lawley et al. 2006; Chaudhuri et al. 2009) led to the discovery of bacterial virulence genes. Additionally, CRISPRi has been applied to target and study essential genes (Qu et al. 2019). 4) Genetic modification of the host (by RNAi) and the pathogen (using a transposon-library) in parallel (O’Connor and Isberg 2014), was used to unravel the genetic interactions between *Legionella* and *Drosophila*, and address functional redundancy of bacterial effectors (O’Connor et al. 2012).

4.4. *In silico* approaches to predict interaction points

An orthogonal approach to experimentally probing the interface between host and pathogen is offered by *in silico* approaches. These cover the prediction of pathogen effector proteins (Burstein et al. 2009; Samudrala, Heffron, and McDermott 2009) and relevant host targets (Schleker, Garcia-Garcia, et al. 2012), as well as understanding the evolution of pathogenicity (Che, Hasan, and Chen 2014), host adaptation (Wheeler, Gardner, and Barquist 2018; Mousavi-Derazmahalleh et al. 2019) or resistance development (Munck et al. 2014).

4.5. Shortcomings and unknowns of current approaches

All of these approaches are powerful and have substantially advanced our understanding of host-pathogen interactions. Yet, each has its specific limitations to be overcome. The knowledge generated through each of the presented studies can be used to improve methodologies and direct advances within other models and approaches.

Despite their strong impact on fueling hypothesis-driven research, global studies continue to suffer from a panel of shortcomings. In the case of large-scale mapping of host-pathogen PPIs, limitations in recapitulating the infection environment remain. For example, PPIs have so far been studied in mammalian cells, either outside the context of infection using plasmid-based over-expression of a single effector, or through lysate-based *in vitro* systems. These approaches can be easily prone to the identification of false-positives due to non-physiologically high abundances of the effectors outside of the context of infection. At the same time, they do not allow probing for interactions that may depend on the presence of additional effectors and can produce false-negatives due to the absence of changes in the cell response to bacterial infection (Auweter et al. 2011; Sontag et al. 2016; D’Costa et al. 2019).

In the case of high-throughput genomics, even though gene-depletion screens have been performed in the *Salmonella* infection context (Andritschke et al. 2016; Yeung et al. 2019), all current approaches use barcoded, pooled mutant libraries, comprised of tens of thousands of individual mutants, followed by sequencing. As infection rates are around 30% in most cell culture approaches, this generates a vast pool of uninfected bystander cells. Although this may be overcome by cell sorting, uninfected cells still limit the sensitivity needed to detect small impacts of gene deletions on the infectious potential.

Mechanistic studies on the other hand allow for very precise elucidation of a single interaction or interdependency, yet they often do not permit the throughput needed to gain a global image and a systemic interaction map. While emerging approaches, such as using organoids and co-culture, give rise to new insights by allowing combinations of players that had so far been inaccessible (Verma et al. 2020), they, as of now, cannot be adapted to higher dimensionalities of perturbations, making them “blind” to heterogeneity and redundancy.

Lastly, *in silico* methods, despite offering a vast resource for hypothesis-driven research, depend on subsequent validation and often suffer from high false-positive rates, with newer approaches aiming at tackling this shortcoming (Goldberg, Rost, and Bromberg 2016). In addition, algorithm-based prediction of novel effector proteins relies on known primary or secondary structure of known effectors, such as short linear motifs (SLMs) or sequence similarity (Schleker, Garcia-Garcia, et al. 2012), and are therefore limited in their applicability.

5. Bibliography of this chapter

- Aguilar, Julieta, John Zupan, Todd A. Cameron, and Patricia C. Zambryski. 2010. "Agrobacterium Type IV Secretion System and Its Substrates Form Helical Arrays around the Circumference of Virulence-Induced Cells." *Proceedings of the National Academy of Sciences of the United States of America* 107 (8): 3758–63.
- Andritschke, Daniel, Sabrina Dilling, Mario Emmenlauer, Tobias Welz, Fabian Schmich, Benjamin Misselwitz, Pauli Rämö, et al. 2016. "A Genome-Wide siRNA Screen Implicates Spire1/2 in SipA-Driven *Salmonella* Typhimurium Host Cell Invasion." *PLoS One* 11 (9): e0161965.
- Arena, Ellen T., Sigrid D. Auweter, L. Caetano M. Antunes, A. Wayne Vogl, Jun Han, Julian A. Guttman, Matthew A. Croxen, et al. 2011. "The Deubiquitinase Activity of the *Salmonella* Pathogenicity Island 2 Effector, SseL, Prevents Accumulation of Cellular Lipid Droplets." *Infection and Immunity* 79 (11): 4392–4400.
- Auweter, Sigrid D., Amit P. Bhavsar, Carmen L. de Hoog, Yuling Li, Y. Alina Chan, Joris van der Heijden, Michael J. Lowden, et al. 2011. "Quantitative Mass Spectrometry Catalogues *Salmonella* Pathogenicity Island-2 Effectors and Identifies Their Cognate Host Binding Partners." *The Journal of Biological Chemistry* 286 (27): 24023–35.
- Azimi, Taher, Maryam Zamirnasta, Mahmood Alizadeh Sani, Mohammad Mehdi Soltan Dallal, and Ahmad Nasser. 2020. "Molecular Mechanisms of *Salmonella* Effector Proteins: A Comprehensive Review." *Infection and Drug Resistance* 13 (January): 11–26.
- Barthel, Manja, Siegfried Hapfelmeier, Leticia Quintanilla-Martínez, Marcus Kremer, Manfred Rohde, Michael Hogardt, Klaus Pfeffer, Holger Rüssmann, and Wolf-Dietrich Hardt. 2003. "Pretreatment of Mice with Streptomycin Provides a *Salmonella* Enterica Serovar Typhimurium Colitis Model That Allows Analysis of Both Pathogen and Host." *Infection and Immunity* 71 (5): 2839–58.
- Batra, Jyoti, Judd F. Hultquist, Dandan Liu, Olena Shtanko, John Von Dollen, Laura Satkamp, Gwendolyn M. Jang, et al. 2018. "Protein Interaction Mapping Identifies RBBP6 as a Negative Regulator of Ebola Virus Replication." *Cell* 175 (7): 1917–30.e13.
- Branchu, Priscilla, Matt Bawn, and Robert A. Kingsley. 2018. "Genome Variation and Molecular Epidemiology of *Salmonella* Enterica Serovar Typhimurium Pathovariants." *Infection and Immunity* 86 (8). <https://doi.org/10.1128/IAI.00079-18>.
- Brooks, Andrew B. E., Daniel Humphreys, Vikash Singh, Anthony C. Davidson, Susan D. Arden, Folma Buss, and Vassilis Koronakis. 2017. "MYO6 Is Targeted by *Salmonella* Virulence Effectors to Trigger PI3-Kinase Signaling and Pathogen Invasion into Host Cells." *Proceedings of the National Academy of Sciences of the United States of America* 114 (15): 3915–20.
- Brückner, Anna, Cécile Polge, Nicolas Lentze, Daniel Auerbach, and Uwe Schlattner. 2009. "Yeast Two-Hybrid, a Powerful Tool for Systems Biology." *International Journal of Molecular Sciences* 10 (6): 2763–88.
- Burstein, David, Tal Zusman, Elena Degtyar, Ram Viner, Gil Segal, and Tal Pupko. 2009. "Genome-Scale Identification of *Legionella Pneumophila* Effectors Using a Machine Learning Approach." *PLoS Pathogens* 5 (7): e1000508.

- Casanova, James E. 2017. "Bacterial Autophagy: Offense and Defense at the Host-Pathogen Interface." *Cellular and Molecular Gastroenterology and Hepatology* 4 (2): 237–43.
- Chang, Shu-Jung, Sheng Chih Jin, Xuyao Jiao, and Jorge E. Galán. 2019. "Unique Features in the Intracellular Transport of Typhoid Toxin Revealed by a Genome-Wide Screen." *PLoS Pathogens* 15 (4): e1007704.
- Chaudhuri, Roy R., Sarah E. Peters, Stephen J. Pleasance, Helen Northen, Chrissie Willers, Gavin K. Paterson, Danielle B. Cone, et al. 2009. "Comprehensive Identification of *Salmonella* Enterica Serovar Typhimurium Genes Required for Infection of BALB/c Mice." *PLoS Pathogens* 5 (7): e1000529.
- Che, Dongsheng, Mohammad Shabbir Hasan, and Bernard Chen. 2014. "Identifying Pathogenicity Islands in Bacterial Pathogenomics Using Computational Approaches." *Pathogens* 3 (1): 36–56.
- Chou, Seemay, Heather Upton, Katherine Bao, Ursula Schulze-Gahmen, Avi J. Samelson, Nanhai He, Anna Nowak, et al. 2013. "HIV-1 Tat Recruits Transcription Elongation Factors Dispersed along a Flexible AFF4 Scaffold." *Proceedings of the National Academy of Sciences of the United States of America* 110 (2): E123–31.
- Claudi, Beatrice, Petra Spröte, Anna Chirkova, Nicolas Personnic, Janine Zankl, Nura Schürmann, Alexander Schmidt, and Dirk Bumann. 2014. "Phenotypic Variation of *Salmonella* in Host Tissues Delays Eradication by Antimicrobial Chemotherapy." *Cell* 158 (4): 722–33.
- Coburn, Bryan, Inna Sekirov, and B. Brett Finlay. 2007. "Type III Secretion Systems and Disease." *Clinical Microbiology Reviews* 20 (4): 535–49.
- Colonne, Punsiri M., Caylin G. Winchell, and Daniel E. Voth. 2016. "Hijacking Host Cell Highways: Manipulation of the Host Actin Cytoskeleton by Obligate Intracellular Bacterial Pathogens." *Frontiers in Cellular and Infection Microbiology* 6 (September): 107.
- Costa, Luciana F., Juliana P. S. Mol, Ana Patricia C. Silva, Auricélio A. Macêdo, Teane M. A. Silva, Geraldo E. S. Alves, Sebastian Winter, et al. 2016. "Iron Acquisition Pathways and Colonization of the Inflamed Intestine by *Salmonella* Enterica Serovar Typhimurium." *International Journal of Medical Microbiology: IJMM* 306 (8): 604–10.
- Costa, Tiago R. D., Catarina Felisberto-Rodrigues, Amit Meir, Marie S. Prevost, Adam Redzej, Martina Trokter, and Gabriel Waksman. 2015. "Secretion Systems in Gram-Negative Bacteria: Structural and Mechanistic Insights." *Nature Reviews. Microbiology* 13 (6): 343–59.
- Cummins, Joanne, and Cormac G. M. Gahan. 2012. "Signature Tagged Mutagenesis in the Functional Genetic Analysis of Gastrointestinal Pathogens." *Gut Microbes* 3 (2): 93–103.
- Davis, Kimberly M., and Ralph R. Isberg. 2016. "Defining Heterogeneity within Bacterial Populations via Single Cell Approaches." *BioEssays: News and Reviews in Molecular, Cellular and Developmental Biology* 38 (8): 782–90.
- Davis, Zoe H., Erik Verschueren, Gwendolyn M. Jang, Kevin Kleffman, Jeffrey R. Johnson, Jimin Park, John Von Dollen, et al. 2015. "Global Mapping of Herpesvirus-Host Protein Complexes Reveals a Transcription Strategy for Late Genes." *Molecular Cell* 57 (2): 349–60.

- D'Costa, Vanessa M., Etienne Coyaud, Kirsten C. Boddy, Estelle M. N. Laurent, Jonathan St-Germain, Taoyingnan Li, Sergio Grinstein, Brian Raught, and John H. Brumell. 2019. "BioID Screen of Salmonella Type 3 Secreted Effectors Reveals Host Factors Involved in Vacuole Positioning and Stability during Infection." *Nature Microbiology*, October. <https://doi.org/10.1038/s41564-019-0580-9>.
- Deleu, Sandrine, Kuicheon Choi, Jeff M. Reece, and Stephen B. Shears. 2006. "Pathogenicity of Salmonella: SopE-Mediated Membrane Ruffling Is Independent of Inositol Phosphate Signals." *FEBS Letters* 580 (7): 1709–15.
- Diacovich, Lautaro, and Jean-Pierre Gorvel. 2010. "Bacterial Manipulation of Innate Immunity to Promote Infection." *Nature Reviews. Microbiology* 8 (2): 117–28.
- Di Domenico, Enea Gino, Iliaria Cavallo, Martina Pontone, Luigi Toma, and Fabrizio Ensoli. 2017. "Biofilm Producing Salmonella Typhi: Chronic Colonization and Development of Gallbladder Cancer." *International Journal of Molecular Sciences* 18 (9). <https://doi.org/10.3390/ijms18091887>.
- Drecktrah, Dan, Seamus Levine-Wilkinson, Tapen Dam, Seth Winfree, Leigh A. Knodler, Trina A. Schroer, and Olivia Steele-Mortimer. 2008. "Dynamic Behavior of Salmonella-Induced Membrane Tubules in Epithelial Cells." *Traffic* 9 (12): 2117–29.
- Eisenreich, Wolfgang, Thomas Rudel, Jürgen Heesemann, and Werner Goebel. 2019. "How Viral and Intracellular Bacterial Pathogens Reprogram the Metabolism of Host Cells to Allow Their Intracellular Replication." *Frontiers in Cellular and Infection Microbiology* 9 (March): 42.
- Famelis, Nikolaos, Angel Rivera-Calzada, Gianluca Degliesposti, Maria Wingender, Nicole Mietrach, J. Mark Skehel, Rafael Fernandez-Leiro, et al. 2019. "Architecture of the Mycobacterial Type VII Secretion System." *Nature* 576 (7786): 321–25.
- Figueira, Rita, Kathryn G. Watson, David W. Holden, and Sophie Helaine. 2013. "Identification of Salmonella Pathogenicity Island-2 Type III Secretion System Effectors Involved in Intramacrophage Replication of *S. Enterica* Serovar Typhimurium: Implications for Rational Vaccine Design." *mBio* 4 (2): e00065.
- Fink, Susan L., and Brad T. Cookson. 2007. "Pyroptosis and Host Cell Death Responses during Salmonella Infection." *Cellular Microbiology* 9 (11): 2562–70.
- Fossum, Even, Caroline C. Friedel, Seesandra V. Rajagopala, Björn Titz, Armin Baiker, Tina Schmidt, Theo Kraus, et al. 2009. "Evolutionarily Conserved Herpesviral Protein Interaction Networks." *PLoS Pathogens* 5 (9): e1000570.
- Gal-Mor, Ohad, Erin C. Boyle, and Guntram A. Grassl. 2014. "Same Species, Different Diseases: How and Why Typhoidal and Non-Typhoidal Salmonella Enterica Serovars Differ." *Frontiers in Microbiology* 5 (August): 391.
- Garai, Preeti, Divya Prakash Gnanadhas, and Dipshikha Chakravorty. 2012. "Salmonella Enterica Serovars Typhimurium and Typhi as Model Organisms: Revealing Paradigm of Host-Pathogen Interactions." *Virulence* 3 (4): 377–88.
- Goldberg, Tatyana, Burkhard Rost, and Yana Bromberg. 2016. "Computational Prediction Shines Light on Type III Secretion Origins." *Scientific Reports* 6 (October): 34516.
- Gorvel, Jean Pierre, and Edgardo Moreno. 2002. "Brucella Intracellular Life: From Invasion to Intracellular Replication." *Veterinary Microbiology* 90 (1-4): 281–97.

- Green, Erin R., and Joan Meccas. 2016. "Bacterial Secretion Systems: An Overview." *Microbiology Spectrum* 4 (1). <https://doi.org/10.1128/microbiolspec.VMBF-0012-2015>.
- Günster, Regina A., Sophie A. Matthews, David W. Holden, and Teresa L. M. Thurston. 2017. "SseK1 and SseK3 Type III Secretion System Effectors Inhibit NF- κ B Signaling and Necroptotic Cell Death in Salmonella-Infected Macrophages." *Infection and Immunity* 85 (3). <https://doi.org/10.1128/IAI.00010-17>.
- Hansen-Wester, I., and M. Hensel. 2001. "Salmonella Pathogenicity Islands Encoding Type III Secretion Systems." *Microbes and Infection / Institut Pasteur* 3 (7): 549–59.
- Haraga, Andrea, Maikke B. Ohlson, and Samuel I. Miller. 2008. "Salmonellae Interplay with Host Cells." *Nature Reviews. Microbiology* 6 (1): 53–66.
- Helaine, Sophie, Angela M. Cheverton, Kathryn G. Watson, Laura M. Faure, Sophie A. Matthews, and David W. Holden. 2014. "Internalization of Salmonella by Macrophages Induces Formation of Nonreplicating Persisters." *Science* 343 (6167): 204–8.
- Hensel, M., J. E. Shea, C. Gleeson, M. D. Jones, E. Dalton, and D. W. Holden. 1995. "Simultaneous Identification of Bacterial Virulence Genes by Negative Selection." *Science* 269 (5222): 400–403.
- Ho, Brian T., Tao G. Dong, and John J. Mekalanos. 2014. "A View to a Kill: The Bacterial Type VI Secretion System." *Cell Host & Microbe* 15 (1): 9–21.
- Holden, David W. 2002. "Trafficking of the Salmonella Vacuole in Macrophages." *Traffic* 3 (3): 161–69.
- Hood, Rachel D., Pragya Singh, Fosheng Hsu, Tüzün Güvener, Mike A. Carl, Rex R. S. Trinidad, Julie M. Silverman, et al. 2010. "A Type VI Secretion System of *Pseudomonas Aeruginosa* Targets a Toxin to Bacteria." *Cell Host & Microbe* 7 (1): 25–37.
- Jacobs, J. L., J. W. Gold, H. W. Murray, R. B. Roberts, and D. Armstrong. 1985. "Salmonella Infections in Patients with the Acquired Immunodeficiency Syndrome." *Annals of Internal Medicine* 102 (2): 186–88.
- Jäger, Stefanie, Peter Cimerancic, Natali Gulbahce, Jeffrey R. Johnson, Kathryn E. McGovern, Starlynn C. Clarke, Michael Shales, et al. 2011. "Global Landscape of HIV-Human Protein Complexes." *Nature* 481 (7381): 365–70.
- Jäger, Stefanie, Natali Gulbahce, Peter Cimerancic, Joshua Kane, Nanhai He, Seemay Chou, Iván D'Orso, et al. 2011. "Purification and Characterization of HIV-Human Protein Complexes." *Methods* 53 (1): 13–19.
- Jäger, Stefanie, Dong Young Kim, Judd F. Hultquist, Keisuke Shindo, Rebecca S. LaRue, Eunju Kwon, Ming Li, et al. 2011. "Vif Hijacks CBF- β to Degrade APOBEC3G and Promote HIV-1 Infection." *Nature* 481 (7381): 371–75.
- Jean Beltran, Pierre M., Joel D. Federspiel, Xinlei Sheng, and Ileana M. Cristea. 2017. "Proteomics and Integrative Omic Approaches for Understanding Host-Pathogen Interactions and Infectious Diseases." *Molecular Systems Biology* 13 (3): 922.
- Jennings, Elliott, Teresa L. M. Thurston, and David W. Holden. 2017. "Salmonella SPI-2 Type III Secretion System Effectors: Molecular Mechanisms And Physiological Consequences." *Cell Host & Microbe* 22 (2): 217–31.

- Joshi, Avatar, Benjamin Kostiuk, Andrew Rogers, Jennifer Teschler, Stefan Pukatzki, and Fitnat H. Yildiz. 2017. "Rules of Engagement: The Type VI Secretion System in *Vibrio Cholerae*." *Trends in Microbiology* 25 (4): 267–79.
- Joung, J. K., E. I. Ramm, and C. O. Pabo. 2000. "A Bacterial Two-Hybrid Selection System for Studying Protein-DNA and Protein-Protein Interactions." *Proceedings of the National Academy of Sciences of the United States of America* 97 (13): 7382–87.
- Karve, Sayali S., Suman Pradhan, Doyle V. Ward, and Alison A. Weiss. 2017. "Intestinal Organoids Model Human Responses to Infection by Commensal and Shiga Toxin Producing *Escherichia Coli*." *PloS One* 12 (6): e0178966.
- Killackey, Samuel A., Matthew T. Sorbara, and Stephen E. Girardin. 2016. "Cellular Aspects of *Shigella* Pathogenesis: Focus on the Manipulation of Host Cell Processes." *Frontiers in Cellular and Infection Microbiology* 6 (March): 38.
- Knodler, Leigh A., Bruce A. Vallance, Michael Hensel, Daniela Jäckel, B. Brett Finlay, and Olivia Steele-Mortimer. 2003. "Salmonella Type III Effectors PipB and PipB2 Are Targeted to Detergent-Resistant Microdomains on Internal Host Cell Membranes." *Molecular Microbiology* 49 (3): 685–704.
- Knuff, Katelyn, and B. Brett Finlay. 2017. "What the SIF Is Happening—The Role of Intracellular Salmonella-Induced Filaments." *Frontiers in Cellular and Infection Microbiology* 7 (July): 3235.
- Kolodziejek, Anna M., Melissa A. Altura, Junping Fan, Erik M. Petersen, Matthew Cook, Peter S. Brzovic, and Samuel I. Miller. 2019. "Salmonella Translocated Effectors Recruit OSBP1 to the Phagosome to Promote Vacuolar Membrane Integrity." *Cell Reports* 27 (7): 2147–56.e5.
- Krieger, Viktoria, David Liebl, Yuying Zhang, Roopa Rajashekar, Petr Chlanda, Katrin Giesker, Deepak Chikkaballi, and Michael Hensel. 2014. "Reorganization of the Endosomal System in Salmonella-Infected Cells: The Ultrastructure of Salmonella-Induced Tubular Compartments." *PLoS Pathogens* 10 (9): e1004374.
- Kumar, Yadunanda, and Raphael H. Valdivia. 2009. "Leading a Sheltered Life: Intracellular Pathogens and Maintenance of Vacuolar Compartments." *Cell Host & Microbe* 5 (6): 593–601.
- LaRock, Christopher N., and Brad T. Cookson. 2013. "Burning down the House: Cellular Actions during Pyroptosis." *PLoS Pathogens* 9 (12): e1003793.
- LaRock, Doris L., Anu Chaudhary, and Samuel I. Miller. 2015. "Salmonellae Interactions with Host Processes." *Nature Reviews. Microbiology* 13 (4): 191–205.
- Lasica, Anna M., Miroslaw Ksiazek, Mariusz Madej, and Jan Potempa. 2017. "The Type IX Secretion System (T9SS): Highlights and Recent Insights into Its Structure and Function." *Frontiers in Cellular and Infection Microbiology* 7 (May): 215.
- Lauber, Frédéric, Justin C. Deme, Susan M. Lea, and Ben C. Berks. 2018. "Type 9 Secretion System Structures Reveal a New Protein Transport Mechanism." *Nature* 564 (7734): 77–82.
- Lawley, Trevor D., Kaman Chan, Lucinda J. Thompson, Charles C. Kim, Gregory R. Govoni, and Denise M. Monack. 2006. "Genome-Wide Screen for Salmonella Genes Required for Long-Term Systemic Infection of the Mouse." *PLoS Pathogens* 2 (2): e11.

- Lees, Emily A., Jessica L. Forbester, Sally Forrest, Leanne Kane, David Goulding, and Gordon Dougan. 2019. "Using Human Induced Pluripotent Stem Cell-Derived Intestinal Organoids to Study and Modify Epithelial Cell Protection Against Salmonella and Other Pathogens." *Journal of Visualized Experiments: JoVE*, no. 147 (May). <https://doi.org/10.3791/59478>.
- Leo, Jack C., Iwan Grin, and Dirk Linke. 2012. "Type V Secretion: Mechanism(s) of Autotransport through the Bacterial Outer Membrane." *Philosophical Transactions of the Royal Society of London. Series B, Biological Sciences* 367 (1592): 1088–1101.
- Liss, Viktoria, A. Leoni Swart, Alexander Kehl, Natascha Hermanns, Yuying Zhang, Deepak Chikkaballi, Nathalie Böhles, Jörg Deiwick, and Michael Hensel. 2017. "Salmonella Enterica Remodels the Host Cell Endosomal System for Efficient Intravacuolar Nutrition." *Cell Host & Microbe* 21 (3): 390–402.
- Logan, Savannah L., Jacob Thomas, Jinyuan Yan, Ryan P. Baker, Drew S. Shields, Joao B. Xavier, Brian K. Hammer, and Raghuvveer Parthasarathy. 2018. "The Vibrio Cholerae Type VI Secretion System Can Modulate Host Intestinal Mechanics to Displace Gut Bacterial Symbionts." *Proceedings of the National Academy of Sciences of the United States of America* 115 (16): E3779–87.
- Lossi, Nadine S., Nathalie Rolhion, Anthony I. Magee, Cliona Boyle, and David W. Holden. 2008. "The Salmonella SPI-2 Effector SseJ Exhibits Eukaryotic Activator-Dependent Phospholipase A and Glycerophospholipid : Cholesterol Acyltransferase Activity." *Microbiology* 154 (Pt 9): 2680–88.
- Lu, Xiaoxi, Shuang Xie, Lulu Ye, Linda Zhu, and Qinghua Yu. 2020. "Lactobacillus Protects Against S. Typhimurium-Induced Intestinal Inflammation by Determining the Fate of Epithelial Proliferation and Differentiation." *Molecular Nutrition & Food Research* 64 (5): e1900655.
- Maier, Lisa, Médéric Diard, Mikael E. Sellin, Elsa-Sarah Chouffane, Kerstin Trautwein-Weidner, Balamurugan Periaswamy, Emma Slack, et al. 2014. "Granulocytes Impose a Tight Bottleneck upon the Gut Luminal Pathogen Population during Salmonella Typhimurium Colitis." *PLoS Pathogens* 10 (12): e1004557.
- Matsumoto, Hiroyuki, and Glenn M. Young. 2009. "Translocated Effectors of Yersinia." *Current Opinion in Microbiology* 12 (1): 94–100.
- McClelland, M., K. E. Sanderson, J. Spieth, S. W. Clifton, P. Latreille, L. Courtney, S. Porwollik, et al. 2001. "Complete Genome Sequence of Salmonella Enterica Serovar Typhimurium LT2." *Nature* 413 (6858): 852–56.
- Mirrashidi, Kathleen M., Cherilyn A. Elwell, Erik Verschueren, Jeffrey R. Johnson, Andrew Frando, John Von Dollen, Oren Rosenberg, et al. 2015. "Global Mapping of the Inc-Human Interactome Reveals That Retromer Restricts Chlamydia Infection." *Cell Host & Microbe* 18 (1): 109–21.
- Monack, D. M., and J. A. Theriot. 2001. "Actin-Based Motility Is Sufficient for Bacterial Membrane Protrusion Formation and Host Cell Uptake." *Cellular Microbiology* 3 (9): 633–47.
- Mousavi-Derazmahalleh, Mahsa, Steven Chang, Geoff Thomas, Mark Derbyshire, Phillip E. Bayer, David Edwards, Matthew N. Nelson, et al. 2019. "Prediction of Pathogenicity Genes Involved in Adaptation to a Lupin Host in the Fungal Pathogens Botrytis Cinerea and Sclerotinia Sclerotiorum via Comparative Genomics." *BMC Genomics* 20 (1): 385.

- Mulye, Minal, Dhritiman Samanta, Seth Winfree, Robert A. Heinzen, and Stacey D. Gilk. 2017. "Elevated Cholesterol in the *Coxiella Burnetii* Intracellular Niche Is Bacteriolytic." *mBio* 8 (1). <https://doi.org/10.1128/mBio.02313-16>.
- Munck, Christian, Heidi K. Gumpert, Annika I. Nilsson Wallin, Harris H. Wang, and Morten O. A. Sommer. 2014. "Prediction of Resistance Development against Drug Combinations by Collateral Responses to Component Drugs." *Science Translational Medicine* 6 (262): 262ra156.
- Nairz, Manfred, Andrea Schroll, Thomas Sonnweber, and Günter Weiss. 2010. "The Struggle for Iron - a Metal at the Host-Pathogen Interface." *Cellular Microbiology* 12 (12): 1691–1702.
- Namakchian, Mahsa, Kristin Kassler, Heinrich Sticht, Michael Hensel, and Jörg Deiwick. 2018. "Structure-Based Functional Analysis of Effector Protein SifA in Living Cells Reveals Motifs Important for *Salmonella* Intracellular Proliferation." *International Journal of Medical Microbiology: IJMM* 308 (1): 84–96.
- Navarro-Garcia, Fernando, Fernando Ruiz-Perez, Ángel Cataldi, and Mariano Larzábal. 2019. "Type VI Secretion System in Pathogenic *Escherichia Coli*: Structure, Role in Virulence, and Acquisition." *Frontiers in Microbiology* 10 (August): 1965.
- Navarro, Lorena, Neal M. Alto, and Jack E. Dixon. 2005. "Functions of the *Yersinia* Effector Proteins in Inhibiting Host Immune Responses." *Current Opinion in Microbiology* 8 (1): 21–27.
- Nedialkova, Lubov Petkova, Rémy Denzler, Martin B. Koeppel, Manuel Diehl, Diana Ring, Thorsten Wille, Roman G. Gerlach, and Bärbel Stecher. 2014. "Inflammation Fuels Colicin Ib-Dependent Competition of *Salmonella* Serovar Typhimurium and *E. Coli* in Enterobacterial Blooms." *PLoS Pathogens* 10 (1): e1003844.
- Nickerson, K. P., S. Senger, Y. Zhang, R. Lima, S. Patel, L. Ingano, W. A. Flavahan, et al. 2018. "*Salmonella* Typhi Colonization Provokes Extensive Transcriptional Changes Aimed at Evading Host Mucosal Immune Defense During Early Infection of Human Intestinal Tissue." *EBioMedicine* 31 (May): 92–109.
- Ninio, Shira, and Craig R. Roy. 2007. "Effector Proteins Translocated by *Legionella Pneumophila*: Strength in Numbers." *Trends in Microbiology* 15 (8): 372–80.
- Nishino, Kunihiko, Tammy Latifi, and Eduardo A. Groisman. 2006. "Virulence and Drug Resistance Roles of Multidrug Efflux Systems of *Salmonella Enterica* Serovar Typhimurium." *Molecular Microbiology*. <https://doi.org/10.1111/j.1365-2958.2005.04940.x>.
- O'Connor, Tamara J., Dana Boyd, Marion S. Dorer, and Ralph R. Isberg. 2012. "Aggravating Genetic Interactions Allow a Solution to Redundancy in a Bacterial Pathogen." *Science* 338 (6113): 1440–44.
- O'Connor, Tamara J., and Ralph R. Isberg. 2014. "iMAD, a Genetic Screening Strategy for Dissecting Complex Interactions between a Pathogen and Its Host." *Nature Protocols* 9 (8): 1916–30.
- Ohl, M. E., and S. I. Miller. 2001. "*Salmonella*: A Model for Bacterial Pathogenesis." *Annual Review of Medicine* 52: 259–74.

- Okeke, Iruka N., Ramanan Laxminarayan, Zulfiqar A. Bhutta, Adriano G. Duse, Philip Jenkins, Thomas F. O'Brien, Ariel Pablos-Mendez, and Keith P. Klugman. 2005. "Antimicrobial Resistance in Developing Countries. Part I: Recent Trends and Current Status." *The Lancet Infectious Diseases* 5 (8): 481–93.
- Oliva, Giulia, Tobias Sahr, and Carmen Buchrieser. 2018. "The Life Cycle of *L. Pneumophila*: Cellular Differentiation Is Linked to Virulence and Metabolism." *Frontiers in Cellular and Infection Microbiology* 8 (January): 3.
- Organization, World Health, and Others. 2017. "WHO Publishes List of Bacteria for Which New Antibiotics Are Urgently Needed [Internet]." *Genebra: World Health Organization*.
- Penn, Bennett H., Zoe Netter, Jeffrey R. Johnson, John Von Dollen, Gwendolyn M. Jang, Tasha Johnson, Yamini M. Ohol, et al. 2018. "An Mtb-Human Protein-Protein Interaction Map Identifies a Switch between Host Antiviral and Antibacterial Responses." *Molecular Cell* 71 (4): 637–48.e5.
- Perrett, Charlotte A., and Daoguo Zhou. 2013. "Salmonella Type III Effector SopB Modulates Host Cell Exocytosis." *Emerging Microbes & Infections* 2 (5): e32.
- Porwollik, Steffen, Carlos A. Santiviago, Pui Cheng, Fred Long, Prerak Desai, Jennifer Fredlund, Shabarinath Srikumar, et al. 2014. "Defined Single-Gene and Multi-Gene Deletion Mutant Collections in Salmonella Enterica Sv Typhimurium." *PLoS One* 9 (7): e99820.
- Pucciarelli, M. Graciela, and Francisco García-Del Portillo. 2017. "Salmonella Intracellular Lifestyles and Their Impact on Host-to-Host Transmission." *Microbiology Spectrum* 5 (4). <https://doi.org/10.1128/microbiolspec.MTBP-0009-2016>.
- Québatte, Maxime, and Christoph Dehio. 2017. "Systems-Level Interference Strategies to Decipher Host Factors Involved in Bacterial Pathogen Interaction: From RNAi to CRISPRi." *Current Opinion in Microbiology* 39 (October): 34–41.
- Qu, Jiuxin, Neha K. Prasad, Michelle A. Yu, Shuyan Chen, Amy Lyden, Nadia Herrera, Melanie R. Silvis, et al. 2019. "Modulating Pathogenesis with Mobile-CRISPRi." *Journal of Bacteriology* 201 (22). <https://doi.org/10.1128/JB.00304-19>.
- Rajagopala, Seesandra Venkatappa, Kelly T. Hughes, and Peter Uetz. 2009. "Benchmarking Yeast Two-Hybrid Systems Using the Interactions of Bacterial Motility Proteins." *Proteomics* 9 (23): 5296–5302.
- Ramos-Morales, Francisco. 2012. "Impact of Salmonella Enterica Type III Secretion System Effectors on the Eukaryotic Host Cell." *ISRN Cell Biology* 2012 (December). <https://doi.org/10.5402/2012/787934>.
- Ruiz-Albert, Javier, Xiu-Jun Yu, Carmen R. Beuzón, Abigail N. Blakey, Edouard E. Galyov, and David W. Holden. 2002. "Complementary Activities of SseJ and SifA Regulate Dynamics of the Salmonella Typhimurium Vacuolar Membrane." *Molecular Microbiology* 44 (3): 645–61.
- Samudrala, Ram, Fred Heffron, and Jason E. McDermott. 2009. "Accurate Prediction of Secreted Substrates and Identification of a Conserved Putative Secretion Signal for Type III Secretion Systems." *PLoS Pathogens* 5 (4): e1000375.

- Scallan, Elaine, Robert M. Hoekstra, Frederick J. Angulo, Robert V. Tauxe, Marc-Alain Widdowson, Sharon L. Roy, Jeffery L. Jones, and Patricia M. Griffin. 2011. "Foodborne Illness Acquired in the United States--Major Pathogens." *Emerging Infectious Diseases* 17 (1): 7–15.
- Schleker, Sylvia, Javier Garcia-Garcia, Judith Klein-Seetharaman, and Baldo Oliva. 2012. "Prediction and Comparison of Salmonella-Human and Salmonella-Arabidopsis Interactomes." *Chemistry & Biodiversity* 9 (5): 991–1018.
- Schleker, Sylvia, Jingchun Sun, Balachandran Raghavan, Matthew Srnc, Nicole Müller, Mary Koepfinger, Leelavati Murthy, Zhongming Zhao, and Judith Klein-Seetharaman. 2012. "The Current Salmonella-Host Interactome." *PROTEOMICS--Clinical Applications* 6 (1-2): 117–33.
- Schroeder, Gunnar N. 2017. "The Toolbox for Uncovering the Functions of Legionella Dot/Icm Type IVb Secretion System Effectors: Current State and Future Directions." *Frontiers in Cellular and Infection Microbiology* 7: 528.
- Selkig, Joel, Megan Stanifer, André Mateus, Karin Mitosch, Inigo Barrio-Hernandez, Mandy Rettel, Heeyoung Kim, et al. 2020. "SARS-CoV-2 Infection Remodels the Host Protein Thermal Stability Landscape." <https://doi.org/10.21203/rs.3.rs-105193/v1>.
- Seto, Shintaro, Kunio Tsujimura, and Yukio Koide. 2011. "Rab GTPases Regulating Phagosome Maturation Are Differentially Recruited to Mycobacterial Phagosomes." *Traffic* 12 (4): 407–20.
- Shah, Priya S., Nichole Link, Gwendolyn M. Jang, Phillip P. Sharp, Tongtong Zhu, Danielle L. Swaney, Jeffrey R. Johnson, et al. 2018. "Comparative Flavivirus-Host Protein Interaction Mapping Reveals Mechanisms of Dengue and Zika Virus Pathogenesis." *Cell* 175 (7): 1931–45.e18.
- Shah, Priya S., Jason A. Wojcechowskyj, Manon Eckhardt, and Nevan J. Krogan. 2015. "Comparative Mapping of Host-Pathogen Protein-Protein Interactions." *Current Opinion in Microbiology* 27 (October): 62–68.
- Sontag, Ryan L., Ernesto S. Nakayasu, Roslyn N. Brown, George S. Niemann, Michael A. Sydor, Octavio Sanchez, Charles Ansong, et al. 2016. "Identification of Novel Host Interactors of Effectors Secreted by Salmonella and Citrobacter." *mSystems* 1 (4). <https://doi.org/10.1128/mSystems.00032-15>.
- Stapels, Daphne A. C., Peter W. S. Hill, Alexander J. Westermann, Robert A. Fisher, Teresa L. Thurston, Antoine-Emmanuel Saliba, Isabelle Blommestein, Jörg Vogel, and Sophie Helaine. 2018. "Salmonella Persists Undermine Host Immune Defenses during Antibiotic Treatment." *Science* 362 (6419): 1156–60.
- Strauss, E. J., and S. Falkow. 1997. "Microbial Pathogenesis: Genomics and beyond." *Science* 276 (5313): 707–12.
- Stynen, Bram, Hélène Tourneu, Jan Tavernier, and Patrick Van Dijck. 2012. "Diversity in Genetic in Vivo Methods for Protein-Protein Interaction Studies: From the Yeast Two-Hybrid System to the Mammalian Split-Luciferase System." *Microbiology and Molecular Biology Reviews: MMBR* 76 (2): 331–82.
- Tait, S. W. G., G. Ichim, and D. R. Green. 2014. "Die Another Way—non-Apoptotic Mechanisms of Cell Death." *Journal of Cell Science*. <https://jcs.biologists.org/content/127/10/2135.short>.

- Tattoli, Ivan, Matthew T. Sorbara, Dajana Vuckovic, Arthur Ling, Fraser Soares, Leticia A. M. Carneiro, Chloe Yang, Andrew Emili, Dana J. Philpott, and Stephen E. Girardin. 2012. "Amino Acid Starvation Induced by Invasive Bacterial Pathogens Triggers an Innate Host Defense Program." *Cell Host & Microbe* 11 (6): 563–75.
- Thakur, Aneesh, Heidi Mikkelsen, and Gregers Jungersen. 2019. "Intracellular Pathogens: Host Immunity and Microbial Persistence Strategies." *Journal of Immunology Research* 2019 (April): 1356540.
- Thiennimitr, Parameth, Sebastian E. Winter, Maria G. Winter, Mariana N. Xavier, Vladimir Tolstikov, Douglas L. Huseby, Torsten Sterzenbach, Renée M. Tsois, John R. Roth, and Andreas J. Bäuml. 2011. "Intestinal Inflammation Allows *Salmonella* to Use Ethanolamine to Compete with the Microbiota." *Proceedings of the National Academy of Sciences of the United States of America* 108 (42): 17480–85.
- Threlfall, E. John. 2002. "Antimicrobial Drug Resistance in *Salmonella*: Problems and Perspectives in Food- and Water-Borne Infections." *FEMS Microbiology Reviews* 26 (2): 141–48.
- Toledo, Alvaro, and Jorge L. Benach. 2015. "Hijacking and Use of Host Lipids by Intracellular Pathogens." *Microbiology Spectrum* 3 (6). <https://doi.org/10.1128/microbiolspec.VMBF-0001-2014>.
- Tsois, R. M., S. M. Townsend, E. A. Miao, S. I. Miller, T. A. Ficht, L. G. Adams, and A. J. Bäuml. 1999. "Identification of a Putative *Salmonella* Enterica Serotype Typhimurium Host Range Factor with Homology to IpaH and YopM by Signature-Tagged Mutagenesis." *Infection and Immunity* 67 (12): 6385–93.
- Uetz, Peter, Yu-An Dong, Christine Zeretzke, Christine Atzler, Armin Baiker, Bonnie Berger, Seesandra V. Rajagopala, et al. 2006. "Herpesviral Protein Networks and Their Interaction with the Human Proteome." *Science* 311 (5758): 239–42.
- Verma, Smriti, Stefania Senger, Bobby J. Cherayil, and Christina S. Faherty. 2020. "Spheres of Influence: Insights into *Salmonella* Pathogenesis from Intestinal Organoids." *Microorganisms* 8 (4). <https://doi.org/10.3390/microorganisms8040504>.
- Wagner, Samuel, Iwan Grin, Silke Malmshaimer, Nidhi Singh, Claudia E. Torres-Vargas, and Sibel Westerhausen. 2018. "Bacterial Type III Secretion Systems: A Complex Device for the Delivery of Bacterial Effector Proteins into Eukaryotic Host Cells." *FEMS Microbiology Letters* 365 (19). <https://doi.org/10.1093/femsle/fny201>.
- Wasylnka, Julie A., Malina A. Bakowski, Jason Szeto, Maikke B. Ohlson, William S. Trimble, Samuel I. Miller, and John H. Brummell. 2008. "Role for Myosin II in Regulating Positioning of *Salmonella*-Containing Vacuoles and Intracellular Replication." *Infection and Immunity* 76 (6): 2722–35.
- Westermann, Alexander J., Lars Barquist, and Jörg Vogel. 2017. "Resolving Host-Pathogen Interactions by Dual RNA-Seq." *PLoS Pathogens* 13 (2): e1006033.
- Westermann, Alexander J., Konrad U. Förstner, Fabian Amman, Lars Barquist, Yanjie Chao, Leon N. Schulte, Lydia Müller, Richard Reinhardt, Peter F. Stadler, and Jörg Vogel. 2016. "Dual RNA-Seq Unveils Noncoding RNA Functions in Host-Pathogen Interactions." *Nature* 529 (7587): 496–501.

- Wheeler, Nicole E., Paul P. Gardner, and Lars Barquist. 2018. "Machine Learning Identifies Signatures of Host Adaptation in the Bacterial Pathogen *Salmonella* Enterica." *PLoS Genetics* 14 (5): e1007333.
- Winter, Sebastian E., Parameth Thiennimitr, Maria G. Winter, Brian P. Butler, Douglas L. Huseby, Robert W. Crawford, Joseph M. Russell, et al. 2010. "Gut Inflammation Provides a Respiratory Electron Acceptor for *Salmonella*." *Nature* 467 (7314): 426–29.
- Yeung, Amy T. Y., Yoon Ha Choi, Amy H. Y. Lee, Christine Hale, Hannes Ponstingl, Derek Pickard, David Goulding, et al. 2019. "A Genome-Wide Knockout Screen in Human Macrophages Identified Host Factors Modulating *Salmonella* Infection." *mBio* 10 (5). <https://doi.org/10.1128/mBio.02169-19>.
- Yuan, Xiao-Yan, Ying Wang, and Ming-Yi Wang. 2018. "The Type IV Secretion System in *Helicobacter Pylori*." *Future Microbiology* 13 (July): 1041–54.
- Yu, Hong B., Matthew A. Croxen, Amanda M. Marchiando, Rosana B. R. Ferreira, Ken Cadwell, Leonard J. Foster, and B. Brett Finlay. 2014. "Autophagy Facilitates *Salmonella* Replication in HeLa Cells." *mBio* 5 (2): e00865–14.
- Yu, Xiu-Jun, Mei Liu, and David W. Holden. 2016. "Salmonella Effectors SseF and SseG Interact with Mammalian Protein ACBD3 (GCP60) To Anchor *Salmonella*-Containing Vacuoles at the Golgi Network." *mBio* 7 (4). <https://doi.org/10.1128/mBio.00474-16>.
- Zhang, Shuping, Robert A. Kingsley, Renato L. Santos, Helene Andrews-Polymenis, Manuela Raffatellu, Josely Figueiredo, Jairo Nunes, Renee M. Tsois, L. Garry Adams, and Andreas J. Bäuml. 2003. "Molecular Pathogenesis of *Salmonella* Enterica Serotype Typhimurium-Induced Diarrhea." *Infection and Immunity* 71 (1): 1–12.
- Zhou, D., L. M. Chen, and L. Hernandez. 2001. "A *Salmonella* Inositol Polyphosphatase Acts in Conjunction with Other Bacterial Effectors to Promote Host Cell Actin Cytoskeleton Rearrangements and Bacterial" *Molecular*. <https://onlinelibrary.wiley.com/doi/abs/10.1046/j.1365-2958.2001.02230.x>.

Chapter II

Establishing AP/QMS to map the STm infection interactome

Chapter II: Establishing AP/QMS to map the STm infection interactome**1. Summary**

Facultatively intracellular bacteria target diverse host proteins and hijack various cellular processes to induce and maintain infection. To promote its survival, *Salmonella enterica* serovar Typhimurium (STm) uses two distinct Type 3 secretion systems (T3SS) for translocation of effector protein to the host cytoplasm. Despite extensive efforts, there is only limited knowledge of their protein targets. This chapter describes my efforts to set up a systematic approach to map host-pathogen protein-protein interactions (PPIs) during STm infection.

To achieve this, we created a library comprising 32 STm strains expressing a chromosomally tagged effector. This allows for immunoprecipitation (IP), while maintaining endogenous levels of effector expression and translocation. I infected epithelial and macrophage cell lines with this strain library, to assess effector secretion dynamics and optimize experimental conditions. Affinity-Purification coupled to Quantitative Mass-Spectrometry (AP/QMS) in the presence or absence of crosslinking reagent DSP was then used to elucidate the STm interactome (Figure II.1A) within two different host cell lines: HeLa epithelial cells and RAW264.7 macrophages. This chapter describes in detail the optimization process of the AP/QMS workflow, the quality control, as well as the rationale behind the described setup, regarding both experimental and computational steps (Figure II.1B).

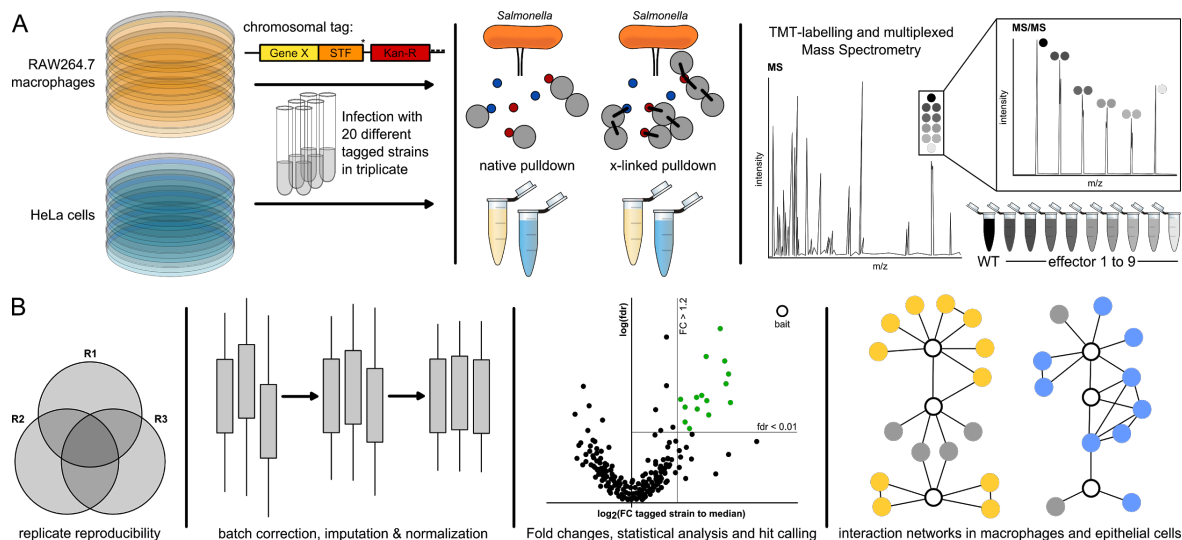


Figure II.1 Graphical abstract. (A) STm 14028s strains expressing chromosomally STF-tagged effectors were applied in infection of RAW264.7 or HeLa cells (MOI ~100:1) in biological triplicates. At 20 hours post infection (hpi), two different harvesting strategies - native, and after crosslinking with Dithiobis(succinimidyl propionate) (DSP) - were applied and samples were subjected to anti-FLAG immunoprecipitation. SPI-1 (blue) and SPI-2 (red) effectors, as well as host proteins (grey) are shown in the schematic, here black lines indicate crosslinking. Immunoprecipitates were reduced, alkylated and digested with trypsin and then combined in a TMT-10plex (one untagged wildtype (WT) control and nine different tagged-effectors). (B) All proteins that were detected by two or more unique peptides and that were present in at least two out of three replicates passed the initial analysis stage. After batch effect removal, variance normalization and imputation as described in the Experimental Procedures, hits were called (detailed description in this chapter) and networks were built from the final hit list. *This figure has been published as Figure 1 in (Walch et al. 2020).*

2. Contributions

Dr. Joel Selkrig and Keith Fernandez contributed to the construction of the tagged-effector strain library by generating 25 of the 32 strains. I conducted all experimental work presented or used in this chapter. Mandy Rettel conducted the sample preparation for mass spectrometry and operated the machines. Dr. Frank Stein, together with input from Dr. Joel Selkrig, Dr. Athanasios Typas, Dr. Mikhail Savitski and myself set up the pipeline for data analysis (protein query, data normalization, limma analysis). All further data analysis (thresholding, quality control) was conducted by me with input from Dr. Frank Stein, Dr. Joel Selkrig and Dr. Athanasios Typas. The work presented here is part of the following published preprint (bioRxiv), which is currently under revision at Cell Host&Microbe:

Walch, Philipp, Joel Selkrig, Leigh A. Knodler, Mandy Rettel, Frank Stein, Keith Fernandez, Cristina Viéitez, et al. 2020. "Global Mapping of *Salmonella* Enterica-Host Protein-Protein Interactions during Infection." *bioRxiv*, Cold Spring Harbor Laboratory. <https://doi.org/10.1101/2020.05.04.075937>.

3. Library construction of tagged-effector strains and large-scale infection

In order to allow for affinity-tag-based IP, while preserving endogenous levels of effector expression and translocation, we decided to introduce a chromosomal 2xStrep-TEV-3xFLAG (STF)-tag C-terminally of a panel of effectors (full detail on the methodology can be found in Chapter VII, section VII.7). In brief, we used the donor plasmid pJPS1 to amplify the STF-tag and a downstream kanamycin resistance cassette with homology to the C-terminal region of the effector of interest and to a location ~20 base pairs downstream of the end of the gene (Figure II.2). This fragment was then incorporated into the genome using λ -red recombinase (Datsenko and Wanner 2000; Uzzau et al. 2001). An adapted strategy was applied for *sifA*, where the STF affinity-tag was introduced between D136 and I137, in order to preserve the C-terminal prenylation motif required for SifA function.

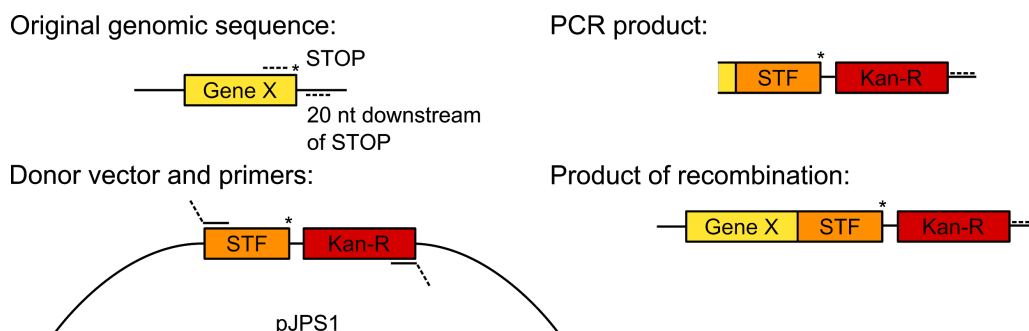


Figure II.2 Cloning strategy for introducing the chromosomal STF-tag. Using pJPS1 as the template plasmid, the STF-tag and downstream KanR-cassette were amplified and inserted C-terminally of the effector of interest using homologous recombination (λ -red recombinase), the asterisk denotes the stop-codon.

We chose two different cell lines, HeLa (as a model for epithelial cells) and RAW264.7 (as a model for macrophages) for infection. These two are broadly used models in the field, which makes the results more easily comparable to the literature. In addition, using cell lines instead of primary cells allows for an easy upscaling and therefore high

sensitivity despite the low levels of translocated effector protein. A more detailed elaboration on the use of primary cells can be found in Chapter III, section 6.2.

Using Western Blot (WB) in an infection time-course, I assessed that harvesting cells 20 hours post infection (hpi) gives the largest yield of translocated effector protein in the host cytoplasm, which is in concordance with detection of largest bacterial load (Figure II.3A). I then isolated cells at 20 hpi for the entire panel of tagged effectors to determine which were detected in the cytoplasm of either of the two cell lines. To assess effector translocation, I observed the presence of tagged effector proteins in the Tx-100 soluble fraction of the whole cell lysate. This comprises of the proteins present in the cytoplasm as well as those localized to membranes or organelles (except the nucleus), which get solubilized by the detergent, while *Salmonella* stay intact.

Of the 32 effectors which were STF-tagged, I was able to detect 28 in the Tx-100-insoluble fraction (i.e. they were expressed) and 20 in the Tx-100-soluble fraction (i.e. they were translocated). The presence of these effectors in the Tx-100-soluble fraction in HeLa and RAW264.7 is displayed in Figure II.3B. There are multiple explanations for the absence of detectable effector signal in the TX-100-soluble fraction:

- 1) The effector is translocated at too low levels to be detected by Western Blot.
- 2) The assessed time point (20 hpi) may not be universally optimal for all effectors. This is especially the case for SPI-1 effectors, against which the late time point generates an overall bias.
- 3) The effector is not expressed at high levels in the assessed cell lines, but might exert its relevance in other cell types.
- 4) The effector is localized to a cellular compartment that is not completely (or at all) solubilized during harvesting of the lysate.
- 5) The affinity-tag impedes translocation, folding or stability of the effector protein.

The list of all tagged effectors and their performance regarding expression (presence in the Tx-100 insoluble fraction) and secretion are summarized in Table II.1 (section II.7.1). For all subsequent experiments, IP was performed on the STF-tagged effector present in the Tx-100 soluble fraction.

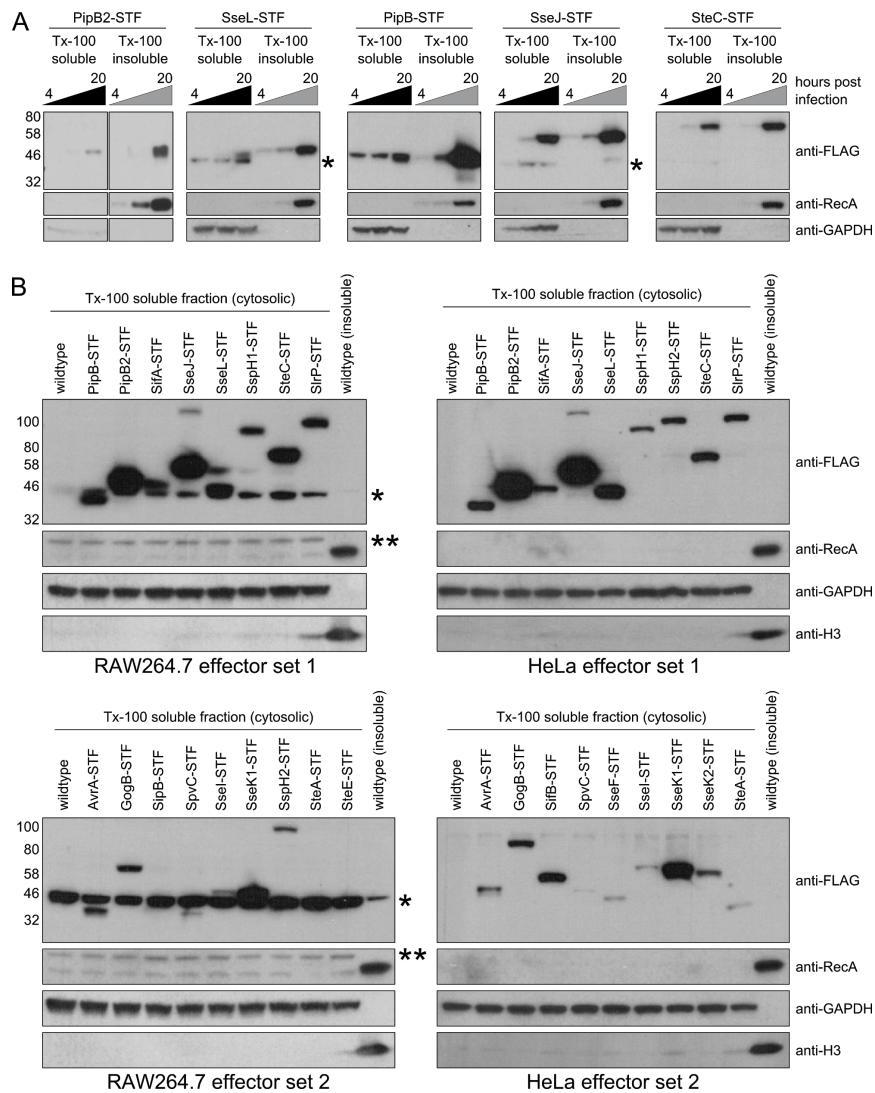


Figure II.3 Time-course infection, expression and translocation at 20 hpi. (A) Expression and translocation of PipB2, SseL, PipB, SseJ and SteC was assessed over time. At 4, 8 and 20 hpi, cells were harvested in Tx-100. Soluble and insoluble fractions obtained after centrifugation were assessed with anti-FLAG, anti-RecA (bacterial loading control) and anti-GAPDH (host cytosolic loading control). Single asterisk denotes an unspecific band of the anti-FLAG antibody in the cytoplasmic fraction of RAW264.7, double asterisk denotes an unspecific band occurring with RecA-antibody (B) At 20 hpi, cells were lysed in Tx-100 and separated into soluble and insoluble fractions. Anti-FLAG immunoblotting was used to probe the translocation into the cytosolic fraction of the indicated effectors. Panel B shows the Tx-100 soluble fractions of the four 10-plexes used in the final experiment, asterisks (unspecific bands) and loading controls as in panel A. *This figure has been published as Figure S1 in (Walch et al. 2020).*

4. Optimization of the AP/QMS workflow

The tagging strategy we chose for this study allows for multiple degrees of freedom in experimental design, possible comparisons and mass spec settings. I evaluated the various combinations for their feasibility, reproducibility and gain of information with respect to the following dimensions:

- 1) Label-free proteomics vs multiplexing with TMT-labeling
- 2) Use of the crosslinker dithiobis-succinimidylpropionate (DSP) vs native pulldown
- 3) Immunoprecipitation *via* Strep-tag vs FLAG-tag

Determining these was essential for streamlining the final workflow and experimental layout of this study.

4.1. Label-free proteomics vs multiplexing with TMT-labeling

For most proteomic large-scale studies to this point, label-free MS has been used to calculate enrichments. There are, however, two main shortcomings of label-free MS: 1) the necessity for pseudo-counts, as each enrichment is calculated with respect to the wildtype control, and zero counts in IP sample or control are thus not possible; and 2) an increased run time, which lowers the throughput of the methodology, as all samples are measured on separate mass spec runs. Pseudo-counts are introduced when calculating the enrichment of a protein that was not detected in either the wildtype or IP sample. The requirement for null-counts arises from the way logarithmic enrichments are calculated from the protein abundance, given by the intensity-based absolute quantification (iBAQ) value namely as:

$$\log_2(FC) = \log_2\left(\frac{iBAQ.IP(\text{protein } X)}{iBAQ.WT(\text{protein } X)}\right)$$

In this fold change (FC) calculation, neither the numerator nor the denominator can take the value zero. Therefore, if a protein is not detected in either sample, an artificial pseudo-abundance has to be introduced in order to make this expression mathematically valid. Usual pseudo-counts are either setting the iBAQ value to 1 or alternatively setting it to the lowest iBAQ value detected in the experiment. However, this has the drawback that it gives rise to very large (or very small) $\log(FC)$ values, which depend solely on the detection of a protein in one or the other sample. This is exemplified in Figure II.4A, where I plotted FLAG- vs Strep-enrichments after IP on SteC-STF with respect to wildtype control in unlabeled MS. The distinct clouds of very highly enriched targets in the two IPs originate solely from proteins that were only detected in either IP sample or control, making this approach very susceptible to false positives and false negatives.

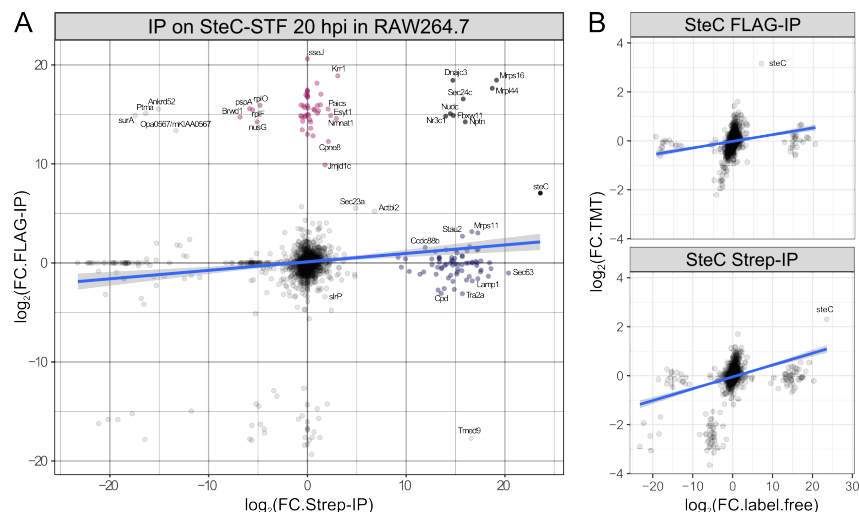


Figure II.4 Quantification in label-free MS and comparison to TMT-multiplexing. (A) Label-free enrichments after Strep-IP vs FLAG-IP on SteC-STF 20 hpi in RAW264.7. Differentially enriched proteins are colored in red (FLAG) and blue (Strep). Enrichments were calculated with respect to untagged control, the minimal detected iBAQ value was used as pseudo-count to deal with missing values. (B) iBAQ-based enrichments (label free) vs enrichments calculated after TMT-labelling (all with respect to untagged control) of SteC-STF FLAG- or Strep-IP 20 hpi in RAW264.7. SteC is indicated in the plots. The blue line shows the overall correlation of the two enrichment methods (including clouds of points with very high or very low iBAQ-enrichment score).

These issues can be mitigated by using TMT-labelling and multiplexing, which eliminates the necessity of pseudo-counts, as the occurrence of any given peptide for each protein is simultaneously selected across all TMT-channels in MS1, and the abundance (reporter ion intensity) within each TMT channel is measured in the subsequent MS2 scan. Therefore, all proteins will have been measured in all channels of one TMT-10-plex, and no zero-values occur. This advantage becomes evident in the comparison of the enrichments obtained after TMT-labelling vs iBAQ-based enrichments for FLAG-IP and Strep-IP on SteC-STF (Figure II.4B). The enrichment values along the y-axis (TMT-labelling) follow a continuous Gaussian distribution around zero, while the iBAQ-based enrichment values (x-axis) display a trimodal distribution. The inflated iBAQ-values causing this likely represent false positives due to missing values. Their absence along the y-axis demonstrates that TMT-labelling prior to MS can increase the accuracy of the study. Additionally, TMT-labelling allows for multiplexing and running up to 10 different IP samples at the same time, which saves mass spec instrument time and enables higher sample throughput.

4.2. Use of the crosslinker DSP vs native pulldown

A common consideration in large-scale AP/MS studies is the use of a crosslinking agent, which allows the capture of transient interactions but increases the unspecific background with respect to a native pulldown. In order to assess the applicability and usefulness of a crosslinking reagent in this setup, I tested varying concentrations of the reversible, membrane-permeable crosslinker dithiobis(succinimidyl propionate) (DSP) prior to harvesting. DSP is amine-reactive and contains a disulfide bond at its center. Hence, covalent bonds introduced by DSP between amines of interacting proteins can be reversed using reducing conditions, which simplifies the identification of the interacting proteins by mass spec.

I next determined the minimal necessary concentration to detect crosslinking as well as the dynamic concentration range. Using PAGE in non-reducing conditions, and subsequent Western Blot, I observed reduction of the abundance of low molecular weight (MW), monomeric SseJ-STF (~52 kDa) with increasing concentration of DSP. Subjecting the same samples to reducing conditions and SDS-PAGE, the overall abundance of SseJ-STF remained constant (Figure II.5A), indicating that SseJ-STF is present in higher MW complexes in the native sample, and those do not migrate past the stacking gel. I therefore concluded that using DSP at a concentration of 1mM creates stable high MW complexes of tagged effectors (here SseJ-STF) and their interaction partners, which stay intact throughout the harvesting process, but can be broken down in reducing conditions. I decided to optimize this process on SseJ for two reasons:

- 1) Due to its high level of expression and translocation at 20 hpi, visualization by Western Blot is easier. Besides, if the concentration of DSP is high enough for SseJ, we can assume sufficiency for lowly abundant effectors.
- 2) SseJ is a very well characterized effector with previously described interaction partners. Therefore, quality control of the PPIs identified in MS is more straightforward.

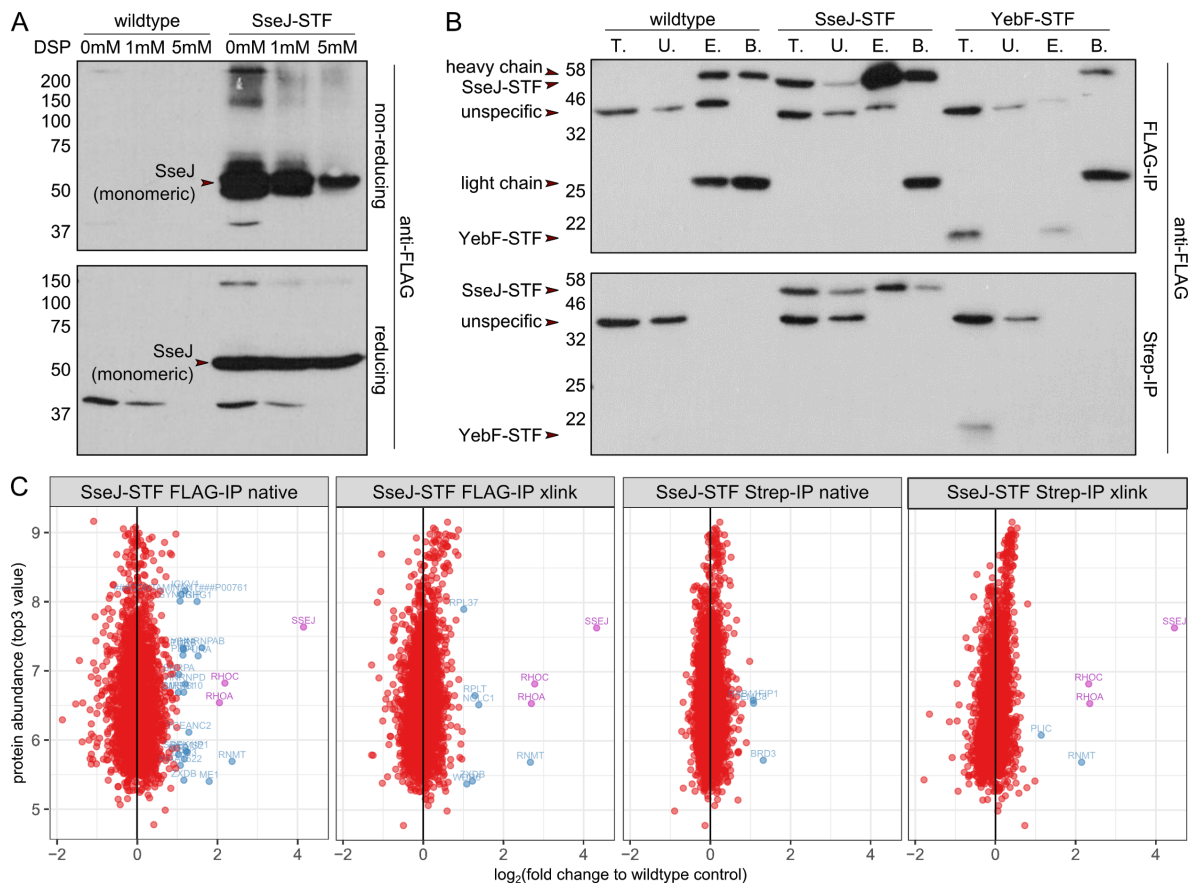


Figure II.5 Use of the crosslinker DSP prior to cell lysis and comparing Strep- and FLAG-IP. (A) Cells were infected with wildtype STm or SseJ-STF expressing STm. At 20 hpi, varying concentrations of DSP were added to the cells for 2 hours at 4°C. Lysates were harvested using Triton-X100 and anti-FLAG immunoblot was performed after PAGE in reducing and non-reducing conditions. With increasing concentration of DSP, the low-MW, monomeric form of SseJ-STF (indicated on the blot) decreases in abundance under non-reducing conditions. (B) At 20 hpi, cells were harvested under native conditions and subjected to FLAG- and Strep-IP. Intermediate fractions were collected and assessed by Western Blot (T = total fraction, U = unbound fraction, E = elution, B = beads). Bands corresponding to tagged effectors, as well as unspecific bands or heavy and light chain of the antibody are indicated. (C) Enrichment after TMT-labelling with respect to untagged control vs top3 value for each protein detected in native / crosslinked FLAG- / Strep-IP. The top3 value denotes the average signal of the three most highly abundant peptides of a given protein. Non-hits are represented by red dots, hits are indicated in blue and the bait (SseJ), as well as known interaction partners RhoA and RhoC in purple. All depicted conditions were assessed in the same TMT-multiplex.

4.3. Immunoprecipitation *via* Strep-tag vs FLAG-tag

We chose the chromosomal STF-tag to have two orthogonal affinity tags available for IP. In order to assess the information content and reproducibility between FLAG- and Strep-IP, I compared them by Western Blot, as well as TMT-multiplexed MS-quantification. For this comparison, I infected RAW264.7 with a SseJ-STF strain (high level of translocation into the host cytoplasm), a YebF-STF strain (low level of translocation into host cytoplasm), as well as wildtype STm as (untagged) control. The quantification after mass spec was calculated with respect to wildtype.

While the highly abundant SseJ-STF immunoprecipitated equally well in both FLAG- and Strep-IP, more lowly abundant effectors, such as YebF, were more readily detected in the FLAG-IP (Figure II.5B). This indicated that pull-down on the 3x-FLAG-tag was more efficient. In addition, using FLAG-IP, I detected the bait SseJ, its known interaction partners RhoA and RhoC, as well as a vast panel of other, less strongly

enriched interactors, in both the native and crosslinked sample (Figure II.5C). After Strep-IP of the native lysate, however, I could not even detect the bait in significant amounts. This could be improved through crosslinking, yet the number of detected interaction partners was still lower compared to FLAG-IP (Figure II.5C). Altogether, this data indicated a higher pulldown efficiency with the FLAG-IP, and I therefore decided to proceed only with this and also reduce the size of this large-scale endeavor.

4.4. Final experimental set-up for the large-scale AP/QMS study

Taking all previous considerations into account, I performed a multiplexed evaluation run. Thereby, I determined reproducibility and gain of information between the different conditions. This also served as a pilot for the large-scale screen. I chose the following set-up for the TMT-10plex: wildtype (native), wildtype (native, technical replicate), WT (native, biological replicate), WT (crosslinked), SseJ-STF (native), SseJ-STF (crosslinked), SteC-STF (native), SteC-STF (crosslinked), YebF-STF (native), YebF (crosslinked).

By plotting the correlation between all samples, one can see that technical replicates (two wildtype samples from the same day) displayed a very high correlation ($R^2 = 0.99$), while correlation among biological replicates was lower, but still excellent ($R^2 = 0.9$) (Figure II.6A, black and green boxes, respectively). Comparison to crosslinked samples revealed that there is a slightly different protein fingerprint within crosslinked samples (Figure II.6, dark green box, $R^2 = 0.88$). I therefore concluded that using both conditions (native and after crosslinking) would provide additional information and two partly distinct interactomes.

In addition, I could obtain a list of target proteins which were enriched in pulldowns on SseJ-STF and SteC-STF (data not shown). This preliminary list included the known SseJ-interaction partners RhoA and RhoC, as well as FMNL1 for SteC, which we later validated and characterized in this work (see Chapters III and IV).

To summarize, after a thorough optimization and quality assessment, I decided to multiplex FLAG-IPs on 9 effectors with one wildtype control in each run. For the large-scale study, I performed two of these 10-plex runs (with two different sets of effectors) for each cell line and each condition in triplicate, which sums up to a total of 24 individual datasets, which are all accessible at the proteomeXchange consortium (Deutsch et al. 2020) via the PRIDE (Perez-Riverol et al. 2019) repository (project accession number: PXD018375).

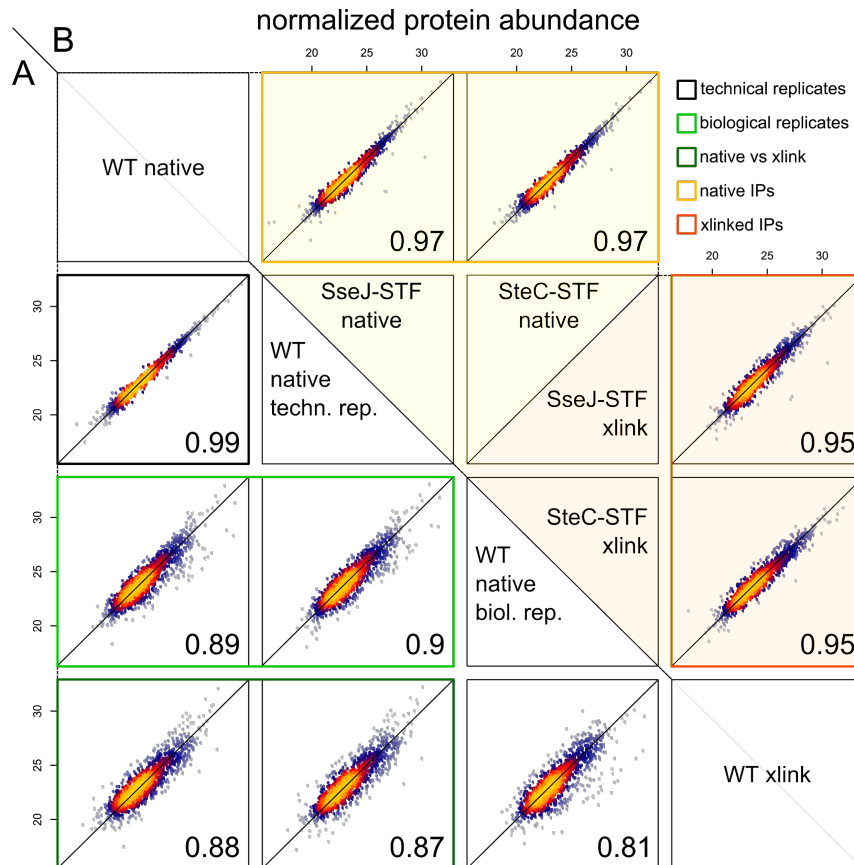


Figure II.6 Correlations between technical and biological replicates, and between native vs crosslinked harvest. A) Normalized protein abundance correlates very well ($R^2 = 0.99$) between technical replicates (black box) while correlation between biological replicates ($R^2 \cong 0.9$) is less pronounced (light green box). Comparison between native and crosslinked samples (dark green box) reveals somewhat distinct patterns of background proteins in the wildtype (unlabeled) control ($R^2 \cong 0.88$). B) IPs on tagged effectors do not significantly alter the distribution of normalized protein abundances within native (light orange box, $R^2 = 0.97$) or crosslinked (dark orange box, $R^2 = 0.9$) conditions. This indicates that only few proteins significantly change abundance (i.e. hits), while most proteins are of similar abundance as in the wildtype control (i.e. background).

5. Large-scale proteomics and quality control

The peptide lists that were obtained from MS were analyzed using Mascot (v2.2.07) and IsobarQuant (Franken et al. 2015) and searched using the appropriate Uniprot databases (full detail of search parameters and included modifications is described in Chapter VII). Only proteins with at least 2 unique peptides and a false discovery rate (fdr) less than 0.01 were considered for further analysis. Figure II.7 gives an overview over the number of proteins identified in, and the overlap between, the replicates in the different conditions. We only considered proteins that were identified in at least two of the three replicates for enrichment score calculations (overall 74.9% of all proteins (detected in at least one replicate) for HeLa, 72.3% for RAW264.7).

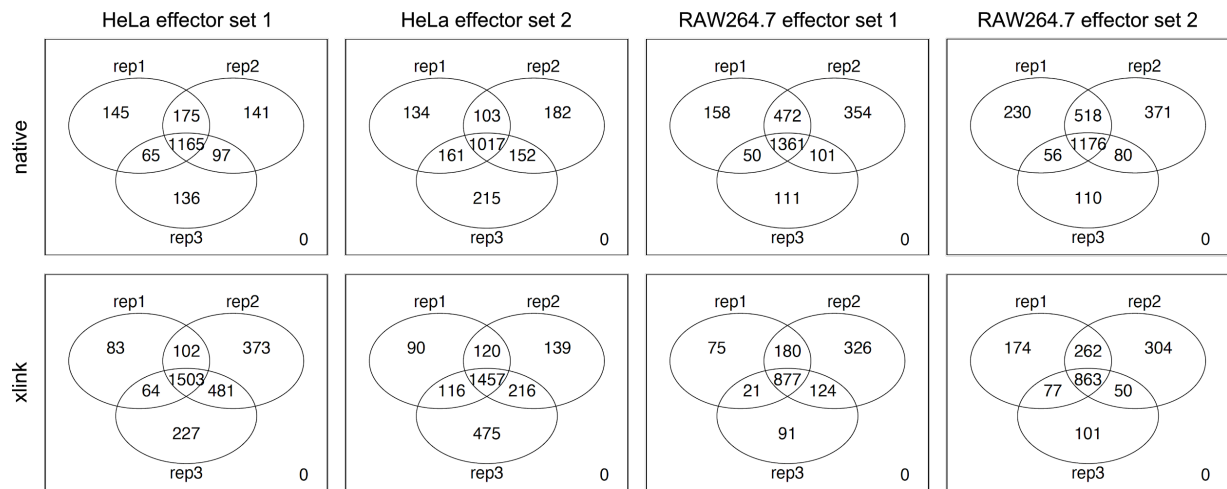


Figure II.7 Overlap between replicates in the different conditions and cell lines. Only proteins detected in at least two replicates were used in further analysis. A large majority of proteins is detected across all three replicates of a given condition, the number of proteins detected overall varies strongly between cell lines and conditions. The effector sets indicated in this figure correspond to those depicted in Figure II.3B. *This figure has been published as Figure S2A in (Walch et al. 2020).*

The raw protein abundance signal obtained by MS displayed strong replicate dependence (Figure II.8). In order to mitigate and correct for this, the data was batch-cleaned (i.e. batch effects originating from individual TMT-multiplexes were removed) and normalized with respect to mean and variance (see Chapter VII, section VII.14.3 for further detail). Variance stabilization normalization (Huber et al. 2002) is based on an additive-multiplicative error model and calculates a robust variation of a maximum-likelihood estimator. After normalization (called data calibration), the dependence of the variance on the mean was modeled, and the data was transformed while maintaining variance stability.

In a last step, in order to account for missing values in one of the three replicates, imputation was used to generate a third abundance value. Imputation is a commonly used tool in proteomics (Webb-Robertson et al. 2015) and relies on estimating a missing value based on the average abundance of all proteins with comparable abundance to the missing protein in the two replicates where data was available. The number of replicates each protein was identified in was listed alongside the fold enrichments and statistical significance. Thereby, PPIs relying on imputed values could be followed throughout the analysis to avoid a bias and reduce the occurrence of false positives caused by imputation.

By comparing the median and interquartile range across all proteins, we could observe a removal of systemic, batch-dependent differences between the replicates (Figure II.8A, panels 2-4). Furthermore, we noticed that, while the raw data mainly clusters by replicate in PCA, the batch-cleaning and normalization successfully removes batch effects and we can see clustering by effector (most strongly for PipB2, SseJ, SteC and PipB; Figure II.8B).

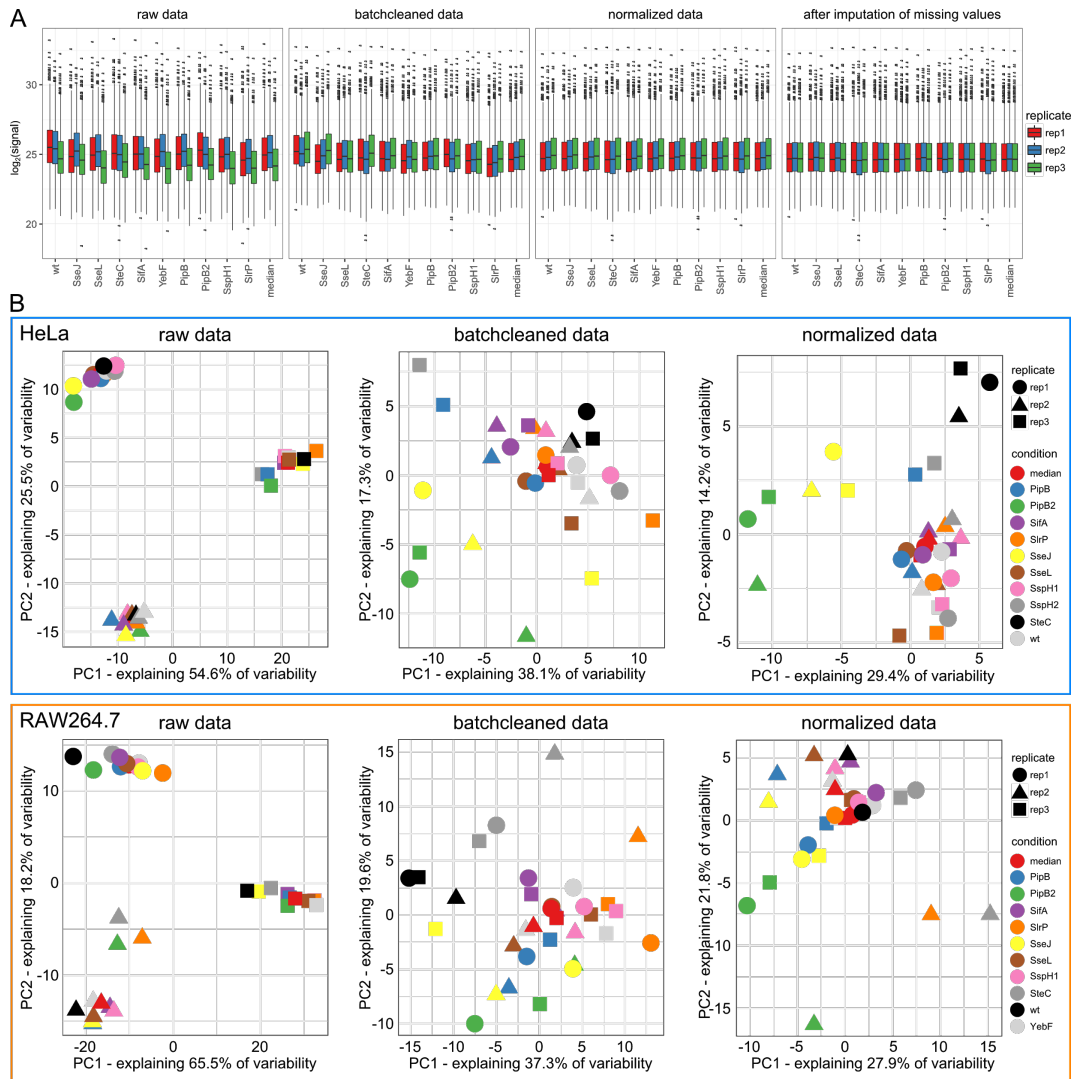


Figure II.8 Batch effect removal and signal normalization reduces variability between replicates. (A) Distributions of logarithmic abundance signal of all proteins identified are shown as boxplots with median and interquartile range for each of the channels in the TMT-10plex. The data is displayed after the individual steps of the computational workup (raw data, after batch-cleaning, after normalization and after imputation). Throughout the steps, the medians and variances across the replicates and samples get stabilized. The three replicates are indicated as shown in the legend. (B) PCA representation of the three replicates of the first batch of effectors in HeLa (blue) and RAW264.7 (orange), after the computational workup steps. The percentage of variance which can be explained by the individual principal components is indicated on the axes. While samples cluster according to their replicate in the raw data, samples with the same bait cluster more closely after batch-cleaning and normalization. Replicates and effector baits are depicted as shown in the legend.

Finally, as we expect the data to be sparse in enriched protein targets, it is useful to look at the distribution of p-values across the entire dataset. As expected, I observed a uniform distribution of larger p-values and a peak at very low ones for both cell lines across both conditions (Figure II.9). This shows that the data is of appropriate quality, batch effects have been removed and that we can expect an overall false discovery rate of 7.4% (Holmes and Huber 2018). This is calculated by dividing the sum of background p-values as indicated by the dotted line in Figure II.9 by the sum of p-values < 0.01). Overall, crosslinked samples had a larger number of detected interactions, as well as a more pronounced peak of small p-values.

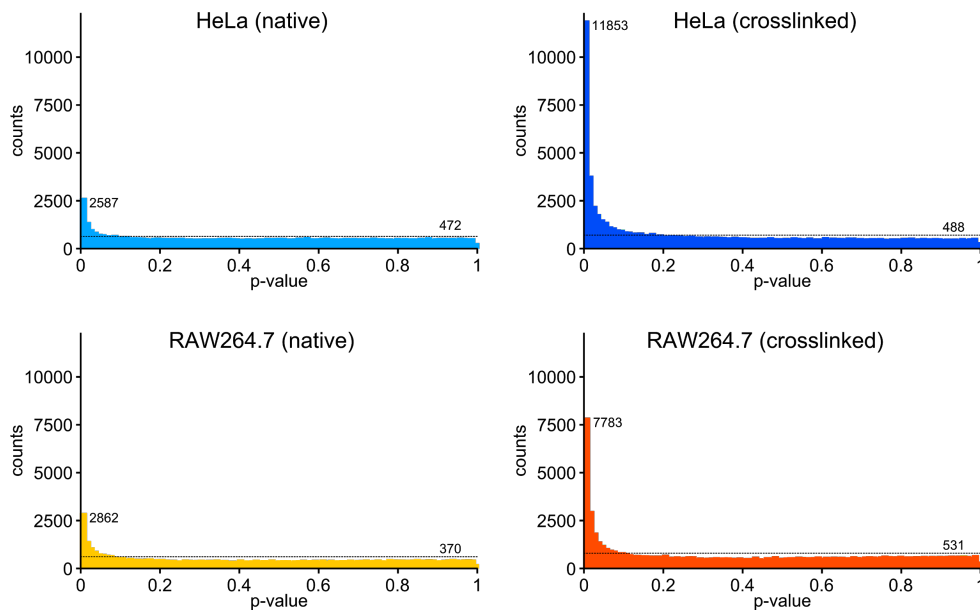


Figure II.9 Distribution of p-values across both cell lines and conditions. P-values calculated with limma were binned with size 0.01 and their counts in each bin are displayed as a histogram for each condition (HeLa native (light blue), HeLa crosslinked (dark blue), RAW264.7 native (light orange) and RAW264.7 crosslinked (dark orange)). In each histogram, the count of the bin $p\text{-value} < 0.01$ is indicated. In addition, the average count of randomly distributed p-values (expected) is shown as a dotted line. For the generation of the histograms, p-values were extracted from Table S2 of (Walch et al. 2020), and were consequently calculated with respect to both, the untagged control and the median of the TMT10-plex. This is discussed in further detail in section 6.1 of this chapter.

6. Calculating enrichments and thresholding

The generated dataset spans more than 119,000 effector-target pairs across the different cell lines and conditions (62,946 in HeLa, 56,412 in RAW264.7). In order to assess PPIs and perform hit-calling, three important analysis steps were undertaken:

1. Enrichment calculation i.e. fold change (FC)
2. Statistical reliability calculation i.e. false discovery rate (fdr)
3. Determination of thresholds to distinguish hits from background

6.1. Calculation of the enrichment values

When assessing AP-MS data, the strength of an interaction is most commonly described by the FC between the abundance of a given protein in the test sample compared to its abundance in a negative control. In the case of this dataset, due to the layout of the TMT-multiplex, there are however two ways the FC can be calculated:

- 1) with respect to the abundance of a given protein in the untagged control (host cells infected with wildtype STm) sample or
- 2) with respect to the median abundance of a given protein across all 10 channels.

While the first option describes the “traditional” way of calculating FCs, the second one has two main advantages. Firstly, the fold enrichments are more robust, as they are calculated with respect to a total of 9 samples instead of one. Secondly, it filters out background binding present in all effector samples and that might not be biologically meaningful. Calculating FCs with respect to the median however relies on the assumption that effectors have distinct panels of interaction partners, i.e. that targets are to some degree effector-specific.

Indeed, calculating FCs with respect to the median of the 10-plex (FC-to-median), as compared to the wildtype strongly decreases the variance and improves the signal-to-noise ratio (Figure II.10). This is especially true for crosslinked samples, where the background in tagged effector samples was distinct and slightly higher compared to the untagged control. Applying calculation of the FC with respect to the wildtype control, this leads to false identification of background proteins as “highly enriched”, the variance in the FC-to-median method remains low. This indicates that a large number of interactions occur non-specifically once a FLAG-tag is present, and calculating the FC with respect to the median allows for an easier extraction of specific target proteins of a given effector (Figure II.10).

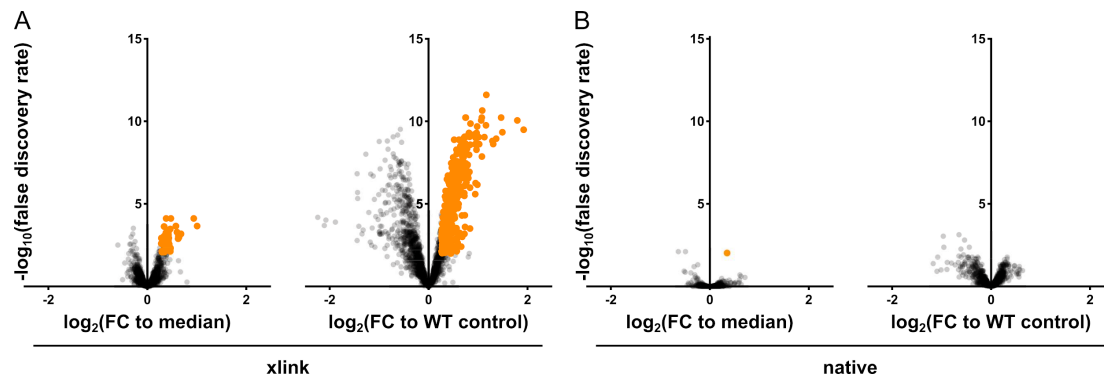


Figure II.10 Comparison of FC-calculation with respect to median and wildtype control. (A) Logarithmic fold-enrichments for proteins obtained through FLAG-IP on SteE-STF (as an example of an effector with few specific interactions) in RAW264.7 after crosslinking shown as volcano plots vs $-\log_{10}(\text{fdr})$. The enrichments were calculated with respect to the median abundance of each protein across the TMT-10plex (first panel) or to the untagged control (second panel). Proteins crossing the hit calling thresholds ($\text{FC} > 1.2$, $\text{fdr} < 0.01$) are colored in orange, all others in grey. Calculating the FC with respect to the median improves signal-to-noise ratio compared to calculation with respect to wildtype. (B) As in panel A, but for native pull-down. *This figure has been published as Figure S2B in (Walch et al. 2020).*

6.2. Calculation of the statistical reliability

Apart from FC, another important measure of any given PPI is its statistical reliability. As three independent, biological replicates were conducted for each effector, we have the ability to detect targets which only display a low FC, but do so consistently across replicates. Due to the inherently low abundance of translocated effector protein in the host cytosol, we expect only a small fraction of each host target protein to interact with any given effector. This means that even low, but reproducible FC are of importance.

In order to enhance the detection of statistically significant PPIs, we applied two different methods to calculate the fdr:

- 1) The limma tool (Ritchie et al. 2015) was used for initial calculation of fdr values,
- 2) T-values from the limma output were also applied in the fdrtool (Strimmer 2008).

In case the limma T-values displayed a standard deviation deviating from 1 to a degree where no convergence of significant hits was detected, the alternative fdr values from the fdrtool were used (Figure II.11).

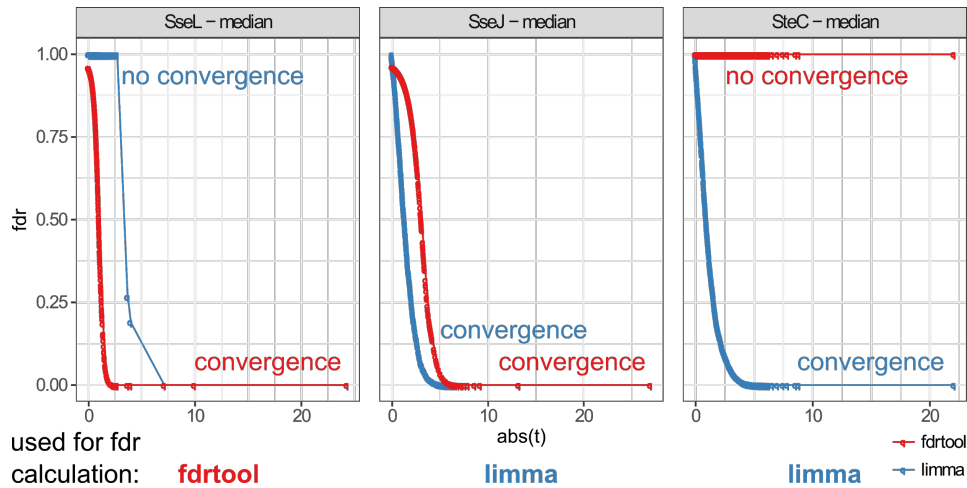


Figure II.11 Comparing limma and fdrtool for fdr-calculation. The absolute value of the t-statistics in limma is plotted vs the fdr calculated using either limma (blue) or fdrtool (red). Three exemplary plots are shown. In each case, the convergence is indicated. For the final calculation of false discovery rates the method which converged better was used (as indicated) for each sample individually.

6.3. Determination of thresholds to distinguish hits from background

Finally, these two measures for PPIs have to be used in a consistent way to call hits across effectors. Yet the dataset is complex, comprising two different cell types from distinct biological backgrounds and highly diverse amounts of expression and translocation across effectors (as seen by Western Blot, Figure II.3).

Indeed, the lowly expressed and translocated effectors, such as AvrA or GogB, displayed overall lower FCs compared to highly expressed and translocated ones, such as PipB2, SteC or SseJ. This indicates that the magnitude of detected fold enrichments strongly depends on the amount of translocated protein. For the fdr, this was however not true, indicating that the dynamic range is indeed in the lower FC values for many of the assessed effectors. Hence, we can be stringent on the fdr cutoff, which I set to $\text{fdr} < 0.01$ as minimum fdr requirement to allow for small, yet reproducible enrichments to be picked up and thereby avoid false negatives.

Setting stringent FC cutoffs across all samples results in many effectors having no interaction partners at all (Figure II.12A) and the median number of targets per effector decreasing strongly (Figure II.12B). I observed that the critical point at which both the number of effectors for which I can identify at least one interaction partner, and the median number of targets per effector start dropping is 1.2 (Figure II.12). Therefore, in order to avoid losing lowly enriched targets, especially for effectors with a low level of translocation, I chose the fold change cutoff $\text{FC} > 1.2$ for hit calling.

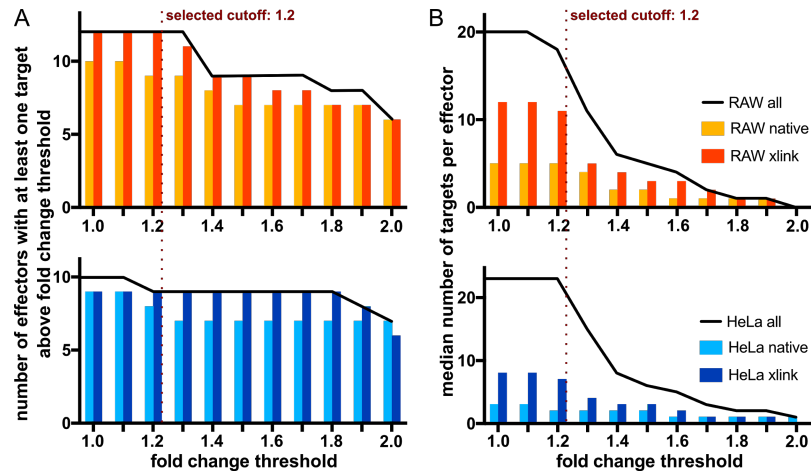


Figure II.12 Increasing the FC-threshold reduces diversity in effectors with enriched targets. (A) For RAW264.7 (orange) and HeLa (blue), the number of baits (maximum 18) for which the bait, and at least one significant PPI was detected using the FC values indicated on the x-axis. An *fdr* threshold of 0.01 was chosen in all cases. In both cell lines, this was done for the native samples (brighter shade) or the crosslinked samples (darker shade) individually, or for both conditions combined (black line). The number of effectors for which the bait and at least one PPI can be detected decreases with increasing FC requirement. (B) Coloring as in panel A, but the median number of targets per effector are displayed. The variance in the number of PPIs detected for the various effectors is very large, with few effectors (e.g. PipB2, SseJ, SteC) harboring hundreds of PPIs and others (e.g. AvrA, GogB, SspH1, SifB) showing fewer than 10. As final FC-cutoff, 1.2 was chosen, as justified in text.

As described before, the number of targets that passed these thresholds varied greatly from one effector to another. To adjust the thresholds on an effector-dependent level, I implemented a second layer of threshold refining by capping the number of targets per effector. This was done by only considering the most highly enriched and most significant targets as hits. Besides, as conservative thresholds are prone to producing false negatives, I wanted to ensure that hits identified in one IP condition (native or crosslinked) were not missed in the other. Therefore, targets that were identified and surpassing the FC criterion in both conditions were retained even if they only met a lower *fdr* requirement ($fdr < 0.05$). This is justified, as PPIs meeting the initial FC requirement in both conditions are very likely biologically meaningful interactions. Thus, the final hit-calling method was chosen as follows:

- 1) Initial thresholds: $FC > 1.2$; $fdr < 0.01$, this was applied to each dataset individually (387 PPIs in RAW264.7 and 612 PPIs in HeLa passed this stage, overlaps between native and crosslinked: 7.8% in RAW264.7, 6.5% in HeLa).
- 2) Refining of overlap: Native and crosslinked data for each effector were combined and if a PPI surpassed the FC criterion in both conditions, the *fdr* requirement in both conditions was lowered to $fdr < 0.05$, in order to retain PPIs in the overlap (number of PPIs is the same as after step 1, overlaps between native and crosslinked: 19.6% in RAW264.7, 9.8% in HeLa).
- 3) Capping per effector: The PPIs which passed step 2 were ranked according to their FC and according to their *fdr* in each condition. All PPIs identified in both conditions, as well as the top 20 PPIs for each of the rankings (*fdr*, FC in each condition) were kept as hits, resulting in 237 PPIs in RAW264.7 (crosslinked vs native overlap: 32.1%) and 238 PPIs in HeLa (crosslinked vs native overlap: 25.2%) passing the aforementioned filters.

7. Appendix

7.1. Tagged effector strain library

To probe effector-target interactions in this study, we created a library of 32 chromosomally affinity-tagged effector strains. These STm strains can be used for AP/QMS experiments and are available to the research community. All strains have been validated by PCR and the expression and translocation have been assessed by Western Blot and, where applicable, AP/QMS. Table II.1 summarizes the location of the STF-tag, as well as the performance in this study.

Table II.1. STF-tagged effector library. Effector proteins secreted via the SPI-1 or SPI-2 T3SS were STF-tagged in their endogenous locus. Performance with respect to expression, translocation and detectability in mass spectrometry are indicated. *This table is published as Supplementary Table S1 in (Walch et al. 2020).*

gene name	gene number	tag location	expressed (RAW264.7, 20hpi)	Injected (Tx-100 soluble)	bait detected in MS	T3SS
AvrA	STM14_3462	C-terminal (aa 278)	yes	yes	yes	I
CigR	STM14_4534	C-terminal (aa 159)	yes	no	--	II
GogB	STM14_3164	C-terminal (aa 497)	yes	yes	yes	II
PipB	STM14_1233	C-terminal (aa 291)	yes	yes	yes	II
PipB2	STM14_3350	C-terminal (aa 350)	yes	yes	yes	II (& I)
SifA	STM14_1400	internally (aa 136)	yes	yes	yes	II
SifB	STM14_1940	C-terminal (aa 316)	yes	yes	yes	II
SipA (SspA)	STM14_3481	C-terminal (aa 685)	yes	no	--	I
SipB (SspB)	STM14_3484	C-terminal (aa 593)	yes	yes	no	I
SipC (SspC)	STM14_3483	C-terminal (aa 409)	yes	no	--	I
SlrP	STM14_928	C-terminal (aa 765)	yes	yes	yes	I & II
SopA	STM14_2557	C-terminal (aa 782)	yes	no	--	I
SopB (SigD)	STM14_1237	C-terminal (aa 561)	no	--	--	I
SopD2	STM14_1098	C-terminal (aa 319)	no	--	--	II
SptP	STM14_3477	C-terminal (aa 543)	yes	no	--	I
SpvB	STM14_5562	C-terminal (aa 591)	yes	no	--	II
SpvC	STM14_5561	C-terminal (aa 241)	yes	yes	no	II (& I)
SrgE	STM14_1877	C-terminal (aa 488)	yes	no	--	II
SseF	STM14_1700	C-terminal (aa 260)	yes	yes	no	II
SseG	STM14_1701	C-terminal (aa 229)	no	--	--	II
SseI	STM14_1193	C-terminal (aa 322)	yes	yes	yes	II
SseJ	STM14_1974	C-terminal (aa 408)	yes	yes	yes	II
SseK1	STM14_4996	C-terminal (aa 336)	yes	yes	yes	II
SseK2	STM14_2428	C-terminal (aa 335)	yes	yes	yes	II
SseL	STM14_2824	C-terminal (aa 317)	yes	yes	yes	II
SspH1	STM14_1483	C-terminal (aa 700)	yes	yes	yes	I & II
SspH2	STM14_2769	C-terminal (aa 788)	yes	yes	yes	II
SteA	STM14_1912	C-terminal (aa 210)	yes	yes	no	I & II
SteB	STM14_1970	C-terminal (aa 133)	no	--	--	II & (I)
SteC	STM14_2050	C-terminal (aa 457)	yes	yes	yes	II
SteD	STM14_2638	C-terminal (aa 111)	yes	no	--	II
SteE	STM14_3166	C-terminal (aa 181)	yes	yes	no	I & II

7.2. Volcano Plots of AP/QMS study

To summarize the generated data, all enrichments with a significantly enriched bait in one condition are displayed in the following Volcano plots (Figures II.13 to II.16):

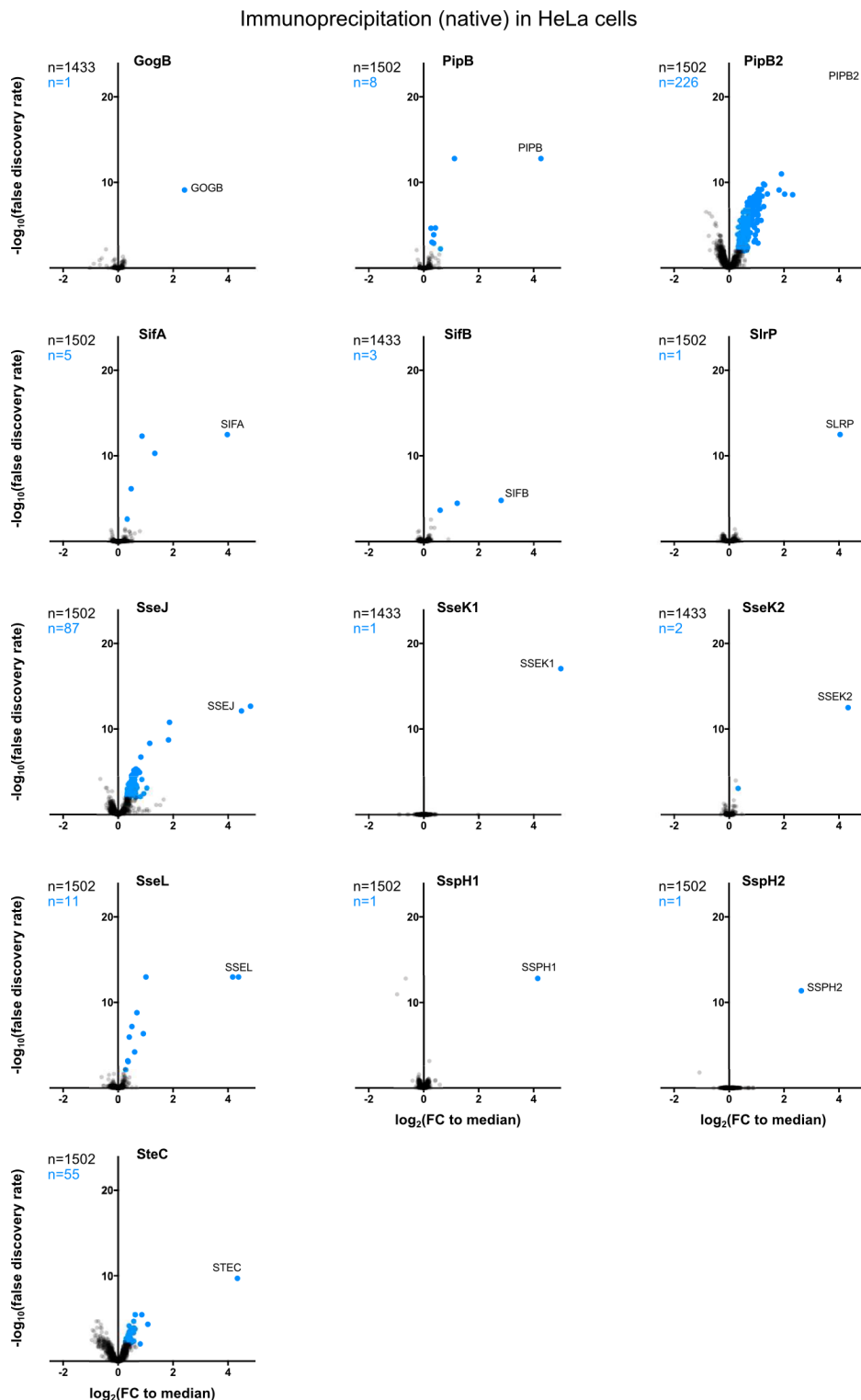


Figure II.13 Enrichments after native IP in HeLa cells. Proteins passing the initial threshold ($\text{FC} > 1.2$, $\text{fdr} < 0.01$) are displayed in blue. The bait protein is indicated by name. Numbers of total proteins identified and hits are indicated. Fold changes were calculated with respect to the median of the TMT-10plex. *This figure has been published as Figure S3 in (Walch et al. 2020).*

Immunoprecrecipitation (x-linked) in HeLa cells

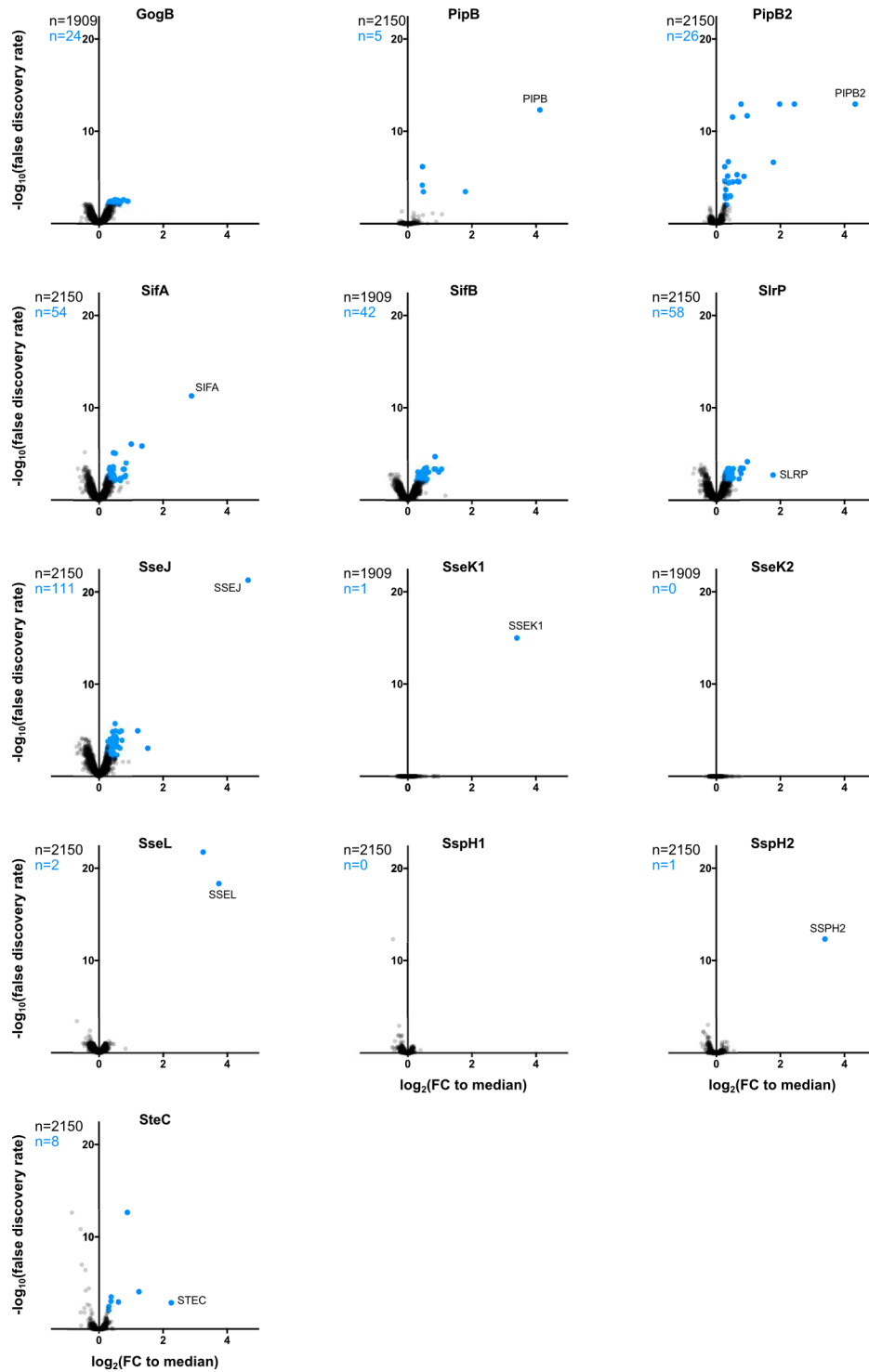


Figure II.14 Enrichments after IP under crosslinking conditions in HeLa cells. Coloring and calculation as described for Figure II.13. This figure has been published as Figure S4 in (Walch et al. 2020).

Immunoprecipitation (native) in RAW264.7 cells

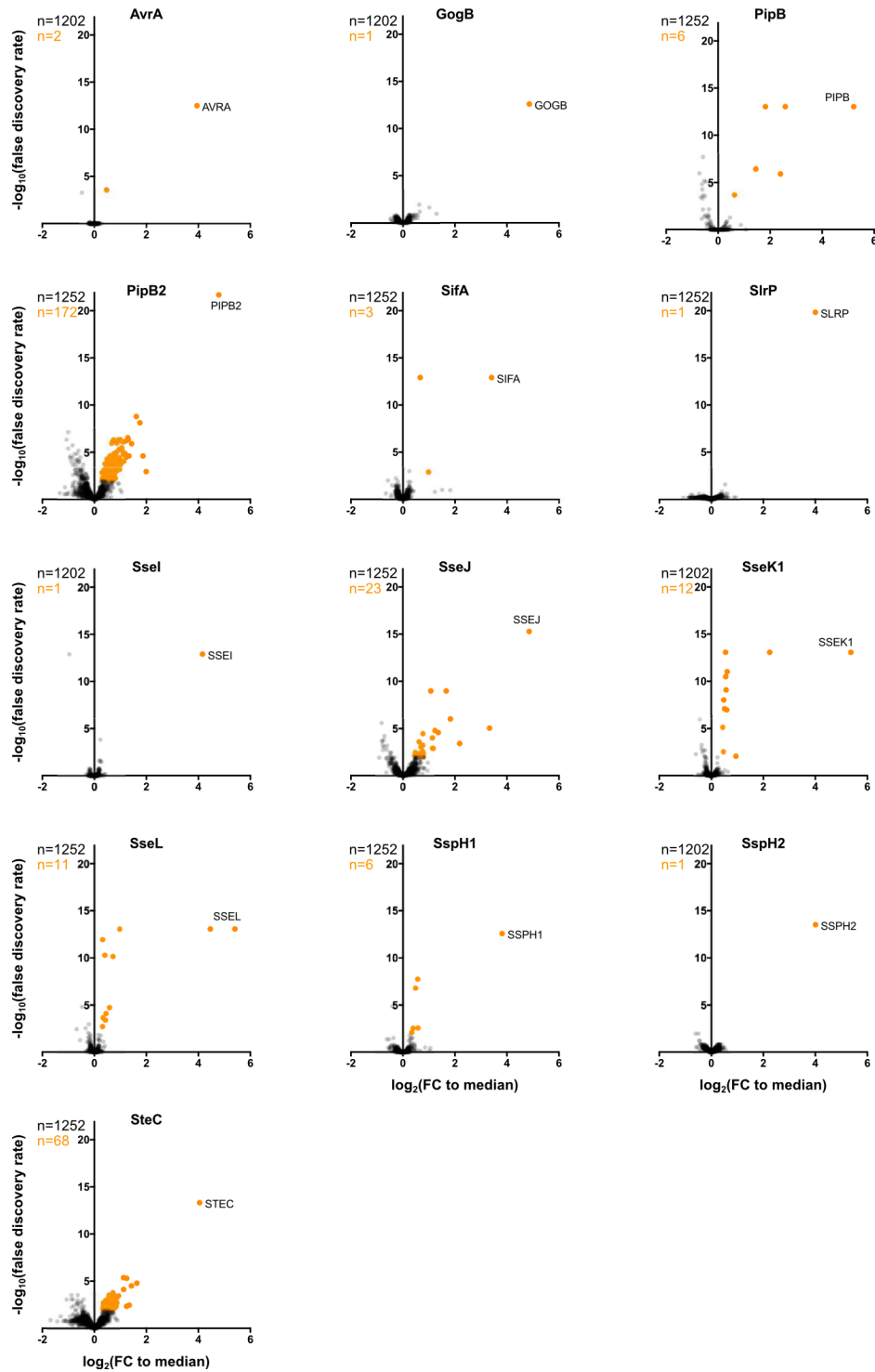


Figure II.15 Enrichments after native IP in RAW264.7. Proteins passing the initial threshold ($\text{FC} > 1.2$, $\text{fdr} < 0.01$) are displayed in gold. Calculations and display as described in the legend for Figure II.13. *This figure has been published as Figure S5 in (Walch et al. 2020).*

Immunoprecipitation (x-linked) in RAW264.7 cells

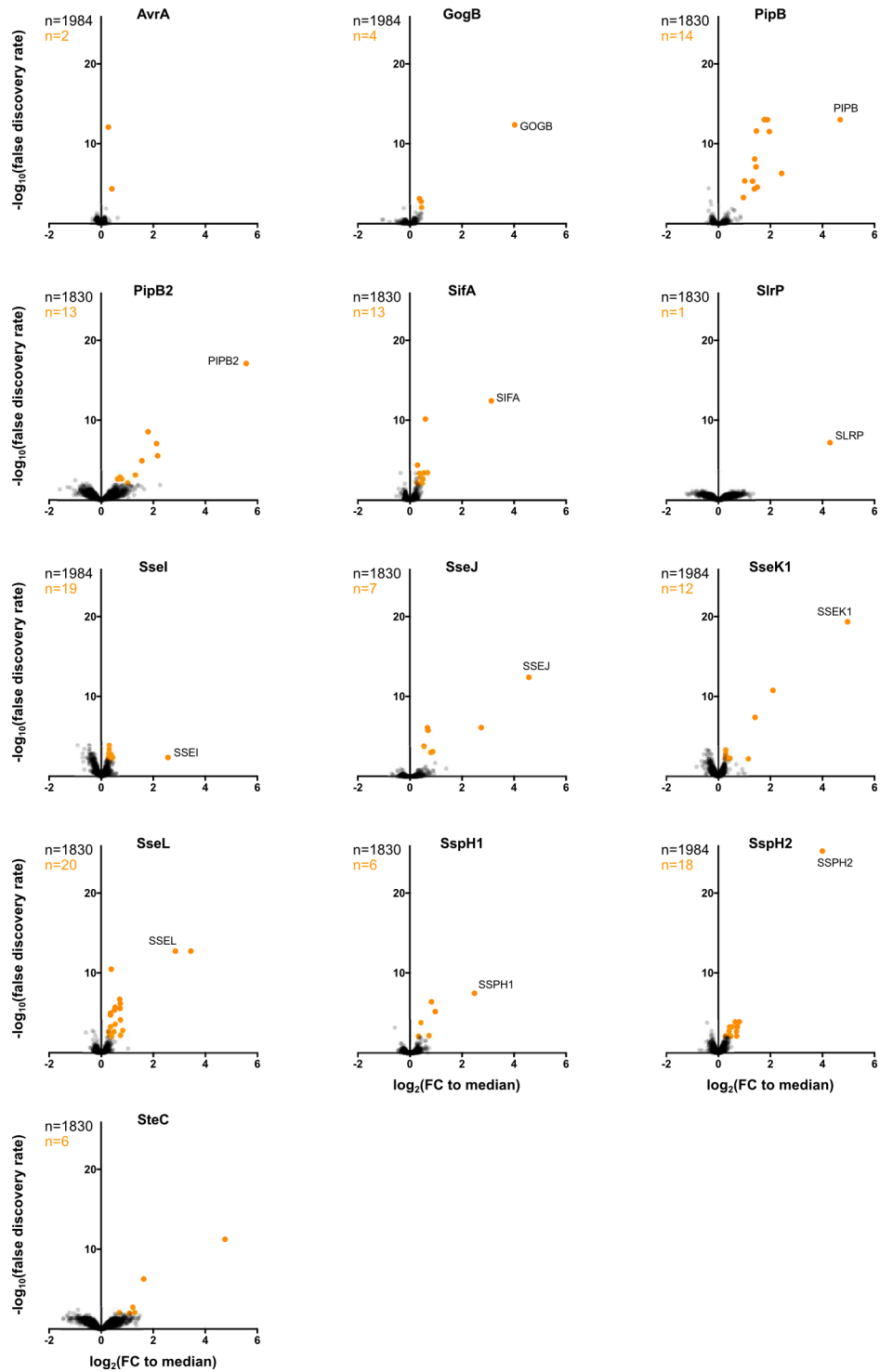


Figure II.16 Enrichments after IP under crosslinking conditions in RAW264.7. Coloring and calculation as described for Figure II.15. This figure has been published as Figure S6 in (Walch et al. 2020).

8. Bibliography of this chapter

- Datsenko, K. A., and B. L. Wanner. 2000. "One-Step Inactivation of Chromosomal Genes in *Escherichia Coli* K-12 Using PCR Products." *Proceedings of the National Academy of Sciences of the United States of America* 97 (12): 6640–45.
- Deutsch, Eric W., Nuno Bandeira, Vagisha Sharma, Yasset Perez-Riverol, Jeremy J. Carver, Deepti J. Kundu, David García-Seisdedos, et al. 2020. "The ProteomeXchange Consortium in 2020: Enabling 'big Data' approaches in Proteomics." *Nucleic Acids Research* 48 (D1): D1145–52.
- Franken, Holger, Toby Mathieson, Dorothee Childs, Gavain M. A. Sweetman, Thilo Werner, Ina Tögel, Carola Doce, et al. 2015. "Thermal Proteome Profiling for Unbiased Identification of Direct and Indirect Drug Targets Using Multiplexed Quantitative Mass Spectrometry." *Nature Protocols* 10 (10): 1567–93.
- Holmes, Susan, and Wolfgang Huber. 2018. *Modern Statistics for Modern Biology*. Cambridge University Press.
- Huber, Wolfgang, Anja von Heydebreck, Holger Sültmann, Annemarie Poustka, and Martin Vingron. 2002. "Variance Stabilization Applied to Microarray Data Calibration and to the Quantification of Differential Expression." *Bioinformatics* 18 Suppl 1: S96–104.
- Perez-Riverol, Yasset, Attila Csordas, Jingwen Bai, Manuel Bernal-Llinares, Suresh Hewapathirana, Deepti J. Kundu, Avinash Inuganti, et al. 2019. "The PRIDE Database and Related Tools and Resources in 2019: Improving Support for Quantification Data." *Nucleic Acids Research* 47 (D1): D442–50.
- Ritchie, Matthew E., Belinda Phipson, Di Wu, Yifang Hu, Charity W. Law, Wei Shi, and Gordon K. Smyth. 2015. "Limma Powers Differential Expression Analyses for RNA-Sequencing and Microarray Studies." *Nucleic Acids Research* 43 (7): e47.
- Strimmer, Korbinian. 2008. "Fdrtool: A Versatile R Package for Estimating Local and Tail Area-Based False Discovery Rates." *Bioinformatics* 24 (12): 1461–62.
- Uzzau, S., N. Figueroa-Bossi, S. Rubino, and L. Bossi. 2001. "Epitope Tagging of Chromosomal Genes in *Salmonella*." *Proceedings of the National Academy of Sciences of the United States of America* 98 (26): 15264–69.
- Walch, Philipp, Joel Selkrig, Leigh A. Knodler, Mandy Rettel, Frank Stein, Keith Fernandez, Cristina Viéitez, et al. 2020. "Global Mapping of *Salmonella* Enterica-Host Protein-Protein Interactions during Infection." *Cold Spring Harbor Laboratory*. <https://doi.org/10.1101/2020.05.04.075937>.
- Webb-Robertson, Bobbie-Jo M., Holli K. Wiberg, Melissa M. Matzke, Joseph N. Brown, Jing Wang, Jason E. McDermott, Richard D. Smith, et al. 2015. "Review, Evaluation, and Discussion of the Challenges of Missing Value Imputation for Mass Spectrometry-Based Label-Free Global Proteomics." *Journal of Proteome Research* 14 (5): 1993–2001.

Chapter III

Large-scale identification of novel effector-target interactions

Chapter III: Large-scale identification of novel effector-target interactions**1. Summary**

Using the STF-tagged STm library in AP/QMS, I generated a vast effector-target interaction dataset that expands the known host-pathogen interactome during *Salmonella enterica* infection. Across 15 effectors, two cell lines and two harvesting conditions, I identified 446 effector-target interactions, of which 25 had previously been described in literature. From these, I built two networks, one for each cell line, and assessed the STm interactomes by identification of key host processes, GO-term enrichment, determination of effector promiscuity and cell line- or condition-specificity of the identified PPIs. Subsequently, I selected a subset of novel interactions for validation using reciprocal co-IP, by which I could demonstrate an accuracy of at least 59% through validating 13 out of 22 new PPIs, as well as validation in primary bone marrow-derived macrophages (pBMDMs).

In this chapter, I describe the identification of a plethora of novel host-pathogen PPIs and underline their validity by recapitulating known biology, as well as validating a subset of novel PPIs. The majority of effectors interacted with a panel of host proteins, yet they converged on targeted host processes. I used this information to build new associations between STm effectors, either through physical interactions or functional relationships. The dataset presented here provides a systems-wide host-bacterial pathogen physical interactome resource, to our knowledge, the first in an infection context and with effectors being expressed and translocated at endogenous levels.

2. Contributions

Analysis and visualization of the list of hit proteins (network building and analysis, GO-term enrichment, analysis of cell line and condition specificity) was conducted by me with input and feedback from Dr. Joel Selkrig and Dr. Athanasios Typas. I performed all experimental work presented in and used for this chapter (assessment of bacterial secretion, reciprocal validation, validation in pBMDMs). Mandy Rettel conducted sample preparation for mass spectrometry (IP in pBMDMs) and operated the machines. Dr. Frank Stein conducted the initial data analysis with input from Dr. Joel Selkrig, Dr. Athanasios Typas, Dr. Mikhail Savitski and myself. Additional data analysis, statistical tests and visualization was performed by myself with input from Dr. Joel Selkrig, Dr. Athanasios Typas and Dr. Sarah Kaspar. Murine bone marrow for BMDM extraction was provided by Prof. Wolf-Dietrich Hardt (ETH Zurich). The work presented here is part of the following published preprint (bioRxiv), which is currently under revision at Cell Host&Microbe:

Walch, Philipp, Joel Selkrig, Leigh A. Knodler, Mandy Rettel, Frank Stein, Keith Fernandez, Cristina Viéitez, et al. 2020. "Global Mapping of *Salmonella Enterica*-Host Protein-Protein Interactions during Infection." *bioRxiv*, Cold Spring Harbor Laboratory. <https://doi.org/10.1101/2020.05.04.075937>.

3. Large-scale AP/MS identifies hundreds of novel effector-target PPIs

Taking the concluding subsections of Chapter II into account and applying the method for hit-calling outlined there, I detected 447 non-redundant PPIs (including 1 contaminant, IgG-heavy chain) across 15 effectors and 2 tested cell lines, excluding the detection of bait proteins. Of those, 25 occurred between an effector and another bacterial protein, while 421 were effector-host. 25 of these were previously reported, those are summarized in Table III.1 (section III.7), and the remaining 396 were novel. All identified PPIs are accessible at proteomeXchange (Deutsch et al. 2020) via the PRIDE (Perez-Riverol et al. 2019) repository (project accession number: PXD018375).

Even though not all effectors were detected in each condition, significantly enriched interaction partners were identified for a total of 15 effectors (12 in RAW264.7 and 9 in HeLa, Figure III.1A, left Venn diagram). For several effectors (SlrP in RAW264.7, GogB, SspH1, SspH2 and SseK1 in HeLa), no PPI passed the threshold criteria, even though a bait was detected (Figure III.1A, right Venn diagram). This absence of significant protein-interaction partners can be due to a multitude of reasons, such as a disruption of effector functionality by the tag, non-proteinaceous targets (Nawabi, Catron, and Haldar 2008; Knodler et al. 2009; McShan et al. 2016) or a multitude of transient interactions. A detailed discussion of possible reasons is given in Chapter VI, section 1.5.

Effectors where I detected the bait and at least one significant target had on average 19.7 PPIs in RAW264.7 and 26.4 PPIs in HeLa, with a large variance across the panel of effectors (Figure III.1B). This indicates a strong promiscuity of STm effector proteins inside the host cytoplasm during infection. Instead of having a single specific host protein interaction partner, several effectors interacted with a vast panel of host proteins, such as PipB2, for which we detected 59 PPIs in RAW264.7 and 48 PPIs in HeLa cells (Figure III.1B). Thus, for bacterial pathogens, pleiotropic effects, in this case the action of a single effector on multiple host targets or processes, might constitute the rule, rather than being the exception (Takahashi-Kanemitsu, Knight, and Hatakeyama 2020; Hamon et al. 2012). Furthermore, several of these novel PPIs may not be direct, but rather mediated through other host factors (it is a common problem in AP methodologies that indirect interaction partners are piggybacked (Nesvizhskii 2012; Teng et al. 2015)). This can also explain the binding of effectors to a large number of host proteins that are involved in the same process. The convergence of STm effectors on distinct host processes is discussed in further detail in the following section and in Chapter VI, section 1.3.

We were unable to capture several well-characterized PPIs that had previously been described, such as SifA-SKIP (Jackson et al. 2008; Diacovich et al. 2009; Zhao et al. 2015) and AvraA-MKK7 (Jones et al. 2008; Du and Galán 2009). A possible explanation is that AP/MS approaches commonly suffer from false negatives (Verschueren et al. 2015), but many other possible reasons exist (see Discussion in Chapter VI, section 1.5).

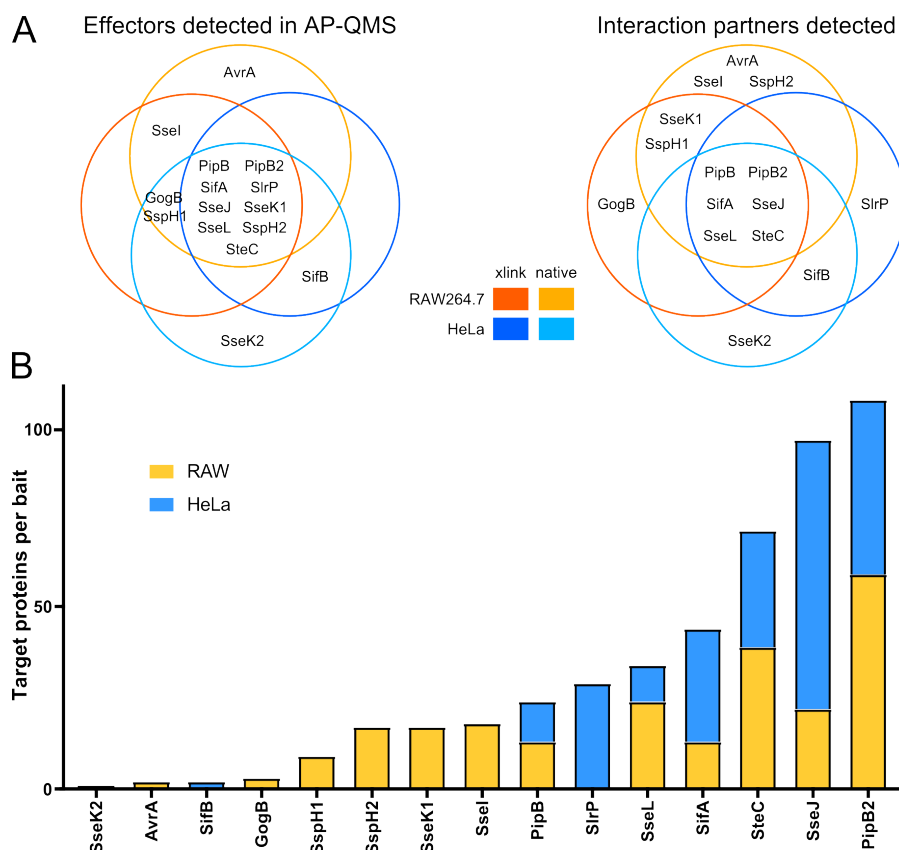


Figure III.1 Number of PPIs detected for each bait. A) Venn diagrams showing the recovery of STF-tagged bait across the different cell lines and pulldown conditions (left panel), as well as STF-tagged effectors with at least one significantly enriched target protein (right panel). B) The number of target proteins identified in the pulldowns on the respective STF-tagged effector are plotted per cell line - RAW264.7 in gold, HeLa in blue - irrespective of pulldown condition (native vs crosslinked). *This figure has been adapted from Figure S7A in (Walch et al. 2020).*

4. Network construction and analysis

I used the PPIs selected as “hits” in each cell line to build two distinct interaction networks (Figure III.2), where each node represents a bait or target protein and each edge depicts either an identified PPI or a known functional interaction, listed in STRING DB, version 11 (Szklarczyk et al. 2019). A list of all STRING functional interactions can be found in Table S5 of (Walch et al. 2020). More detail on the network building in cytoscape version 3.7.2 (Shannon et al. 2003) can be found Chapter VII.

4.1. STm effector PPIs converge on biologically relevant cellular processes

The two networks contained several previously identified or characterized PPIs (Figure III.2, black nodes). For example in RAW264.7, SseJ directly interacts with the host Rho-GTPase proteins RhoA and RhoB (Ohlson et al. 2008), which we detect as highly enriched in both the native and crosslinked SseJ pulldown (RhoA: $\log_2(\text{FC}) > 2.74$; $\text{FDR} < 9.35 \cdot 10^{-6}$, RhoB: $\log_2(\text{FC}) = 2.18$; $\text{FDR} = 3.88 \cdot 10^{-4}$ corrected for multiple testing). Several other previously reported interactions were also recovered e.g. PipB2-KLC1, PipB2-KIF5B, SseL-OSBP and Ssel-ACADM (Sontag et al. 2016; Henry et al. 2006; Auweter et al. 2012) (Figure III.2A). Similarly, in HeLa cells we were able to recover previously described PPIs, such as SseJ-RHOA, PipB2-KIF5, PipB2-KLC1 and SseL-OSBP (Ohlson et al. 2008; Henry et al. 2006; Auweter et al. 2012) (Figure III.2B). RhoB

was detected as a hit for SseJ in RAW264.7 but not in HeLa cells, likely due to its low expression in the latter (not even detected as background in HeLa cells). This indicates that there are substantial differences in the background proteome and the effector PPI profile between the two cell lines. This is evaluated in further detail in section 5 of this chapter.

Interestingly, I found that several host protein complexes were targeted by STm effectors including ion transport, respiration, myosins, the T-complex, cholesterol transport, the spliceosome, 40S ribosome and the establishment of SNARE complex (Figure III.2). While not necessarily all PPIs linked to a given cellular process or protein complex are direct, and in fact may originate from piggybacking, this nonetheless shows the relevance of these particular host processes during *Salmonella* infection. In addition, we saw convergence of multiple STm effectors on the same host protein, complex or cellular process. In RAW264.7 macrophages, several solute carrier proteins (SLCs), which are involved in the transport of ions and small molecules (Schaller and Lauschke 2019), were found to interact with both SseJ and PipB2 (Figure III.2A). In HeLa cells, SifB displayed PPIs with the RAB proteins Rab10 and Rab13, the former of which was also a target of PipB2 (Figure III.2B).

I observed the *Salmonella* effector SifA interacting with various proteins of the SNARE complex, mainly Vacuolar Sorting Proteins (VPSs), as well as the actin-related protein 2/3 complex subunit 4 (ARPC4). SNARE proteins, as well as the ARP2/3 complex and other host targets identified in this work (e.g. KLC1, KIF5B) have been shown to localize to the SCV at early stages of the infection in previous studies (Santos et al. 2015). Finding these host proteins associated with STm effectors 20 hpi therefore shows an extension of the timeframe, and suggests that several of these target proteins stay associated with the SCV through PPIs with STm effectors. Furthermore, the specific interactions of SifA with SNARE proteins and other cytoskeleton-dependent trafficking proteins underlines its role in the stability, protection and maturation of the SCV during infection (Creasey and Isberg 2014; Beuzón et al. 2000).

In both cell lines, SteC, which has been linked to actin rearrangements in proximity to the SCV (Poh et al. 2008), displayed PPIs with host targets being involved in mRNA splicing. This suggests a potential regulatory role of SteC in host-transcript splicing across both cell types. Similarly, SifA formed PPIs with several mRNA splicing-related proteins, such as SFPQ, in addition to the PPIs captured with VPS proteins (Figure III.2B). Both examples suggest that effectors are multifactorial in their functionality and hence target distinct biological processes. We cannot conclude whether these different processes are targeted sequentially or simultaneously, as we only look at a single time point. However, by investigating the PPIs at other time points during infection, more detail on the multifunctionality of effectors could be generated.

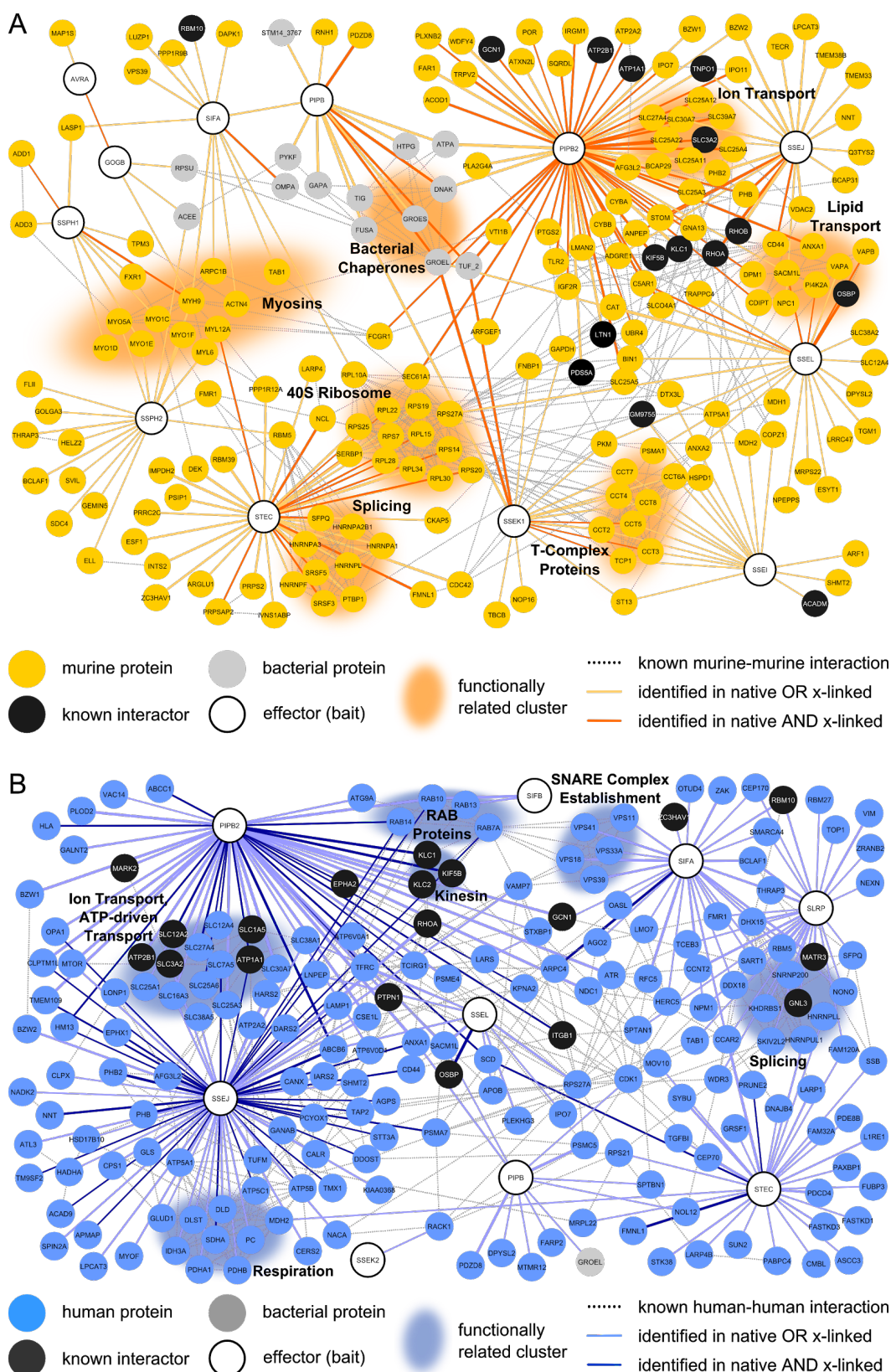


Figure III.2 *Salmonella*-host PPI networks in RAW264.7 and HeLa. (A) RAW264.7 PPI network spanning 12 STm effectors (white) and their host targets (gold for novel, black for previously described) and bacterial proteins (grey) at 20 hpi. The edges are colored according to the type of interaction and the thickness is proportional to the fold change of the respective PPI. The network was created in cytoscape version 3.7.2. (Shannon et al. 2003) and functional interactions were obtained from STRING DB version 11 (Szklarczyk et al. 2019). (B) HeLa PPI network spanning 9 STm effectors. Coloring, edge formatting and network generation are as described in panel A and the figure legend. *This figure has been adapted from Figures 2 and 3 in (Walch et al. 2020).*

4.2. Connectivity of the networks

Several of the biological processes introduced above served as effector convergence points, such as myosin MYH9 as a common target of SspH1, SspH2, GogB and SifA in RAW264.7. Ion transport proteins SLC3A2 and SLC30A7 were common targets linking SseJ and PipB2, as well as several T-complex proteins linking SseK1 and SseL. In HeLa cells, the Phosphatidylinositol-3-phosphatase SAC1 (SACM1L), which plays a role in the cycling of phosphatidylinositol in conjunction with OSBP (Mesmin et al. 2017) was a connection point for SseL, PipB and PipB2. Also, the Ras-related protein Rab10, which is involved in intracellular vesicle and membrane trafficking (Babbey et al. 2006; Hutagalung and Novick 2011) was a common target of SseJ, PipB2 and SifB. These linkage points indicate potential effector co-operation, whether direct or indirect, in parallel or sequentially, on related host cellular processes (Figure III.3)

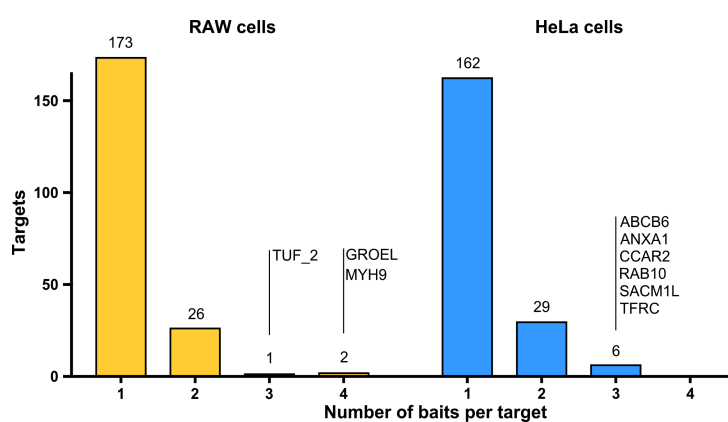


Figure III.3 Connectivity of the interaction networks as indicated by the number of effectors binding to a given host protein. Histogram showing separating target proteins according to the number of effector baits shown to interact with each protein. For proteins being identified in at least 3 individual effector pull-downs, the protein name is indicated. Target proteins in RAW264.7 are depicted in gold, those in HeLa in blue. *This figure has been published as Figure S7C in (Walch et al. 2020).*

4.3. GO-term enrichment analysis

In order to dig deeper into these functional clusters and to go beyond known host functional interactions and interaction hubs, I evaluated Gene Ontology (GO)-term enrichments within the targets in both cell lines (Ashburner et al. 2000; Gene Ontology Consortium 2021). Several processes were highly enriched in both cell lines, such as ion transport, vesicular transport and fusion, response to hormonal stimulus or general processes involved in host-symbiont or host-microbe interactions (Figure III.4A).

I found ion transport to be mainly targeted by PipB2 and SseJ, both through their interactions with ATP-dependent transporters and SLC proteins. Similarly, vesicle-mediated transport was mainly impacted by a small group of effectors, mainly PipB2, SseJ and SifA (Figure III.4B). Other processes, such as responses to hormone stimulus, were affected by a much broader panel of effector proteins, with almost all effectors targeting host factors involved in this process (Figure III.4B). This indicates a lower specificity, but can also originate from a more systemic importance of the process for the infection progression.

While the aforementioned processes were enriched across both cell lines, I also determined host cell type-specific enriched GO-terms. Cytoskeleton-dependent intracellular transport (mainly through SspH1 and SspH2, grouped under “ion transport after GO-term grouping), positive regulation of cell death (mainly through SseJ, SteC and PipB2) as well as upregulation of endocytosis were more pronounced in RAW264.7. In particular, transport along the cytoskeleton, as well as lipid trafficking have previously been found important for maintenance of the SCV (Wasylnka et al. 2008; Nawabi, Catron, and Haldar 2008; Arena et al. 2011).

On the other hand, oxidation of organic compounds, epithelial cell migration or catabolic processes were specific to HeLa cells (Figure III.4). In addition, interactions of SseJ, PipB2, SifA and SifB with RAB proteins and components of the SNARE complex were specifically enriched in HeLa cells (Figure III.2B). While this is the first reporting of physical interactions through these specific effectors, the involvement of the associated host processes has previously been implicated in STm infection (Stévenin et al. 2019; Kyei et al. 2006; Rzomp et al. 2003; Stein, Müller, and Wandinger-Ness 2012).

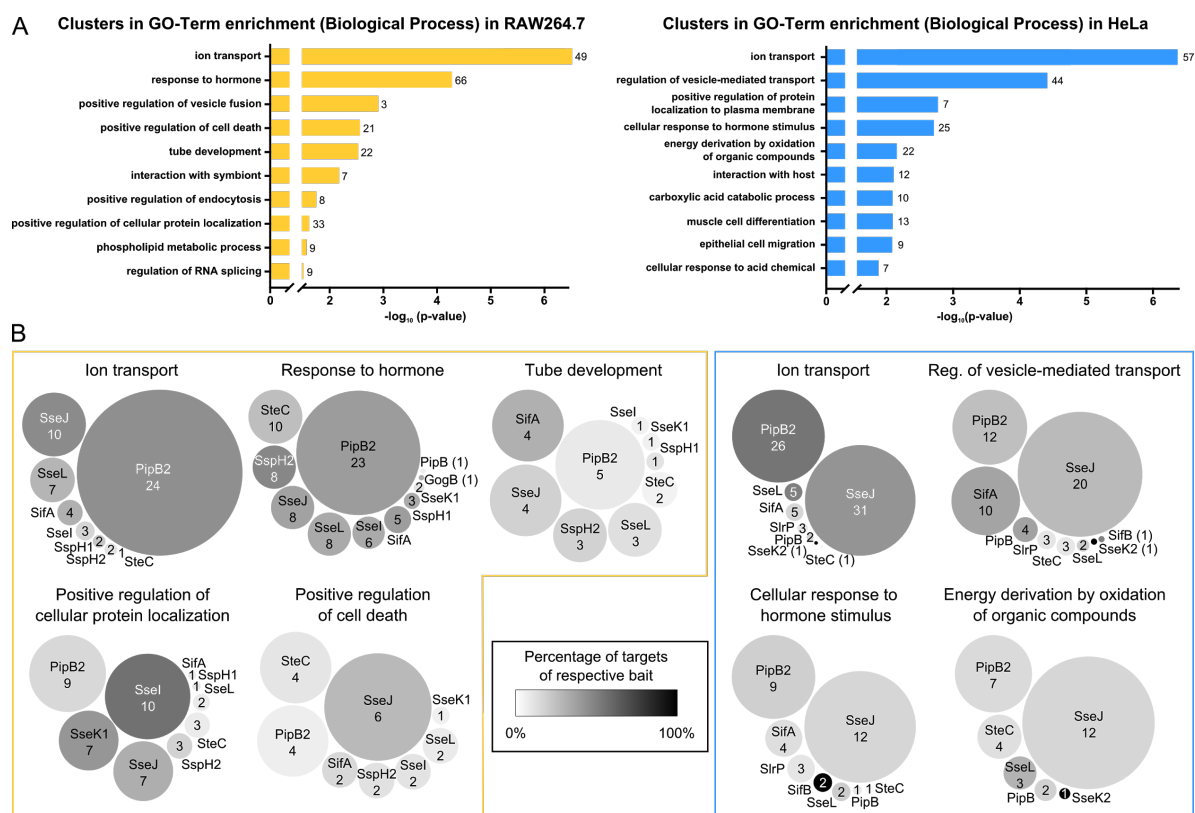


Figure III.4 GO-term enrichments (Biological Process) across both cell lines. (A) Enriched processes identified in GO-term analysis (Biological Processes) in RAW264.7 (in gold) and HeLa (in blue) with respect to the background proteome identified in the AP/QMS experiment. The top 10 clusters of GO-terms are ordered by negative logarithmic significance after Benjamini-Hochberg correction for multiple testing (Benjamini and Hochberg 1995; Bindea et al. 2009). *n* indicates the number of target proteins which were present in the respective clusters. (B) Bubble plots of effectors displaying PPIs with targets listed in the indicated GO-terms. Size signifies the relative number of targets bound by a given effector per term (absolute number is indicated). Coloring signifies the percentage of PPIs per effector being involved a given GO-term (as indicated in the legend). *This figure has been adapted from Figures 2C, 3C and S7B in (Walch et al. 2020).*

Due to the differences in host cell background (murine vs human) and cell type (macrophage vs epithelial cell), it is expected that only a subset of enriched biological processes is shared between the two. These commonalities might reflect the common features of living in an intracellular niche: the rewiring of lipid trafficking, small molecule and ion transport or modulating host cell responses. Distinctly enriched processes could allude to differences in the host proteome or in intracellular dynamics within epithelial cells and macrophages. This is highlighted in section 5.

4.4. Bacterial-bacterial interactions

In addition to the PPIs with various host proteins, I observed several effector interactions with bacterial cytosolic proteins, as well as some effector-effector interactions (such as AvrA-GogB or SifA-PipB). The latter is very intriguing and largely missing from literature because effector interactions are typically studied out of the context of infection or by ectopic effector expression, making interactions with other effectors difficult or impossible to detect. Although some of these interactions may be indirect and mediated through a common host factor that both effectors bind simultaneously, this finding nonetheless supports the concept of effector cooperation and convergence on influencing the same cellular processes. For one of the effector pairs, AvrA and GogB, convergence on inflammation has been previously described. While AvrA exerts its anti-inflammatory and anti-apoptotic effect through reducing MKK7-mediated JNK-signalling (Jones et al. 2008; Du and Galán 2009), GogB inhibits I κ B degradation, thereby reducing inflammation (Pilar et al. 2012). Despite the lack of a common target, the observation of their physical interaction strongly suggests a direct cooperation of GogB and AvrA in regulating and dampening inflammatory processes.

We also detected 25 interactions between effectors and other bacterial proteins (mostly cytosolic) – note that this is only possible in an infection context. Examples for these interactions are PipB-GroEL, PipB-STM14_3767 or PipB-DnaK (Figure III.3). To exclude the possibility that these interactions are due to contamination of my sample (partial lysis of bacterial cells within the host, which could lead to these PPIs occurring in the host cytoplasm), I validated the specific presence of GroEL and the bacterial acetyl-CoA hydrolase STM14_3767, but not of other abundant bacterial proteins, such as RecA in the cytoplasm of RAW264.7 cells during infection (Figure III.5). RecA was only detected in the Tx100-insoluble fraction, therefore making partial bacterial lysis improbable. This finding suggests a secretion of several bacterial proteins, among them STM14_3767 and GroEL into the host cytoplasm upon infection. For GroEL, secretion has been described in other bacterial pathogens, such as *Helicobacter pylori*, *Bacillus subtilis* or *Francisella novicida* (Yang et al. 2011; González-López et al. 2013; Pierson et al. 2011; McCaig, Koller, and Thanassi 2013). At this point, I cannot conclude whether the secretion of the bacterial proteins identified in PPIs occurs *via* translocation through a secretion system, or through other means of protein export. To do so, one would need to assess the presence of GroEL and STM14_3767 in the host cytoplasm after infection with SPI-1 (Δ prgK) or SPI-2 (Δ ssaV) deficient STM.

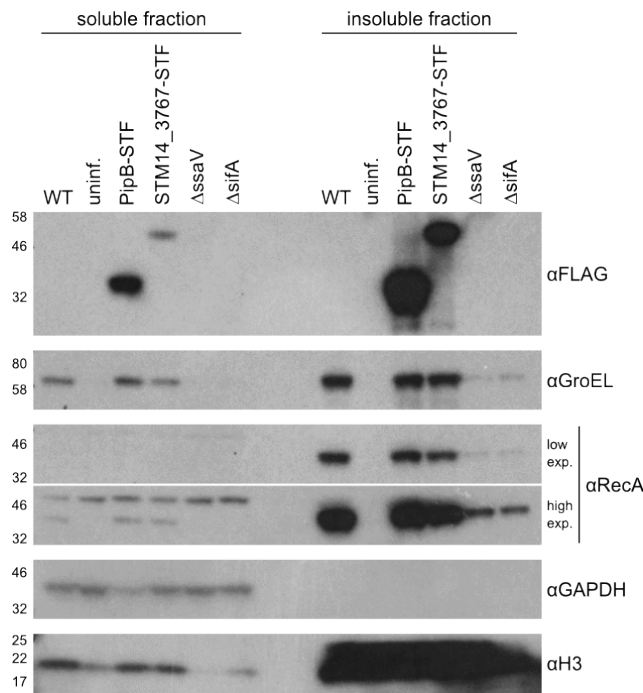


Figure III.5 GroEL and STM14_3767, but not other highly abundant bacterial proteins (RecA), are present in the host cytoplasm during infection. Cells were infected with various strains (wildtype, two C-terminally STF-tagged strains, a Δ ssaV mutant (T3SS2 translocation deficient) and a Δ sifA mutant (displaying a decreased stability of the SCV; all at MOI = 100:1) and harvested 20 hpi in Tx100. Lysates were separated into Tx100-soluble and -insoluble fractions and probed by SDS-PAGE and subsequent Western Blot using the antibodies indicated on the right hand side: α FLAG to probe for effector translocation, α GroEL, α RecA (bacterial loading control), α GAPDH (cytoplasmic fraction), α H3 (nuclear control). I could, in addition to the STM effector PipB, observe the presence of GroEL and STM14_3767, but not RecA, in the Tx100-soluble (cytoplasmic) fraction. *This figure has been adapted from Supplementary Figure S8 in (Walch et al. 2020).*

5. Cell line- and condition-specificity

As discussed in the previous chapter, I assessed PPIs in both native harvesting conditions as well as after crosslinking with the reversible, membrane-permeable crosslinker DSP in order to also capture transient and weaker PPIs. When comparing the overlap between native and crosslinked samples, I noticed several interactions, such as SifA-VSP39 or SifA-RBM10, which specifically occurred only after crosslinking in both cell lines. This suggests that these interactions may occur transiently.

There is however only a partial overlap between native and crosslinked samples in both cell lines (Figure III.6A and B, Venn diagrams). Fisher's exact test showed that while the overlap is only partial, it is highly significant (p-value < 0.0001). This can have a multitude of reasons:

- 1) Pulldown after crosslinking is less efficient (as seen by Western Blot, data not shown), possibly due to inaccessibility of the affinity tag within the crosslinked complex. This leads to a lower abundance of the bait protein and can therefore lower enrichment scores.
- 2) The nonspecific background obtained through IP after crosslinking (as discussed in Chapter II) lowers the signal-to-noise ratio compared to native pulldown.

- 3) Due to the additional experimental steps (crosslinking, quenching) and the resulting increased incubation times during harvesting and sample preparation, the recovery of some (weaker) PPIs could be impacted. This is relevant as only a fraction of PPIs is covalently crosslinked by DSP due to its efficiency. Therefore, we expect to also capture several non-crosslinked interactions within the crosslinked sample.
- 4) The stringency of thresholding could lead to an increased number of false negatives. I tried mitigating this through improvements in the hit calling method (as described in Chapter II), but false negatives cannot be completely rectified.

I found 28 PPIs that were conserved within both cell lines or across IP conditions. Six of these were identified in all four datasets, and three of these were novel: SteC-FMNL1, SseJ-CD44 and SseJ-PHB. Other PPIs were obtained in three out of four conditions, making it very likely that they are false negatives in the fourth condition. Among those, several were newly identified in this work: e.g. PipB2-ANXA1, PipB-GroEL or SseL-SACM1L. The large majority of PPIs (418 out of 446) within the AP/MS dataset however are specific to either RAW264.7 or HeLa (Figure III.6C).

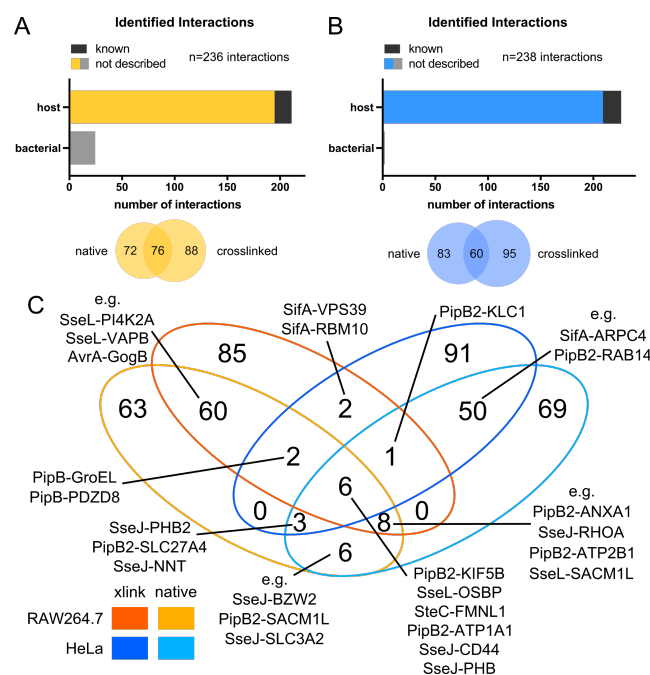


Figure III.6 Overlap between native and crosslinked samples as well as across cell lines reveals several conserved PPIs. (A) PPIs identified in RAW264.7 infection for 20h are grouped according to their origin (murine host vs bacterial) and colored according to whether they are novel (gold, grey) or previously described (black). Venn diagram shows overlap in PPIs between native and crosslinked pulldown as well as the number of PPIs identified specifically in one condition. (B) As in panel A, but for HeLa cells. Host color coding is blue. (C) Venn diagram spanning both cell lines and conditions. Exemplary PPIs are given for overlaps. *This figure has been adapted from Figures 2B, 3B and 4A in (Walch et al. 2020).*

I further investigated the reasons for the lack of overlap between the two cell lines and the only partial overlap between the two IP conditions by assessing the correlation of all proteins (most of them are background). While correlations within the same cell line and condition (i.e. the correlation of the two panels of effectors that were probed) was

very high ($0.853 < R^2 < 0.872$; Figure III.7A-D), the correlation between native and crosslinked IP within one cell line was much lower ($R^2 = 0.604$ in RAW264.7, $R^2 = 0.425$ in HeLa; Figure III.7E and F), as expected between two different sample types. This can serve as possible explanation why only a minority of PPIs was detected in both native and crosslinked IP.

Similarly, the correlation between the two cell lines was low for both of the conditions ($R^2 = 0.464$ in native IP, $R^2 = 0.539$ in crosslinked IP; Figure III.7G and H), as expected for different cell types originating from different species. In line with that, for about one third of PPIs that were identified in one cell line only, the corresponding host target protein was not detected in the other cell line (Figure III.7I - L). The proteins accounting for the remaining cell type specific PPIs were detected at comparable abundances (Figure III.7G and H).

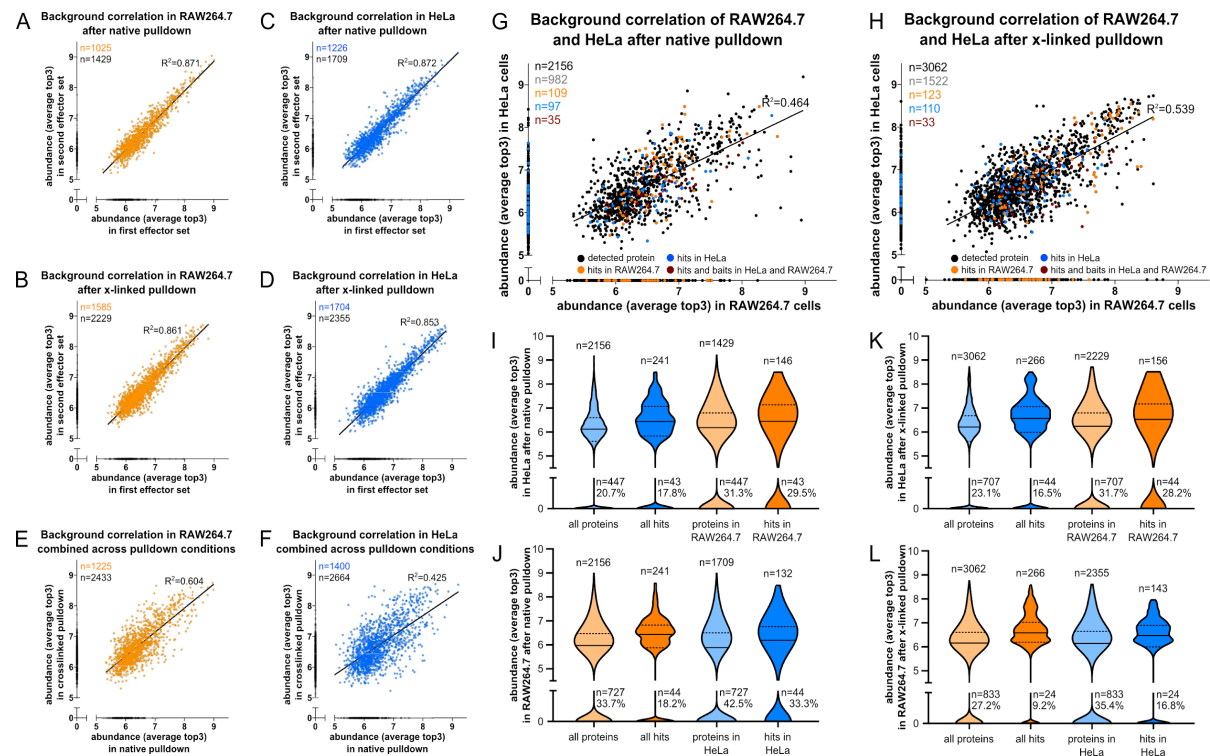


Figure III.7 Comparison of background proteome determined in AP/QMS of RAW264.7 and HeLa. Orthologs were called using protein name, as well as OMA-browser (Altenhoff et al. 2018). If no ortholog was identified in the data or if a given protein was not observed in a given condition or cell line, its abundance was defined as 0. (A-H) Scatterplots comparing the protein abundances of each protein determined in the two datasets as indicated in the title, as well as the correlation between the two: (A) effector sets in RAW264.7 native pulldown, (B) effector sets in RAW264.7 crosslinked pulldown, (C) effector sets in HeLa native pulldown, (D) effector sets in HeLa crosslinked pulldown, (E) native vs crosslinked pulldown in RAW264.7, (F) native vs crosslinked pulldown in HeLa. (G) RAW264.7 vs HeLa in native pulldown. (H) RAW264.7 vs HeLa in crosslinked pulldown. In panels G and H, proteins are indicated as follows: all proteins (black), proteins present in both cell lines (grey), hits in RAW264.7 (gold), hits in HeLa (blue), hits in both cell lines (red). (I-L) Violin plots summarizing the abundance distributions in panels G and H respectively. (I) Abundance distribution of the various groups in HeLa cells, native IP, i.e. projection of the different classes of proteins onto the y-axis in panel G. (J) Abundance distribution of the various groups in RAW264.7 cells, native IP, i.e. projection onto the x-axis in panel G. (K) Abundance distribution of the various groups in HeLa cells, crosslinked IP, i.e. projection onto the y-axis in panel H. (L) Abundance distribution of the various groups in RAW264.7 cells, crosslinked IP, i.e. projection the x-axis in panel H. *This figure has been published as Supplementary Figure S9 in (Walch et al. 2020).*

The remaining differences in host cell interactomes can be attributed to other explanations, such as the occurrence of false negatives. However, the infection cycles are known to be distinct in the two cell types, which is also reflected in the GO-term enrichments of PPIs detected. While STm can break free from the SCV and hyperproliferate in the cytoplasm of epithelial cells, such an escape is not possible in macrophages, due to the fast degradation of cytoplasmic bacteria (Knodler et al. 2010; Castanheira and García-Del Portillo 2017). This difference in intracellular lifestyle could hint towards different pools of host proteins that are accessible as interaction partners for STm effectors within the two host cell lines. Furthermore, differences in host species (murine macrophages vs human epithelial cells), as well as distinct protein expression profiles within the two cell lines contribute to the differences in PPIs detected in this work.

In conclusion, of the 446 PPIs identified in this work, only a small fraction (28 interactions) could be identified in both cell lines. The reasons for these largely disjunct profiles are mainly biological and can be explained through different background proteome compositions, as well as distinct STm infection dynamics. Independent of cell line, the two assessed IP conditions (native vs crosslinked) displayed only a partial, yet significant overlap. While this has mainly technical reasons, it also allows for the detection of PPIs in two distinct conditions and thereby a better insight into STm biology within the host cell.

6. Validation

6.1. Validation *via* reciprocal immunoprecipitation

As the large majority of interactions identified in the large-scale AP/MS study have not been described before, it is important to independently validate a subset of these novel PPIs. To do so, I selected a panel of 12 target proteins, which represent a total of 22 distinct PPIs within the dataset. These were chosen to span both cell lines and conditions, as well as different strengths of interaction as indicated by $\log(\text{FC})$. Thereby, a representative distribution of weaker and stronger interactions was guaranteed (Figure III.8A and B). If all conditions are taken into account (cell line, native vs crosslinked), the selected targets account for 37 individual interactions, as several effector-target pairs were recovered in more than one pulldown condition. This subset of PPIs was then assessed by reciprocal pulldown, using target specific antibodies, which are listed in Table VII.1. A full overview of targets and PPIs that were assessed, including their performance in the reciprocal validation can be found in Table S8 of (Walch et al. 2020). In all cases, an additional STm effector of similar translocation abundance, yet without detectable PPI to the target (i.e. a non-cognate effector), was chosen as negative control (Figure III.8A).

I was able to recover the target protein in 7 of the 12 assessed cases, accounting for 13 of the 22 PPIs (22 of the 37 PPIs when taking into account all individual conditions). Of those, I successfully validated 8 of the 13 PPIs in at least one of the tested conditions, accounting for 61.5%, and I saw no interaction with any of the 6 tested non-

cognate controls for a total of 19 assessed interactions (Figure III.8C, left table). When counting each condition as individual experiment, 13 of 22 PPIs, i.e. 59.1%, could be validated via reciprocal immunoprecipitation, with all 14 assessed non-cognate controls displaying no interaction (total number of probed interactions: 36, Figure III.8C, right table). There are multiple reasons for the inability to recapitulate all PPIs of the subset:

- 1) Despite the stringency of the thresholds applied for hit-calling, false positives are possible.
- 2) Due to the experimental setup, the cell population that is harvested contains about 20 - 40% of infected cells, as not all cells get infected, and some infected cells die throughout the assay. In addition, even within infected cells, the protein levels of STm effectors have been shown to be lower than those of host proteins (Selkrig et al. 2018). Both of these lead to most host protein being not bound, even by an abundantly translocated and well-characterized STm interactor, hence making such reciprocal IPs less sensitive.
- 3) While the anti-FLAG antibody displays a very high efficiency in pulldown, and a commercially available antibody-coated bead slurry could be used for pulldown, the host target antibodies varied in their efficacy in pulling down the host protein and in associating with the protein A or protein G agarose beads used for reciprocal IP. This leads to lower co-IP efficiencies.

Consistent with the last two points, I was more readily able to validate PPIs that displayed a higher FC (Figure III.8B). Nonetheless, I was still able to successfully validate the majority of PPIs within the selected subset using reciprocal IP, which is orthogonal to the initial AP/MS work, yet not as sensitive. This strengthens the validity of the interactions detected with our new method and reported here.

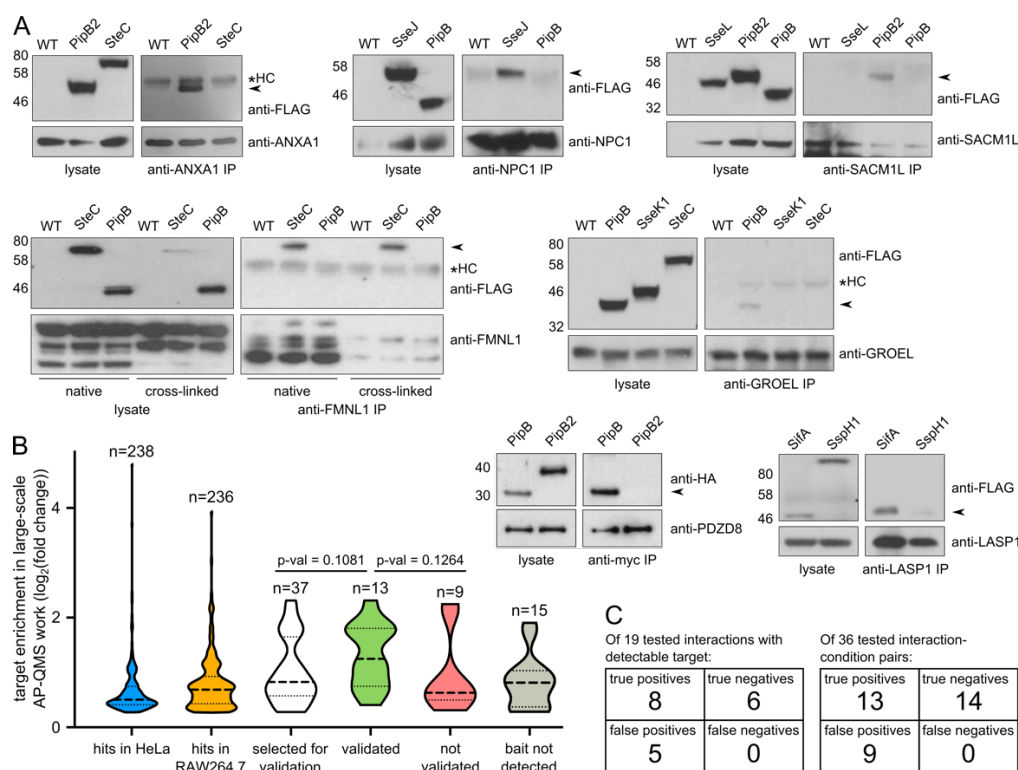


Figure III.8 Validation via reciprocal co-IP using specific antibodies against a panel of novel target proteins. (A) Western Blots depicting reciprocal co-IP as validation. Further detail about the experimental setup and procedure is given in Chapter VII. In each blot, a non-cognate effector with a similar level of expression or translocation is used as negative control. One representative blot per interaction is shown. Experiments were conducted in duplicate, and as a single experiment for LASP1 and GroEL pulldown. Arrows indicate the validated interaction. (B) Violin plot showing the distribution of $\log_2(\text{FC})$ enrichment within the different groups: All hits in HeLa (blue) or RAW264.7 (orange), the subset of interaction selected for validation (white), the PPIs where reciprocal validation was successful (green), unsuccessful (red) or not possible as the host target (i.e. the bait of the reciprocal pulldown) could not be detected (grey). Median and interquartile range are indicated by dotted lines. P-values obtained from two-sided Mann-Whitney test are indicated. (C) Summarizing tables containing all assessed interaction-condition pairs (including negative controls). Numbers of true / false positives / negatives are indicated. *This figure has been adapted from Figure 4B, C and D in (Walch et al. 2020).*

6.2. Validation in primary bone marrow derived macrophages (pBMDMs)

To show the physiological relevance of the identified PPIs in primary cells, we decided to perform infection and AP/QMS in murine primary bone marrow derived macrophages (pBMDMs). Thereby, we also sought to push the boundaries of the methodology and test its applicability in primary cells. First, I assessed the expression and translocation of a set of effectors that were secreted to large extents in RAW264.7 macrophages: SseJ, SseL, SteC and PipB2. While all effectors were expressed in pBMDMs (Tx-100 insoluble fraction), only SseJ, SteC and PipB2 could be recovered in the cytoplasmic (Tx-100 soluble) fraction (Figure III.9A). These lower levels of otherwise strongly translocated effectors can have several reasons, such as:

- 1) A lower number of host cells used in the experiment. In our hands, each mouse yielded around 10 to 20 million pBMDMs, and to be conservative on the number of mice that need to be sacrificed, we used 10-times fewer host cells compared to the AP/QMS work in cell lines.
- 2) A lower infection rate in pBMDMs compared to RAW264.7 cells (Gog et al. 2012).

- 3) The known lower degree of intracellular proliferation in pBMDMs and/or more efficient clearance of the bacterium once inside the cell (Hensel et al. 1998).
- 4) A higher death rate of (infected) pBMDMs compared to RAW264.7 (Monack et al. 1996), which could result in a lower fraction of infected cells 20 hpi.
- 5) Presumably, there are differences in the infection dynamics and targeted pathways across the two cell lines, requiring a different panel of effectors to be translocated.

Due to their distinct profile of interaction partners, I then decided to conduct a small-scale AP/QMS experiment using SteC-STF and PipB2-STF STm 20 hpi in biological triplicate. Untagged (wildtype) STm14028S served as negative control in the following TMT-multiplex layout: 3x WT, 3x SteC-STF, 3x PipB2-STF. This layout with these effectors then allows for two distinct quantifications: 1) with respect to untagged control and 2) with respect to the other effector. For this experiment, pBMDMs from 6 mice were used to yield 9 million cells per effector in each replicate, which is more than 10 times less than the number of RAW264.7 macrophages used for each effector.

As expected, the overall dynamic range of the enrichment of target proteins was too small to apply the same stringent cutoffs as in the large-scale AP/QMS work. Therefore, we decided to compare the two effectors SteC and PipB2 against each other and subsequently assess the distribution of FCs of previously identified hits (in RAW264.7 and HeLa cells) versus all proteins. I also established that comparing two effectors against each other was better at removing the background, rather than merely comparing each effector to the untagged control. This is in line with the enrichment calculation and analysis established for the larger AP/QMS set. Given that these two effectors only share a single interaction partner across RAW264.7 and HeLa, there is also little risk of omitting meaningful interactions while removing the background.

Interestingly, the vast majority of host targets (38 of 43 for SteC and 42 of 64 for PipB2) was more strongly enriched in the IP of the effector they were targeted by in RAW264.7 and HeLa (Figure III.9B). This translates to a significant deviation of the distribution of hits from the distribution of all proteins as calculated by Mann-Whitney test (Figure III.9C). Hence, despite the low dynamic range, a majority of PPIs that were identified in the large-scale AP/QMS work hold true in a primary cell line. This finding demonstrates the adaptability of the AP/QMS approach to other cell types or cell lines, yet also indicates the necessity of large numbers of infected cells (the scale was reduced to one tenth) to provide the necessary dynamic range to detect meaningful PPIs at endogenous effector levels.

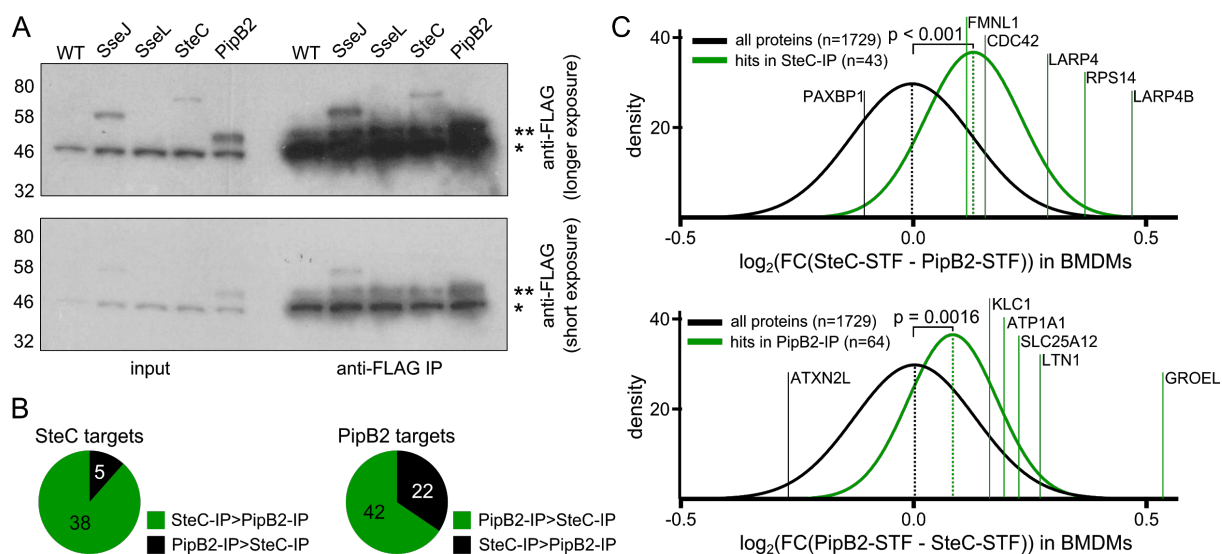


Figure III.9 Validation of successful effector translocation and capture of previously identified PPIs in pBMDMs. (A) Translocation of a panel of STm effectors in pBMDMs 20 hpi with SseJ-STF, SseL-STF, SteC-STF and PipB2-STF shown by Western Blot. Tx-100 soluble lysate fraction, as well as FLAG-IP elutions were assessed with anti-FLAG-antibody. Asterisks denote unspecific bands: *: cytosolic macrophage protein, **: non-specific FLAG-IP protein. (B) The absolute numbers and fraction of hits that were more strongly enriched in pBMDMs (green) and those that weren't (black) are shown in pie charts. (C) Distribution of fold changes (densities) across all proteins (black lines), as well as hits (green lines) in SteC (left) and PipB2 (right). AP/QMS was performed in pBMDMs 20 hpi with wt STm, SteC-STF and PipB2-STF in triplicate and analyzed in the same TMT-multiplex. FCs were calculated between the two effectors and densities were acquired after binning. Representative hits are annotated by name and Mann-Whitney test (two-tailed) was used to calculate significant deviation from the distribution of all proteins. *The data in this figure will be included in a revised version of (Walch et al. 2020).*

We calculated that using primary cells in the original large-scale framework would require an unrealistic number of cells and hence mouse bone marrow. As 6 mice were required for one tenth of the original input number of cells for one TMT-multiplex, we could expect the necessary number of mice to be at least 120 times as high (i.e. bone marrow from at least 720 mice), as the AP/QMS work was based on 12 TMT-multiplexes per cell line, each requiring 10 times the amount of mice used in this small scale validation. While the harvesting of pBMDMs from mice can be optimized to yield a higher number of cells (Troupin et al. 2013), even reducing this number 3- to 5-fold is neither ethically nor practically justifiable. In conclusion, using established cell lines for the large-scale approach and subsequently validating a subset of meaningful interactions in primary cells allows for both, the necessary breadth of the approach and the physiological validity (as also discussed in Chapter I, section I.4).

7. Comparison to previous AP/MS studies mapping *Salmonella* effector PPIs

This dataset is to my knowledge the first one to systematically map STm-host PPIs in an infection context with endogenous levels of effector proteins. Hence its comparability to previously published data is not straightforward. As described in further detail in Chapter I, using non-physiological conditions can cause biases in the detection of PPIs, yet several of these have been described and validated in further detail, establishing them as *bona fide* PPIs. In the work described in this chapter, I could recapitulate several of these well described PPIs (e.g. SseJ and Rho-GTPases

(Ohlson et al. 2008; Christen et al. 2009; Auweter et al. 2011), PipB2 and kinesin (Henry et al. 2006; D'Costa et al. 2019) or SseL and OSBP (Auweter et al. 2012, 2011)), underlining the validity of the data presented here.

In addition, the dataset discussed in this chapter shares overlaps with other previously published systematic approaches:

- 1) In a study by Auweter *et al.*, the authors use ectopic effector expression for a panel of 13 STm effectors in HEK-293T cells, and furthermore purify 11 STm effectors in *E. coli* (Auweter et al. 2011). Of the 15 interactions described in this work, I was able to recover two (SseL-OSBP and SseJ-RhoA).
- 2) Sontag *et al.* probed interactions for a set of eight effectors *in vitro* by AP/MS on RAW264.7 lysates incubated with purified effector proteins. Their study shares three effectors (SseI, SseL and SspH1) with ours, and we share an overlap of two PPIs, SseI-ACADM and SseI-Gm9755 (Sontag et al. 2016). In addition, while the authors identify several PPIs of SseI and GtgA to small solute carrier (SLC) proteins, we observed SLCs as common targets of PipB2 and SseJ, indicating a more general relevance of SLCs during infection. This is in line with their role in cytokine signalling, innate immunity and infections (Awomoyi 2007; Singh et al. 2016; Nguyen et al. 2018).
- 3) In a recent study using Bio-ID to probe effector-target interactions, D'Costa *et al.* assessed a panel of 5 effectors (PipB2, SifA, SopD2, SseF and SseG) by tagging them with BirA (a biotin ligase) and ectopically expressing them in HeLa cells. PipB2 and SifA are shared between the two studies and 16 PPIs for PipB2, as well as 4 PPIs for SifA could be recovered in both studies (D'Costa et al. 2019).

Furthermore, various cellular processes that have been previously implicated in STm infection, such as actin-related transport, ion transport, lipid metabolism and transport and establishment of the SNARE complex, are recapitulated in this work.

8. Appendix

Of the 421 PPIs between STm effector proteins and host cell targets, 25 had previously been described. These, alongside details on the experimental settings used in the previous studies are listed in Table III.1.

Table III.1. List of previously described protein-protein interactions recapitulated in this study. The effector-target interaction pair, as well as the experimental system used in the respective study are indicated. *This table has been published as Supplementary Table S4 in (Walch et al. 2020).*

Interaction	Experimental settings and systems	References
PipB2-ATP1A1	Bio-ID after ectopic expression of BirA-fusion in HeLa cells	(D'Costa et al. 2019)
PipB2-ATP2B1	Bio-ID and AP-MS after ectopic expression of BirA-fusion in HeLa cells	(D'Costa et al. 2019)
PipB2-EPHA2	Bio-ID after ectopic expression of BirA-fusion in HeLa cells	(D'Costa et al. 2019)
PipB2-GCN1	AP-MS after ectopic expression of BirA-fusion in HeLa cells	(D'Costa et al. 2019)
PipB2-ITGB1	Bio-ID after ectopic expression of BirA-fusion in HeLa cells	(D'Costa et al. 2019)
PipB2-KIF5B	Bio-ID after ectopic expression of BirA-fusion in HeLa cells Co-purification of ectopically expressed effector and target in HeLa cells	(D'Costa et al. 2019)(Henry et al. 2006) (Henry et al. 2006)
PipB2-KLC1	Bio-ID after ectopic expression of BirA-fusion in HeLa cells Co-purification of ectopically expressed effector and target in HeLa cells	(D'Costa et al. 2019)(Henry et al. 2006) (Henry et al. 2006; Schleker et al. 2012)
PipB2-KLC2	Bio-ID after ectopic expression of BirA-fusion in HeLa cells Co-purification of ectopically expressed effector and target in HeLa cells	(D'Costa et al. 2019)(Henry et al. 2006) (Henry et al. 2006; Schleker et al. 2012)
PipB2-LTN1	AP-MS after ectopic expression of BirA-fusion in HeLa cells	(D'Costa et al. 2019)
PipB2-MARK2	Bio-ID after ectopic expression of BirA-fusion in HeLa cells	(D'Costa et al. 2019)
PipB2-PDS5A	AP-MS after ectopic expression of BirA-fusion in HeLa cells	(D'Costa et al. 2019)
PipB2-PTPN1	Bio-ID after ectopic expression of BirA-fusion in HeLa cells	(D'Costa et al. 2019)
PipB2-SLC12A2	Bio-ID after ectopic expression of BirA-fusion in HeLa cells	(D'Costa et al. 2019)
PipB2-SLC1A5	Bio-ID after ectopic expression of BirA-fusion in HeLa cells	(D'Costa et al. 2019)
PipB2-SLC3A2	Bio-ID after ectopic expression of BirA-fusion in HeLa cells	(D'Costa et al. 2019)
PipB2-TNPO1	AP-MS after ectopic expression of BirA-fusion in HeLa cells	(D'Costa et al. 2019)
SifA-GNL3	Bio-ID after ectopic expression of BirA-fusion in HeLa cells	(D'Costa et al. 2019)
SifA-MATR3	Bio-ID after ectopic expression of BirA-fusion in HeLa cells	(D'Costa et al. 2019)
SifA-RBM10	AP-MS after ectopic expression of BirA-fusion in HeLa cells	(D'Costa et al. 2019)
SifA-ZC3HAV1	Bio-ID after ectopic expression of BirA-fusion in HeLa cells	(D'Costa et al. 2019)
Ssel-ACADM	AP-MS after incubation of recombinant effector in HeLa or RAW cell lysates	(Sontag et al. 2016)
Ssel-Gm9755	AP-MS after incubation of recombinant effector in HeLa or RAW cell lysates	(Sontag et al. 2016)
SseJ-RhoA	Y2H, colocalization In vitro binding, activation upon expression in HeLa cells	(Ohlson et al. 2008; Christen et al. 2009; Auweter et al. 2011; Schleker et al. 2012)
SseJ-RhoB	Y2H, colocalization	(Ohlson et al. 2008)
SseL-OSBP	AP-MS after ectopic expression of HA-fusion in HEK-293T cells Mechanistic follow-up in vitro using protein truncations	(Auweter et al. 2012, 2011; Schleker et al. 2012)

9. Bibliography of this chapter

- Arena, Ellen T., Sigrid D. Auweter, L. Caetano M. Antunes, A. Wayne Vogl, Jun Han, Julian A. Guttman, Matthew A. Croxen, et al. 2011. "The Deubiquitinase Activity of the Salmonella Pathogenicity Island 2 Effector, SseL, Prevents Accumulation of Cellular Lipid Droplets." *Infection and Immunity* 79 (11): 4392–4400.
- Ashburner, M., C. A. Ball, J. A. Blake, D. Botstein, H. Butler, J. M. Cherry, A. P. Davis, et al. 2000. "Gene Ontology: Tool for the Unification of Biology. The Gene Ontology Consortium." *Nature Genetics* 25 (1): 25–29.
- Auweter, Sigrid D., Amit P. Bhavsar, Carmen L. de Hoog, Yuling Li, Y. Alina Chan, Joris van der Heijden, Michael J. Lowden, et al. 2011. "Quantitative Mass Spectrometry Catalogues Salmonella Pathogenicity Island-2 Effectors and Identifies Their Cognate Host Binding Partners." *The Journal of Biological Chemistry* 286 (27): 24023–35.
- Auweter, Sigrid D., Hong B. Yu, Ellen T. Arena, Julian A. Guttman, and B. Brett Finlay. 2012. "Oxysterol-Binding Protein (OSBP) Enhances Replication of Intracellular Salmonella and Binds the Salmonella SPI-2 Effector SseL via Its N-Terminus." *Microbes and Infection / Institut Pasteur* 14 (2): 148–54.
- Awomoyi, Agnes A. 2007. "The Human Solute Carrier Family 11 Member 1 Protein (SLC11A1): Linking Infections, Autoimmunity and Cancer?" *FEMS Immunology and Medical Microbiology* 49 (3): 324–29.
- Babbey, Clifford M., Nahid Ahktar, Exing Wang, Carlos Chih-Hsiung Chen, Barth D. Grant, and Kenneth W. Dunn. 2006. "Rab10 Regulates Membrane Transport through Early Endosomes of Polarized Madin-Darby Canine Kidney Cells." *Molecular Biology of the Cell* 17 (7): 3156–75.
- Benjamini, Yoav, and Yocef Hochberg. 1995. "Controlling the False Discovery Rate: A Practical and Powerful Approach to Multiple Testing." *Journal of the Royal Statistical Society* 57 (1): 289–300.
- Beuzón, C. R., S. Méresse, K. E. Unsworth, J. Ruíz-Albert, S. Garvis, S. R. Waterman, T. A. Ryder, E. Boucrot, and D. W. Holden. 2000. "Salmonella Maintains the Integrity of Its Intracellular Vacuole through the Action of SifA." *The EMBO Journal* 19 (13): 3235–49.
- Bindea, Gabriela, Bernhard Mlecnik, Hubert Hackl, Pornpimol Charoentong, Marie Tosolini, Amos Kirilovsky, Wolf-Herman Fridman, Franck Pagès, Zlatko Trajanoski, and Jérôme Galon. 2009. "ClueGO: A Cytoscape Plug-in to Decipher Functionally Grouped Gene Ontology and Pathway Annotation Networks." *Bioinformatics* 25 (8): 1091–93.
- Castanheira, Sónia, and Francisco García-Del Portillo. 2017. "Salmonella Populations inside Host Cells." *Frontiers in Cellular and Infection Microbiology* 7 (October): 432.
- Christen, Matthias, Lisette H. Coye, Jill S. Hontz, Doris L. LaRock, Richard A. Pfuetzner, Megha, and Samuel I. Miller. 2009. "Activation of a Bacterial Virulence Protein by the GTPase RhoA." *Science Signaling* 2 (95): ra71.
- Creasey, Elizabeth A., and Ralph R. Isberg. 2014. "Maintenance of Vacuole Integrity by Bacterial Pathogens." *Current Opinion in Microbiology* 17 (February): 46–52.

- D'Costa, Vanessa M., Etienne Coyaud, Kirsten C. Boddy, Estelle M. N. Laurent, Jonathan St-Germain, Taoyingnan Li, Sergio Grinstein, Brian Raught, and John H. Brumell. 2019. "BioID Screen of Salmonella Type 3 Secreted Effectors Reveals Host Factors Involved in Vacuole Positioning and Stability during Infection." *Nature Microbiology*, October. <https://doi.org/10.1038/s41564-019-0580-9>.
- Deutsch, Eric W., Nuno Bandeira, Vagisha Sharma, Yasset Perez-Riverol, Jeremy J. Carver, Deepti J. Kundu, David García-Seisdedos, et al. 2020. "The ProteomeXchange Consortium in 2020: Enabling 'big Data' approaches in Proteomics." *Nucleic Acids Research* 48 (D1): D1145–52.
- Diacovich, Lautaro, Audrey Dumont, Daniel Lafitte, Elodie Soprano, Aude-Agnès Guilhon, Christophe Bignon, Jean-Pierre Gorvel, Yves Bourne, and Stéphane Méresse. 2009. "Interaction between the SifA Virulence Factor and Its Host Target SKIP Is Essential for Salmonella Pathogenesis." *The Journal of Biological Chemistry* 284 (48): 33151–60.
- Du, Fangyong, and Jorge E. Galán. 2009. "Selective Inhibition of Type III Secretion Activated Signaling by the Salmonella Effector AvrA." *PLoS Pathogens* 5 (9): e1000595.
- Gene Ontology Consortium. 2021. "The Gene Ontology Resource: Enriching a Gold Mine." *Nucleic Acids Research* 49 (D1): D325–34.
- Gog, Julia R., Alicia Murcia, Natan Osterman, Olivier Restif, Trevelyan J. McKinley, Mark Sheppard, Sarra Achouri, et al. 2012. "Dynamics of Salmonella Infection of Macrophages at the Single Cell Level." *Journal of the Royal Society, Interface / the Royal Society* 9 (75): 2696–2707.
- González-López, Marco Antonio, Norma Velázquez-Guadarrama, María Elena Romero-Espejel, and José de Jesús Olivares-Trejo. 2013. "Helicobacter Pylori Secretes the Chaperonin GroEL (HSP60), Which Binds Iron." *FEBS Letters* 587 (12): 1823–28.
- Hamon, Mélanie Anne, David Ribet, Fabrizia Stavru, and Pascale Cossart. 2012. "Listeriolysin O: The Swiss Army Knife of Listeria." *Trends in Microbiology* 20 (8): 360–68.
- Henry, Thomas, Carole Couillault, Patrick Rockenfeller, Emmanuel Boucrot, Audrey Dumont, Nina Schroeder, Aurélie Hermant, et al. 2006. "The Salmonella Effector Protein PipB2 Is a Linker for Kinesin-1." *Proceedings of the National Academy of Sciences of the United States of America* 103 (36): 13497–502.
- Hensel, M., J. E. Shea, S. R. Waterman, R. Mundy, T. Nikolaus, G. Banks, A. Vazquez-Torres, C. Gleeson, F. C. Fang, and D. W. Holden. 1998. "Genes Encoding Putative Effector Proteins of the Type III Secretion System of Salmonella Pathogenicity Island 2 Are Required for Bacterial Virulence and Proliferation in Macrophages." *Molecular Microbiology* 30 (1): 163–74.
- Hutagalung, Alex H., and Peter J. Novick. 2011. "Role of Rab GTPases in Membrane Traffic and Cell Physiology." *Physiological Reviews* 91 (1): 119–49.
- Jackson, Laurie K., Parwez Nawabi, Cristiana Hentea, Everett A. Roark, and Kasturi Haldar. 2008. "The Salmonella Virulence Protein SifA Is a G Protein Antagonist." *Proceedings of the National Academy of Sciences of the United States of America* 105 (37): 14141–46.

- Jones, Rheinallt M., Huixia Wu, Christy Wentworth, Liping Luo, Lauren Collier-Hyams, and Andrew S. Neish. 2008. "Salmonella AvrA Coordinates Suppression of Host Immune and Apoptotic Defenses via JNK Pathway Blockade." *Cell Host & Microbe* 3 (4): 233–44.
- Knodler, Leigh A., Bruce A. Vallance, Jean Celli, Seth Winfree, Bryan Hansen, Marinieve Montero, and Olivia Steele-Mortimer. 2010. "Dissemination of Invasive Salmonella via Bacterial-Induced Extrusion of Mucosal Epithelia." *Proceedings of the National Academy of Sciences of the United States of America* 107 (41): 17733–38.
- Knodler, Leigh A., Seth Winfree, Dan Drecktrah, Robin Ireland, and Olivia Steele-Mortimer. 2009. "Ubiquitination of the Bacterial Inositol Phosphatase, SopB, Regulates Its Biological Activity at the Plasma Membrane." *Cellular Microbiology* 11 (11): 1652–70.
- Kyei, George B., Isabelle Vergne, Jennifer Chua, Esteban Roberts, James Harris, Jagath R. Junutula, and Vojo Deretic. 2006. "Rab14 Is Critical for Maintenance of Mycobacterium Tuberculosis Phagosome Maturation Arrest." *The EMBO Journal* 25 (22): 5250–59.
- McCaig, William D., Antonius Koller, and David G. Thanassi. 2013. "Production of Outer Membrane Vesicles and Outer Membrane Tubes by Francisella Novicida." *Journal of Bacteriology* 195 (6): 1120–32.
- McShan, Andrew C., Asokan Anbanandam, Sikta Patnaik, and Roberto N. De Guzman. 2016. "Characterization of the Binding of Hydroxyindole, Indoleacetic Acid, and Morpholinoaniline to the Salmonella Type III Secretion System Proteins SipD and SipB." *ChemMedChem* 11 (9): 963–71.
- Mesmin, Bruno, Joëlle Bigay, Joël Polidori, Denisa Jamecna, Sandra Lacas-Gervais, and Bruno Antony. 2017. "Sterol Transfer, PI4P Consumption, and Control of Membrane Lipid Order by Endogenous OSBP." *The EMBO Journal* 36 (21): 3156–74.
- Monack, D. M., B. Raupach, A. E. Hromockyj, and S. Falkow. 1996. "Salmonella Typhimurium Invasion Induces Apoptosis in Infected Macrophages." *Proceedings of the National Academy of Sciences of the United States of America* 93 (18): 9833–38.
- Nawabi, Parwez, Drew M. Catron, and Kasturi Haldar. 2008. "Esterification of Cholesterol by a Type III Secretion Effector during Intracellular Salmonella Infection." *Molecular Microbiology* 68 (1): 173–85.
- Nesvizhskii, Alexey I. 2012. "Computational and Informatics Strategies for Identification of Specific Protein Interaction Partners in Affinity Purification Mass Spectrometry Experiments." *Proteomics* 12 (10): 1639–55.
- Nguyen, Ngan N. T., Yun-Sook Lim, Lap P. Nguyen, Si C. Tran, Trang T. D. Luong, Tram T. T. Nguyen, Hang T. Pham, et al. 2018. "Hepatitis C Virus Modulates Solute Carrier Family 3 Member 2 for Viral Propagation." *Scientific Reports* 8 (1): 15486.
- Ohlson, Maikke B., Zhiwei Huang, Neal M. Alto, Marie-Pierre Blanc, Jack E. Dixon, Jijie Chai, and Samuel I. Miller. 2008. "Structure and Function of Salmonella SifA Indicate That Its Interactions with SKIP, SseJ, and RhoA Family GTPases Induce Endosomal Tubulation." *Cell Host & Microbe* 4 (5): 434–46.

- Perez-Riverol, Yasset, Attila Csordas, Jingwen Bai, Manuel Bernal-Llinares, Suresh Hewapathirana, Deepti J. Kundu, Avinash Inuganti, et al. 2019. "The PRIDE Database and Related Tools and Resources in 2019: Improving Support for Quantification Data." *Nucleic Acids Research* 47 (D1): D442–50.
- Pierson, Tony, Demetrios Matrakas, Yuka U. Taylor, Ganiraju Manyam, Victor N. Morozov, Weidong Zhou, and Monique L. van Hoek. 2011. "Proteomic Characterization and Functional Analysis of Outer Membrane Vesicles of *Francisella Novicida* Suggests Possible Role in Virulence and Use as a Vaccine." *Journal of Proteome Research* 10 (3): 954–67.
- Pilar, Ana Victoria C., Sarah A. Reid-Yu, Colin A. Cooper, David T. Mulder, and Brian K. Coombes. 2012. "GogB Is an Anti-Inflammatory Effector That Limits Tissue Damage during *Salmonella* Infection through Interaction with Human FBXO22 and Skp1." *PLoS Pathogens* 8 (6): e1002773.
- Poh, John, Charlotte Odendall, Ad Spanos, Cliona Boyle, Mei Liu, Paul Freemont, and David W. Holden. 2008. "SteC Is a *Salmonella* Kinase Required for SPI-2-Dependent F-Actin Remodelling." *Cellular Microbiology* 10 (1): 20–30.
- Rzomp, Kimberly A., Luella D. Scholtes, Benjamin J. Briggs, Gary R. Whittaker, and Marci A. Scidmore. 2003. "Rab GTPases Are Recruited to Chlamydial Inclusions in Both a Species-Dependent and Species-Independent Manner." *Infection and Immunity* 71 (10): 5855–70.
- Santos, José Carlos, Magalie Duchateau, Jennifer Fredlund, Allon Weiner, Adeline Mallet, Christine Schmitt, Mariette Matondo, Véronique Hourdel, Julia Chamot-Rooke, and Jost Enninga. 2015. "The COPII Complex and Lysosomal VAMP7 Determine Intracellular *Salmonella* Localization and Growth." *Cellular Microbiology* 17 (12): 1699–1720.
- Schaller, Lena, and Volker M. Lauschke. 2019. "The Genetic Landscape of the Human Solute Carrier (SLC) Transporter Superfamily." *Human Genetics* 138 (11-12): 1359–77.
- Schleker, Sylvia, Jingchun Sun, Balachandran Raghavan, Matthew Srnec, Nicole Müller, Mary Koepfinger, Leelavati Murthy, Zhongming Zhao, and Judith Klein-Seetharaman. 2012. "The Current *Salmonella*-Host Interactome." *PROTEOMICS--Clinical Applications* 6 (1-2): 117–33.
- Selkrig, Joel, Nan Li, Jacob Bobonis, Annika Hausmann, Anna Sueki, Haruna Imamura, Bachir El Debs, et al. 2018. "Spatiotemporal Proteomics Uncovers Cathepsin-Dependent Host Cell Death during Bacterial Infection." *bioRxiv*. <https://doi.org/10.1101/455048>.
- Singh, Kshipra, Nicole T. Al-Greene, Thomas G. Verriere, Lori A. Coburn, Mohammad Asim, Daniel P. Barry, Margaret M. Allaman, et al. 2016. "The L-Arginine Transporter Solute Carrier Family 7 Member 2 Mediates the Immunopathogenesis of Attaching and Effacing Bacteria." *PLoS Pathogens* 12 (10): e1005984.
- Sontag, Ryan L., Ernesto S. Nakayasu, Roslyn N. Brown, George S. Niemann, Michael A. Sydor, Octavio Sanchez, Charles Ansong, et al. 2016. "Identification of Novel Host Interactors of Effectors Secreted by *Salmonella* and *Citrobacter*." *mSystems* 1 (4). <https://doi.org/10.1128/mSystems.00032-15>.

- Stein, Mary-Pat, Matthias P. Müller, and Angela Wandinger-Ness. 2012. “Bacterial Pathogens Commandeer Rab GTPases to Establish Intracellular Niches.” *Traffic* 13 (12): 1565–88.
- Stévenin, Virginie, Yuen-Yan Chang, Yoann Le Toquin, Magalie Duchateau, Quentin Gai Gianetto, Chak Hon Luk, Audrey Salles, et al. 2019. “Dynamic Growth and Shrinkage of the Salmonella-Containing Vacuole Determines the Intracellular Pathogen Niche.” *Cell Reports* 29 (12): 3958–73.e7.
- Szklarczyk, Damian, Annika L. Gable, David Lyon, Alexander Junge, Stefan Wyder, Jaime Huerta-Cepas, Milan Simonovic, et al. 2019. “STRING v11: Protein-Protein Association Networks with Increased Coverage, Supporting Functional Discovery in Genome-Wide Experimental Datasets.” *Nucleic Acids Research* 47 (D1): D607–13.
- Takahashi-Kanemitsu, Atsushi, Christopher T. Knight, and Masanori Hatakeyama. 2020. “Molecular Anatomy and Pathogenic Actions of Helicobacter Pylori CagA That Underpin Gastric Carcinogenesis.” *Cellular & Molecular Immunology* 17 (1): 50–63.
- Teng, Ben, Can Zhao, Xiaoqing Liu, and Zengyou He. 2015. “Network Inference from AP-MS Data: Computational Challenges and Solutions.” *Briefings in Bioinformatics* 16 (4): 658–74.
- Trouplin, Virginie, Nicolas Boucherit, Laurent Gorvel, Filippo Conti, Giovanna Mottola, and Eric Ghigo. 2013. “Bone Marrow-Derived Macrophage Production.” *Journal of Visualized Experiments: JoVE*, no. 81 (November): e50966.
- Verschueren, Erik, John Von Dollen, Peter Cimermancic, Natali Gulbahce, Andrej Sali, and Nevan J. Krogan. 2015. “Scoring Large-Scale Affinity Purification Mass Spectrometry Datasets with MiST.” *Current Protocols in Bioinformatics / Editorial Board, Andreas D. Baxevanis ... [et Al.]* 49 (March): 8.19.1–8.19.16.
- Walch, Philipp, Joel Selkrig, Leigh A. Knodler, Mandy Rettel, Frank Stein, Keith Fernandez, Cristina Viéitez, et al. 2020. “Global Mapping of Salmonella Enterica-Host Protein-Protein Interactions during Infection.” *Cold Spring Harbor Laboratory*. <https://doi.org/10.1101/2020.05.04.075937>.
- Wasylnka, Julie A., Malina A. Bakowski, Jason Szeto, Maikke B. Ohlson, William S. Trimble, Samuel I. Miller, and John H. Brumell. 2008. “Role for Myosin II in Regulating Positioning of Salmonella-Containing Vacuoles and Intracellular Replication.” *Infection and Immunity* 76 (6): 2722–35.
- Yang, Chun-Kai, Hosam E. Ewis, Xiaozhou Zhang, Chung-Dar Lu, Hae-Jin Hu, Yi Pan, Ahmed T. Abdelal, and Phang C. Tai. 2011. “Nonclassical Protein Secretion by Bacillus Subtilis in the Stationary Phase Is Not due to Cell Lysis.” *Journal of Bacteriology* 193 (20): 5607–15.
- Zhao, Weidong, Thomas Moest, Yaya Zhao, Aude-Agnès Guilhon, Christophe Buffat, Jean-Pierre Gorvel, and Stéphane Méresse. 2015. “The Salmonella Effector Protein SifA Plays a Dual Role in Virulence.” *Scientific Reports* 5 (August): 12979.

Chapter IV

Biological implications of identified effector-target interactions

Chapter IV: Biological implications of identified effector-target interactions

1. Summary

To illustrate the utility of our new PPI dataset as a resource for discovering novel infection biology and to further characterize some of the underlying interactions, I present here two vignettes on the interplay between *Salmonella* and host cells. Firstly, I show that the *Salmonella* effectors SifA, SseJ and SseL cooperate to control cholesterol transport at the *Salmonella* Containing Vacuole (SCV). This process was linked to *Salmonella* infection through PPIs with multiple host factors, and I will highlight the interactions with the Niemann-Pick C1 protein (NPC1) and Oxysterol-binding protein (OSBP). Secondly, I elucidate a novel mechanism by which the STm kinase SteC promotes host actin-bundling *via* direct interaction and phosphorylation of formin-like proteins. A third vignette, which is not presented in this work, concerns the interaction of PipB with the organelle contact site protein PDZD8 (Figure IV.1, (Walch et al. 2020)). Our collaborator Dr. Leigh Knodler uncovered that PipB directly binds and recruits PDZD8 to the SCV and further identified the domains within both proteins that are essential for this interaction.

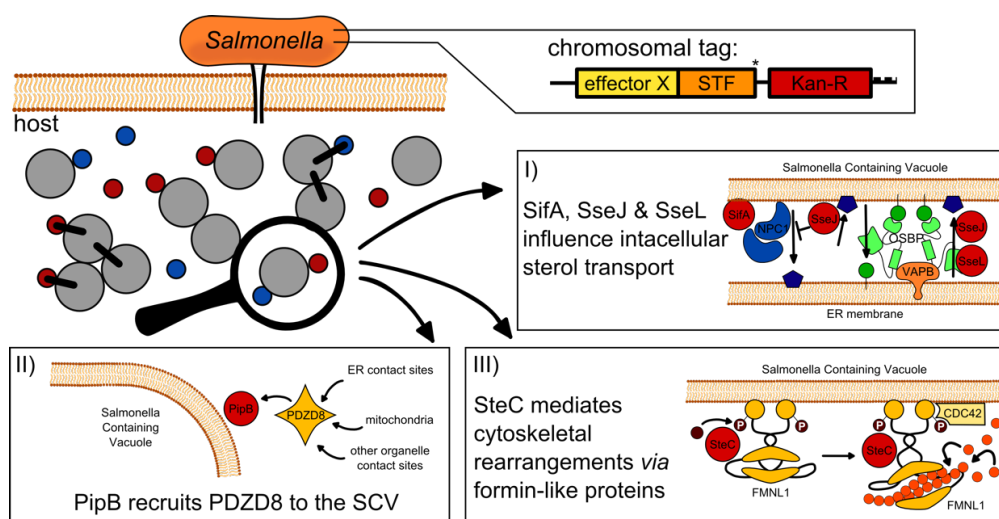


Figure IV.1 Graphical abstract of the chapter. To showcase the biological relevance of the AP/QMS dataset obtained through infection with a library of STm strains endogenously expressing affinity-tagged effectors, we characterized three aspects of novel biology: (I) studying the role of the effectors SifA, SseJ and SseL in cholesterol transport; (II) resolving the interaction between PipB and its host target PDZD8; and (III) delineating the missing link (formin-like proteins) in the role of SteC on actin-bundling. This chapter covers vignettes I) and III) in detail. II) is described in (Walch et al. 2020).

2. Contributions

Experimental work for the separate TMT-run was performed by me, followed by MS-sample preparation by Mandy Rettel and initial MS-data analysis by Dr. Frank Stein. Subsequent analysis and visualization were conducted by myself. All experimentation related to NPC1-localization and filipin staining was performed by me, with input from Dr. Joel Selkrig, Dr. Magdalena Zimoń and Dr. Leigh Knodler. NPC1-knockout cell lines were provided by Dr. Willem Annaert (VIB, KU-Leuven). Confocal microscopy was performed at the EMBL ALMF together with Dr. Joel Selkrig.

SteC purified by Dr. Joel Selkrig and FMNL1 and FMNL2 constructs were provided by Dr. Klemens Rottner. SEC was performed together with Dr. Joel Selkrig, using equipment and size standards provided by the Müller group at EMBL Heidelberg. The *in vitro* kinase assay was conducted in collaboration with Dr. Cristina Viéitez and Dr. Joel Selkrig, phosphoproteomics (mass spectrometry and data analysis) was done by Dr. Clement Potel. Actin bundling infection experiments and imaging were conducted by myself using cell lines provided by Dr. Klemens Rottner and Dr. Frieda Kage. The work described in this chapter is, alongside the third biological vignette on the characterization of the interaction between PipB and PDZD8, is part of the following published preprint (bioRxiv), which is currently under revision at Cell Host&Microbe:

Walch, Philipp, Joel Selkrig, Leigh A. Knodler, Mandy Rettel, Frank Stein, Keith Fernandez, Cristina Viéitez, et al. 2020. “Global Mapping of Salmonella Enterica-Host Protein-Protein Interactions during Infection.” *bioRxiv*, Cold Spring Harbor Laboratory. <https://doi.org/10.1101/2020.05.04.075937>.

3. SseL and SseJ influence cholesterol trafficking

In the AP/QMS work, STm effectors repeatedly interacted with host proteins that are mediating lipid trafficking. This was reflected in GO-term enrichments, which included: “positive regulation of vesicle fusion” (p-value = $1.25 \cdot 10^{-3}$) and “phospholipid metabolic process” (p-value = $2.78 \cdot 10^{-2}$) in RAW264.7 or “regulation of vesicle-mediated transport” (p-value = $3.86 \cdot 10^{-5}$) in HeLa cells. Lipid trafficking stands out among other biological processes due to its central role in several other downstream processes, such as immune response, protein recruitment and organelle organization (Walpole, Grinstein, and Westman 2018; Lau et al. 2019). In addition to their role in cellular signaling, lipids play a vital role in changing the biological properties of cell membranes (Harayama and Riezman 2018). This has been shown to impact the ability of intracellular pathogens to enter their host cells (Lafont and van der Goot 2005; Brandstaetter, Kendrick-Jones, and Buss 2012; Hume et al. 2017). Furthermore, once inside the cell, various bacterial and viral pathogens have been implicated in altering host lipid trafficking for protection of their replication niche (Catron et al. 2002; Knodler and Steele-Mortimer 2003; Mallo et al. 2008; Bakowski et al. 2010; Altan-Bonnet 2017).

NPC1, OSBP, SACM1L, VAP-A and VAP-B were among the most prominently pulled down proteins, and have all previously been described to be involved in cholesterol transport (Mesmin et al. 2017; Pfeffer 2019). Interactions with these proteins originated mainly from PipB2, SseL and SseJ, and were apparent in both cell lines, as discussed in Chapter III subsection 4.3 and displayed in Figure III.4. While I saw no physical effector-effector interactions related to lipid trafficking, I noticed a strong convergence of multiple STm effectors on proteins involved in lipid and more specifically cholesterol trafficking.

3.1. Effector-effector interactions and functional cooperation are prominent around host intracellular cholesterol trafficking

I first sought to increase the resolution of interactions between SseJ and its host targets involved in cholesterol transport, as SseJ is known to esterify cholesterol (Nawabi, Catron, and Haldar 2008). Additionally, the PPIs detected in the AP/QMS work suggested this effector plays an essential role in cholesterol trafficking. In order to increase the sensitivity and enable the detection of lowly abundant targets and weaker PPIs, I conducted a separate TMT-run, where I combined three biological replicates of SseJ-STF FLAG-IP within the same multiplex, comparing it to a biological triplicate of an untagged control, as well as another STm effector. Thereby, I was able to decrease the complexity of the multiplexed sample by about 3-fold, as instead of diluting each effector-IP 1:10 in the multiplex, the SseJ-IP was only diluted 1:3 in this separate run. I did this in both native and crosslinked conditions, both times with respect to an untagged control. While multiplexing samples in groups of ten enabled the throughput of this study, combining biological replicates in the same run decreases the complexity enough to detect weaker interactions (Figure IV.2A).

Thereby, I was able to recapitulate many of the interactions identified in the large-scale study, e.g. those with NPC1, CD44, OSBP, ATP2B1 and others. Additionally, the detected FC and significance were strongly enhanced due to the decreased dilution. Besides, I detected effector-effector interactions between SseJ and SseL, as well as SseJ and SteC after crosslinking (Figure IV.2A). These interactions could be direct or through one of their common host targets. Nevertheless, this finding further underlines the importance of effector-effector cooperation. The observation that SseJ and SseL co-precipitate is in line with a recent study showing that SseJ and SseL both target OSBP (Kolodziejek et al. 2019), which links and fuels the cholesterol-PI4P exchange between the ER and the Golgi network (Mesmin et al. 2017).

Kolodziejek *et al.* also highlighted the importance of OSBP, as well as VAP-A and -B in maintaining the stability of the SCV (Kolodziejek et al. 2019). Consistently, SseL interacted with OSBP, VAP-A, VAP-B, SACM1L and PI4K2A, all of which are involved in the cholesterol-PI4P antiport and have been linked to maintaining the replicative niche during infection (Amini-Bavil-Olyaei et al. 2013; Roulin et al. 2014; Albulescu et al. 2015). In addition, I detected a reproducibly strong interaction between SseJ and NPC1, the Niemann-Pick disease type C1 protein (Figure IV.2A). The role of this protein is the recycling of cholesterol from the endosomes to the ER, and its absence leads to an aberrant cholesterol distribution in the cell (Pfeffer 2019).

Dissecting the host-pathogen interface during *Salmonella* infection

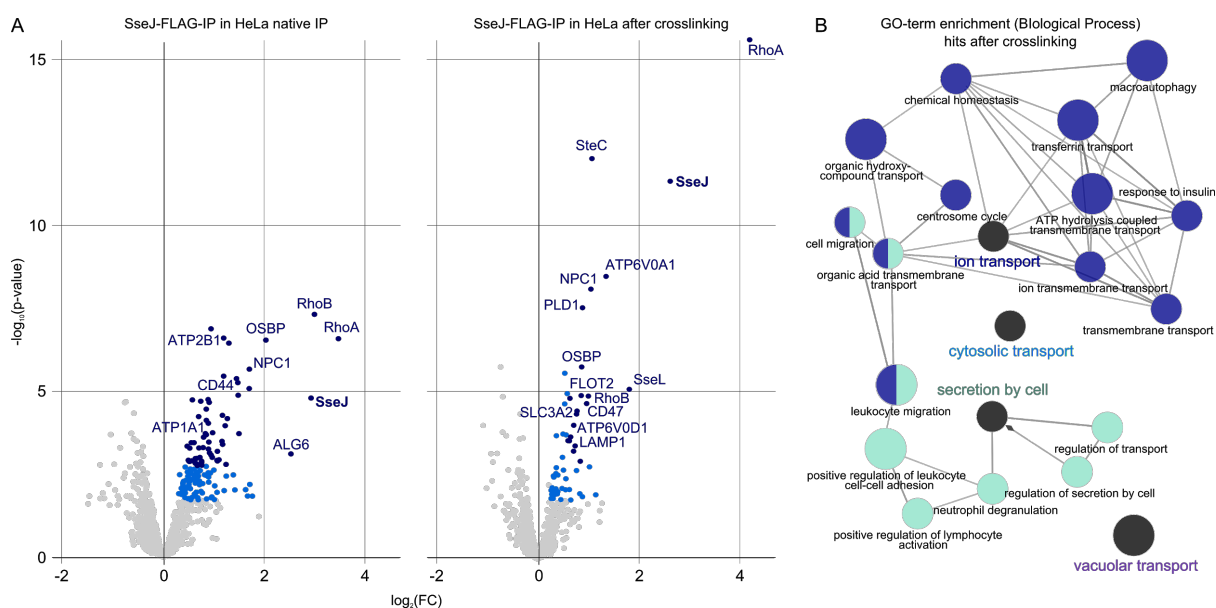


Figure IV.2 Increased resolution of the SseJ-interactome during infection of HeLa cells. (A) Volcano plots displaying the enrichments obtained through native (left) and crosslinked (right) IP on SseJ-STF in HeLa cells 20 hpi with respect to an untagged control. All three replicates were analyzed and measured in the same TMT-10plex run. Proteins with $FC > 1.5$, $fdr < 0.001$ (dark blue), proteins with $FC > 1.2$, $fdr < 0.01$ (light blue) are colored distinctly from all other proteins (grey). The bait, as well as several known, recurring and other highly enriched proteins, are displayed by name. After crosslinking, the STm effectors SseL and SteC co-precipitate with SseJ. (B) GO-term enrichment (Biological Process) using the hits obtained from IP after crosslinking. GO-term fusion and grouping were used, GO-terms associated with the same GO-term group are colored in the same color and the leading GO-term is displayed in dark grey. Panel A has been adapted from Figure 5A in (Walch et al. 2020).

3.2. NPC1 localizes to the SCV during STm infection in SifA-dependent manner

To assess whether there is effector-dependent recruitment of NPC1 to the SCV during infection, we infected HeLa cells with a variety of STm strains: wildtype, *sseJ* and *sseL* knockout mutants ($\Delta sseJ$ and $\Delta sseL$), a double mutant ($\Delta sseJ\Delta sseL$) and a *sifA* mutant ($\Delta sifA$), using an NPC1 knockout HeLa cell line as negative control. At 20 hpi, we performed immunofluorescence using an antibody against endogenous NPC1 and acquired confocal images of the SCV, using LAMP1 as a marker for the intracellular replication compartment.

STm was capable of recruiting NPC1 in wildtype HeLa cells, while, as expected, no NPC1 could be detected in the negative (NPC1-K.O.) control (Figure IV.3). Interestingly, despite SseJ having consistently shown interaction with NPC1, both the $\Delta sseJ$ and the $\Delta sseJ\Delta sseL$ mutants were able to recruit NPC1 to the SCV. This indicates that the interaction between SseJ and NPC1 does not cause its recruitment to the SCV, but may be of other functional nature. It is known that $\Delta sifA$ STm displays reduced vacuolar stability and consequently an increased escape into the host cytoplasm upon infection (Beuzón et al. 2000; Brumell et al. 2001). We hypothesized that SifA may be needed for the recruitment of NPC1 to the SCV, as SifA functions in the recruitment of endosomal vesicles to the SCV through the formation of SIFs (Ohlson et al. 2008; Dumont et al. 2010; Zhao et al. 2015; Knuff and Finlay 2017). Indeed, recruitment of NPC1 to the STm microcolony was abolished both for vacuolar (LAMP1-positive) $\Delta sifA$ STm and for cytosolic (LAMP1-negative) $\Delta sifA$ STm (Figure

IV.3) – the latter as expected. This indicates that SifA plays a crucial role in recruiting NPC1 to the SCV. As I did not identify NPC1 as an interaction partner of SifA, this recruitment likely occurs indirectly, e.g. through redirecting host phagolysosomal membranes containing NPC1 to the SCV via the lysosomal adapter protein PLEKHM1 (McEwan et al. 2015), rather than a direct protein-protein interaction.

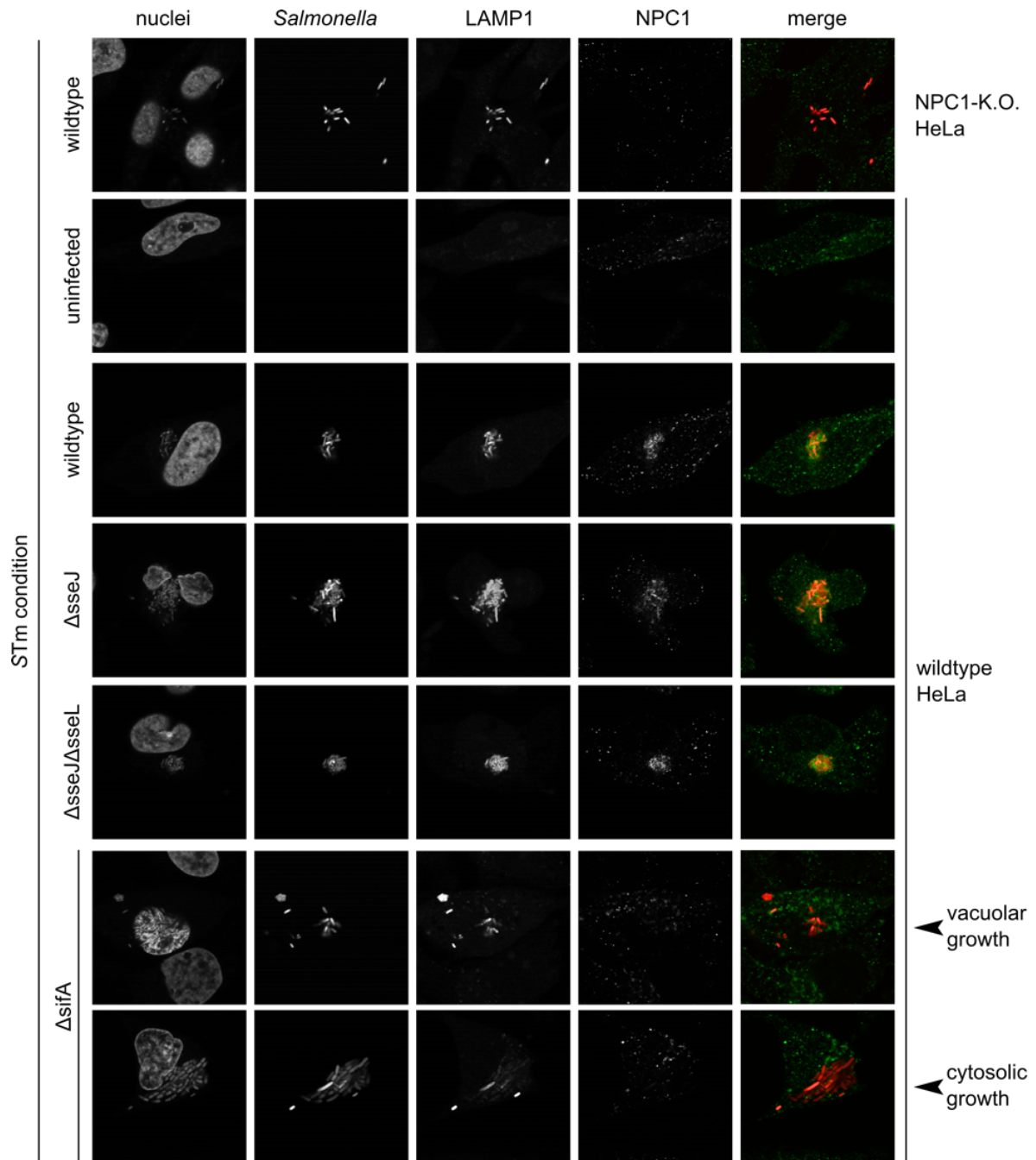


Figure IV.3 Confocal immunofluorescence microscopy images (60x magnification) to assess the recruitment of NPC1 to the SCV in various STm mutant conditions at 12 hpi. Wildtype and NPC1-K.O. HeLa cells were infected with a panel of STm mutants constitutively expressing mCherry. At 12 hpi, cells were fixed, stained with DAPI, permeabilized with saponin and immunofluorescence for the SCV-marker LAMP1, as well as for NPC1 was conducted. The merge shows STm in red and NPC1 in green. *This figure will be part of a revised version of (Walch et al. 2020).*

To quantify the degree of colocalization of NPC1 with the SCV, I additionally performed widefield microscopy, confirming the findings obtained in confocal imaging (Figure IV.4A). Due to the larger number of cells per field of view, widefield images allow for a more straightforward and unbiased calculation of colocalization. To do so, I calculated a colocalization score:

$$\text{colocalization score} = \frac{\text{mean intensity}(\text{NPC1}).\text{Salmonella}}{\text{mean intensity}(\text{NPC1}).\text{host cell}}$$

where the numerator is given by the NPC1 signal at the STm site:

$$\text{mean intensity}(\text{NPC1}).\text{Salmonella} = \frac{\text{integrated intensity}(\text{NPC1}).\text{Salmonella}}{\text{area}(\text{Salmonella})}$$

and the denominator by the overall NPC1 signal throughout the cell:

$$\text{mean intensity}(\text{NPC1}).\text{host cell} = \frac{\text{integrated intensity}(\text{NPC1}).\text{host cell}}{\text{area}(\text{host cell})}$$

In order to calculate these, binary masks for host cells, as well as STm in the SCV were generated by background correction and subsequent image segmentation. This is described in more detail in section VII.20. A colocalization score of 1 therefore indicates a random distribution of NPC1 throughout the cell, while co-localization results in values larger than 1, and active exclusion of NPC1 from the SCV in values smaller than 1.

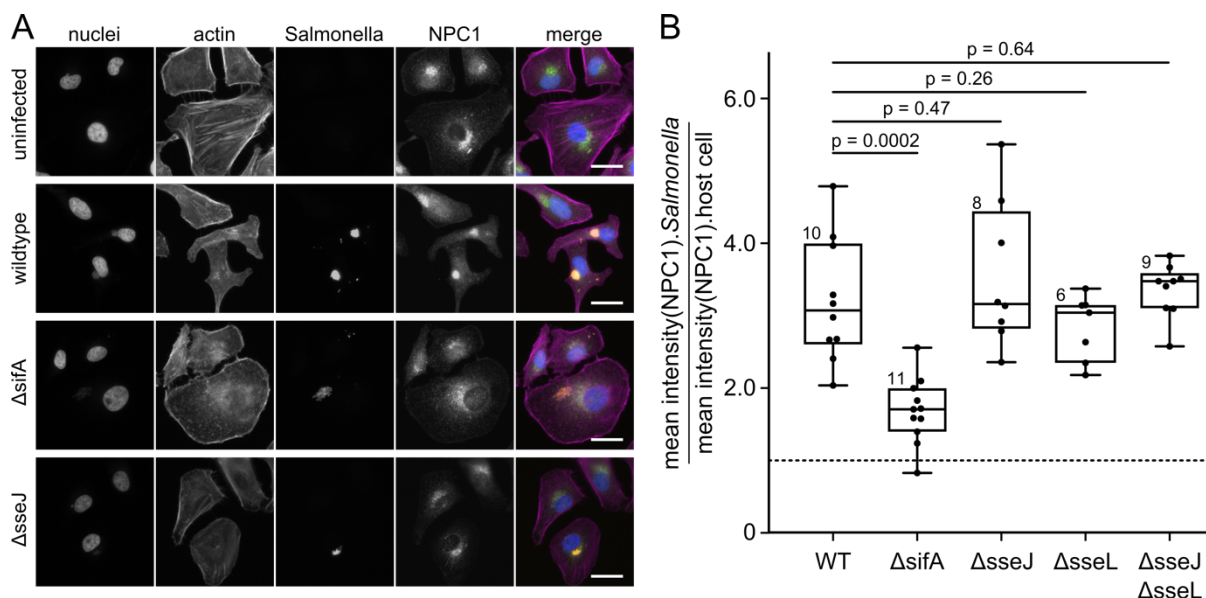


Figure IV.4 Widefield immunofluorescence images and quantification of colocalization between NPC1 and the SCV. (A) Exemplary widefield microscopy images after infection with a panel of STm mutants for 12 hours. Cells were fixed, stained with DAPI (blue) and phalloidin (purple) and immunofluorescence for NPC1 (green) was conducted to assess colocalization of the host protein with intracellular STm (orange). The merge displays the overlay of all channels. (B) Quantification (colocalization score of NPC1 signal with STm) of a total of 44 fields of view across five STm strains. Boxplots display median with interquartile range and whiskers indicate the range between minimum and maximum. Two-tailed T-test with Welch correction was performed to calculate p-values (displayed) and assess significance. $\Delta sifA$ displays the only significant deviation in NPC1-accumulation at the STm site. Panel B will be part of a revised version of (Walch et al. 2020).

By applying this quantification to the widefield images, I was able to confirm the absence of NPC1 at the SCV specifically in $\Delta sifA$ STm, while neither of the other mutant conditions that were assessed significantly reduced the recruitment of NPC1 (Figure IV.4B). The finding that NPC1 is recruited to the SCV during infection is in line with previous reports (Smith et al. 2007; Drecktrah et al. 2008). Here, I was also able to determine that this colocalization is dependent on the STm effector protein SifA.

3.3. The presence of cholesterol at the SCV depends on SifA, SseJ and SseL

Consequently, I hypothesized that the impact of SseJ and SseL on the rewiring of lipid trafficking is linked to NPC1, subsequent to its SifA-dependent recruitment to the SCV. This would be in line with NPC1's known function in recycling cholesterol. To test this hypothesis and expand the knowledge about the roles of these effectors, I infected wildtype and NPC1-KO HeLa cells with a panel of STm mutants ($\Delta sseJ$, $\Delta sseL$, $\Delta sseJ\Delta sseL$, $\Delta sifA$) and stained with filipin 12 hpi. Filipin III is a polyene discovered in *Streptomyces filipinensis*, which binds cholesterol (Bittman and Fischkoff 1972) and is commonly used to probe for the distribution of cholesterol within the cell (Maxfield and Wüstner 2012; Wilhelm et al. 2019).

By using a fluorescent reporter to visualize STm (mCherry) and staining the cell area (CellMask, deep red), as well as LAMP1 using a specific antibody (Alexa Fluor 488), I was able to assess the presence of cholesterol throughout the cell and at the SCV. I observed colocalization of cholesterol and the SCV (Figure IV.5A) which was most strongly pronounced when infecting with wildtype STm. Furthermore, I observed the previously described, aberrant localization of cholesterol in NPC1-KO cells, which manifests in sharp puncti of filipin signal, originating from cholesterol being trapped in the endosomes (Tharkeshwar et al. 2017) (Figure IV.5B).

In the microscopy images (Figure IV.5A), I noticed decreased degrees of cholesterol accumulation at the SCV in several STm-host combinations. In order to quantify this in an unbiased way, I adapted the calculation outlined in chapter 3.2. by replacing the NPC1-signal with the filipin signal:

$$colocalization\ score = \frac{mean\ intensity(filipin). (Salmonella \cap LAMP1)}{mean\ intensity(filipin). host\ cell}$$

where both the numerator (filipin signal at the STm site mask, overlapped with LAMP1 mask to exclude cytosolic STm microcolonies) and the denominator (filipin signal throughout the cell mask) were calculated as before using binary masks for STm, LAMP1 and the cell. Again, a colocalization score of 1 indicates a random distribution of cholesterol throughout the cell. While infection of wildtype HeLa with wildtype STm resulted in a median score of 2.63, this was significantly reduced in infection with $\Delta sseJ$ bacteria (median = 1.83). The $\Delta sseL$ mutant also showed a mild reduction in colocalization (median = 2.07). The $\Delta sseJ\Delta sseL$ double mutant reduced colocalization to levels slightly lower than a $\Delta sseJ$ mutant (median = 1.64). Strikingly, the strongest reduction occurred in the $\Delta sifA$ mutant, where colocalization of filipin and the SCV was

the lowest observed (median = 1.43, Figure IV.5C), indicating that SseJ and SifA are in fact the main drivers of cholesterol accumulation at the SCV. In the case of $\Delta sifA$, the most likely explanation is that the STm effector plays a crucial role in the recruitment of endolysosomal membranes, which are rich in cholesterol, as described above.

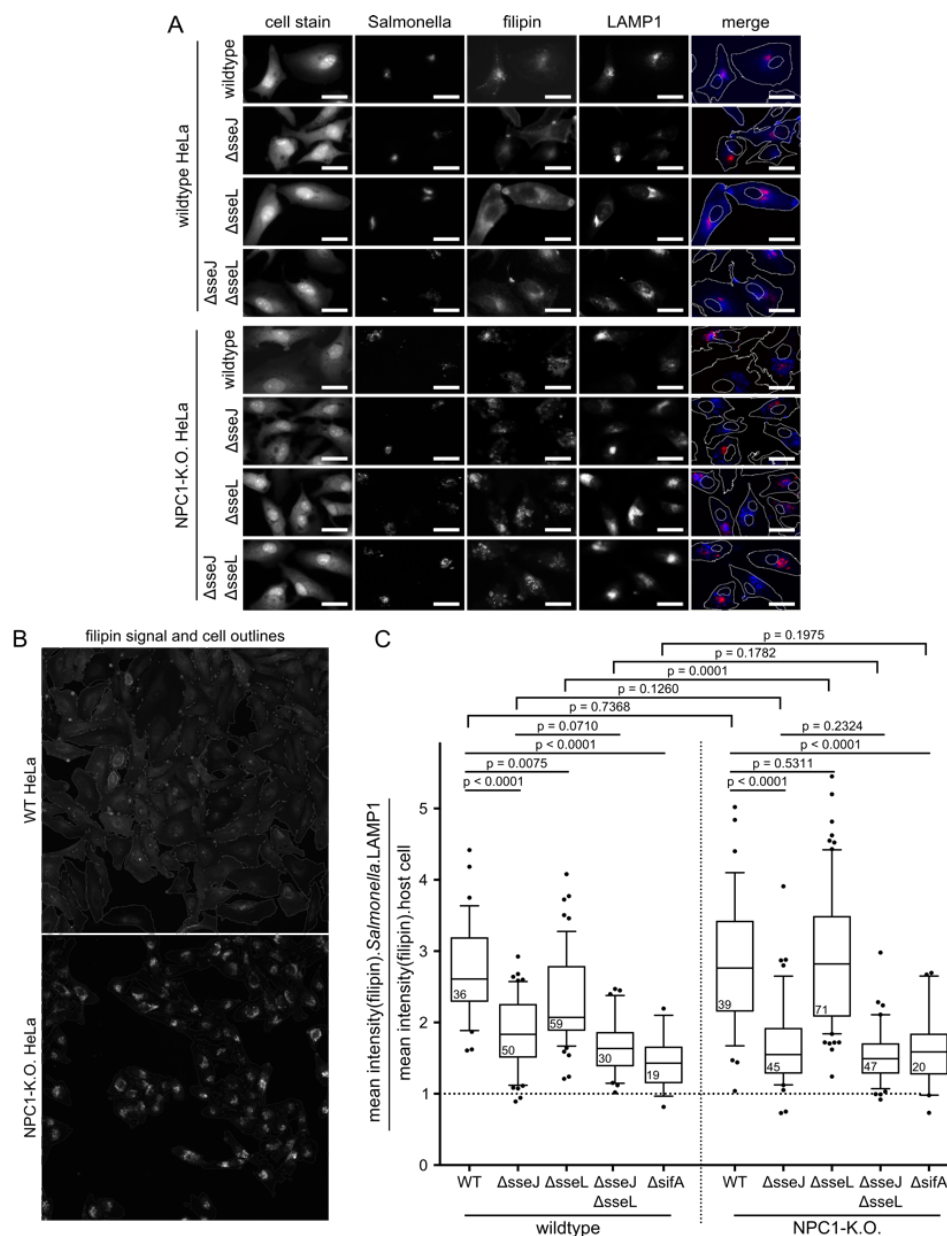


Figure IV.5 Microscopy images of WT and NPC1-KO HeLa cells infected with different STm mutants and stained with filipin 12 hpi. (A) Images of wildtype and NPC1-K.O. HeLa cells were acquired with 20x magnification. CellMask stain is shown in grey, STm in red, filipin in blue and LAMP1 in green. The merge summarizes STm and filipin channels with cell periphery and nuclei (outlines). Scale bar denotes 30 μ m. (B) Microscopy images (20x magnification) of uninfected HeLa wildtype cells (upper panel) and NPC1-K.O. HeLa cells (lower panel) stained for the distribution of cholesterol using filipin. The filipin channel, as well as the cell outlines are shown. (C) To quantify the filipin-staining images, the ratio of filipin signal within the area of the intracellular, vacuolar STm to the overall filipin signal throughout the cell was calculated for a total of 416 fields of view (each one containing on average 20 infected cells). Distribution of colocalization scores in each condition is displayed as a boxplot (spanning interquartile range with the median as a line) with whiskers (from Q10 to Q90). T-test with Welch correction for unequal variances was performed for statistical analysis and p-values are indicated. *This figure has been adapted from Figure 5 in (Walch et al. 2020).*

In a NPC1-KO host background, wildtype STm were able to mitigate the endosomal accumulation of cholesterol, leading to a colocalization score comparable to the one in wildtype HeLa (median = 2.76). Strikingly, Δ sseL bacteria no longer caused a decrease in cholesterol-SCV colocalization (median = 2.82), indicating that the small impact SseL has on cholesterol trafficking is dependent on the presence of NPC1. On the other hand, the decrease of cholesterol accumulation that I observed for Δ sseJ and Δ sseJ Δ sseL strains remained similar to that observed during infection of wildtype HeLa cells (median = 1.55 and median = 1.49, respectively; Figure IV.5C).

3.4. The OSBP-inhibitor OSW-1 reduces cholesterol accumulation at the SCV

To further unravel the impact of OSBP-mediated cholesterol trafficking in conjunction with STm effector action, I decided to assess the impact of the OSBP-inhibitor OSW-1 (Burgett et al. 2011; Albuлесcu et al. 2015; Mesmin et al. 2017; Roberts et al. 2019) on the cholesterol distribution during infection with various STm mutants. First, I assessed a workable range of concentrations, where OSW-1 does not display a cytotoxic effect on host cells and does not inhibit infection as it had been previously described (Y. Zhou et al. 2005; Albuлесcu et al. 2015; Roberts et al. 2019). To study this, I infected HeLa cells with wildtype STm and, starting from 0 hpi, treated with a concentration series of OSW-1 (ranging from 0.25nM to 128nM). At 20 hpi, I assessed cell viability and infection by microscopy and subsequent analysis in CellProfiler. In line with previous reports on monitoring the effect of OSBP inhibition on cholesterol trafficking (Burgett et al. 2011; Mesmin et al. 2017; Roberts et al. 2019), I determined a concentration of 1 nM (Figure IV.6A).

Next, I infected WT HeLa with different STm mutant strains (WT, Δ sseJ, Δ sseL, Δ sseJ Δ sseL) and, in parallel to *Salmonella* infection (see section VII.10.1), treated the cells with OSW-1, using DMSO in media as control. At 12 hpi, the cells were fixed, stained with CellMask and filipin, imaged on a widefield microscope and colocalization was quantified as described in the previous section. Interestingly, OSW-1 reduced localization of cholesterol at the SCV in all tested STm strains (for WT: median(untreated) = 2.54, median(treated) = 1.81, Figure IV.6). While there were slight differences in colocalization score of the various STm mutants, the dynamic range is reduced so much by OSBP inhibition that additional effects of effector deletion were difficult to discern. This indicates that OSBP is indeed an essential player in promoting cholesterol influx to the SCV during STm infection, which is in line with previous reports of OSBP's function as a cholesterol-PI4P antiporter within the cell and during infection (Auweter et al. 2012; Albuлесcu et al. 2015; Mesmin et al. 2017).

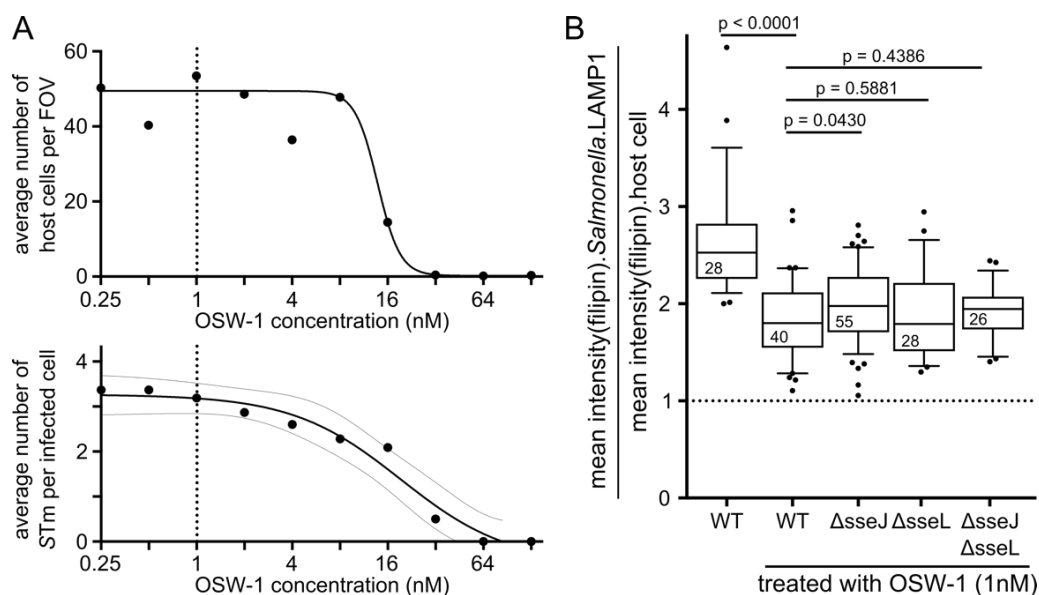


Figure IV.6 Quantification of colocalization between STm and cholesterol after treatment with the OSBP-inhibitor OSW-1. A) Concentration-dependent effect of OSW-1 on host cell viability (quantified as number of cells per field of view after 20-hour treatment, upper graph) and STm infection (quantified by average number of STm per infected cell at 20 hpi, lower graph). X-axis is depicted in log₂-scale and data points were fitted with a sigmoidal curve (4 parameter logistic, implemented in GraphPad Prism, version 7). B) HeLa cells were infected with a panel of STm mutants and, subsequent to infection, treated with 1 nM OSW-1, with DMSO as untreated control. At 12 hpi, cells were fixed and stained for unesterified cholesterol with filipin. Widefield images were acquired and colocalization was quantified as described in the previous sections. n indicates the number of fields of view analyzed for each condition and p-values were calculated with two-sided T-test with Welsh correction.

3.5. Hypothesis on biological action

The findings described in this subchapter suggest a complex and interdependent network underlying cholesterol transport. During infection, SifA, SseJ and SseL, recruit, interact with and modulate several host targets, such as OSBP or NPC1. Thereby, STm actively modulate host processes and alter cholesterol trafficking, which impacts accumulation of cholesterol at the SCV, in turn changing the proteome on the surface of the vacuole. While the interconnectivity of these STm effectors and host pathways is highly complex (Figure IV.7), I can conclude the following points:

- 1) During infection, SifA is required for the recruitment of NPC1 to the SCV. While this does not necessarily occur through a direct PPI, I could show the necessity of SifA presence for NPC1 localization to the vacuole.
- 2) Once at the vacuole, SseJ interacts with NPC1. As NPC1 is exporting cholesterol from the membrane it is bound to (Pfeffer 2019), and as *sseJ* knockout reduces the cholesterol content of the SCV membrane, this interaction is likely inhibiting NPC1 function, which means that one of the roles SseJ plays during infection is the retention of cholesterol at the SCV. This could be (also) due its enzymatic function as a cholesterol acyltransferase.
- 3) SseL and SseJ are required for cholesterol influx to the SCV, this occurs, at least in part, through OSBP, and OSBP-inhibition reduces the cholesterol content of the SCV.

- 4) I hypothesize that SseL is functionally dependent on NPC1, as in NPC1-knockout cells, the cholesterol is retained in the endosomal compartment, making it unavailable for OSBP-mediated transport to the SCV.

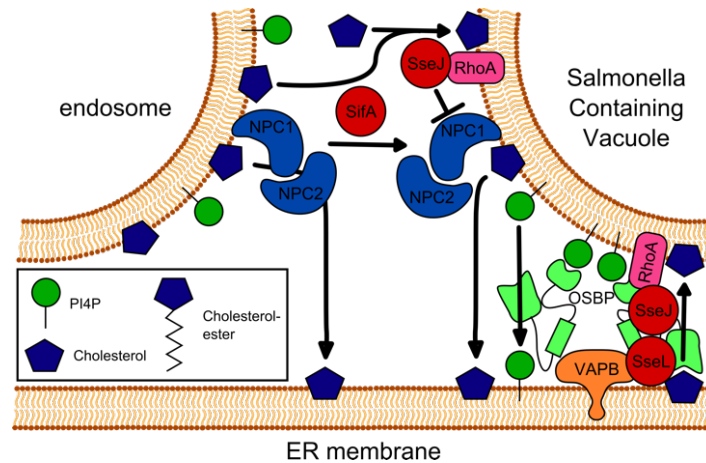


Figure IV.7 The complex interplay of STm effectors and host cell targets. Schematic summarizing the demonstrated interaction points between the pathogen and the host with respect to cholesterol trafficking. STm effectors are shown in red, host targets in various colors (NPC1: blue, OSBP: green, VAPB: orange, RhoA: pink).

Effector deletions have been shown to impact vacuolar stability (Ruiz-Albert et al. 2002; Zhao et al. 2015; Stévenin et al. 2019). It remains to be shown whether STm effectors impact cholesterol trafficking and other processes throughout the infection timeline to actively stabilize or destabilize the vacuole. This has been demonstrated for the early SCV, where several effectors affect membrane trafficking to mediate and maintain the balance between vacuolar and cytosolic lifestyle (Stévenin et al. 2019).

4. SteC modulates actin rearrangements via formin-like proteins

Cytoskeletal rearrangements are of vital importance to STm during infection, first in the early stages for uptake into epithelial cells (D. Zhou et al. 2001; Patel and Galán 2005), and in later stages for maturation and movement of the SCV (Fu and Galán 1998; Odendall et al. 2012). *Salmonella* has been shown to utilize host cytoskeletal structure for various transport processes and several effector proteins play a role in remodeling the cytoskeletal organization (Galan and Zhou 2000). One of these is the STm effector SteC, which can trigger actin bundle formation in close proximity to the SCV. Yet, despite the fact that several interaction partners of SteC have been identified, their impact on actin bundling does not explain the whole extent of the effect exerted by SteC (Poh et al. 2008; Odendall et al. 2012; Fernandez-Piñar et al. 2012). This indicates that there are still missing links between the molecular function of SteC and its biological role during infection.

One of the most consistently recovered PPIs in the dataset is the interaction of the bacterial kinase SteC with the host formin-like protein 1 (FMNL1), which is the main formin-like protein in macrophages (Yayoshi-Yamamoto, Taniuchi, and Watanabe 2000). FMNL1, among other FMNL proteins, plays a central role in cytoskeletal organization (Bai et al. 2011) due to its function as actin nucleator (Dehapiot et al. 2020). In addition to observing the co-purification of SteC and FMNL1 very consistently across cell lines and conditions after IP on SteC-STF, I validated their interaction through reciprocal co-IP in both RAW264.7 and HeLa (as discussed in Chapter III).

4.1. SteC and FMNL1 interact *in vitro*

We then sought to describe this interaction in more detail, and therefore, as a first step, subjected purified SteC (wildtype, full-length), as well as purified SteC_{K256H} (catalytically inactive) to an *in vitro* binding assay with recombinantly expressed FMNL1₁₋₃₈₅ (N-terminal domain), which we received from our collaborator Dr. Klemens Rottner. I analyzed the formation of a higher MW complex by size exclusion chromatography (SEC), in collaboration with Dr. Joel Selkrig.

We observed that SteC, SteC_{K256H}, and FMNL1₁₋₃₈₅ migrated as multimeric protein species prior to pre-incubation together (Figure IV.13A, orange and blue traces). When subjecting the proteins to pre-incubation with each other, the migration behavior changed and we observed a higher MW complex occurring for both, incubation with SteC and SteC_{K256H} (Figure IV.8A, green trace). These results indicate that:

- 1) SteC and the N-terminal domain of FMNL1 form a complex *in vitro* through direct binding
- 2) This interaction is stable enough to be detected through SEC
- 3) This interaction is independent of the catalytic activity of SteC.

Due to the breadth of the retention time peaks in SEC, it is difficult to make conclusive statements about the stoichiometry of these interactions, which all appear to be highly multimeric (MW > 500kDa).

4.2. *In vitro* phosphorylation of FMNL1 by SteC and phosphosite identification via phosphoproteomics

In a second step, I wanted to test the hypothesis whether FMNL1 serves as a direct substrate to SteC. To do so, I performed an *in vitro* phosphorylation assay using [³²P]-γ-ATP and later determined phosphorylation sites on FMNL1 and FMNL2 via phosphoproteomics. This was done in collaboration with Dr. Cristina Viéitez and Dr. Clement Potel.

In the *in vitro* kinase assay, we could recapitulate autophosphorylation on SteC, which had been previously reported (Poh et al. 2008). Furthermore, when incubating SteC together with FMNL1₁₋₃₈₅, FMNL1 was phosphorylated by wildtype SteC, but not by the catalytically inactive SteC_{K256H} (Figure IV.8B). This underlines that FMNL1 serves as a direct substrate of SteC and can be phosphorylated without the need of other cofactors.

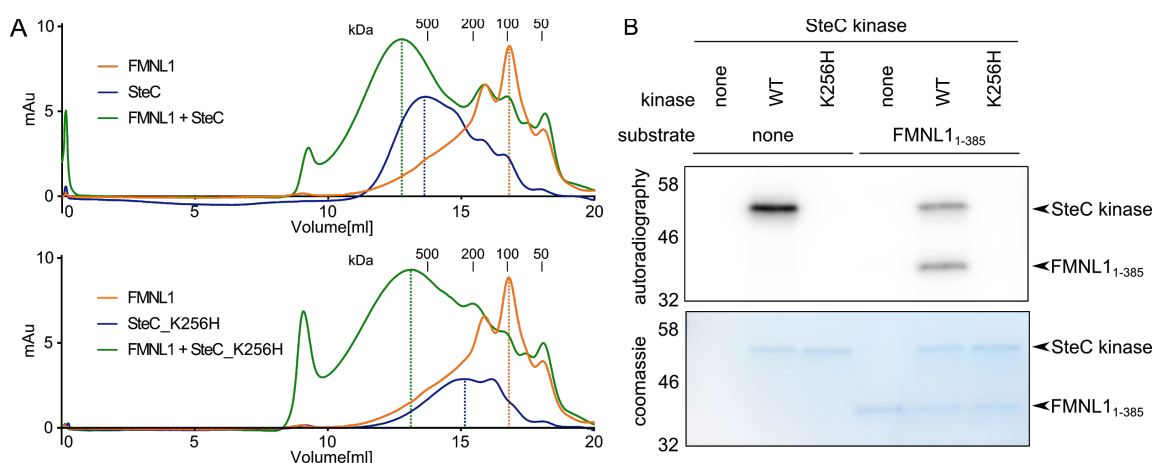


Figure IV.8 SteC directly binds and phosphorylates FMNL1 *in vitro*. (A) SEC chromatograms of FMNL1₁₋₃₈₅ (orange), SteC (blue, upper panel) or SteC_{K256H} (blue, lower panel). Upon pre-incubation of the FMNL1 with SteC (green), a shift of the trace towards lower elution volume (i.e. a higher MW) can be detected. Protein mass corresponding to various retention times is indicated (BioRad protein standard with 1.35 - 670 kDa range was used). (B) Autoradiography and staining with Coomassie after *in vitro* phosphorylation assay. FMNL1₁₋₃₈₅ was incubated with SteC or SteC_{K256H} in the presence of [³²P]-γ-ATP, protein mixtures were separated via SDS-PAGE and transferred to PVDF. Phosphorylation of FMNL1₁₋₃₈₅ only occurs in the presence of catalytically active SteC (as indicated by the arrows). This figure has been published as Figure 7A and 7B in (Walch et al. 2020).

Next, we performed phosphoproteomics to identify the residues within the FMNL proteins that were phosphorylated by SteC. To do so, we subjected recombinantly expressed N-terminal constructs of FMNL1 and FMNL2 to an *in vitro* kinase assay with SteC, using SteC_{K256H} as a negative control, using two different ATP concentrations, 50 μM and 5 mM (see Chapter VII, section VII.23). In addition to autophosphorylation sites on SteC, we identified multiple phosphosites in both FMNL proteins, which were specifically detected after exposure to catalytically active SteC. A summary of all SteC autophosphorylation sites and phosphorylated FMNL1 and FMNL2 residues can be found in Supplementary Table S10 in (Walch et al. 2020; 50 μM ATP) and in Table IV.1 (5 mM ATP).

Interestingly, these were located in similar domains of the two FMNL proteins (Figure IV.9), most predominantly in a flexible loop within the armadillo repeat (arm2). Among these were two phosphosites (S184 in FMNL1 and S171 in FMNL2), which have previously been shown to play a role in mediating Rho-family GTPase- and Cdc42-binding (Kühn et al. 2015) and which are equivalent within the two proteins. The finding that SteC recognizes and phosphorylates functionally relevant residues within FMNL-family proteins suggests a functional role of the STeC-FMNL1 interaction in the regulation of actin rearrangement *via* Cdc42.

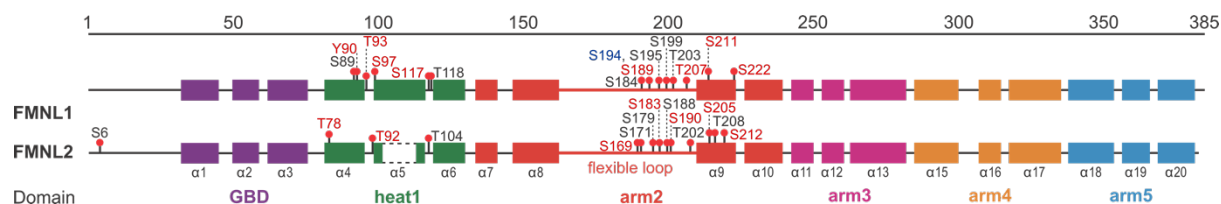


Figure IV.9 Identification of phosphosites in the N-terminal domains of FMNL1 and FMNL2 after incubation with SteC *in vitro*. Schematic maps of FMNL1 and FMNL2 with functional domains and structure elements indicated. Phosphosites that were observed for the two proteins are indicated. For both proteins, the flexible loop of the armadillo repeat is mostly targeted for phosphorylation. Coloring: blue: identified in the first replicate (using 50 μM ATP), red: identified in the second replicate (5 mM ATP), black: identified in both. *This figure has adapted from Figure 7C in (Walch et al. 2020).*

4.3. Quantification of SteC-dependent actin bundling during infection

In a next step, I aimed at linking the molecular interplay between SteC and its host partners to their biological impact during infection. It has previously been shown that SteC is essential for the formation of actin bundles in the vicinity of the STm microcolony during the infection of 3T3 fibroblasts (Poh et al. 2008; Odendall et al. 2012; Imami et al. 2013). As a result, I hypothesized on FMNL proteins being the missing link between SteC and the described phenotype due to their capability of promoting actin rearrangements and polymerization (Bai et al. 2011; Heimsath and Higgs 2012; Block et al. 2012).

In the *in vitro* experiments, I had seen that SteC is able to bind and phosphorylate other FMNL proteins, despite them not being enriched in the AP/QMS data. As FMNL1 is only lowly expressed in 3T3 fibroblast cells (Kage, Winterhoff, et al. 2017), I decided to use cells carrying knockouts of the more ubiquitous FMNL proteins FMNL2 and FMNL3 in my experiments. Although these two FMNL-family members were not detected as direct interaction partners in the AP/QMS work, this could have been due to their lower expression in the two cell lines probed. The phosphoproteomic work shows that SteC can phosphorylate (and hence directly interact with) FMNL2 as well.

When infecting wildtype 3T3 fibroblasts, I observed the SteC-dependent occurrence of actin bundles at the SCV, as previously described (Odendall et al. 2012): When impeding SteC-translocation to the host cytoplasm, either through deletion ($\Delta steC$) or through disruption of the T3SS2 ($\Delta ssaV$), no actin bundling in the proximity of the STm microcolony occurred (Figure IV.10A). Quantifying the colocalization of actin signal

with the SCV similarly to the procedure described in subsection 3.2 of this chapter confirmed a significant drop in actin signal at the location of STm in infection with $\Delta steC$ and $\Delta ssaV$ mutants (Figure IV.10B). Strikingly, for 3T3 fibroblasts that were depleted in FMNL2/3, actin-bundling was strongly reduced, even in infection with wildtype STm, and was only mildly further reduced by $\Delta steC$ (Figure IV.10). This suggests that SteC indeed induces FMNL-dependent actin-bundling.

Interestingly, despite neither wildtype nor the $\Delta steC$ mutant being capable of inducing a substantial amount of actin bundles in the context of FMNL2/3 deletion, I observed a residual effect of SteC. Hence, I sought out to assess the expression of FMNL proteins in the various cell lines using antibodies against FMNL2 (which also bind to FMNL3) and against FMNL1. The latter is only recently available and has an improved specificity towards FMNL1.

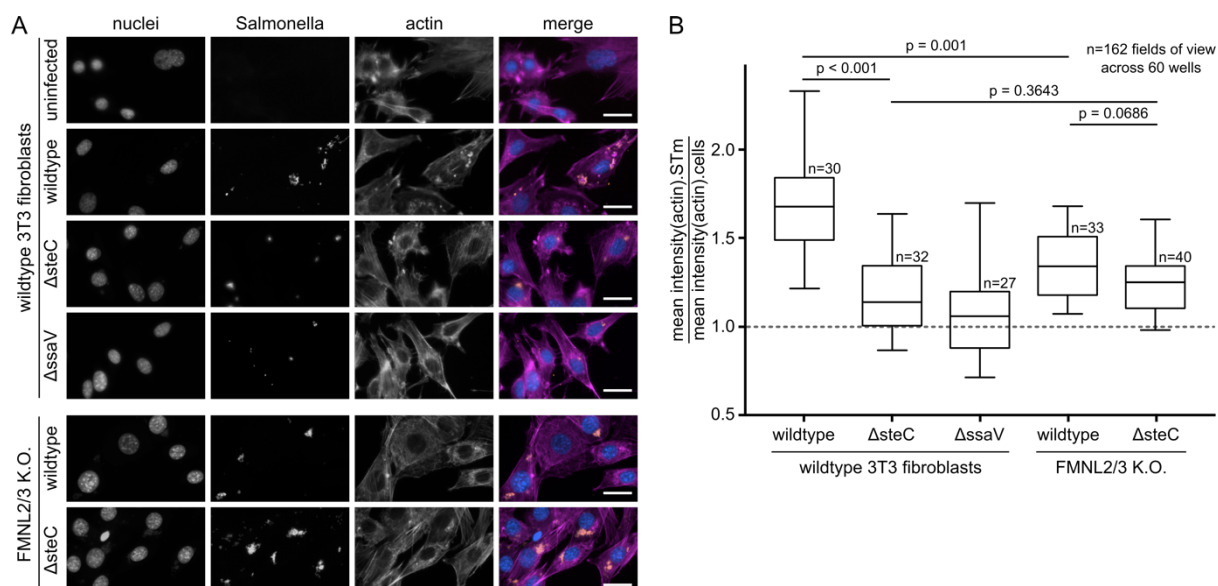


Figure IV.10 SteC induces actin bundles in 3T3 fibroblasts through FMNL2/3. Microscopy images of 3T3 fibroblasts infected with various STm strains (red), stained with DAPI (blue) and phalloidin (purple) after fixation 8 hpi. For wildtype 3T3, two datasets from two independent experiments were collected, and for FMNL2/3-KO clones 9.10 and 46.20 (Kage, Steffen, et al. 2017), each present in 20 wells per experiment, a total of three independent experiments was used. (B) Quantification of panel A as indicated on the y-axis. The mean actin intensity signal at the site of STm was divided by the mean actin intensity throughout the host cell. T-test with Welch correction was used for statistical analysis and p-values are indicated. *This figure has been adapted from Figure 7 in (Walch et al. 2020).*

FMNL2 and FMNL3 were very highly abundant in the 3T3 control samples and not detectable in the two KO-mutant clones used during experimentation. FMNL1 was most highly abundant in RAW264.7, as expected, but also displayed residual levels in 3T3 fibroblasts (Figure IV.11). It is therefore conceivable that the residual actin-bundling detected in the FMNL2/3 depletion context can be attributed to low levels of FMNL1 being present in the cells. Quantifying actin bundling during infection of FMNL1 knockout cells, as well as a triple mutant (depleted in all three proteins), could provide further detail on the residual actin bundling at the SCV, as noticed in the presented experiments.

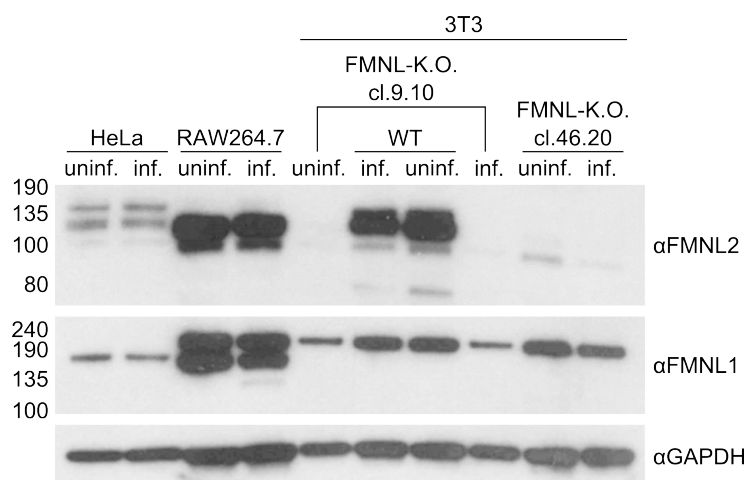


Figure IV.11 Abundance of FMNL proteins across the various cell lines used in experimentation. Western Blot of cleared (Tx100 soluble) lysate of all cell lines used for experimentation (cl.9.10 and cl.46.20 indicate two distinct clones of the FMNL2/3 knockout cell line). Samples were harvested at 8 hpi and antibodies against FMNL1, FMNL2 (which shows cross-reactive behavior towards FMNL3 (Kage, Winterhoff, et al. 2017)) and GAPDH (as the loading control) were used. *This figure has been published as Figure S11 in (Walch et al. 2020).*

4.4. Concluding hypothesis on the biological function

The model I propose for the mechanism underlying actin remodeling during STm infection describes the molecular interplay between effectors and their host target as follows: SteC interacts with formins of the FMNL subfamily. This interaction occurs directly and is independent of the catalytic activity of SteC (as described in section 4.1.). Upon binding, the FMNL protein is phosphorylated at specific residues within its flexible loop (as discussed in section 4.2.), which are known to promote binding of Cdc42 to the FMNL protein (Figure IV.12, left, (Kühn et al. 2015)). Cdc42 then activates FMNL and thereby induces actin polymerization (Kühn et al. 2015), which leads to actin bundling in the vicinity of the SCV (as described in section 4.3.; Figure IV.12, right). Absence of either SteC or the host FMNL protein will lead to a reduction of the characteristic actin bundles in the proximity of the SCV.

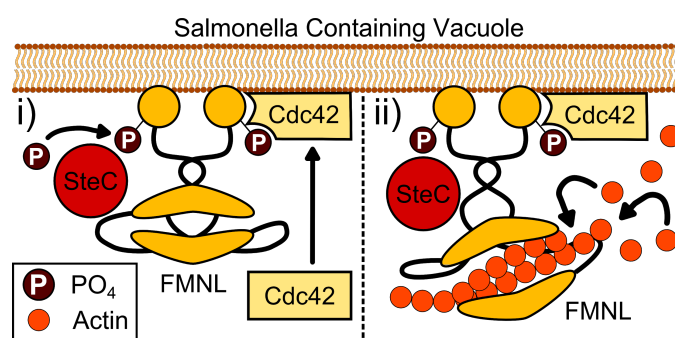


Figure IV.12 Model of the molecular interplay between SteC and host factors to induce actin bundling at the SCV. (i) SteC and FMNL proteins interact directly and SteC phosphorylates its host partner. This phosphorylation recruits Cdc42 and promotes its interaction with the FMNL formin. (ii) Upon binding of Cdc42, the FMNL protein induces actin polymerization and thereby facilitates the formation of actin bundles in the proximity of the STm microcolony.

5. Appendix

Two distinct ATP concentrations were used in the *in vitro* kinase assay coupled to phosphoproteomics to identify phosphosites in FMNL1₁₋₃₈₅ and FMNL2₂₋₄₇₈ after incubation with SteC or SteC_{K256H}. Residues identified in the replicate using 50 μ M ATP can be found in Supplementary Table S10 in (Walch et al. 2020), phosphorylated amino acids identified using 5mM ATP are listed in Table IV.1.

Table VI.1. Phosphosites identified in SteC, FMNL1₁₋₃₈₅ and FMNL2₂₋₄₇₈ after co-incubation. Amino acid (serine, threonine or tyrosine) and position in the respective protein are indicated. The localization probability was required to be larger than 0.75. Sites identified in samples containing SteC_{K256H} were excluded.

Protein name	Phosphosite	Localization probability	Score
Formin-like protein 1	S117	0.947153	215.79
Formin-like protein 1	S184	1	255.96
Formin-like protein 1	S189	0.999918	200.52
Formin-like protein 1	S195	0.997405	293.75
Formin-like protein 1	S199	0.999973	228.3
Formin-like protein 1	S211	0.999981	149.36
Formin-like protein 1	S222	1	126.26
Formin-like protein 1	S89	1	236.31
Formin-like protein 1	S97	0.999997	164.65
Formin-like protein 1	T118	0.999276	328.95
Formin-like protein 1	T203	1	231.21
Formin-like protein 1	T207	0.999998	192.85
Formin-like protein 1	T93	0.960963	63.062
Formin-like protein 2	S169	0.998554	103.75
Formin-like protein 2	S171	1	191.74
Formin-like protein 2	S179	1	272.2
Formin-like protein 2	S183	0.999936	97.441
Formin-like protein 2	S188	0.997501	220.72
Formin-like protein 2	S190	0.903323	187.04
Formin-like protein 2	S205	1	131.42
Formin-like protein 2	S212	0.999989	120.71
Formin-like protein 2	S466	1	228.09
Formin-like protein 2	S6	1	392.79
Formin-like protein 2	T104	0.999276	241.35
Formin-like protein 2	T202	0.999998	131.42
Formin-like protein 2	T208	0.999442	143.46
Formin-like protein 2	T446	1	288.57
Formin-like protein 2	T450	0.999988	230.62
Formin-like protein 2	T467	1	61.815
Formin-like protein 2	T78	0.999999	159.18
Formin-like protein 2	T92	0.999741	46.318
SteC	S240	1	276.2
SteC	S242	1	272.81
SteC	S282	1	307.25
SteC	S295	0.999999	106.93
SteC	S297	1	199.99
SteC	S337	1	131.69
SteC	S369	0.958318	223.46
SteC	S377	1	266.68
SteC	S379	1	190.26
SteC	S75	1	221.6
SteC	S80	0.999958	199.81
SteC	T245	0.999103	271.32
SteC	T308	0.999599	158.77
SteC	T382	1	301.04
SteC	T402	1	412.35
SteC	T406	1	341.83
SteC	T429	1	304.72
SteC	T445	1	259.97
SteC	Y243	0.998137	186.78

6. Bibliography of this chapter

- Albulescu, Lucian, Jeroen R. P. M. Strating, Hendrik Jan Thibaut, Lonneke van der Linden, Matthew D. Shair, Johan Neyts, and Frank J. M. van Kuppeveld. 2015. "Broad-Range Inhibition of Enterovirus Replication by OSW-1, a Natural Compound Targeting OSBP." *Antiviral Research* 117 (May): 110–14.
- Altan-Bonnet, Nihal. 2017. "Lipid Tales of Viral Replication and Transmission." *Trends in Cell Biology* 27 (3): 201–13.
- Amini-Bavil-Olyaei, Samad, Youn Jung Choi, Jun Han Lee, Mude Shi, I-Chueh Huang, Michael Farzan, and Jae U. Jung. 2013. "The Antiviral Effector IFITM3 Disrupts Intracellular Cholesterol Homeostasis to Block Viral Entry." *Cell Host & Microbe* 13 (4): 452–64.
- Auweter, Sigrid D., Hong B. Yu, Ellen T. Arena, Julian A. Guttman, and B. Brett Finlay. 2012. "Oxysterol-Binding Protein (OSBP) Enhances Replication of Intracellular *Salmonella* and Binds the *Salmonella* SPI-2 Effector SseL via Its N-Terminus." *Microbes and Infection / Institut Pasteur* 14 (2): 148–54.
- Bai, Siau Wei, Maria Teresa Herrera-Abreu, Jennifer L. Rohn, Victor Racine, Virginia Tajadura, Narendra Suryavanshi, Stephanie Bechtel, Stefan Wiemann, Buzz Baum, and Anne J. Ridley. 2011. "Identification and Characterization of a Set of Conserved and New Regulators of Cytoskeletal Organization, Cell Morphology and Migration." *BMC Biology* 9 (August): 54.
- Bakowski, Malina A., Virginie Braun, Grace Y. Lam, Tony Yeung, Won Do Heo, Tobias Meyer, B. Brett Finlay, Sergio Grinstein, and John H. Brumell. 2010. "The Phosphoinositide Phosphatase SopB Manipulates Membrane Surface Charge and Trafficking of the *Salmonella*-Containing Vacuole." *Cell Host & Microbe* 7 (6): 453–62.
- Beuzón, C. R., S. Méresse, K. E. Unsworth, J. Ruíz-Albert, S. Garvis, S. R. Waterman, T. A. Ryder, E. Boucrot, and D. W. Holden. 2000. "*Salmonella* Maintains the Integrity of Its Intracellular Vacuole through the Action of SifA." *The EMBO Journal* 19 (13): 3235–49.
- Bittman, R., and S. A. Fischkoff. 1972. "Fluorescence Studies of the Binding of the Polyene Antibiotics Filipin 3, Amphotericin B, Nystatin, and Lagosin to Cholesterol." *Proceedings of the National Academy of Sciences of the United States of America* 69 (12): 3795–99.
- Block, Jennifer, Dennis Breitsprecher, Sonja Kühn, Moritz Winterhoff, Frieda Kage, Robert Geffers, Patrick Duwe, et al. 2012. "FMNL2 Drives Actin-Based Protrusion and Migration Downstream of Cdc42." *Current Biology: CB* 22 (11): 1005–12.
- Brandstaetter, Hemma, John Kendrick-Jones, and Folma Buss. 2012. "Myo1c Regulates Lipid Raft Recycling to Control Cell Spreading, Migration and *Salmonella* Invasion." *Journal of Cell Science* 125 (Pt 8): 1991–2003.

- Brumell, J. H., C. M. Rosenberger, G. T. Gotto, S. L. Marcus, and B. B. Finlay. 2001. "SifA Permits Survival and Replication of *Salmonella* Typhimurium in Murine Macrophages." *Cellular Microbiology* 3 (2): 75–84.
- Burgett, Anthony W. G., Thomas B. Poulsen, Kittikhun Wangkanont, D. Ryan Anderson, Chikako Kikuchi, Kousei Shimada, Shuichi Okubo, et al. 2011. "Natural Products Reveal Cancer Cell Dependence on Oxysterol-Binding Proteins." *Nature Chemical Biology* 7 (9): 639–47.
- Catron, Drew M., Matthew D. Sylvester, Yvonne Lange, Madhusudan Kadekoppala, Bradley D. Jones, Denise M. Monack, Stanley Falkow, and Kasturi Haldar. 2002. "The *Salmonella*-Containing Vacuole Is a Major Site of Intracellular Cholesterol Accumulation and Recruits the GPI-Anchored Protein CD55." *Cellular Microbiology* 4 (6): 315–28.
- Dehapiot, Benoit, Raphaël Clément, Hervé Alégot, Gabriella Gzásó-Gerhát, Jean-Marc Philippe, and Thomas Lecuit. 2020. "Assembly of a Persistent Apical Actin Network by the Formin Frl/Fmnl Tunes Epithelial Cell Deformability." *Nature Cell Biology* 22 (7): 791–802.
- Drecktrah, Dan, Seamus Levine-Wilkinson, Tapen Dam, Seth Winfree, Leigh A. Knodler, Trina A. Schroer, and Olivia Steele-Mortimer. 2008. "Dynamic Behavior of *Salmonella*-Induced Membrane Tubules in Epithelial Cells." *Traffic* 9 (12): 2117–29.
- Dumont, Audrey, Emmanuel Boucrot, Stéphanie Drevensek, Vanessa Daire, Jean-Pierre Gorvel, Christian Poüs, David W. Holden, and Stéphane Méresse. 2010. "SKIP, the Host Target of the *Salmonella* Virulence Factor SifA, Promotes Kinesin-1-Dependent Vacuolar Membrane Exchanges." *Traffic* 11 (7): 899–911.
- Fernandez-Piñar, Pablo, Ainel Alemán, John Sondek, Henrik G. Dohlman, María Molina, and Humberto Martín. 2012. "The *Salmonella* Typhimurium Effector SteC Inhibits Cdc42-Mediated Signaling through Binding to the Exchange Factor Cdc24 in *Saccharomyces Cerevisiae*." *Molecular Biology of the Cell* 23 (22): 4430–43.
- Fu, Y., and J. E. Galán. 1998. "The *Salmonella* Typhimurium Tyrosine Phosphatase SptP Is Translocated into Host Cells and Disrupts the Actin Cytoskeleton." *Molecular Microbiology* 27 (2): 359–68.
- Galan, J. E., and D. Zhou. 2000. "Striking a Balance: Modulation of the Actin Cytoskeleton by *Salmonella*." *Proceedings of the National Academy of Sciences of the United States of America* 97 (16): 8754–61.
- Harayama, Takeshi, and Howard Riezman. 2018. "Understanding the Diversity of Membrane Lipid Composition." *Nature Reviews. Molecular Cell Biology* 19 (5): 281–96.
- Heimsath, Ernest G., Jr, and Henry N. Higgs. 2012. "The C Terminus of Formin FMNL3 Accelerates Actin Polymerization and Contains a WH2 Domain-like Sequence That Binds Both Monomers and Filament Barbed Ends." *The Journal of Biological Chemistry* 287 (5): 3087–98.

- Hume, Peter J., Vikash Singh, Anthony C. Davidson, and Vassilis Koronakis. 2017. "Swiss Army Pathogen: The Salmonella Entry Toolkit." *Frontiers in Cellular and Infection Microbiology* 7 (August): 348.
- Imami, Koshi, Amit P. Bhavsar, Hongbing Yu, Nat F. Brown, Lindsay D. Rogers, B. Brett Finlay, and Leonard J. Foster. 2013. "Global Impact of Salmonella Pathogenicity Island 2-Secreted Effectors on the Host Phosphoproteome." *Molecular & Cellular Proteomics: MCP* 12 (6): 1632–43.
- Kage, Frieda, Anika Steffen, Adolf Ellinger, Carmen Ranftler, Christian Gehre, Cord Brakebusch, Margit Pavelka, Theresia Stradal, and Klemens Rottner. 2017. "FMNL2 and -3 Regulate Golgi Architecture and Anterograde Transport Downstream of Cdc42." *Scientific Reports* 7 (1): 9791.
- Kage, Frieda, Moritz Winterhoff, Vanessa Dimchev, Jan Mueller, Tobias Thalheim, Anika Freise, Stefan Brühmann, et al. 2017. "FMNL Formins Boost Lamellipodial Force Generation." *Nature Communications* 8 (March): 14832.
- Knodler, Leigh A., and Olivia Steele-Mortimer. 2003. "Taking Possession: Biogenesis of the Salmonella-Containing Vacuole." *Traffic* 4 (9): 587–99.
- Knuff, Katelyn, and B. Brett Finlay. 2017. "What the SIF Is Happening-The Role of Intracellular Salmonella-Induced Filaments." *Frontiers in Cellular and Infection Microbiology* 7 (July): 335.
- Kolodziejek, Anna M., Melissa A. Altura, Junping Fan, Erik M. Petersen, Matthew Cook, Peter S. Brzovic, and Samuel I. Miller. 2019. "Salmonella Translocated Effectors Recruit OSBP1 to the Phagosome to Promote Vacuolar Membrane Integrity." *Cell Reports* 27 (7): 2147–56.e5.
- Kühn, Sonja, Constanze Erdmann, Frieda Kage, Jennifer Block, Lisa Schwenkmezger, Anika Steffen, Klemens Rottner, and Matthias Geyer. 2015. "The Structure of FMNL2-Cdc42 Yields Insights into the Mechanism of Lamellipodia and Filopodia Formation." *Nature Communications* 6 (May): 7088.
- Lafont, Frank, and F. Gisou van der Goot. 2005. "Bacterial Invasion via Lipid Rafts." *Cellular Microbiology* 7 (5): 613–20.
- Lau, Nicole, Amanda L. Haeberle, Brittany J. O’Keeffe, Eleanor A. Latomanski, Jean Celli, Hayley J. Newton, and Leigh A. Knodler. 2019. "SopF, a Phosphoinositide Binding Effector, Promotes the Stability of the Nascent Salmonella-Containing Vacuole." *PLoS Pathogens* 15 (7): e1007959.
- Mallo, Gustavo V., Marianela Espina, Adam C. Smith, Mauricio R. Terebiznik, Ainel Alemán, B. Brett Finlay, Lucia E. Rameh, Sergio Grinstein, and John H. Brumell. 2008. "SopB Promotes Phosphatidylinositol 3-Phosphate Formation on Salmonella Vacuoles by Recruiting Rab5 and Vps34." *The Journal of Cell Biology* 182 (4): 741–52.
- Maxfield, Frederick R., and Daniel Wüstner. 2012. "Analysis of Cholesterol Trafficking with Fluorescent Probes." *Methods in Cell Biology* 108: 367–93.

- McEwan, David G., Benjamin Richter, Beatrice Claudi, Christoph Wigge, Philipp Wild, Hesso Farhan, Kieran McGourty, et al. 2015. "PLEKHM1 Regulates Salmonella-Containing Vacuole Biogenesis and Infection." *Cell Host & Microbe* 17 (1): 58–71.
- Mesmin, Bruno, Joëlle Bigay, Joël Polidori, Denisa Jamecna, Sandra Lacas-Gervais, and Bruno Antony. 2017. "Sterol Transfer, PI4P Consumption, and Control of Membrane Lipid Order by Endogenous OSBP." *The EMBO Journal* 36 (21): 3156–74.
- Nawabi, Parwez, Drew M. Catron, and Kasturi Haldar. 2008. "Esterification of Cholesterol by a Type III Secretion Effector during Intracellular Salmonella Infection." *Molecular Microbiology* 68 (1): 173–85.
- Odendall, Charlotte, Nathalie Rolhion, Andreas Förster, John Poh, Douglas J. Lamont, Mei Liu, Paul S. Freemont, Andrew D. Catling, and David W. Holden. 2012. "The Salmonella Kinase SteC Targets the MAP Kinase MEK to Regulate the Host Actin Cytoskeleton." *Cell Host & Microbe* 12 (5): 657–68.
- Ohlson, Maikke B., Zhiwei Huang, Neal M. Alto, Marie-Pierre Blanc, Jack E. Dixon, Jijie Chai, and Samuel I. Miller. 2008. "Structure and Function of Salmonella SifA Indicate That Its Interactions with SKIP, SseJ, and RhoA Family GTPases Induce Endosomal Tubulation." *Cell Host & Microbe* 4 (5): 434–46.
- Patel, Jayesh C., and Jorge E. Galán. 2005. "Manipulation of the Host Actin Cytoskeleton by Salmonella--All in the Name of Entry." *Current Opinion in Microbiology* 8 (1): 10–15.
- Pfeffer, Suzanne R. 2019. "NPC Intracellular Cholesterol Transporter 1 (NPC1)-Mediated Cholesterol Export from Lysosomes." *The Journal of Biological Chemistry* 294 (5): 1706–9.
- Poh, John, Charlotte Odendall, Ad Spanos, Cliona Boyle, Mei Liu, Paul Freemont, and David W. Holden. 2008. "SteC Is a Salmonella Kinase Required for SPI-2-Dependent F-Actin Remodelling." *Cellular Microbiology* 10 (1): 20–30.
- Roberts, Brett L., Zachary C. Severance, Ryan C. Bensen, Anh T. Le, Naga Rama Kothapalli, Juan I. Nuñez, Hongyan Ma, et al. 2019. "Transient Compound Treatment Induces a Multigenerational Reduction of Oxysterol-Binding Protein (OSBP) Levels and Prophylactic Antiviral Activity." *ACS Chemical Biology* 14 (2): 276–87.
- Roulin, Pascal S., Mark Lötzerich, Federico Torta, Lukas B. Tanner, Frank J. M. van Kuppeveld, Markus R. Wenk, and Urs F. Greber. 2014. "Rhinovirus Uses a Phosphatidylinositol 4-Phosphate/cholesterol Counter-Current for the Formation of Replication Compartments at the ER-Golgi Interface." *Cell Host & Microbe* 16 (5): 677–90.
- Ruiz-Albert, Javier, Xiu-Jun Yu, Carmen R. Beuzón, Abigail N. Blakey, Edouard E. Galyov, and David W. Holden. 2002. "Complementary Activities of SseJ and SifA Regulate Dynamics of the Salmonella Typhimurium Vacuolar Membrane." *Molecular Microbiology* 44 (3): 645–61.

- Smith, Adam C., Won Do Heo, Virginie Braun, Xiuju Jiang, Chloe Macrae, James E. Casanova, Marci A. Scidmore, Sergio Grinstein, Tobias Meyer, and John H. Brumell. 2007. "A Network of Rab GTPases Controls Phagosome Maturation and Is Modulated by *Salmonella* Enterica Serovar Typhimurium." *The Journal of Cell Biology* 176 (3): 263–68.
- Stévenin, Virginie, Yuen-Yan Chang, Yoann Le Toquin, Magalie Duchateau, Quentin Gai Gianetto, Chak Hon Luk, Audrey Salles, et al. 2019. "Dynamic Growth and Shrinkage of the *Salmonella*-Containing Vacuole Determines the Intracellular Pathogen Niche." *Cell Reports* 29 (12): 3958–73.e7.
- Tharkeshwar, Arun Kumar, Jesse Trekker, Wendy Vermeire, Jarne Pauwels, Ragna Sannerud, David A. Priestman, Danielle Te Vruchte, et al. 2017. "A Novel Approach to Analyze Lysosomal Dysfunctions through Subcellular Proteomics and Lipidomics: The Case of NPC1 Deficiency." *Scientific Reports* 7 (January): 41408.
- Walch, Philipp, Joel Selkrig, Leigh A. Knodler, Mandy Rettel, Frank Stein, Keith Fernandez, Cristina Viéitez, et al. 2020. "Global Mapping of *Salmonella* Enterica-Host Protein-Protein Interactions during Infection." *Cold Spring Harbor Laboratory*. <https://doi.org/10.1101/2020.05.04.075937>.
- Walpole, Glenn F. W., Sergio Grinstein, and Johannes Westman. 2018. "The Role of Lipids in Host-Pathogen Interactions." *IUBMB Life* 70 (5): 384–92.
- Wilhelm, Léa P., Laetitia Voilquin, Toshihide Kobayashi, Catherine Tomasetto, and Fabien Alpy. 2019. "Intracellular and Plasma Membrane Cholesterol Labeling and Quantification Using Filipin and GFP-D4." In *Intracellular Lipid Transport: Methods and Protocols*, edited by Guillaume Drin, 137–52. New York, NY: Springer New York.
- Yayoshi-Yamamoto, S., I. Taniuchi, and T. Watanabe. 2000. "FRL, a Novel Formin-Related Protein, Binds to Rac and Regulates Cell Motility and Survival of Macrophages." *Molecular and Cellular Biology* 20 (18): 6872–81.
- Zhao, Weidong, Thomas Moest, Yaya Zhao, Aude-Agnès Guilhon, Christophe Buffat, Jean-Pierre Gorvel, and Stéphane Méresse. 2015. "The *Salmonella* Effector Protein SifA Plays a Dual Role in Virulence." *Scientific Reports* 5 (August): 12979.
- Zhou, D., L. M. Chen, L. Hernandez, S. B. Shears, and J. E. Galán. 2001. "A *Salmonella* Inositol Polyphosphatase Acts in Conjunction with Other Bacterial Effectors to Promote Host Cell Actin Cytoskeleton Rearrangements and Bacterial Internalization." *Molecular Microbiology* 39 (2): 248–59.
- Zhou, Yan, Celia Garcia-Prieto, Dennis A. Carney, Rui-Hua Xu, Helene Pelicano, Ying Kang, Wensheng Yu, et al. 2005. "OSW-1: A Natural Compound with Potent Anticancer Activity and a Novel Mechanism of Action." *Journal of the National Cancer Institute* 97 (23): 1781–85.

Chapter V

Screening a genome-wide *STm* knockout library during infection

Chapter V: Screening a genome-wide STm knockout library during infection

1. Summary

The host-pathogen interface consists of a complex interplay of protein-protein interactions, post-translational modifications and other rewiring of cellular pathways and machineries. In the case of STm, effector proteins get translocated to the host cytoplasm *via* Type-III Secretion Systems (T3SS) and they play a central role in rewiring the host response. To broaden our understanding of *Salmonella*-host interface and to elucidate the genes and proteins that are essential during the various stages of the infection process, a look beyond effector-target protein-protein interactions is required.

This chapter describes an unbiased approach of studying *Salmonella* genes that play a role in the initiation and maintenance of infection. These had previously been identified in the lab using a high-throughput microscopy-based screening of *Salmonella* knockout mutants. In addition to recapitulating previous knowledge, we present a large pool of novel biology on STm genes involved in various stages of the infection process. This made proper quality control and validation necessary, which is presented in this chapter. Lastly, we predicted secretion of a previously uncharacterized protein, YebF, as a $\Delta yebF$ mutant displayed microscopy feature fingerprint that was highly similar to that of $\Delta sseJ$. I demonstrated that YebF is indeed secreted to the host cytoplasm and identified protein-protein interactions to host targets upon infection.

2. Contributions

The work described in sections 4.1 and 4.2 (high-throughput screening, microscopy and data analysis) have mainly been performed by Dr. Bachir El Debs. He initiated the project and conducted the majority of the screening and data analysis part, in collaboration with the lab of Dr. Wolfgang Huber. I joined the screening for the third replicate of the RAW264.7 macrophage infection and subsequently conducted the validation described in section 4.3 (selecting subset, generating strains, infection, microscopy and data analysis), with input from Dr. Athanasios Typas and Dr. Bachir El Debs. Furthermore, I performed the experimental work described in section 4.4. Mass spectrometry was conducted by Mandy Rettel and Dr. Frank Stein at the PCF (EMBL Heidelberg), with input from Dr. Mikhail Savitski and myself. The work described in this chapter is part of a manuscript currently in preparation, with Dr. Bachir El Debs and myself as co-first authors.

3. Background and significance

Large-scale proteomic studies, as the one presented in the previous chapters, are essential for deepening the understanding of how *Salmonella* directly rewire host pathways and promote infection. Yet despite their power, they focus on physical protein-protein interactions and what the *Salmonella* secreted proteins may target during infection. There are however layers of interaction that transcend effector-target interactions - such as pathogen processes that are dependent on the host (e.g.

metabolic), such as their replication environment, or the immunological response by the host to the invading pathogen.

Studying genetic interactions between microbe and host has some similarities to chemical genetics, where a library of pathogen mutant strains is subjected to a panel of stress conditions to elucidate the impact of genes on bacterial survival in certain stresses (Spring 2005; Nichols et al. 2011; French et al. 2016). Understanding the host response traditionally occurs in a very targeted and highly mechanistic fashion and does not take place on a high-throughput scale (Günster et al. 2017; Chen et al. 2020). Of the described approaches for understanding the genetic interplay between host and pathogen on a global scale, the libraries used in these studies have so far been pooled (Chaudhuri et al. 2009; Napier et al. 2016; Jeng et al. 2019; Yeung et al. 2019). While this allows for easy upscaling due to advances in sequencing technologies, it is insensitive to small impacts, as a highly complex library is followed in a heterogeneous mixture of infected and bystander cells with replicating, non-replicating and inactive bacteria. In addition, pooled libraries generally rely on a one-dimensional readout – fitness (Chaudhuri et al. 2009; Napier et al. 2016; Jeng et al. 2019; Yeung et al. 2019). Increasing the dimensionality of the phenotype through multiparametric analysis can overcome this and allows a more detailed dissection of gene functionality, as well as the discovery of novel virulence genes.

To understand the impact of each non-essential gene on infection in an unbiased way, we profiled a comprehensive library of STm single-gene knockout mutants during infection of two host cell lines across four time points. We used high-throughput microscopy to extract hundreds of image features that go beyond conventional phenotypes, such as infection rate or intracellular growth. Furthermore, the platform I present can easily be adapted to other conditions or pathogens, and can be amended by additional levels of complexity, such as the presence of drugs, stresses or varying host genetic backgrounds.

4. Genome-wide knockout screen of *Salmonella* mutants during infection

To motivate the work performed for the validation and functional characterization, sections 4.1 and 4.2 will briefly describe the work mainly performed by Dr. Bachir El Debs (see Contributions, section V.2).

4.1. High-throughput screening and microscopy

In order to elucidate the impact of various STm genes, and related biological processes on the infective potential and intracellular proliferation, the previously described STm knockout library was transformed with a plasmid constitutively expressing mCherry (pFCcGi). This library was then used for infection of HeLa and RAW264.7 cells in 384-well format, using the gentamicin protection assay described in Chapter VII, sections VII.10. and VII.24. At four different time points (0, 4, 8 and 20 hpi), the infected cells were fixed in paraformaldehyde and stained for DAPI and actin. For each well, four

fields of view (20x magnification) were acquired using automated image acquisition and plate loading (Figure V.1, upper panel).

That way, around 400,000 images were obtained and subsequently analyzed using a custom-made CellProfiler-based pipeline. Cells were segmented and a total of 2774 unbiased features in HeLa cells and 1723 features in RAW264.7 cells were extracted for each cell. For each mutant, mean, standard deviation and informative percentiles (median, Q95, Q99) were calculated and this vast dataset was reduced to 527 orthogonal and reproducible features across 3692 mutants (Figure V.1, lower panel). The number of features was subsequently reduced further by medoid clustering to 68.

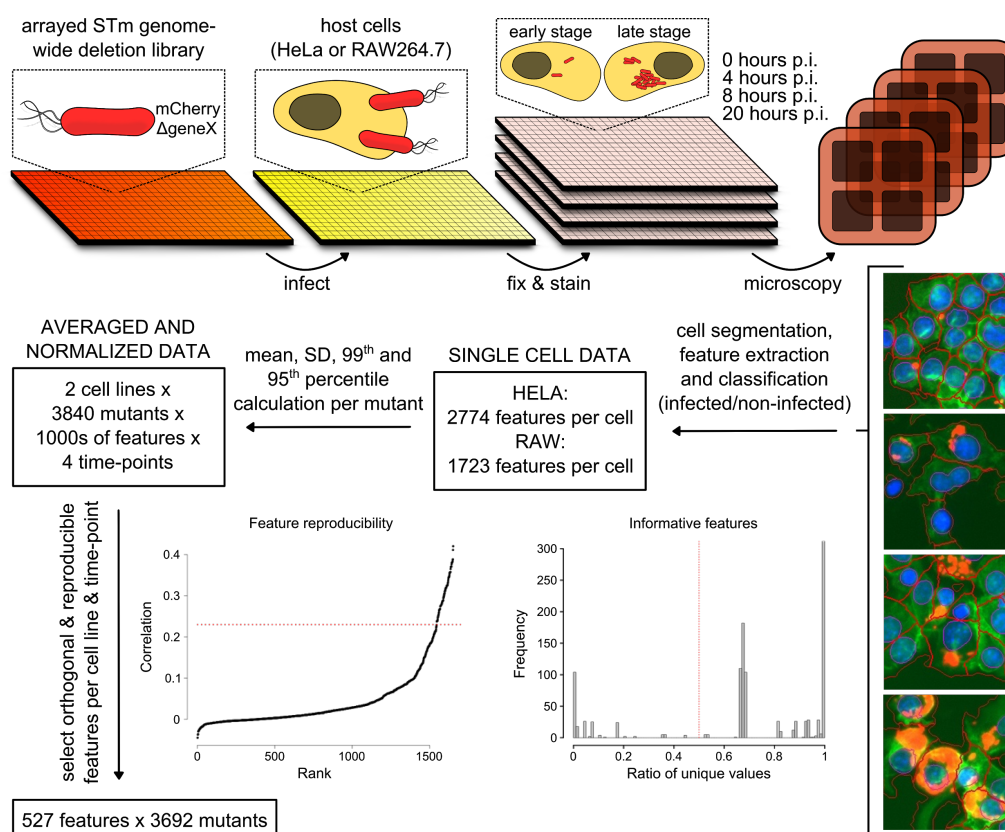


Figure V.1. Experimental workflow and high-throughput microscopy data analysis. Host cells (HeLa and RAW264.7) were infected with an arrayed library of 3840 mutants, each harboring a single gene deletion by replacement of the target gene with a kanamycin resistance cassette, and expressing mCherry. Infection was carried out in 384-well plate format in triplicate for each cell line and at 0 hpi, 4 hpi, 8 hpi and 20 hpi, cells were washed, fixed in PFA and stained using phalloidin and DAPI. Using automated high-throughput image acquisition on a Nikon Eclipse Ti microscope, four images were acquired per well. Cells were segmented and features extracted, quantified and classified. For each mutant and each feature, statistical values were calculated and orthogonal (i.e. informative) and reproducible features were selected. Thereby a total of 527 features (across the two cell lines and all time points) were selected and can be compared across 3692 individual mutant strains. *This figure displays work conducted by Dr. Bachir El Debs.*

4.2. Data analysis and overview of screening results

In addition to the unbiased evaluation of features, one can assess the performance of all mutants with respect to their ability to cause infection (i.e. infection rate at 0 hpi), as well as their proliferative potential (Integrated STm intensity at 20 hpi). As expected, the vast majority of mutants did not confer any significant impact in infectious potential

or intracellular proliferation (Figure V.2 grey bars and dots), however a subset of mutants displayed significant decreases in either cell entry (Figure V.2A and B) or proliferation (Figure V.2C and D).

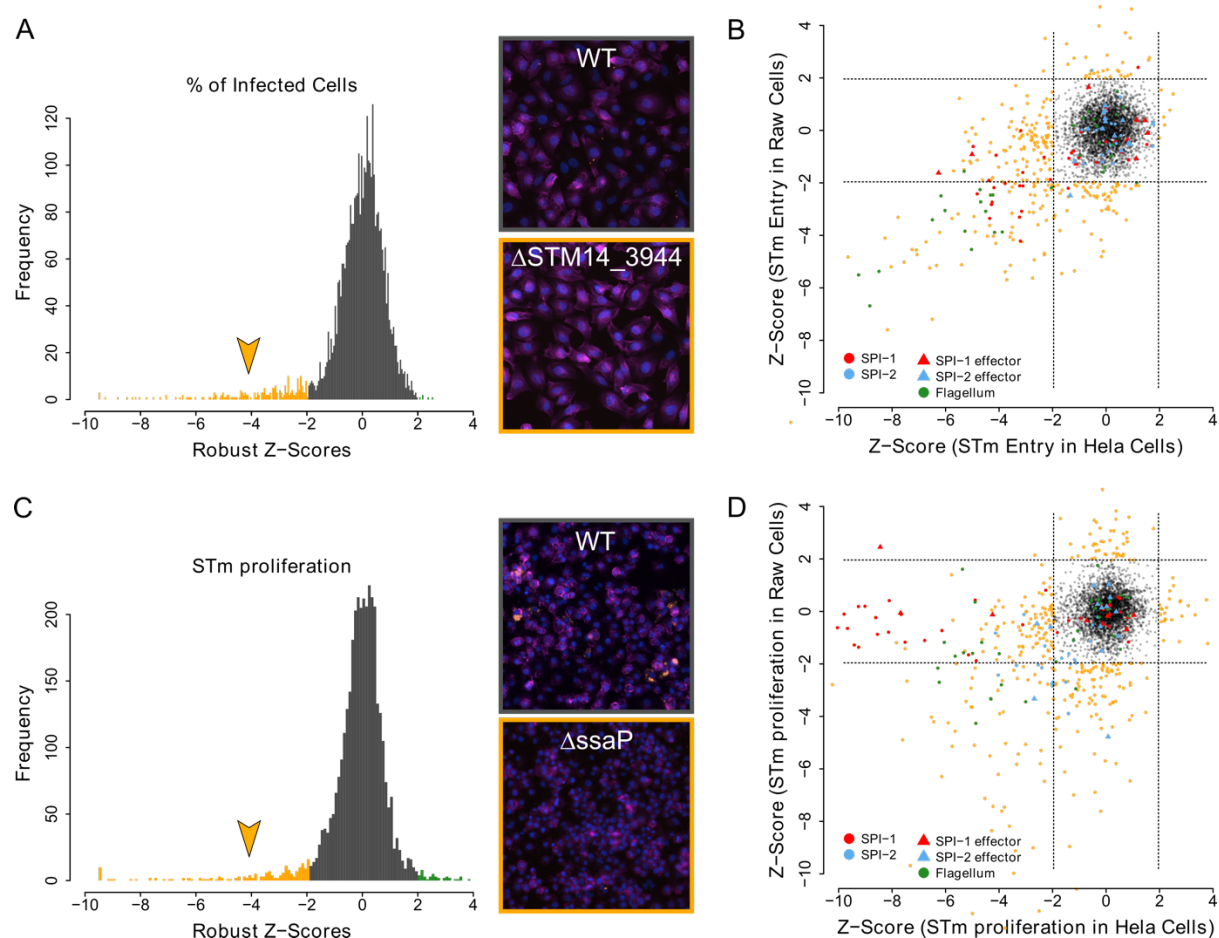


Figure V.2. Cell entry and intracellular proliferation of all tested STm single gene knockout mutants in HeLa cells and RAW264.7. A) Distribution of robust z-scores (infection rate in HeLa cells) for all mutants. Z-scores were binned and are colored as follows: z-score < -2 in gold, z-score > 2 in green, all others in grey. As an example, infection of HeLa cells (0 hpi) with wildtype STm (which does not display a defect in cell entry in HeLa cells) is shown compared to infection of HeLa cells (0 hpi) with Δ STM14_3944 STm, which has a significantly decreased z-score (as indicated by the golden arrow), and hence a strong invasion defect in HeLa cells. B) Z-scores for entry in HeLa cells are plotted *versus* entry in RAW264.7. Knockout mutants displaying abs(z-score) > 2 in at least one cell line are shown in gold, all others in grey. Components (circles) and effectors (triangles) of the SPI-1 (red) and SPI-2 (blue) T3SS, as well as components of the flagellum (green circles) are highlighted. C) Robust z-score distribution for intracellular proliferation in RAW264.7 (measured by integrated STm intensity at 20 hpi). Coloring as in panel A. As an example, infection RAW264.7 cell infection (20 hpi) with wildtype STm is compared to the Δ ssaP strain, which displays a strong defect in intracellular proliferation and hence a low z-score (as indicated by the golden arrow). D) Z-scores for intracellular proliferation in RAW264.7 and HeLa are plotted against each other, as indicated. Coloring and highlighting as in panel B. *This figure is based on work conducted by and data generated and analyzed by Dr. Bachir El Debs.*

By zooming into different groups of bacterial proteins, we can recapitulate the known biology of effector proteins and other well described machineries, such as the flagellum. The latter is mostly required for cell motility and invasion (Figure V.2B, green dots), but not intracellular proliferation (Figure V.2D, green dots). SPI-1 components of the T3SS impact the invasion predominantly in HeLa cells (Figure V.2B, red dots),

while only few SPI-1 effectors exert a significant impact on cell invasion and proliferation (Figure V.2B and D, red triangles). Lastly, single gene deletions of SPI-2 effectors generally do not cause significant impact on cell invasion or intracellular proliferation (Figure V.2B and D, blue triangles), but deletions in components of the SPI-2 encoded T3SS reduce the intracellular proliferation in both cell lines (Figure V.2D, blue dots).

4.3. Small-scale validation reveals high accuracy and specificity

In addition to the known biology on virulence factors in *Salmonella* described in the previous section, this dataset offers a vast pool of novel insights into bacterial genes that are required for the initiation or maintenance of infection. Therefore, a validation of a subset of mutants is required for quality control of the screening data. Thereby, we can assess the specificity, accuracy and sensitivity of the high-throughput methodology and data analysis.

I selected a subset of mutants that displayed a significant impairment of infectious potential or intracellular proliferation in either of the cell lines. I chose those with an impairment in all conditions, as well as mutants with cell-line- or time-point-specific defects, avoiding a bias towards a specific condition. As described in further detail in Chapter VII, I re-transduced the mutants from the library into clean wildtype STm 14028S background using P22 phage transduction and validated the newly generated strains by PCR. This serves as quality control as well as to make sure that the mutants subjected to the validation process indeed harbor the correct gene deletion.

P22 transduction and subsequent PCR-validation was successful for 14 strains, which I then used to infect RAW264.7 macrophages and HeLa cells. At 0 and 20 hpi, I assessed whether the gene deletion had an effect on cell entry or intracellular proliferation, where a reduction to <75% of either infection rate or integrated STm intensity with respect to wildtype infection was counted as impairment. This assessment was then compared with the screening data, where gene deletions were called hits if they displayed a z-score < -2.

Validation was equally successful throughout the different categories (cell entry / intracellular proliferation in HeLa / RAW264.7), with an overall accuracy of 76.8% and a sensitivity of 78.9% (Figure V.3A). As several of the selected mutants only displayed a significant impairment in one or two of the four tested conditions, there is an overall bias towards true negatives. When looking at each of the assessed strains individually, it became evident that in most cases, only one condition could not be validated (Figure V.3B). For all those where two conditions showed disparities between the high-throughput screen and the validation ($\Delta allR$, Δfdx and $\Delta hilA$), the false positives or negatives occurred either within the same cell line or the same time point.

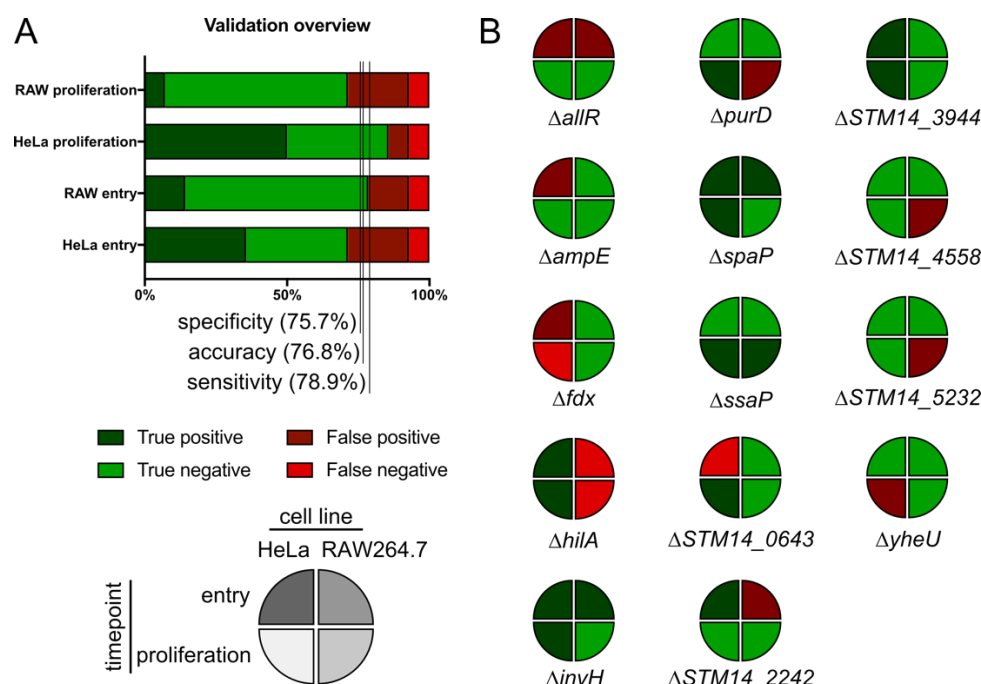


Figure V.3. Small-scale validation of high-throughput screening data. A) Using a subset of single gene knockout mutants in a clean 14028S background (cleaned up by P22 phage transduction), entry and intracellular proliferation were assessed in both host cell backgrounds. True positives, false positives, true negatives and false negatives for each condition are shown as indicated by color and overall specificity, accuracy and sensitivity were calculated. B) Performance of each mutant (indicated by name) in the four assessed conditions. Layout of the circles as shown in the bottom left and coloring as in panel A.

4.4. YebF: a secreted protein with a feature fingerprint similar to SseJ

To add more biological meaning to the vast amount of data that we generated in the screen, and to prove that the quantification of unbiased microscopy features can be used to synthesize novel hypotheses, we selected an STm gene of unknown function, *yebF*, for further characterization. We had noticed that the feature fingerprint generated by deletion of *yebF* was highly correlated to the one of *sseJ* (Figure V.4A). This was curious, as SseJ is a well described translocated STm effector, and while secretion had been reported for YebF in *E. coli* (Prehna et al. 2012), there have not been any studies on the STm protein YebF.

We hypothesized that YebF might get transported to the host cytoplasm during infection. To test this hypothesis, I introduced an affinity-tag at the C-terminus of YebF, maintaining chromosomal expression and thereby endogenous protein levels. The advantages of this tagging method have been extensively described in other chapters of this work. Indeed, I was able to detect YebF-STF in the Tx-100 soluble (cytosolic) fraction of RAW264.7 macrophages 20 hpi (Figure V.4B). This indicates that YebF is indeed transported to the host cytosol during infection, which renders it a putative effector protein.

To understand which host processes YebF might target during infection and whether this can explain the feature fingerprint similarity, I performed FLAG-IP after infection in four independent experiments: twice in HeLa cells (20 hpi) and twice in RAW264.7 macrophages (20 hpi). For other tagged effectors assessed in parallel, the bait could be recovered in mass spectrometry in most cases (as discussed in previous chapters, sections II.4, III.3 and IV.3.1). In the case of YebF-STF, bait detection was only possible in one of the four experiments. A potential explanation for this is the size of YebF (12.8 kDa without tag) as well as its amino acid sequence. During trypsinization prior to MS, there are only a few possible peptides that match the minimum size requirement of at least 7 amino acids for peptide detection (Figure V.4C, see section VII.14.3). Yet despite the difficulties of detecting the YebF-STF bait, several interaction partners could be captured.

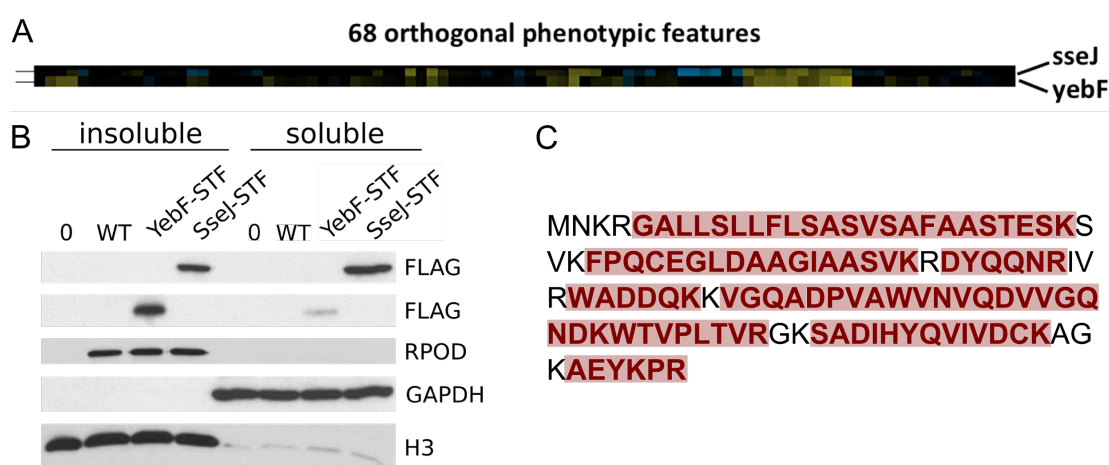


Figure V.4. Characterization of YebF, a *Salmonella* protein which is secreted during infection. A) Comparison of $\Delta sseJ$ and $\Delta yebF$ STm microscopy feature fingerprints obtained from the screen reveals a high similarity of the two knockout strains. B) Secretion of SseJ-STF and YebF-STF into the host cytoplasm (Tx-100 soluble fraction) during STm infection (20 hpi) shown by Western Blot. Secreted effectors in the Tx-100 soluble and insoluble fractions were probed with anti-FLAG antibody, bacterial control (RpoD), cytosolic control (GAPDH) and nuclear control (histone H3) are shown for quality control. C) Amino acid sequence of YebF (without STF-tag). Digesting YebF with trypsin yields the highlighted and bold peptides (by prediction, only peptides >500 Da are shown).

As these difficulties are mainly technical, it is justifiable to assess the enriched host proteins despite absence of the bait. To further improve confidence in the interaction partners, it is useful to focus on the overlap between the four different experiments in which the YebF interactome was assessed. Starting with the experiment where YebF-STF was identified, I evaluated the overlap between the various studies and could thereby reduce the number of candidate interaction partners to 71 across both IP-conditions (41 in native IP, 48 in IP after crosslinking). To do so, I filtered target proteins with a fold change > 1.5 and checked for their enrichments in the other experiments, keeping them if they displayed a fold change > 1.2 and a p-value < 0.05 in at least one other YebF-STF immunoprecipitation.

Focusing on the most highly enriched targets (Figure V.5) reveals several interaction partners involved in TLR signaling (e.g. FLII, LRRFIP1, LRRFIP2, (Dai et al. 2009)) as

well as filaments associated with the nucleus and its envelope (e.g. VIM, LMNB1, (Lin and Worman 1995; Challa and Stefanovic 2011)). Interestingly, in addition to these, prohibitin-2 (PHB2), which co-precipitated with SseJ-STF in the large-scale study, was highly enriched in native IP on YebF in RAW264.7 and HeLa cells. PHB2 has pleiotropic functionality, depending on its cellular localization (Bavelloni et al. 2015). When localized to the plasma membrane, PHB2 is involved in various processes, including cell migration (Fu, Yang, and Bach 2013) and CD86-mediated NF- κ B signaling (Lucas et al. 2013). In infection with *S. typhi*, prohibitins are targeted by the Vi protein to reduce IL-8 production and suppress the innate immune response (Sharma and Qadri 2004; Bavelloni et al. 2015).

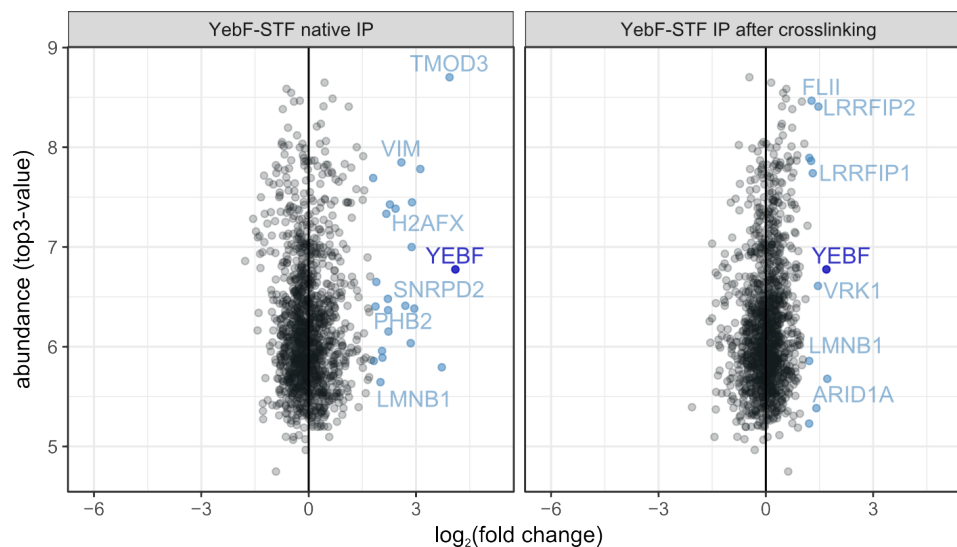


Figure V.5. YebF interaction partners during infection after native and crosslinked IP. Scatterplots of logarithmic fold change versus abundance (top3 value) obtained from a single replicate infection and immunoprecipitation experiment performed in RAW264.7 cells (harvested at 20 hpi). YebF-STF bait is shown in dark blue. For each protein, a p-value was calculated based on the quantiles of the distribution of all proteins (Cox and Mann 2008). Significantly enriched interaction partners (p -value < 0.001) are shown in light blue and all other proteins in grey. Target proteins that were identified in at least one other, independent experiment on YebF-STF are indicated by name. To generate this list, all proteins with a fold change > 1.5 in the single-replicate experiment and with FC > 1.2 and p -value < 0.05 were considered as candidates.

4.5. Conclusion and wider potential of the workflow

In conclusion, we present here a comprehensive dataset that characterizes the effect of single gene deletions in feature fingerprints that are based on unbiased features extracted from high-throughput microscopy. Thereby, we push the characterization of genes that are relevant during infection beyond invasion or proliferation defects. This has three advantages:

- 1) As the features are unbiased, the fingerprints allow for an assessment of the impact of the gene deletion, independent of a specific phenotypic readout
- 2) As the features are high-dimensional, fingerprints are more sensitive in identifying changes conferred by gene deletions
- 3) By comparing feature fingerprints, we can build hypotheses on gene function and relation

We have demonstrated the high quality and accuracy of the data generated in the screen. Furthermore, we have demonstrated that the high dimensionality of the unbiased microscopy features can be utilized to predict the function of previously uncharacterized proteins by similarity to known virulence factors. This can be further generalized by combining feature fingerprints with protein motif similarities to uncover novel infection biology. In addition, the presented high-throughput workflow can be expanded to include other layers of complexity, such as genetic modifications on the host side or the presence of chemical compounds or other stresses.

Such a study would require the selection of subsets of genes on the host- and the pathogen-side, the arraying of single gene deletion STm strains in 384-plate format and the generation of stable, genetically host cell lines. The ensuing screening can be conducted using the same liquid handling platform required for the genome-wide *Salmonella* knock-out screen presented here, as well as the automated microscopy, image analysis, feature quantification and statistics I outlined in this chapter (Figure V.6).

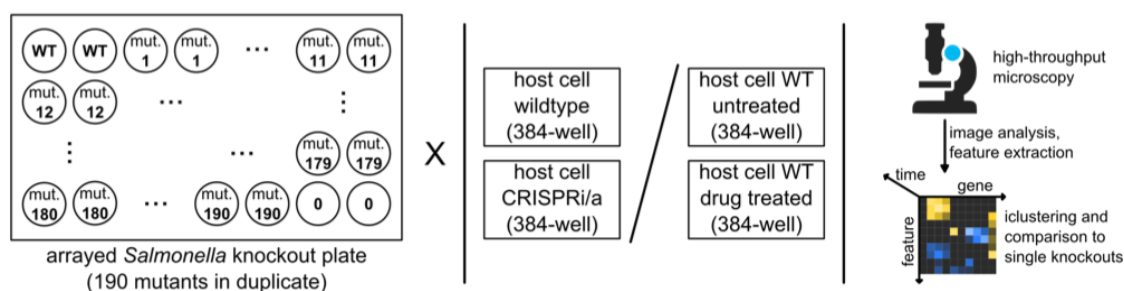


Figure V.6. Layout of a gene-gene interaction screening study in the context of infection. An arrayed library of single gene knockout *Salmonella* mutants in 384-well format, including a wildtype and a bacteria-free control (left) can be used to infect a variety of host backgrounds. These include stable knockout cell lines (e.g. using CRISPR-Cas9), genetically perturbed host cell lines (using CRISPR-i/a) or host cell lines treated with an array of human-targeted drugs. The screen requires an automated liquid handler and the setup allows for a readout by automated cell staining and imaging using high-throughput microscopy. Using an analysis pipeline as the one outlined in Chapter V, unbiased features can be extracted and pairs of genetic perturbations on the host- and the pathogen-side can be clustered, compared and further characterized.

5. Bibliography of this chapter

- Bavelloni, Alberto, Manuela Piazzini, Mirco Raffini, Irene Faenza, and William L. Blalock. 2015. "Prohibitin 2: At a Communications Crossroads." *IUBMB Life* 67 (4): 239–54.
- Challa, Azariyas A., and Branko Stefanovic. 2011. "A Novel Role of Vimentin Filaments: Binding and Stabilization of Collagen mRNAs." *Molecular and Cellular Biology* 31 (18): 3773–89.
- Chaudhuri, Roy R., Sarah E. Peters, Stephen J. Pleasance, Helen Northen, Chrissie Willers, Gavin K. Paterson, Danielle B. Cone, et al. 2009. "Comprehensive Identification of *Salmonella* Enterica Serovar Typhimurium Genes Required for Infection of BALB/c Mice." *PLoS Pathogens* 5 (7): e1000529.
- Chen, Meixin, Hui Sun, Maikel Boot, Lin Shao, Shu-Jung Chang, Weiwei Wang, Tukiet T. Lam, Maria Lara-Tejero, E. Hesper Rego, and Jorge E. Galán. 2020. "Itaconate Is an Effector of a Rab GTPase Cell-Autonomous Host Defense Pathway against *Salmonella*." *Science* 369 (6502): 450–55.
- Cox, Jürgen, and Matthias Mann. 2008. "MaxQuant Enables High Peptide Identification Rates, Individualized P.p.b.-Range Mass Accuracies and Proteome-Wide Protein Quantification." *Nature Biotechnology* 26 (12): 1367–72.
- Dai, Penggao, Sun Yong Jeong, Yanbao Yu, Taohua Leng, Weidong Wu, Ling Xie, and Xian Chen. 2009. "Modulation of TLR Signaling by Multiple MyD88-Interacting Partners Including Leucine-Rich Repeat Fli-I-Interacting Proteins." *Journal of Immunology* 182 (6): 3450–60.
- French, Shawn, Chand Mangat, Amrita Bharat, Jean-Philippe Côté, Hirota Mori, and Eric D. Brown. 2016. "A Robust Platform for Chemical Genomics in Bacterial Systems." *Molecular Biology of the Cell* 27 (6): 1015–25.
- Fu, Ping, Zhiyong Yang, and Leon A. Bach. 2013. "Prohibitin-2 Binding Modulates Insulin-like Growth Factor-Binding Protein-6 (IGFBP-6)-Induced Rhabdomyosarcoma Cell Migration." *The Journal of Biological Chemistry* 288 (41): 29890–900.
- Günster, Regina A., Sophie A. Matthews, David W. Holden, and Teresa L. M. Thurston. 2017. "SseK1 and SseK3 Type III Secretion System Effectors Inhibit NF- κ B Signaling and Necroptotic Cell Death in *Salmonella*-Infected Macrophages." *Infection and Immunity* 85 (3). <https://doi.org/10.1128/IAI.00010-17>.
- Jeng, Edwin E., Varun Bhadkamkar, Nnejiuwa U. Ibe, Haley Gause, Lihua Jiang, Joanne Chan, Ruiqi Jian, et al. 2019. "Systematic Identification of Host Cell Regulators of *Legionella Pneumophila* Pathogenesis Using a Genome-Wide CRISPR Screen." *Cell Host & Microbe* 26 (4): 551–63.e6.
- Lin, F., and H. J. Worman. 1995. "Structural Organization of the Human Gene (LMNB1) Encoding Nuclear Lamin B1." *Genomics* 27 (2): 230–36.

- Lucas, Christopher R., Hector M. Cordero-Nieves, Robert S. Erbe, Jaclyn W. McAlees, Sumeena Bhatia, Richard J. Hodes, Kerry S. Campbell, and Virginia M. Sanders. 2013. "Prohibitins and the Cytoplasmic Domain of CD86 Cooperate to Mediate CD86 Signaling in B Lymphocytes." *Journal of Immunology* 190 (2): 723–36.
- Napier, Brooke A., Sky W. Brubaker, Timothy E. Sweeney, Patrick Monette, Gregory H. Rothmeier, Nina A. Gertsvolf, Andreas Puschnik, Jan E. Carette, Purvesh Khatri, and Denise M. Monack. 2016. "Complement Pathway Amplifies Caspase-11-Dependent Cell Death and Endotoxin-Induced Sepsis Severity." *The Journal of Experimental Medicine* 213 (11): 2365–82.
- Nichols, Robert J., Saunak Sen, Yoe Jin Choo, Pedro Beltrao, Matylda Zietek, Rachna Chaba, Sueyoung Lee, et al. 2011. "Phenotypic Landscape of a Bacterial Cell." *Cell* 144 (1): 143–56.
- Prehna, Gerd, Guijin Zhang, Xiandi Gong, Marek Duszyk, Mark Okon, Lawrence P. McIntosh, Joel H. Weiner, and Natalie C. J. Strynadka. 2012. "A Protein Export Pathway Involving Escherichia Coli Porins." *Structure* 20 (7): 1154–66.
- Sharma, Amita, and Ayub Qadri. 2004. "Vi Polysaccharide of Salmonella Typhi Targets the Prohibitin Family of Molecules in Intestinal Epithelial Cells and Suppresses Early Inflammatory Responses." *Proceedings of the National Academy of Sciences of the United States of America* 101 (50): 17492–97.
- Spring, David R. 2005. "Chemical Genetics to Chemical Genomics: Small Molecules Offer Big Insights." *Chemical Society Reviews* 34 (6): 472–82.
- Yeung, Amy T. Y., Yoon Ha Choi, Amy H. Y. Lee, Christine Hale, Hannes Ponstingl, Derek Pickard, David Goulding, et al. 2019. "A Genome-Wide Knockout Screen in Human Macrophages Identified Host Factors Modulating Salmonella Infection." *mBio* 10 (5). <https://doi.org/10.1128/mBio.02169-19>.

Chapter VI

Discussion and Outlook

Chapter VI: Discussion and Outlook

This thesis expands the knowledge of the *Salmonella* host-pathogen interface during infection through two orthogonal ways: 1) systematically mapping effector-target protein-protein interactions and 2) studying the impact of gene depletion in *Salmonella* on infection. Both are global and systematic approaches, and subsequent validation and mechanistic characterization have been described in this thesis. Parts have been made available to the scientific community in the accompanying publication:

Walch, Philipp, Joel Selkrig, Leigh A. Knodler, Mandy Rettel, Frank Stein, Keith Fernandez, Cristina Viéitez, et al. 2020. “Global Mapping of Salmonella Enterica-Host Protein-Protein Interactions during Infection.” *bioRxiv*, Cold Spring Harbor Laboratory. <https://doi.org/10.1101/2020.05.04.075937>.

1. Effector-target PPIs at the host-pathogen interface

1.1. Brief recap of results

In a first step, I probed the effector-target interface and identified a total of 446 protein-protein interactions (PPIs) spanning 15 STm effectors, two different host cell lines (macrophages and epithelial cells) and two distinct pulldown conditions. I was able to recapitulate known biology by recovering 25 previously described interactions, yet the large majority of observed PPIs are novel. What sets this apart from previous AP/MS studies at the host-pathogen interface is the more physiological setting: using endogenous levels of effector, rather than ectopic expression, and thus retaining an infection context.

To make this possible, we generated a library containing 32 tagged-effector STm strains spanning T3SS1- and T3SS2-dependent translocation. Each strain carries a chromosomal STF-tag at the C-terminus of a given effector (except for SifA, where the tag was placed internally to not disrupt effector localization and functionality). Therefore, this work offers two distinct resources to the community: a vast landscape of interactions, a subset of which has additionally been validated by reciprocal immunoprecipitation, as well as a collection of strains which can be probed in other conditions. Such an expansion could include other relevant host cells, such as dendritic cells or M-cells, probing other time points or infection conditions (such as priming with interferon-gamma or LPS), or assessing spatiotemporal dynamics and cellular localization of specific PPIs.

1.2. Connectivity and specificity within the STm effector interaction network

For the majority of effector proteins, I discovered a multitude of interaction partners co-purifying in AP/QMS, rather than a specific, singular target protein. In many cases, the identified host proteins were functionally related, which gave rise to a highly interconnected network of targeted cellular processes shared by different effectors. It is important to note that not all observed PPIs are necessarily direct, but could also be mediated by host proteins that co-purify as part of a larger protein complex. Indeed, piggybacking, or the co-precipitation of additional host binding partners, is common in

affinity purification studies (Nesvizhskii 2012; Teng et al. 2015). Hence the stickiness or promiscuity of bacterial effectors is most likely biochemical in nature and may occur through interactions between host factors. Furthermore, many effectors targeted biologically distinct protein families or complexes, suggesting that they are multifunctional during infection. While we cannot conclude whether these PPIs occur simultaneously or sequentially, multifunctional effectors are an important concept that had so far only been suggested for pathogens with a very small number of secreted effectors (Backert and Blaser 2016).

Despite the high degree of promiscuity displayed by most STm effectors, the majority of PPIs that I identified were specific to the host background (418 PPIs). Only 28 interactions were observed across both cell lines. Stringent thresholds in hit calling, as well as the difference in expression level within the two cell types, mainly account for such cell-type specific differences. In addition, STm infection follows varying dynamics in epithelial *versus* macrophage cells, and this discrepancy of infection trajectories can cause cell type-specific PPIs.

Besides assessing PPIs in two different cell lines, I applied two orthogonal conditions for harvesting and pulldown. In half of the samples, I used the membrane permeable crosslinker DSP to capture weak PPIs and those occurring transiently. Comparing native harvest and harvest after crosslinking, I observed a differential enrichment of host targets and consequently only a partial overlap between the two immunoprecipitation (IP) conditions. This is likely caused by technical differences as explained in detail in Chapter III, section III.5. Albeit not applied in this study, the application of crosslinking agents prior to immunoprecipitation can also be used to discern direct binding partners from indirect ones. This is especially elegant when coupled with mass spectrometry (Navare et al. 2015; Sinz 2018; Iacobucci, Götze, and Sinz 2020), in which case not only the direct binding partners, but also the interaction site can be determined.

1.3. New insights into STm host-pathogen interactions

In the large-scale AP/MS study, I identified a broad spectrum of enriched host processes and protein families targeted by STm effectors. In this section, I will discuss the further characterization of three biological processes, as well as additional pieces of interesting novel biology that can be investigated in the future.

1.3.1. SseJ, SseL and other effectors are involved in cholesterol trafficking

A biological process I observed to be targeted by a multitude of effectors, mainly PipB2, SseJ and SseL, was cholesterol trafficking. This was attributable to a panel of host proteins (such as OSBP, VAP-A and -B, ANXA1 or NPC1), which is consistent with previously reported data (Wyles, McMaster, and Ridgway 2002; Auweter et al. 2012; Mesmin et al. 2017; Kolodziejek et al. 2019). In this thesis, as described in Chapter IV, I present further molecular evidence of SseJ and SseL cooperating physically and

functionally during infection by impacting lipid transport, more precisely cholesterol influx to and efflux from the SCV.

Both effectors were shown to be required for cholesterol accumulation at the SCV, as measured by filipin staining, albeit SseJ to a larger extent than SseL. When probing their effects in a NPC1-deletion background, the impact of SseL on cholesterol accumulation at the SCV was entirely mitigated, while the SseJ effect became dominant. This, together with previous reports that during infection both NPC1 and SseJ localize at *Salmonella*-induced filaments (Ohlson et al. 2005; Drecktrah et al. 2008), indicates that SseJ and SseL coordinate the maintenance of cholesterol at the SCV *via* NPC1. In contrast to the physical interaction between SseJ and NPC1, which we could identify in AP/QMS, the dependence of SseL function on the presence of NPC1 is of functional nature and most likely not through a direct interaction. To further probe the role of *Salmonella* effectors as well as host proteins such as NPC1 or OSBP on cholesterol trafficking, other readouts may be useful. While filipin stains all unesterified cholesterol, fluorescent probes such as BODIPY (Hölttä-Vuori et al. 2008; Wüstner et al. 2016) can be spiked in to monitor the dynamics of cholesterol trafficking during infection.

While the recruitment of NPC1 to the *Salmonella*-containing vacuole (SCV) did not depend on the presence of SseJ, a deletion of the STm effector protein SifA abolished presence of NPC1 in proximity of intracellular *Salmonella*. This is striking, as in a recently published study, SseJ and SseL were shown to play a role in SCV stability. Knockout of both *sseJ* and *sseL* decreased the fraction of vacuolar STm and caused an increased cytoplasmic escape (Kolodziejek et al. 2019). In addition, deletion of *sifA* has also been associated with a decreased stability of the SCV and an increase in cytoplasmic proliferation (Zhao et al. 2015).

The digitonin permeabilization assay employed in the study by Kolodziejek *et al.* requires harsh treatment prior to staining, affects cell morphology and thereby has the potential to introduce artefacts. It will therefore be highly interesting to probe vacuolar stability during infection using a more direct and less invasive assay. A recently developed dual-color fluorescent reporter strain for cytosolic escape (Hausmann et al. 2020) presents a simple and versatile tool to study the effect of NPC1-deletion or -inhibition, OSBP-inhibition through OSW-1 as well as effector deletion, on SCV stability. These assays can further be coupled to other readouts, such as measuring host cell death *via* LDH assay or monitoring lipid trafficking by filipin staining or BODIPY supplementation.

The SifA-dependent recruitment of NPC1 to the SCV, the newly identified physical interaction between NPC1 and SseJ, as well as the functional dependence of SseL on the presence of NPC1 places this host lipid transporter at the center of the interplay between *Salmonella* and their host. It is reasonable to believe that the host protein NPC1 fuels the efflux of cholesterol from the endosomal compartment, as well as

presumably the SCV towards the ER. SseJ, and to a lesser extent SseL, counteract this by funneling cholesterol towards the SCV. While it remains to be shown whether NPC1 impacts vacuolar stability during *Salmonella* infection, there is evidence from other pathogens that it plays a crucial role during infection. More specifically, NPC1 is the receptor for the Ebola glycoprotein and is required for viral entry (H. Wang et al. 2016). This suggests a function as a “gatekeeper” protein between the endosomal compartment, the cytoplasm and the lumen.

1.3.2. SteC interacts with FMNLs to trigger actin polymerization

In previous work, SteC had been described to mediate actin reorganization and polymerization during infection through HSP70 and by hijacking MAPK signaling (Odendall et al. 2012; Imami et al. 2013). However, the impact SteC exerted on actin bundling could not be entirely explained through these host proteins, indicating that there is a missing piece in this model. One of the most abundant, novel PPIs that I identified occurred between the *Salmonella* effector kinase SteC and formin-like (FMNL) proteins, most predominantly FMNL1. The *in vivo* and *in vitro* interaction between SteC and FMNL proteins, which I described and characterized in this work, offers a previously undescribed link between the interplay of SteC and the host cytoskeleton.

I demonstrated that SteC can directly phosphorylate FMNL proteins in an *in vitro* kinase assay and identified phosphosites in conserved functional regions. Interestingly, two of these, S184 in FMNL1 and its equivalent amino acid site in FMNL2 (S171), were previously shown to promote CDC42 recruitment and interaction, which in turn induces FMNL-driven actin polymerization (Kühn et al. 2015). In the AP/QMS dataset, CDC42 is indeed co-enriched in IP on SteC in RAW264.7 cells, further suggesting that SteC plays a role in FMNL-CDC42-dependent actin rearrangements at the SCV. I hypothesize that SteC directly binds and phosphorylates FMNL proteins, thereby promoting CDC42 binding and recruiting this complex to the SCV, where actin polymerization is then triggered through CDC42-dependent activation of FMNL proteins.

While past studies identified T3SS2-dependent actin bundling in the presence of dominant negative CDC42 (Unsworth et al. 2004), further mechanistic work will be needed to fully unravel the interplay. This includes elucidating the molecular rearrangements occurring upon SteC-binding, identifying the affinity and specificity of SteC to bind different FMNLs, understanding the degree of involvement of CDC42, as well as reconciling these findings with the previously described role of MAPK-dependent signaling in SteC-driven actin regulation (Odendall et al. 2012). Furthermore, it is striking that the interaction between SteC and FMNL proteins occurred as a stable interaction *in vitro* (as seen *via* size-exclusion chromatography) and *in vivo* (as interaction partner in native IP). While kinases generally interact transiently with their substrates, the stable nature of the PPI between SteC and FMNL proteins could allude to a specificity of SteC for formin-like proteins. Lastly, there may

be a panel of other substrates that are phosphorylated by SteC and remain to be identified.

1.3.3. Other protein families and biological processes targeted by effector PPIs

In addition to the two vignettes of novel biology I described in further detail in Chapter IV, there was a vast panel of strong interactions that can fuel novel hypotheses and be further characterized experimentally.

As part of a collaboration, we explored further the strong and conserved interaction between the STm effector PipB and its host target protein PDZD8 (Walch et al. 2020). There, we showed that PDZD8 recruitment to the SCV is contingent on PipB. PDZD8 regulates organelle contact sites in various cell types and colocalizes with the Ras-related protein Rab7 (Hirabayashi et al. 2017; Guillén-Samander, Bian, and De Camilli 2019). Furthermore, the region required for binding Rab7, the coiled-coil domain at the C-terminus of PDZD8 (Guillén-Samander, Bian, and De Camilli 2019), was also essential for establishing the interaction with PipB in this study (Walch et al. 2020). Additionally, PDZD8 has been reported to play a role in impairing intracellular Herpes Simplex Virus replication during infection. It does so through binding moesin and thereby regulating the cytoskeleton (Henning et al. 2011). The function on the cytoskeleton has also been established outside of the context of (viral) infection (Bai et al. 2011). One can therefore speculate that PipB localizes to the SCV surface, where it recruits and binds PDZD8. There, in conjunction with Rab7, PipB may promote organelle contact sites and tethering between late endosomes, the endoplasmic reticulum or mitochondria and the SCV. While it remains unclear how this is beneficial to the intracellular pathogen, proximity of other organelles might be crucial for the rewiring of transport processes, SCV protection and intracellular survival.

A family of proteins that was targeted by several STm effectors, especially in epithelial cells, were Rab-GTPases. Rab10, Rab13 and Rab14 co-purified with PipB2 and SifB. These three host proteins had previously been implicated in various host cell processes. Rab10 is involved in regulating ER dynamics and is responsible for the generation of new ER tubules (English and Voeltz 2013). Furthermore, Rab10 is involved in transport of vesicles containing surface proteins (such as TRL4 or GLUT4) to the cell membrane (D. Wang et al. 2010; Sano et al. 2008), a function also performed by Rab8b and Rab13, depending on the cell type (Sun et al. 2010). Rab13 furthermore plays a role in the assembly of tight junctions through regulation of PKA signaling (Köhler, Louvard, and Zahraoui 2004). Both Rab13 and Rab14 are also involved in recycling at the TGN, and Rab14 is found in early endosomes (Nokes et al. 2008; Junutula et al. 2004; Kitt et al. 2008).

For all Rab proteins identified in this study, there are previously described links to various infectious diseases (Stein, Müller, and Wandinger-Ness 2012). Rab13 and Rab14 are recruited to the intracellular replication compartment of *M. tuberculosis*, where Rab14 is required to prevent maturation and subsequent fusion with the

lysosome and pathogen clearance (Kyei et al. 2006). Rab10 is associated with phagosomes of *Mycobacterium*, where it exerts a protective function (Cardoso, Jordao, and Vieira 2010), as well as in some species of *Chlamydia* (Rzomp et al. 2003). It is therefore highly interesting to look into the alteration of Rab-dependent vesicle trafficking in *Salmonella* infection and pathogenesis, especially since Rab proteins, including Rab29 and Rab32, have been associated with the intracellular pathogenicity of the human-specific bacterium *Salmonella enterica* serovar Typhi (Spanò, Liu, and Galán 2011; Baldassarre et al. 2019).

Another protein family that was enriched as targets of effector PPIs were vesicular sorting proteins (VPS family) associated with the formation of the SNARE complex. Most PPIs with VPS proteins were with the STm effector SifA, which has been linked to the formation of SIFs (Ohlson et al. 2008). VPS proteins have previously been described to play a role in *Salmonella* infection (Patrick et al. 2018). In addition, there are various reports on how other intracellular pathogens, such as *Mycobacterium*, target VPS proteins to rewire vesicle trafficking (Philips 2008; Bach et al. 2008). This is especially true for viral infections, where a multitude of different viruses, including Ebola (Silvestri et al. 2007), HIV (Garrus et al. 2001) and EIAV (Tanzi, Piefer, and Bates 2003) have been reported to utilize VPS function for particle budding and virion release.

Besides Rab-GTPases and VPS proteins, both of which are associated with vesicular trafficking, I identified various other protein families as effector targets that might merit a deeper characterization. A prominent group of proteins are myosins, which were predominantly identified in PPIs with SspH1 and SspH2 in RAW264.7. Several members of the unconventional myosin protein family co-purified with these effectors. One of those, Myo1c, has been implicated in lipid-raft formation and recycling, and therefore STm invasion (Brandstaetter, Kendrick-Jones, and Buss 2012). Other myosin-proteins regulate production of phospholipids and membrane ruffling (Brooks et al. 2017), the positioning of the SCV close to the nucleus (Wasylnka et al. 2008) or degradation of cytoplasmic bacteria (Tumbarello et al. 2015). Therefore, targeting myosin proteins to hijack their motor function or their association with specific lipids occurs throughout the infection trajectory.

Small solute carrier (SLC) proteins were highly enriched as interaction partners of PipB2 and SseJ. SLCs represent a large and diverse family of transporters of various exogenous and endogenous small molecules (Schaller and Lauschke 2019), which are shifting into focus as promising drug targets (Superti-Furga et al. 2020). Other large-scale proteomic studies have identified members of this family as interaction partners of *Salmonella* effectors (D'Costa et al. 2019). While no mechanistic studies of SLC proteins during bacterial infection have been conducted, their functional importance for various cellular processes, such as cell survival (Besecker et al. 2008), signal transduction (Vlachodimou, IJzerman, and Heitman 2019) and ion homeostasis (Fredriksson et al. 2008) is heavily investigated.

1.3.4. Bacterial-bacterial PPIs in the host cytoplasm

The unique setup of this study allowed the detection of PPIs between effectors and other bacterial proteins occurring in the host cell. To exclude the possibility that interactions between bacterial proteins originate from partial lysis of the bacterial cell, I validated the presence of GroEL and STM14_3767 in the cytoplasm, as examples of identified bacterial interaction partners. RecA, another highly abundant bacterial protein, could only be detected in the bacterial fraction, excluding partial lysis as a main factor underlying these PPIs. In addition, I used reciprocal immunoprecipitation to validate the PPI between PipB and GroEL in the host cytoplasm upon infection.

Understanding how bacterial proteins interact and cooperate during infection is very important and has so far only rarely been studied. In addition to a recent study identifying the functional cooperation of SseJ and SseL (Kolodziejek et al. 2019), the two *Salmonella* effectors SseF and SseG have been shown to interact and link the SCV to the Golgi network, thereby securing the intracellular replication niche *via* the host protein ABCD3 (Deiwick et al. 2006; Yu, Liu, and Holden 2016).

In the large-scale AP/MS work, I identified two effector-effector interactions: PipB-SifA and AvrA-GogB. In addition, I observed co-enrichments of SseL and SteC when immunoprecipitating SseJ. As both PipB and SifA have been shown to localize at SIFs (Knodler et al. 2003; Brumell, Goosney, and Finlay 2002), their interaction could be mediated through a common interaction partner or occur due to their colocalization. For AvrA and GogB, a functional relationship in modulating inflammation is possible. Both proteins have been implicated in dampening inflammatory response during infection (Jones et al. 2008; F. Du and Galán 2009; Pilar et al. 2012). Previous reports demonstrated their action through different host proteins, making the physical interaction I identified in this work even more striking, alluding to a functional relevance of how these two cooperate. More mechanistic work will further elucidate the exact interplay of STm effectors on up- or down-regulating inflammation during infection. While the SseJ-SseL interaction is most likely mediated through their concerted effect on OSBP (Kolodziejek et al. 2019), the nature and functionality of the SseJ-SteC interaction remains to be investigated.

1.4. Outlook on the global mapping of the STm-host interplay

In this work, I was able to recapitulate known biology by identifying 25 previously described interactions. Comparing this study to past large-scale systematic efforts to probe STm-host PPIs is important. However, this is a challenging endeavor since previous studies that have systematically probed the STm-host interactome were not performed in an infection context and were commonly using effector overexpression (Auweter et al. 2011; Sontag et al. 2016). Therefore, the absence of overlap between other work and this study can be due to multiple reasons, including our methodological approach to use physiological effector levels and preserve the infection context. As the overabundance of effector proteins by over-expression can lead to nonspecific interactions, and as taking PPIs out of the infection context can increase the

occurrence of artifacts, it is not surprising the data presented here only partially overlap with those pre-existing studies of much smaller scale.

Throughout this thesis, I have highlighted the overlaps and discrepancies between my work and previously reported studies (Auweter et al. 2011; Sontag et al. 2016; D'Costa et al. 2019). This has most extensively been done in Chapter III, sections III.7 and III.8. I was thereby able to establish a higher level of confidence in a panel of previously reported interactions, such as SseJ-RhoA and SseL-OSBP, both of which have been described in further detail by more mechanistic studies (Ohlson et al. 2008; Christen et al. 2009; Schleker et al. 2012; Auweter et al. 2012). Furthermore, the findings in this work underline the importance of several host protein families, such as SLCs, which have been linked to cytokine release, viral and bacterial infections as well as innate immunity (Awomoyi 2007; Singh et al. 2016; Nguyen et al. 2018). These processes could be targeted by various STm effectors to modulate inflammation, protection of the SCV as well as cell invasion.

It would be exciting to combine these existing approaches with our methodology to probe the transient host-pathogen interactome during infection in further detail and to add a second layer of spatiotemporal complexity. Besides that, using catalytically inactive effectors as baits could arrest transient processes in the binding stage and thereby enhance the capture of transient target proteins. Also, expanding the spectrum of detectable interactions to non-proteinaceous molecules, such as lipids, (deoxy-)ribonucleotides or sugars by combining AP/MS approaches with metabolomics or lipidomics (Haberkant et al. 2013; Maeda et al. 2013; Saliba et al. 2014) would be a fascinating linking point to existing methodologies and could deepen our knowledge of effector functionality in the host cytoplasm.

Furthermore, the knowledge generated in this work could be used to predict a multitude of features at the host-pathogen interface. Common motifs on host targets of STm effectors can be exploited to predict other interaction partners or to enrich the biological function of the interaction during infection. This is most straightforward for post-translational modifications introduced by *Salmonella* effectors (Ye et al. 2007; Poh et al. 2008; Diao et al. 2008; Narayanan and Edelman 2014; LaRock, Chaudhary, and Miller 2015), by using motifs and patterns in substrates of STm effectors such as the phosphosites targeted by SteC.

Lastly, despite the vast extent of previously described effector proteins contained in our library, current knowledge may suffer from underestimation of the entire repertoire of (effector) proteins translocated upon infection (Li et al. 2018; Niemann et al. 2011). Recent approaches in proteomics allow for an unbiased identification and profiling of secreted proteins across intracellular pathogens (Mahdavi et al. 2014). In addition, genetic screening, coupled to unbiased phenotypic fingerprinting, as exemplified in this work with *yebF* (Chapter V, section V.4.4), represents a powerful tool to identify or predict effectors *de novo*. By applying these methodologies, the full arsenal of STm

effector proteins can be uncovered and, due to its versatility, the library that I presented in this work can easily be amended. Thereby, further PPIs occurring during infection can be identified and the interaction map between STm and host further resolved.

1.5. Shortcomings and potential pitfalls

It has previously been reported that introducing an affinity tag can impede proper effector localization or function. This has been studied in most detail for SifA, which has a C-terminal prenylation motif (Brumell, Goosney, and Finlay 2002). Consequently, we adapted our tagging strategy in this specific case. It is however not known whether similar disruption of effector functionality could occur for any of the remaining 31 effectors in the library. In addition, assessing effector functionality may require effector-specific assays, as for a large number of STm effectors, a single gene knockout does not confer a strong phenotype (R. Figueira et al. 2013). Low abundance of the tagged protein can indicate a decreased stability or expression, which could be the case for the otherwise highly expressed effectors SseF and SseG, but further effector-specific phenotypic testing will be required for the majority of effectors.

We assessed expression (i.e. presence in the insoluble fraction) and translocation (i.e. presence in the cytoplasmic fraction) for the entire library and were able to detect 20 effectors within the cytoplasm during infection (of 28 that were expressed). There are plausible several reasons for failure to detect effector translocation:

- 1) the C-terminal STF-tag could impede protein expression, folding, stability or T3SS-translocation
- 2) the effector is not expressed or translocated at the given time point tested
- 3) the effector is not expressed in the tested cell line
- 4) the amount of translocated effector is so low that our detection is not sensitive enough

Of the panel of 15 effector proteins for which we could detect reproducible translocation by AP/QMS in the two cell lines, five did not display any significant PPIs (SlrP in RAW264.7 and GogB, SseK1, SspH1 and SspH2 in HeLa cells). Again, there are multiple possible explanations for this finding:

- 1) the C-terminal tag could have disrupted protein stability, functionality, localization or binding to host targets,
- 2) the effector might display highly promiscuous behavior or a multitude of transient interactions (as many of them have enzymatic activity),
- 3) the interaction partner may be non-proteinaceous, such as lipids, metabolites or nucleotides (Nawabi, Catron, and Haldar 2008; Knodler et al. 2009; McShan et al. 2016).

Lastly, we were unable to recapitulate a number of well-described and rigorously characterized interactions, such as AvrA and MKK7 (Jones et al. 2008; F. Du and

Galán 2009) or SifA and SKIP (Jackson et al. 2008; Diacovich et al. 2009; Zhao et al. 2015). This could be due to tagging, condition, cell line, time-point, stringency of the enrichment threshold, limitations of the MS or methodological false negatives.

1.6. Conclusion and outlook

In conclusion, by maintaining physiological conditions and the infection context in large scale, this work provides a breakthrough in proteomic host-pathogen studies. The data presented here can be used for hypothesis building and as starting points for other unbiased and more systematic studies. This includes the understanding of effector cooperation, which is of very high relevance in intracellular pathogens, especially those with large arsenals of translocated effectors. Understanding the interplay between pathogen and host in an infection context, how translocated effector proteins hijack and modify host signaling and how these lead to pathogenicity are invaluable to both understanding the molecular mechanisms of infection and discovering targets for antimicrobial therapies.

There are multiple ways in which the methodology presented here can be broadened and adapted to other contexts. It would be fascinating to probe the host-pathogen interface dynamically over different time points and assess the host-specificity by using further host cell backgrounds. By focusing on an earlier time point, one could overcome the bias towards SPI-2 effectors, which are most abundantly secreted at the later stages of infection. To overcome the low amount of effector bait protein that is inevitably linked, the scale would need to be increased or low-copy plasmids can be used for effector expression. That way, a more physiological methodology to broaden the knowledge on effector-target PPIs of SopF (Cheng et al. 2017; Xu et al. 2019; Lau et al. 2019), SopB (Knodler, Finlay, and Steele-Mortimer 2005; Mallo et al. 2008; Bakowski et al. 2010), AvrA (Jones et al. 2008; F. Du and Galán 2009) and others could be developed.

In addition, through combining the approach presented here with already existing alternatives, non-proteinaceous targets, post-translational modifications, such as ubiquitinylation or phosphorylation, and transient interactions can be included and enriched for. Lastly, I hope that this work incentivizes similar approaches in other intracellular pathogens which translocate effector proteins. *Salmonella enterica* serovar Typhimurium is one of the best studied intracellular model organisms, where we show that using an unbiased global AP/QMS approach we are still able to uncover hidden biology. I anticipate that further adaptation of our AP/QMS approach to other pathogens can fuel the identification of host-pathogen PPIs across the entire infection biology community.

2. Host-pathogen interface beyond effector PPIs

2.1. Unbiased approaches and their advantages

The application of unbiased high-throughput methodologies has deepened the knowledge of the interconnectivity between the host and the pathogen during infection. Recent advances cover the elucidation of essential host factors for infection using the CRISPR-Cas technology (Napier et al. 2016; Xu et al. 2019; Jeng et al. 2019; R. Wang et al. 2020), the identification of bacterial genes that play a role during infection (Chaudhuri et al. 2009; Xu et al. 2019), the screening of drugs modulating infection (Barrows et al. 2016) or the attribution of changes to the host or pathogen transcriptome (*via* dual RNAseq) and proteome (*via* mass spectrometry) upon infection (Bojkova et al. 2020; Pisu et al. 2020).

Main advantages of unbiased approaches include their genome-wide scale, their multifactoriality, their increased statistical robustness and their capability to uncover novel biology in an unprecedented way (Eckhardt et al. 2020). By not excluding components by default, unexpected interdependencies can be discovered. Thereby, unbiased approaches can fuel and initiate hypothesis-driven research.

2.2. New insights into interdependency

In this work, two distinct and orthogonal unbiased approaches have been applied:

- the identification of host protein targets for a library of translocated *Salmonella* effector proteins
- the assessment of bacterial genes that play a role during infection

While the former has been thoroughly discussed in the previous section, I will now focus on the interdependency beyond the effector-target protein-protein interaction interface.

Upon entry into the host cell, *Salmonella* encounters and proliferates in a hostile environment. Host defenses, as well as nutrient depletion inside the SCV require rewiring of host cell pathways and lay the basis for the interdependency between host and pathogen. Changes to the bacterial metabolism, as well as a metabolic interplay between the host and the pathogen have been reported to play a major role (Olive and Sassetti 2016; Bumann and Schothorst 2017). Specifically, swift adaptation to lower ATP production (Lee, Pontes, and Groisman 2013), as well as a reduced ribosome biosynthesis (Pontes, Yeom, and Groisman 2016), alongside changes to the hosts lipid metabolism (Walpole, Grinstein, and Westman 2018) or lactate production during infection (Gillis et al. 2018) are used to gain competitive advantage over gut microbiota, survive intracellularly and persist antimicrobial treatment (Harms, Maisonneuve, and Gerdes 2016; Bumann and Schothorst 2017).

The data presented in the various parts of this study can be used to further shed light into which bacterial proteins are required for intracellular survival and which host metabolic pathways are affected, hijacked and up- or down-regulated during infection.

By combining knowledge from effector-target interactions, the effect of single-gene knockouts on infection and the changes in abundance and thermal stability across the host proteome with additional mechanistic follow-up, we can build further hypotheses about how the host and pathogen metabolism are interwoven during infection.

Furthermore, this study presents a vast dataset which can, in addition to mechanistic follow-up characterization on specific interaction points, be exploited to predict bacterial protein function. As showcased with the secreted protein YebF, which came into focus due to its feature fingerprint-similarity to the translocated SPI-2 effector SseJ, it is possible to infer parts of a proteins' functionalities from phenotypic changes upon genetic deletion. This principle can be expanded to other protein classes and can be enhanced further by including additional features of effectors, such as sequence similarity (McDermott et al. 2011) or the occurrence of Short Linear Motifs (SLiMs, (Sámano-Sánchez and Gibson 2020)). Furthermore, the biological role of previously uncharacterized effector proteins is more easily accessible to research. For the majority of known STm effectors, single gene deletion does not confer a significant decrease in infection rate of intracellular proliferation (A. R. Figueira 2011), and in many cases, no phenotype is described for deletion. By expanding the dimensionality of microscopy features as presented in this study, we enable the research community to attribute specific and observable, phenotypic changes to the absence of single bacterial proteins, thereby fueling hypotheses for effector function during infection.

2.3. Next developments in the field of host-pathogen interactions

Recent advances in the field of host-*Salmonella* interactions include the screening of host factors that are required for the initiation and maintenance of infection by using RNAi (Misselwitz et al. 2011; Thornbrough et al. 2012; Curt et al. 2014) or CRISPR-Cas9-mediated knockout (Napier et al. 2016; Yeung et al. 2019; Xu et al. 2019). This can be fine-tuned further by adjusting the host transcription to a finer degree using CRISPR-interference (D. Du et al. 2017) or CRISPR-activation (Heaton et al. 2017) using modified Cas9, in the context of *Salmonella* infection. Furthermore, using these setups for genetic modification of the host, and combining these with genetic perturbations on the pathogen side will yield a deepened understanding of genetic interactions occurring during infection: By attributing antagonisms and synergies to pairs of host and pathogen genes (O'Connor et al. 2012).

To further understand connection points between the host and the pathogen, and to elucidate ways to disrupt the means by which *Salmonella* promotes its intracellular survival, it is highly meaningful to study a combination of genetic interactions between host and pathogen, alongside chemogenomics in the context of infection. This can either be done independently, by comparing results of chemical genomics screening studies in *Salmonella* with knockout infection screens, or simultaneously, by adding another layer of complexity to an infection screen. These include genetic perturbation on the host side, as well as different stresses, such as temperature, oxygen level and treatment with an antibiotic or a human-targeted drug. This would allow the

identification of interaction points between the host and the pathogen that can be therapeutically targeted, and enables a better understanding of the impact of individual STM genes on the development of resistance to existing treatments.

In addition to genomic advances, novel proteomic-based techniques that do not rely on the identification of interaction partners of a specific protein, but rather explore the proteome as a whole, have fueled the understanding of host-pathogen interactions on a global scale. These include assessing the changes in host protein expression, localization, or post-translational modifications upon challenge with a pathogen (Ribet and Cossart 2010; Imami et al. 2013; Zhang et al. 2020; Selkrig, Li, et al. 2020). This can be extended by an additional layer of complexity through the introduction of knockouts or mutations on either host or pathogen side. Furthermore, the changes in protein abundance and thermal stability can be assessed by Thermal Proteome Profiling (TPP, (Savitski et al. 2014; Franken et al. 2015)). Here, changes in thermal stability can be used as a proxy for protein binding, post-translational modification or conformational change. While its original application lies in the discovery of changes introduced by drug treatment to identify cellular drug targets (Savitski et al. 2014), recent advances have also probed the effect of pathogens on the host cell (Selkrig, Stanifer, et al. 2020).

Adapting TPP to *Salmonella* infection and probing changes in abundance and thermal stability occurring to the host proteome upon infection would deepen the knowledge on host rewiring, as it has for viral infections (Selkrig, Stanifer, et al. 2020). By additionally introducing single gene deletions on the pathogen side, changes that occur upon infection can be attributed to specific bacterial proteins, such as individual SPI-1 and SPI-2 effectors. Using previous reports about effector functionality and interactions (Schleker et al. 2012; LaRock, Chaudhary, and Miller 2015; Walch et al. 2020), such a study could be validated and benchmarked and the knowledge about how *Salmonella* rewires host cells beyond the effector-target interface could be further expanded.

Lastly, all presented advances can be further developed by transferring the technology and methodology to other, more complex or meaningful host systems as well as other pathogens.

2.4. Conclusion and further outlook

As indicated in the previous sections, the field of host-pathogen interactions has the potential to develop into various dimensions and directions, trying to describe the complex interplay between host and pathogen. Among those that I did not present in this chapter are the incorporation of commensal bacteria, which play an impactful role during colonization of the host (Brugiroux et al. 2016; Rogers, Tsolis, and Bäumlner 2021), as well as the development of more complex experimental systems to study the course of infection (Nickerson et al. 2018; Lees et al. 2019; Verma et al. 2020).

During infection of the host, the first barrier invading pathogens encounter, is the colonization resistance, which is mainly conferred by the host microbiome (Brugiroux et al. 2016; Rogers, Tsolis, and Bäumlér 2021). Studies addressing the interactions and competition between commensal gut bacteria and pathogens have highlighted the production of short-chain fatty acids such as propionate or butyrate (Jacobson et al. 2018; Rogers, Tsolis, and Bäumlér 2021), a competition for iron (Deriu et al. 2013), and the maintenance of anaerobic conditions (Litvak et al. 2019) as main factors determining colonization resistance. The interplay between the pathogen, the microbiome and the host is strongly influenced by the induction of inflammation by *Salmonella*, providing a competitive advantage and creating favorable conditions for host cell invasion (Stecher et al. 2007; Spees et al. 2013).

Assessing the interplay between these three entities has so far been limited to animal models, which have continuously evolved to include a controllable and stable microbiome conferring comparable colonization resistance (Brugiroux et al. 2016). An alternative direction is the continuous development of sophisticated *ex vivo* experimental systems that allow for more precise manipulation than animal models, but are of higher complexity than 2-dimensional cell culture, such as organoids or mini-guts (Nickerson et al. 2018; Lees et al. 2019; Verma et al. 2020). In these systems, a variety of infection related processes, such as the interplay between the host intestinal cells and commensal bacteria (Lu et al. 2020) or neutrophil invasion (Karve et al. 2017) have been studied. Building up on these co-culture systems, the host responses can be studied in more detail, taking the impact of commensal bacteria into account.

I am confident that studies as the ones presented in this thesis will fuel hypothesis-driven research, thereby better characterizing the interconnectivity between pathogen and host. Taking a multifaceted systems approach to infection biology, this thesis presents a decisive step into a more holistic understanding of the *Salmonella*-host interface.

3. Bibliography of this chapter

- Auweter, Sigrid D., Amit P. Bhavsar, Carmen L. de Hoog, Yuling Li, Y. Alina Chan, Joris van der Heijden, Michael J. Lowden, et al. 2011. "Quantitative Mass Spectrometry Catalogues *Salmonella* Pathogenicity Island-2 Effectors and Identifies Their Cognate Host Binding Partners." *The Journal of Biological Chemistry* 286 (27): 24023–35.
- Auweter, Sigrid D., Hong B. Yu, Ellen T. Arena, Julian A. Guttman, and B. Brett Finlay. 2012. "Oxysterol-Binding Protein (OSBP) Enhances Replication of Intracellular *Salmonella* and Binds the *Salmonella* SPI-2 Effector SseL via Its N-Terminus." *Microbes and Infection / Institut Pasteur* 14 (2): 148–54.
- Awomoyi, Agnes A. 2007. "The Human Solute Carrier Family 11 Member 1 Protein (SLC11A1): Linking Infections, Autoimmunity and Cancer?" *FEMS Immunology and Medical Microbiology* 49 (3): 324–29.
- Bach, Horacio, Kadamba G. Papavinasasundaram, Dennis Wong, Zakaria Hmama, and Yossef Av-Gay. 2008. "Mycobacterium Tuberculosis Virulence Is Mediated by PtpA Dephosphorylation of Human Vacuolar Protein Sorting 33B." *Cell Host & Microbe* 3 (5): 316–22.
- Backert, Steffen, and Martin J. Blaser. 2016. "The Role of CagA in the Gastric Biology of *Helicobacter Pylori*." *Cancer Research* 76 (14): 4028–31.
- Bai, Siau Wei, Maria Teresa Herrera-Abreu, Jennifer L. Rohn, Victor Racine, Virginia Tajadura, Narendra Suryavanshi, Stephanie Bechtel, Stefan Wiemann, Buzz Baum, and Anne J. Ridley. 2011. "Identification and Characterization of a Set of Conserved and New Regulators of Cytoskeletal Organization, Cell Morphology and Migration." *BMC Biology* 9 (August): 54.
- Bakowski, Malina A., Virginie Braun, Grace Y. Lam, Tony Yeung, Won Do Heo, Tobias Meyer, B. Brett Finlay, Sergio Grinstein, and John H. Brummel. 2010. "The Phosphoinositide Phosphatase SopB Manipulates Membrane Surface Charge and Trafficking of the *Salmonella*-Containing Vacuole." *Cell Host & Microbe* 7 (6): 453–62.
- Baldassarre, Massimiliano, Virtu Solano-Collado, Arda Balci, Heather M. Wilson, Subhankar Mukhopadhyay, Gordon Dougan, and Stefania Spanò. 2019. "Salmonella Typhi Survives in Human Macrophages by Neutralizing the RAB32/BLOC-3 Host-Defence Pathway." *bioRxiv*. <https://doi.org/10.1101/570531>.
- Barrows, Nicholas J., Rafael K. Campos, Steven T. Powell, K. Reddisiva Prasanth, Geraldine Schott-Lerner, Ruben Soto-Acosta, Gaddiel Galarza-Muñoz, et al. 2016. "A Screen of FDA-Approved Drugs for Inhibitors of Zika Virus Infection." *Cell Host & Microbe* 20 (2): 259–70.
- Besecker, Beth, Shengying Bao, Barbara Bohacova, Audrey Papp, Wolfgang Sadee, and Daren L. Knoell. 2008. "The Human Zinc Transporter SLC39A8 (Zip8) Is Critical in Zinc-Mediated Cytoprotection in Lung Epithelia." *American Journal of Physiology. Lung Cellular and Molecular Physiology* 294 (6): L1127–36.
- Bojkova, Denisa, Kevin Klann, Benjamin Koch, Marek Widera, David Krause, Sandra Ciesek, Jindrich Cinatl, and Christian Münch. 2020. "Proteomics of SARS-CoV-2-Infected Host Cells Reveals Therapy Targets." *Nature* 583 (7816): 469–72.
- Brandstaetter, Hemma, John Kendrick-Jones, and Folma Buss. 2012. "Myo1c Regulates Lipid Raft Recycling to Control Cell Spreading, Migration and *Salmonella* Invasion." *Journal of Cell Science* 125 (Pt 8): 1991–2003.

- Brooks, Andrew B. E., Daniel Humphreys, Vikash Singh, Anthony C. Davidson, Susan D. Arden, Folma Buss, and Vassilis Koronakis. 2017. "MYO6 Is Targeted by Salmonella Virulence Effectors to Trigger PI3-Kinase Signaling and Pathogen Invasion into Host Cells." *Proceedings of the National Academy of Sciences of the United States of America* 114 (15): 3915–20.
- Brugiroux, Sandrine, Markus Beutler, Carina Pfann, Debora Garzetti, Hans-Joachim Ruscheweyh, Diana Ring, Manuel Diehl, et al. 2016. "Genome-Guided Design of a Defined Mouse Microbiota That Confers Colonization Resistance against Salmonella Enterica Serovar Typhimurium." *Nature Microbiology* 2 (November): 16215.
- Brumell, John H., Danika L. Goosney, and B. Brett Finlay. 2002. "SifA, a Type III Secreted Effector of Salmonella Typhimurium, Directs Salmonella-Induced Filament (Sif) Formation along Microtubules." *Traffic* 3 (6): 407–15.
- Bumann, Dirk, and Joep Schothorst. 2017. "Intracellular Salmonella Metabolism." *Cellular Microbiology* 19 (10). <https://doi.org/10.1111/cmi.12766>.
- Cardoso, Carla M. P., Luisa Jordao, and Otilia V. Vieira. 2010. "Rab10 Regulates Phagosome Maturation and Its Overexpression Rescues Mycobacterium-Containing Phagosomes Maturation." *Traffic* 11 (2): 221–35.
- Chaudhuri, Roy R., Sarah E. Peters, Stephen J. Pleasance, Helen Northen, Chrissie Willers, Gavin K. Paterson, Danielle B. Cone, et al. 2009. "Comprehensive Identification of Salmonella Enterica Serovar Typhimurium Genes Required for Infection of BALB/c Mice." *PLoS Pathogens* 5 (7): e1000529.
- Cheng, Sen, Lu Wang, Qian Liu, Linlu Qi, Kaiwen Yu, Zhen Wang, Mei Wu, et al. 2017. "Identification of a Novel Salmonella Type III Effector by Quantitative Secretome Profiling." *Molecular & Cellular Proteomics: MCP* 16 (12): 2219–28.
- Christen, Matthias, Lisette H. Coye, Jill S. Hontz, Doris L. LaRock, Richard A. Pfuetzner, Megha, and Samuel I. Miller. 2009. "Activation of a Bacterial Virulence Protein by the GTPase RhoA." *Science Signaling* 2 (95): ra71.
- Curt, Alexander, Jiuli Zhang, Justin Minnerly, and Kailiang Jia. 2014. "Intestinal Autophagy Activity Is Essential for Host Defense against Salmonella Typhimurium Infection in *Caenorhabditis Elegans*." *Developmental and Comparative Immunology* 45 (2): 214–18.
- D'Costa, Vanessa M., Etienne Coyaud, Kirsten C. Boddy, Estelle M. N. Laurent, Jonathan St-Germain, Taoyingnan Li, Sergio Grinstein, Brian Raught, and John H. Brumell. 2019. "BioID Screen of Salmonella Type 3 Secreted Effectors Reveals Host Factors Involved in Vacuole Positioning and Stability during Infection." *Nature Microbiology*, October. <https://doi.org/10.1038/s41564-019-0580-9>.
- Deiwick, Jörg, Suzana P. Salcedo, Emmanuel Boucrot, Sarah M. Gilliland, Thomas Henry, Nele Petermann, Scott R. Waterman, Jean-Pierre Gorvel, David W. Holden, and Stéphane Méresse. 2006. "The Translocated Salmonella Effector Proteins SseF and SseG Interact and Are Required to Establish an Intracellular Replication Niche." *Infection and Immunity* 74 (12): 6965–72.
- Deriu, Elisa, Janet Z. Liu, Milad Pezeshki, Robert A. Edwards, Roxanna J. Ochoa, Heidi Contreras, Stephen J. Libby, Ferric C. Fang, and Manuela Raffatellu. 2013. "Probiotic Bacteria Reduce Salmonella Typhimurium Intestinal Colonization by Competing for Iron." *Cell Host & Microbe* 14 (1): 26–37.

- Diacovich, Lautaro, Audrey Dumont, Daniel Lafitte, Elodie Soprano, Aude-Agnès Guilhon, Christophe Bignon, Jean-Pierre Gorvel, Yves Bourne, and Stéphane Méresse. 2009. "Interaction between the SifA Virulence Factor and Its Host Target SKIP Is Essential for Salmonella Pathogenesis." *The Journal of Biological Chemistry* 284 (48): 33151–60.
- Diao, Jianbo, Ying Zhang, Jon M. Huibregtse, Daoguo Zhou, and Jue Chen. 2008. "Crystal Structure of SopA, a Salmonella Effector Protein Mimicking a Eukaryotic Ubiquitin Ligase." *Nature Structural & Molecular Biology* 15 (1): 65–70.
- Drecktrah, Dan, Seamus Levine-Wilkinson, Tapen Dam, Seth Winfree, Leigh A. Knodler, Trina A. Schroer, and Olivia Steele-Mortimer. 2008. "Dynamic Behavior of Salmonella-Induced Membrane Tubules in Epithelial Cells." *Traffic* 9 (12): 2117–29.
- Du, Dan, Assen Roguev, David E. Gordon, Meng Chen, Si-Han Chen, Michael Shales, John Paul Shen, et al. 2017. "Genetic Interaction Mapping in Mammalian Cells Using CRISPR Interference." *Nature Methods* 14 (6): 577–80.
- Du, Fangyong, and Jorge E. Galán. 2009. "Selective Inhibition of Type III Secretion Activated Signaling by the Salmonella Effector AvrA." *PLoS Pathogens* 5 (9): e1000595.
- Eckhardt, Manon, Judd F. Hultquist, Robyn M. Kaake, Ruth Hüttenhain, and Nevan J. Krogan. 2020. "A Systems Approach to Infectious Disease." *Nature Reviews. Genetics* 21 (6): 339–54.
- English, Amber R., and Gia K. Voeltz. 2013. "Rab10 GTPase Regulates ER Dynamics and Morphology." *Nature Cell Biology* 15 (2): 169–78.
- Figueira, Ana Rita. 2011. "Analysis of Effectors of the Salmonella Typhimurium SPI-2 Type Three Secretion System." Imperial College London. <https://doi.org/10.25560/9287>.
- Figueira, Rita, Kathryn G. Watson, David W. Holden, and Sophie Helaine. 2013. "Identification of Salmonella Pathogenicity Island-2 Type III Secretion System Effectors Involved in Intramacrophage Replication of *S. Enterica* Serovar Typhimurium: Implications for Rational Vaccine Design." *mBio* 4 (2): e00065.
- Franken, Holger, Toby Mathieson, Dorothee Childs, Gavain M. A. Sweetman, Thilo Werner, Ina Tögel, Carola Doce, et al. 2015. "Thermal Proteome Profiling for Unbiased Identification of Direct and Indirect Drug Targets Using Multiplexed Quantitative Mass Spectrometry." *Nature Protocols* 10 (10): 1567–93.
- Fredriksson, Robert, Karl J. V. Nordström, Olga Stephansson, Maria G. A. Hägglund, and Helgi B. Schiöth. 2008. "The Solute Carrier (SLC) Complement of the Human Genome: Phylogenetic Classification Reveals Four Major Families." *FEBS Letters* 582 (27): 3811–16.
- Garrus, J. E., U. K. von Schwedler, O. W. Pornillos, S. G. Morham, K. H. Zavitz, H. E. Wang, D. A. Wettstein, et al. 2001. "Tsg101 and the Vacuolar Protein Sorting Pathway Are Essential for HIV-1 Budding." *Cell* 107 (1): 55–65.
- Gillis, Caroline C., Elizabeth R. Hughes, Luisella Spiga, Maria G. Winter, Wenhan Zhu, Tatiane Furtado de Carvalho, Rachael B. Chanin, et al. 2018. "Dysbiosis-Associated Change in Host Metabolism Generates Lactate to Support Salmonella Growth." *Cell Host & Microbe* 23 (1): 54–64.e6.

- Guillén-Samander, Andrés, Xin Bian, and Pietro De Camilli. 2019. "PDZD8 Mediates a Rab7-Dependent Interaction of the ER with Late Endosomes and Lysosomes." *Proceedings of the National Academy of Sciences of the United States of America*, October. <https://doi.org/10.1073/pnas.1913509116>.
- Haberkant, Per, Reinout Raijmakers, Marjolein Wildwater, Timo Sachsenheimer, Britta Brügger, Kenji Maeda, Martin Houweling, et al. 2013. "In Vivo Profiling and Visualization of Cellular Protein-Lipid Interactions Using Bifunctional Fatty Acids." *Angewandte Chemie* 52 (14): 4033–38.
- Harms, Alexander, Etienne Maisonneuve, and Kenn Gerdes. 2016. "Mechanisms of Bacterial Persistence during Stress and Antibiotic Exposure." *Science* 354 (6318). <https://doi.org/10.1126/science.aaf4268>.
- Hausmann, Annika, Desirée Böck, Petra Geiser, Dorothee L. Berthold, Stefan A. Fattinger, Markus Furter, Judith A. Bouman, et al. 2020. "Intestinal Epithelial NAIP/NLRC4 Restricts Systemic Dissemination of the Adapted Pathogen *Salmonella Typhimurium* due to Site-Specific Bacterial PAMP Expression." *Mucosal Immunology* 13 (3): 530–44.
- Heaton, Brook E., Edward M. Kennedy, Rebekah E. Dumm, Alfred T. Harding, Matthew T. Sacco, David Sachs, and Nicholas S. Heaton. 2017. "A CRISPR Activation Screen Identifies a Pan-Avian Influenza Virus Inhibitory Host Factor." *Cell Reports* 20 (7): 1503–12.
- Henning, Matthew S., Patricia Stiedl, Denis S. Barry, Robert McMahon, Scott G. Morham, Derek Walsh, and Mojgan H. Naghavi. 2011. "PDZD8 Is a Novel Moesin-Interacting Cytoskeletal Regulatory Protein That Suppresses Infection by Herpes Simplex Virus Type 1." *Virology* 415 (2): 114–21.
- Hirabayashi, Yusuke, Seok-Kyu Kwon, Hunki Paek, Wolfgang M. Pernice, Maëla A. Paul, Jino Lee, Parsa Erfani, et al. 2017. "ER-Mitochondria Tethering by PDZD8 Regulates Ca²⁺ Dynamics in Mammalian Neurons." *Science* 358 (6363): 623–30.
- Hölttä-Vuori, Maarit, Riikka-Liisa Uronen, Jarmila Repakova, Emppu Salonen, Ilpo Vattulainen, Pertti Panula, Zaiguo Li, Robert Bittman, and Elina Ikonen. 2008. "BODIPY-Cholesterol: A New Tool to Visualize Sterol Trafficking in Living Cells and Organisms." *Traffic* 9 (11): 1839–49.
- Iacobucci, Claudio, Michael Götze, and Andrea Sinz. 2020. "Cross-Linking/mass Spectrometry to Get a Closer View on Protein Interaction Networks." *Current Opinion in Biotechnology* 63 (June): 48–53.
- Imami, Koshi, Amit P. Bhavsar, Hongbing Yu, Nat F. Brown, Lindsay D. Rogers, B. Brett Finlay, and Leonard J. Foster. 2013. "Global Impact of *Salmonella* Pathogenicity Island 2-Secreted Effectors on the Host Phosphoproteome." *Molecular & Cellular Proteomics: MCP* 12 (6): 1632–43.
- Jackson, Laurie K., Parwez Nawabi, Cristiana Hentea, Everett A. Roark, and Kasturi Haldar. 2008. "The *Salmonella* Virulence Protein SifA Is a G Protein Antagonist." *Proceedings of the National Academy of Sciences of the United States of America* 105 (37): 14141–46.
- Jacobson, Amanda, Lilian Lam, Manohary Rajendram, Fiona Tamburini, Jared Honeycutt, Trung Pham, Will Van Treuren, et al. 2018. "A Gut Commensal-Produced Metabolite Mediates Colonization Resistance to *Salmonella* Infection." *Cell Host & Microbe* 24 (2): 296–307.e7.

- Jeng, Edwin E., Varun Bhadkamkar, Nnejiuwa U. Ibe, Haley Gause, Lihua Jiang, Joanne Chan, Ruiqi Jian, et al. 2019. "Systematic Identification of Host Cell Regulators of Legionella Pneumophila Pathogenesis Using a Genome-Wide CRISPR Screen." *Cell Host & Microbe* 26 (4): 551–63.e6.
- Jones, Rheinallt M., Huixia Wu, Christy Wentworth, Liping Luo, Lauren Collier-Hyams, and Andrew S. Neish. 2008. "Salmonella AvrA Coordinates Suppression of Host Immune and Apoptotic Defenses via JNK Pathway Blockade." *Cell Host & Microbe* 3 (4): 233–44.
- Junutula, Jagath R., Ann M. De Mazière, Andrew A. Peden, Karen E. Ervin, Raj J. Advani, Suzanne M. van Dijk, Judith Klumperman, and Richard H. Scheller. 2004. "Rab14 Is Involved in Membrane Trafficking between the Golgi Complex and Endosomes." *Molecular Biology of the Cell* 15 (5): 2218–29.
- Karve, Sayali S., Suman Pradhan, Doyle V. Ward, and Alison A. Weiss. 2017. "Intestinal Organoids Model Human Responses to Infection by Commensal and Shiga Toxin Producing Escherichia Coli." *PloS One* 12 (6): e0178966.
- Kitt, Khameeka N., Delia Hernández-Deviez, Sarah D. Ballantyne, Elias T. Spiliotis, James E. Casanova, and Jean M. Wilson. 2008. "Rab14 Regulates Apical Targeting in Polarized Epithelial Cells." *Traffic* 9 (7): 1218–31.
- Knodler, Leigh A., B. Brett Finlay, and Olivia Steele-Mortimer. 2005. "The Salmonella Effector Protein SopB Protects Epithelial Cells from Apoptosis by Sustained Activation of Akt." *The Journal of Biological Chemistry* 280 (10): 9058–64.
- Knodler, Leigh A., Bruce A. Vallance, Michael Hensel, Daniela Jäckel, B. Brett Finlay, and Olivia Steele-Mortimer. 2003. "Salmonella Type III Effectors PipB and PipB2 Are Targeted to Detergent-Resistant Microdomains on Internal Host Cell Membranes." *Molecular Microbiology* 49 (3): 685–704.
- Knodler, Leigh A., Seth Winfree, Dan Drecktrah, Robin Ireland, and Olivia Steele-Mortimer. 2009. "Ubiquitination of the Bacterial Inositol Phosphatase, SopB, Regulates Its Biological Activity at the Plasma Membrane." *Cellular Microbiology* 11 (11): 1652–70.
- Köhler, Katja, Daniel Louvard, and Ahmed Zahraoui. 2004. "Rab13 Regulates PKA Signaling during Tight Junction Assembly." *The Journal of Cell Biology* 165 (2): 175–80.
- Kolodziejek, Anna M., Melissa A. Altura, Junping Fan, Erik M. Petersen, Matthew Cook, Peter S. Brzovic, and Samuel I. Miller. 2019. "Salmonella Translocated Effectors Recruit OSBP1 to the Phagosome to Promote Vacuolar Membrane Integrity." *Cell Reports* 27 (7): 2147–56.e5.
- Kühn, Sonja, Constanze Erdmann, Frieda Kage, Jennifer Block, Lisa Schwenkmezger, Anika Steffen, Klemens Rottner, and Matthias Geyer. 2015. "The Structure of FMNL2–Cdc42 Yields Insights into the Mechanism of Lamellipodia and Filopodia Formation." *Nature Communications*. <https://doi.org/10.1038/ncomms8088>.
- Kyei, George B., Isabelle Vergne, Jennifer Chua, Esteban Roberts, James Harris, Jagath R. Junutula, and Vojo Deretic. 2006. "Rab14 Is Critical for Maintenance of Mycobacterium Tuberculosis Phagosome Maturation Arrest." *The EMBO Journal* 25 (22): 5250–59.
- LaRock, Doris L., Anu Chaudhary, and Samuel I. Miller. 2015. "Salmonellae Interactions with Host Processes." *Nature Reviews. Microbiology* 13 (4): 191–205.

- Lau, Nicole, Amanda L. Haeberle, Brittany J. O’Keeffe, Eleanor A. Latomanski, Jean Celli, Hayley J. Newton, and Leigh A. Knodler. 2019. “SopF, a Phosphoinositide Binding Effector, Promotes the Stability of the Nascent Salmonella-Containing Vacuole.” *PLoS Pathogens* 15 (7): e1007959.
- Lee, Eun-Jin, Mauricio H. Pontes, and Eduardo A. Groisman. 2013. “A Bacterial Virulence Protein Promotes Pathogenicity by Inhibiting the Bacterium’s Own F1Fo ATP Synthase.” *Cell* 154 (1): 146–56.
- Lees, Emily A., Jessica L. Forbester, Sally Forrest, Leanne Kane, David Goulding, and Gordon Dougan. 2019. “Using Human Induced Pluripotent Stem Cell-Derived Intestinal Organoids to Study and Modify Epithelial Cell Protection Against Salmonella and Other Pathogens.” *Journal of Visualized Experiments: JoVE*, no. 147 (May). <https://doi.org/10.3791/59478>.
- Li, Menghan, Bing Gu, Rajdeep Bomjan, Meghana Chitale, Daisuke Kihara, and Daoguo Zhou. 2018. “YggG Is a Novel SPI-1 Effector Essential for Salmonella Virulence.” *bioRxiv*. <https://doi.org/10.1101/300152>.
- Litvak, Yael, Khin K. Z. Mon, Henry Nguyen, Ganrea Chanthavixay, Megan Liou, Eric M. Velazquez, Laura Kutter, et al. 2019. “Commensal Enterobacteriaceae Protect against Salmonella Colonization through Oxygen Competition.” *Cell Host & Microbe* 25 (1): 128–39.e5.
- Lu, Xiaoxi, Shuang Xie, Lulu Ye, Linda Zhu, and Qinghua Yu. 2020. “Lactobacillus Protects Against *S. Typhimurium*-Induced Intestinal Inflammation by Determining the Fate of Epithelial Proliferation and Differentiation.” *Molecular Nutrition & Food Research* 64 (5): e1900655.
- Maeda, Kenji, Kanchan Anand, Antonella Chiapparino, Arun Kumar, Mattia Poletto, Marko Kaksonen, and Anne-Claude Gavin. 2013. “Interactome Map Uncovers Phosphatidylserine Transport by Oxysterol-Binding Proteins.” *Nature* 501 (7466): 257–61.
- Mahdavi, Alborz, Janek Szychowski, John T. Ngo, Michael J. Sweredoski, Robert L. J. Graham, Sonja Hess, Olaf Schneewind, Sarkis K. Mazmanian, and David A. Tirrell. 2014. “Identification of Secreted Bacterial Proteins by Noncanonical Amino Acid Tagging.” *Proceedings of the National Academy of Sciences of the United States of America* 111 (1): 433–38.
- Mallo, Gustavo V., Marianela Espina, Adam C. Smith, Mauricio R. Terebiznik, Ainel Alemán, B. Brett Finlay, Lucia E. Rameh, Sergio Grinstein, and John H. Brumell. 2008. “SopB Promotes Phosphatidylinositol 3-Phosphate Formation on Salmonella Vacuoles by Recruiting Rab5 and Vps34.” *The Journal of Cell Biology* 182 (4): 741–52.
- McDermott, Jason E., Abigail Corrigan, Elena Peterson, Christopher Oehmen, George Niemann, Eric D. Cambronne, Danna Sharp, Joshua N. Adkins, Ram Samudrala, and Fred Heffron. 2011. “Computational Prediction of Type III and IV Secreted Effectors in Gram-Negative Bacteria.” *Infection and Immunity* 79 (1): 23–32.
- McShan, Andrew C., Asokan Anbanandam, Sikta Patnaik, and Roberto N. De Guzman. 2016. “Characterization of the Binding of Hydroxyindole, Indoleacetic Acid, and Morpholinoaniline to the Salmonella Type III Secretion System Proteins SipD and SipB.” *ChemMedChem* 11 (9): 963–71.

- Mesmin, Bruno, Joëlle Bigay, Joël Polidori, Denisa Jamecna, Sandra Lacas-Gervais, and Bruno Antony. 2017. "Sterol Transfer, PI4P Consumption, and Control of Membrane Lipid Order by Endogenous OSBP." *The EMBO Journal* 36 (21): 3156–74.
- Misselwitz, Benjamin, Sabrina Dilling, Pascale Vonaesch, Raphael Sacher, Berend Snijder, Markus Schlumberger, Samuel Rout, et al. 2011. "RNAi Screen of *Salmonella* Invasion Shows Role of COPI in Membrane Targeting of Cholesterol and Cdc42." *Molecular Systems Biology* 7 (March): 474.
- Napier, Brooke A., Sky W. Brubaker, Timothy E. Sweeney, Patrick Monette, Gregory H. Rothmeier, Nina A. Gertsvolf, Andreas Puschnik, Jan E. Carette, Purvesh Khatri, and Denise M. Monack. 2016. "Complement Pathway Amplifies Caspase-11-Dependent Cell Death and Endotoxin-Induced Sepsis Severity." *The Journal of Experimental Medicine* 213 (11): 2365–82.
- Narayanan, Lakshmi A., and Mariola J. Edelmann. 2014. "Ubiquitination as an Efficient Molecular Strategy Employed in *Salmonella* Infection." *Frontiers in Immunology* 5 (November): 558.
- Navare, Arti T., Juan D. Chavez, Chunxiang Zheng, Chad R. Weisbrod, Jimmy K. Eng, Richard Siehnel, Pradeep K. Singh, Colin Manoil, and James E. Bruce. 2015. "Probing the Protein Interaction Network of *Pseudomonas Aeruginosa* Cells by Chemical Cross-Linking Mass Spectrometry." *Structure* 23 (4): 762–73.
- Nawabi, Parwez, Drew M. Catron, and Kasturi Haldar. 2008. "Esterification of Cholesterol by a Type III Secretion Effector during Intracellular *Salmonella* Infection." *Molecular Microbiology* 68 (1): 173–85.
- Nesvizhskii, Alexey I. 2012. "Computational and Informatics Strategies for Identification of Specific Protein Interaction Partners in Affinity Purification Mass Spectrometry Experiments." *Proteomics* 12 (10): 1639–55.
- Nguyen, Ngan N. T., Yun-Sook Lim, Lap P. Nguyen, Si C. Tran, Trang T. D. Luong, Tram T. T. Nguyen, Hang T. Pham, et al. 2018. "Hepatitis C Virus Modulates Solute Carrier Family 3 Member 2 for Viral Propagation." *Scientific Reports* 8 (1): 15486.
- Nickerson, K. P., S. Senger, Y. Zhang, R. Lima, S. Patel, L. Ingano, W. A. Flavahan, et al. 2018. "*Salmonella* Typhi Colonization Provokes Extensive Transcriptional Changes Aimed at Evading Host Mucosal Immune Defense During Early Infection of Human Intestinal Tissue." *EBioMedicine* 31 (May): 92–109.
- Niemann, George S., Roslyn N. Brown, Jean K. Gustin, Afke Stufkens, Afshan S. Shaikh-Kidwai, Jie Li, Jason E. McDermott, et al. 2011. "Discovery of Novel Secreted Virulence Factors from *Salmonella* Enterica Serovar Typhimurium by Proteomic Analysis of Culture Supernatants." *Infection and Immunity* 79 (1): 33–43.
- Nokes, Rita L., Ian C. Fields, Ruth N. Collins, and Heike Fölsch. 2008. "Rab13 Regulates Membrane Trafficking between TGN and Recycling Endosomes in Polarized Epithelial Cells." *The Journal of Cell Biology* 182 (5): 845–53.
- O'Connor, Tamara J., Dana Boyd, Marion S. Dorer, and Ralph R. Isberg. 2012. "Aggravating Genetic Interactions Allow a Solution to Redundancy in a Bacterial Pathogen." *Science* 338 (6113): 1440–44.

- Odendall, Charlotte, Nathalie Rolhion, Andreas Förster, John Poh, Douglas J. Lamont, Mei Liu, Paul S. Freemont, Andrew D. Catling, and David W. Holden. 2012. “The *Salmonella* Kinase SteC Targets the MAP Kinase MEK to Regulate the Host Actin Cytoskeleton.” *Cell Host & Microbe* 12 (5): 657–68.
- Ohlson, Maikke B., Kerry Fluhr, Cheryl L. Birmingham, John H. Brumell, and Samuel I. Miller. 2005. “SseJ Deacylase Activity by *Salmonella* Enterica Serovar Typhimurium Promotes Virulence in Mice.” *Infection and Immunity* 73 (10): 6249–59.
- Ohlson, Maikke B., Zhiwei Huang, Neal M. Alto, Marie-Pierre Blanc, Jack E. Dixon, Jijie Chai, and Samuel I. Miller. 2008. “Structure and Function of *Salmonella* SifA Indicate That Its Interactions with SKIP, SseJ, and RhoA Family GTPases Induce Endosomal Tubulation.” *Cell Host & Microbe* 4 (5): 434–46.
- Olive, Andrew J., and Christopher M. Sassetti. 2016. “Metabolic Crosstalk between Host and Pathogen: Sensing, Adapting and Competing.” *Nature Reviews. Microbiology* 14 (4): 221–34.
- Patrick, Kristin L., Jason A. Wojcechowskyj, Samantha L. Bell, Morgan N. Riba, Tao Jing, Sara Talmage, Pengbiao Xu, et al. 2018. “Quantitative Yeast Genetic Interaction Profiling of Bacterial Effector Proteins Uncovers a Role for the Human Retromer in *Salmonella* Infection.” *Cell Systems* 7 (3): 323–38.e6.
- Philips, Jennifer A. 2008. “Mycobacterial Manipulation of Vacuolar Sorting.” *Cellular Microbiology* 10 (12): 2408–15.
- Pilar, Ana Victoria C., Sarah A. Reid-Yu, Colin A. Cooper, David T. Mulder, and Brian K. Coombes. 2012. “GogB Is an Anti-Inflammatory Effector That Limits Tissue Damage during *Salmonella* Infection through Interaction with Human FBXO22 and Skp1.” *PLoS Pathogens* 8 (6): e1002773.
- Pisu, Davide, Lu Huang, Jennifer K. Grenier, and David G. Russell. 2020. “Dual RNA-Seq of Mtb-Infected Macrophages In Vivo Reveals Ontologically Distinct Host-Pathogen Interactions.” *Cell Reports* 30 (2): 335–50.e4.
- Poh, John, Charlotte Odendall, Ad Spanos, Cliona Boyle, Mei Liu, Paul Freemont, and David W. Holden. 2008. “SteC Is a *Salmonella* Kinase Required for SPI-2-Dependent F-Actin Remodelling.” *Cellular Microbiology* 10 (1): 20–30.
- Pontes, Mauricio H., Jinki Yeom, and Eduardo A. Groisman. 2016. “Reducing Ribosome Biosynthesis Promotes Translation during Low Mg²⁺ Stress.” *Molecular Cell* 64 (3): 480–92.
- Ribet, David, and Pascale Cossart. 2010. “Post-Translational Modifications in Host Cells during Bacterial Infection.” *FEBS Letters* 584 (13): 2748–58.
- Rogers, Andrew W. L., Renée M. Tsolis, and Andreas J. Bäumlner. 2021. “*Salmonella* versus the Microbiome.” *Microbiology and Molecular Biology Reviews: MMBR* 85 (1). <https://doi.org/10.1128/MMBR.00027-19>.
- Rzomp, Kimberly A., Luella D. Scholtes, Benjamin J. Briggs, Gary R. Whittaker, and Marci A. Scidmore. 2003. “Rab GTPases Are Recruited to Chlamydial Inclusions in Both a Species-Dependent and Species-Independent Manner.” *Infection and Immunity* 71 (10): 5855–70.
- Saliba, Antoine-Emmanuel, Ivana Vonkova, Stefano Ceschia, Greg M. Findlay, Kenji Maeda, Christian Tischer, Samy Deghou, et al. 2014. “A Quantitative Liposome Microarray to Systematically Characterize Protein-Lipid Interactions.” *Nature Methods* 11 (1): 47–50.

- Sámano-Sánchez, Hugo, and Toby J. Gibson. 2020. "Mimicry of Short Linear Motifs by Bacterial Pathogens: A Drugging Opportunity." *Trends in Biochemical Sciences* 45 (6): 526–44.
- Sano, Hiroyuki, William G. Roach, Grantley R. Peck, Mitsunori Fukuda, and Gustav E. Lienhard. 2008. "Rab10 in Insulin-Stimulated GLUT4 Translocation." *Biochemical Journal* 411 (1): 89–95.
- Savitski, Mikhail M., Friedrich B. M. Reinhard, Holger Franken, Thilo Werner, Maria Fälth Savitski, Dirk Eberhard, Daniel Martinez Molina, et al. 2014. "Tracking Cancer Drugs in Living Cells by Thermal Profiling of the Proteome." *Science* 346 (6205): 1255784.
- Schaller, Lena, and Volker M. Lauschke. 2019. "The Genetic Landscape of the Human Solute Carrier (SLC) Transporter Superfamily." *Human Genetics* 138 (11-12): 1359–77.
- Schleker, Sylvia, Jingchun Sun, Balachandran Raghavan, Matthew Srnec, Nicole Müller, Mary Koepfinger, Leelavati Murthy, Zhongming Zhao, and Judith Klein-Seetharaman. 2012. "The Current Salmonella-Host Interactome." *PROTEOMICS--Clinical Applications* 6 (1-2): 117–33.
- Selkrig, Joel, Nan Li, Annika Hausmann, Matthew S. J. Mangan, Matylda Zietek, André Mateus, Jacob Bobonis, et al. 2020. "Spatiotemporal Proteomics Uncovers Cathepsin-Dependent Macrophage Cell Death during Salmonella Infection." *Nature Microbiology* 5 (9): 1119–33.
- Selkrig, Joel, Megan Stanifer, André Mateus, Karin Mitosch, Inigo Barrio-Hernandez, Mandy Rettel, Heeyoung Kim, et al. 2020. "SARS-CoV-2 Infection Remodels the Host Protein Thermal Stability Landscape." <https://doi.org/10.21203/rs.3.rs-105193/v1>.
- Silvestri, Lynn S., Gordon Ruthel, George Kallstrom, Kelly L. Warfield, Dana L. Swenson, Timothy Nelle, Patrick L. Iversen, Sina Bavari, and M. Javad Aman. 2007. "Involvement of Vacuolar Protein Sorting Pathway in Ebola Virus Release Independent of TSG101 Interaction." *The Journal of Infectious Diseases* 196 Suppl 2 (November): S264–70.
- Singh, Kshipra, Nicole T. Al-Greene, Thomas G. Verriere, Lori A. Coburn, Mohammad Asim, Daniel P. Barry, Margaret M. Allaman, et al. 2016. "The L-Arginine Transporter Solute Carrier Family 7 Member 2 Mediates the Immunopathogenesis of Attaching and Effacing Bacteria." *PLoS Pathogens* 12 (10): e1005984.
- Sinz, Andrea. 2018. "Cross-Linking/Mass Spectrometry for Studying Protein Structures and Protein-Protein Interactions: Where Are We Now and Where Should We Go from Here?" *Angewandte Chemie* 57 (22): 6390–96.
- Sontag, Ryan L., Ernesto S. Nakayasu, Roslyn N. Brown, George S. Niemann, Michael A. Sydor, Octavio Sanchez, Charles Ansong, et al. 2016. "Identification of Novel Host Interactors of Effectors Secreted by *Salmonella* and *Citrobacter*." *mSystems* 1 (4). <https://doi.org/10.1128/mSystems.00032-15>.
- Spanò, Stefania, Xiaoyun Liu, and Jorge E. Galán. 2011. "Proteolytic Targeting of Rab29 by an Effector Protein Distinguishes the Intracellular Compartments of Human-Adapted and Broad-Host *Salmonella*." *Proceedings of the National Academy of Sciences of the United States of America* 108 (45): 18418–23.

- Spees, Alanna M., Christopher A. Lopez, Dawn D. Kingsbury, Sebastian E. Winter, and Andreas J. Bäumlér. 2013. "Colonization Resistance: Battle of the Bugs or Ménage à Trois with the Host?" *PLoS Pathogens* 9 (11): e1003730.
- Stecher, Bärbel, Riccardo Robbiani, Alan W. Walker, Astrid M. Westendorf, Manja Barthel, Marcus Kremer, Samuel Chaffron, et al. 2007. "Salmonella Enterica Serovar Typhimurium Exploits Inflammation to Compete with the Intestinal Microbiota." *PLoS Biology* 5 (10): 2177–89.
- Stein, Mary-Pat, Matthias P. Müller, and Angela Wandinger-Ness. 2012. "Bacterial Pathogens Commandeer Rab GTPases to Establish Intracellular Niches." *Traffic* 13 (12): 1565–88.
- Sun, Yi, Philip J. Bilan, Zhi Liu, and Amira Klip. 2010. "Rab8A and Rab13 Are Activated by Insulin and Regulate GLUT4 Translocation in Muscle Cells." *Proceedings of the National Academy of Sciences of the United States of America* 107 (46): 19909–14.
- Superti-Furga, Giulio, Daniel Lackner, Tabea Wiedmer, Alvaro Ingles-Prieto, Barbara Barbosa, Enrico Girardi, Ulrich Goldmann, et al. 2020. "The RESOLUTE Consortium: Unlocking SLC Transporters for Drug Discovery." *Nature Reviews. Drug Discovery* 19 (7): 429–30.
- Tanzi, Giancarlo O., Andrew J. Piefer, and Paul Bates. 2003. "Equine Infectious Anemia Virus Utilizes Host Vesicular Protein Sorting Machinery during Particle Release." *Journal of Virology* 77 (15): 8440–47.
- Teng, Ben, Can Zhao, Xiaoqing Liu, and Zengyou He. 2015. "Network Inference from AP-MS Data: Computational Challenges and Solutions." *Briefings in Bioinformatics* 16 (4): 658–74.
- Thornbrough, Joshua M., Tom Hundley, Raphael Valdivia, and Micah J. Worley. 2012. "Human Genome-Wide RNAi Screen for Host Factors That Modulate Intracellular Salmonella Growth." *PloS One* 7 (6): e38097.
- Tumbarello, David A., Paul T. Manna, Mark Allen, Mark Bycroft, Susan D. Arden, John Kendrick-Jones, and Folma Buss. 2015. "The Autophagy Receptor TAX1BP1 and the Molecular Motor Myosin VI Are Required for Clearance of Salmonella Typhimurium by Autophagy." *PLoS Pathogens* 11 (10): e1005174.
- Unsworth, Kate E., Michael Way, Mark McNiven, Laura Machesky, and David W. Holden. 2004. "Analysis of the Mechanisms of Salmonella-Induced Actin Assembly during Invasion of Host Cells and Intracellular Replication." *Cellular Microbiology* 6 (11): 1041–55.
- Verma, Smriti, Stefania Senger, Bobby J. Cherayil, and Christina S. Faherty. 2020. "Spheres of Influence: Insights into Salmonella Pathogenesis from Intestinal Organoids." *Microorganisms* 8 (4). <https://doi.org/10.3390/microorganisms8040504>.
- Vlachodimou, Anna, Adriaan P. IJzerman, and Laura H. Heitman. 2019. "Label-Free Detection of Transporter Activity via GPCR Signalling in Living Cells: A Case for SLC29A1, the Equilibrative Nucleoside Transporter 1." *Scientific Reports* 9 (1): 13802.
- Walch, Philipp, Joel Selkrig, Leigh A. Knodler, Mandy Rettel, Frank Stein, Keith Fernandez, Cristina Viéitez, et al. 2020. "Global Mapping of Salmonella Enterica-Host Protein-Protein Interactions during Infection." *Cold Spring Harbor Laboratory*. <https://doi.org/10.1101/2020.05.04.075937>.

- Walpole, Glenn F. W., Sergio Grinstein, and Johannes Westman. 2018. "The Role of Lipids in Host-Pathogen Interactions." *IUBMB Life* 70 (5): 384–92.
- Wang, Di, Jun Lou, Chuan Ouyang, Weilin Chen, Yiqi Liu, Xinyuan Liu, Xuetao Cao, Jianli Wang, and Linrong Lu. 2010. "Ras-Related Protein Rab10 Facilitates TLR4 Signaling by Promoting Replenishment of TLR4 onto the Plasma Membrane." *Proceedings of the National Academy of Sciences of the United States of America* 107 (31): 13806–11.
- Wang, Han, Yi Shi, Jian Song, Jianxun Qi, Guangwen Lu, Jinghua Yan, and George F. Gao. 2016. "Ebola Viral Glycoprotein Bound to Its Endosomal Receptor Niemann-Pick C1." *Cell* 164 (1-2): 258–68.
- Wang, Ruofan, Camille R. Simoneau, Jessie Kulsuptrakul, Mehdi Bouhaddou, Katherine A. Travisano, Jennifer M. Hayashi, Jared Carlson-Stevermer, et al. 2020. "Genetic Screens Identify Host Factors for SARS-CoV-2 and Common Cold Coronaviruses." *Cell*, December. <https://doi.org/10.1016/j.cell.2020.12.004>.
- Wasylnka, Julie A., Malina A. Bakowski, Jason Szeto, Maikke B. Ohlson, William S. Trimble, Samuel I. Miller, and John H. Brumell. 2008. "Role for Myosin II in Regulating Positioning of Salmonella-Containing Vacuoles and Intracellular Replication." *Infection and Immunity* 76 (6): 2722–35.
- Wüstner, Daniel, Frederik W. Lund, Clemens Röhr, and Herbert Stangl. 2016. "Potential of BODIPY-Cholesterol for Analysis of Cholesterol Transport and Diffusion in Living Cells." *Chemistry and Physics of Lipids* 194 (January): 12–28.
- Wyles, Jessica P., Christopher R. McMaster, and Neale D. Ridgway. 2002. "Vesicle-Associated Membrane Protein-Associated Protein-A (VAP-A) Interacts with the Oxysterol-Binding Protein to Modify Export from the Endoplasmic Reticulum." *The Journal of Biological Chemistry* 277 (33): 29908–18.
- Xu, Yue, Ping Zhou, Sen Cheng, Qiuhe Lu, Kathrin Nowak, Ann-Katrin Hopp, Lin Li, et al. 2019. "A Bacterial Effector Reveals the V-ATPase-ATG16L1 Axis That Initiates Xenophagy." *Cell* 178 (3): 552–66.e20.
- Yeung, Amy T. Y., Yoon Ha Choi, Amy H. Y. Lee, Christine Hale, Hannes Ponstingl, Derek Pickard, David Goulding, et al. 2019. "A Genome-Wide Knockout Screen in Human Macrophages Identified Host Factors Modulating Salmonella Infection." *mBio* 10 (5). <https://doi.org/10.1128/mBio.02169-19>.
- Ye, Zhongde, Elaine O. Petrof, David Boone, Erika C. Claud, and Jun Sun. 2007. "Salmonella Effector AvrA Regulation of Colonic Epithelial Cell Inflammation by Deubiquitination." *The American Journal of Pathology* 171 (3): 882–92.
- Yu, Xiu-Jun, Mei Liu, and David W. Holden. 2016. "Salmonella Effectors SseF and SseG Interact with Mammalian Protein ACBD3 (GCP60) To Anchor Salmonella-Containing Vacuoles at the Golgi Network." *mBio* 7 (4). <https://doi.org/10.1128/mBio.00474-16>.
- Zhang, Buyu, Bohao Liu, Yinglin Zhou, Xinxiang Zhang, Qinghua Zou, and Xiaoyun Liu. 2020. "Contributions of Mass Spectrometry-Based Proteomics to Understanding Salmonella-Host Interactions." *Pathogens* 9 (7). <https://doi.org/10.3390/pathogens9070581>.
- Zhao, Weidong, Thomas Moest, Yaya Zhao, Aude-Agnès Guilhon, Christophe Buffat, Jean-Pierre Gorvel, and Stéphane Méresse. 2015. "The Salmonella Effector Protein SifA Plays a Dual Role in Virulence." *Scientific Reports* 5 (August): 12979.

Chapter VII

Experimental Procedures

Chapter VII: Experimental Procedures

I did not use statistical methods to predetermine sample sizes. Methodologies have been previously described in publications authored by myself in the course of my doctoral studies (Walch et al. 2020) and have been adapted here to provide more detail.

1. List of antibodies

The majority of antibodies listed in Table VII.1 have been published as Supplementary Table S14 in (Walch et al. 2020).

Table VII.1. Antibodies used in the study. All antibodies, including manufacturer and catalog number. The application (IP: reciprocal immunoprecipitation, WB: Western Blot, IF: Immunofluorescence) and the dilution for each use are indicated.

Antibody (including target and source)	Origin / Manufacturer	Identifier (Cat #)	Application & Dilution
anti-FMNL1 (produced in rabbit)	LS Bio	LS-C401690	IP: 1:100, WB:1:1000
anti-ANXA1 (produced in rabbit)	proteintech	21990-1-AP	IP: 1:100, WB:1:1000
anti-MAP1S (produced in mouse)	Precision antibodies	AG10006	IP: 1:100, WB:1:1000
anti-TCP1 (produced in rat)	Thermo Fisher	MA3-026	IP: 1:100, WB:1:1000
anti-LASP1 (produced in rabbit)	proteintech	10515-1-AP	IP: 1:100, WB:1:1000
anti-PHB1 (produced in rabbit)	Cell Signalling	#2426	IP: 1:100, WB:1:1000
anti-SACM1L (produced in rabbit)	proteintech	13033-1-AP	IP: 1:100, WB:1:1000
anti-BCLAF1 (produced in rabbit)	Millipore	AB10546	IP: 1:100, WB:1:1000
anti-VPS39 (produced in rabbit)	proteintech	16219-1-AP	IP: 1:100, WB:1:1000
anti-GroEL (produced in rabbit)	donation from Bukau lab	--	IP: 1:100, WB:1:1000
anti-NPC1 (produced in rabbit)	Thermo Fisher	PA1-16817	IP: 1:100, WB:1:1000
anti-FMNL2 (produced in mouse)	abcam	ab57963	WB: 1:1000
anti-Histone H3 (D1H2) (produced in rabbit)	Cell Signalling	#4499S	WB: 1:1000
anti-RecA (produced in rabbit)	abcam	ab63797	WB: 1:5000
anti-GAPDH (D16H11) (HRP-conjugate, produced in rabbit)	Cell Signalling	#8884	WB: 1:2000
anti-FLAG M2 (produced in mouse)	Sigma	F1804	WB: 1:1000
anti-RNA polymerase Sigma 70 (RpoD) [2G10]	Acris antibodies	GTX12088	WB: 1:1000
anti-LAMP1 (produced in rat, Alexa-488 conjugate)	abcam	ab24871	IF: 1:500
anti-NPC1 (polyclonal, produced in rabbit)	Novus biologicals	NB400-148	IF: 1:500
secondary anti-rabbit (Alexa-680 coupled, produced in goat)	abcam	ab175773	IF: 1:1000
secondary anti-rat (HRP-conjugate, produced in rabbit)	abcam	ab6734	WB: 1:5000
secondary anti-mouse (HRP-conjugate, produced in goat)	Sigma	HVZ-A4416-1ML	WB: 1:5000
secondary anti-rabbit (HRP-conjugate, produced in donkey)	Sigma/GE	NA934-1ML	WB: 1:20000

2. List of primers and plasmids

A large number of primers and plasmids listed in Tables VII.2 and VII.3 have been published in Supplementary Tables S11 and S13 in (Walch et al. 2020).

Table VII.2. All plasmids used in the study. Plasmids (including their source or reference), including a description for the use.

Plasmid name	Description	Source / Reference
pFCcGi	Constitute expression of mCherry(FC), AmpR	(Figueira et al. 2013)
pJSP1	pGEM-Teasy backbone containing 2x STREP-TEV-3xFLAG tag and KanR gene from pKD4, AmpR	Produced by Dr. Joel Selkrig (Walch et al. 2020)
pKD46	λ Red recombinase expression vector, AmpR	(Datsenko and Wanner 2000)
pCP20	Plasmid expressing FLP recombinase, AmpR, ts rep	(Datsenko and Wanner 2000)

Table VII.3. All oligos / primers used in the study. The oligo name and identifier of the primer, its sequence and function are listed.

Primer name	Sequence	Use
JPS14_SIFA-STF ¹	GATACCTTTAGCTGTGAAGTCATGGGGAATCTTTATTTTTTA ATGAAAGACGCATCGTGGCCGGATCTTGC	mutagenesis/STF insertion
JPS15_SIFA-STF ¹	TACGATTTTCGCTATATCTTCTCTTAATCATGGCCGTCATTTG TGGATGCGCGGATAACAGAAAGGCCGGG	mutagenesis/STF insertion
JPS28_SIFA-STF ¹	GATACCTTTA GCTGTGAAGT CATGGGGAAT CTTTATTTTT TAATGAAAGA TCGCCCGGAT GGCTGGTCACACCCGCAG	mutagenesis/STF insertion
JPS29_SIFA-STF ¹	TACGATTTTCGCTATATCTTCTCTTAATCATGGCCGTCATTTG TGGATGCGATTTTAAAAA CTTGTCATCGTCATCCTTG	mutagenesis/STF insertion
JPS38_CCDAB DELETION ¹	ATGTAAAAAGAGGTGAATCATGAAGCAGCAATTACAGTG ACAGTGGACGTGTAGGCTGGAGCTGCTTC	mutagenesis/STF insertion
JPS39_CCDAB DELETION ¹	CCTGTTTCGCTGACACGCATATCAGATCCCCCGAACATCAG GTTAATGGCCATATGAATATCCTCCTTA	mutagenesis/STF insertion
JPS30_GOGB_STF_FWD ¹	GTTTTTTCATTAGTTGGTTGGGATAAATAAGCCTAAAAATA GAAATCGTGGCTGGTCACACCCGCAGTTTG	mutagenesis/STF insertion
JPS31_GOGB_STF_REV ¹	GGAGTATATATCCTTAACTCCAATAGGGCTGCTCTATATATA AATATATTAACATATGAATATCCTCCTTAG	mutagenesis/STF insertion
JPS32_SSEK_STF_FWD ¹	TAATGAATACCAGTCAGTTTACGCAAAGTTTCATGGGCGAGG CATGTGCAGGGCTGGTCACACCCGCAGTTTG	mutagenesis/STF insertion
JPS33_SSEK_STF_REV ¹	TTTTTCGCCGAACTTGATAGTTTATGCCAATATTTTTATGTAT TCAATAGCATATGAATATCCTCCTTAG	mutagenesis/STF insertion
JPS34_SSEJ_STF_FWD ¹	GTTTTGCCATAATGTTAGAAAGTTTTATAGCTCATCATTATTC CACTGAA GGCTGGTCACACCCGCAGTTTG	mutagenesis/STF insertion
JPS35_SSEJ_STF_REV ¹	TATTTTCATGCCACCCGGCACTATGATATTGAGCTGTGTTTTG CTCAAGGC CATATGAATATCCTCCTTAG	mutagenesis/STF insertion
JPS42_GOGB_COLONY_FWD ¹	TGGTGAGGCTATTTACACGA	Diagnostic PCR/STF validation
JPS43_GOGB_COLONY_REV ¹	TTTTCAACGCATGCCCGAAT	Diagnostic PCR/STF validation
JPS44_SSEK_COLONY_FWD ¹	GTTGATCGCAATAACACCCG	Diagnostic PCR/STF validation
JPS45_SSEK_COLONY_REV ¹	GTTCTGAACAGCACTGCGAT	Diagnostic PCR/STF validation
JPS46_SSEJ_COLONY_FWD ¹	AGGCGGCCAGTAATATTGGTT	Diagnostic PCR/STF validation
JPS47_SSEJ_COLONY_REV ¹	CGGTGGCGATTTATCGACTCTA	Diagnostic PCR/STF validation
JPS58_SPVC_STF_FWD ¹	TGCAGAGACAGGCTTACGTGAGGAACCGTTTTATCGTTTTG ATGACAGAG GGCGGCTGGTCACACCCGCAGTTTG	mutagenesis/STF insertion
JPS59_SPVC_STF_REV ¹	AAA TTA ATG AGC ATT TAA AAT AGC TGT TTA ACG GCG TTT ACT GTT CCG TT CATATGAATATCCTCCTTAG	mutagenesis/STF insertion
JPS60_STEC_STF_FWD ¹	CGGAGGAAGGGACTCTGTGGCTAAGGTATTAAGGATGAA TTAAAAAAA GGCGGCTGGTCACACCCGCAGTTTG	mutagenesis/STF insertion
JPS61_STEC_STF_REV ¹	ATA ATT GAT CGG TAA ATC TGT AGC GAA TGT GCC CCC GGC GAT TCG CAG AA CATATGAATATCCTCCTTAG	mutagenesis/STF insertion
JPS62_SSPH1_STF_FWD ¹	TTGTGGATGAGGTGCTGGGTAGCTATCTGACAGCCCGGTG GCGTCTTAAC GGCGGCTGGTCACACCCGCAGTTTG	mutagenesis/STF insertion
JPS63_SSPH1_STF_REV ¹	GAT GTT GTT TGT CCA GGA ATA TCT TTG TTC ACC GCA CCA CAT TCG CCT GG CATATGAATATCCTCCTTAG	mutagenesis/STF insertion
JPS64_SSEI_STF_FWD ¹	GATGGTTTAATACCTTTAAAAAGCAAAAAATTTCTTAATAG GTAAAAATG GGCGGCTGGTCACACCCGCAGTTTG	mutagenesis/STF insertion
JPS65_SSEI_STF_REV ¹	CAA AAT TTA AGT GGA CAC TAT CAT CGC CGG ATT GAC AGG GTT CTG ACA GA CATATGAATATCCTCCTTAG	mutagenesis/STF insertion
JPS66_PIPB2_STF_FWD ¹	TGTCTACAAGCACACAACACTCTTTAACGAATTTTATAGTG AAAAATTT GGCGGCTGGTCACACCCGCAGTTTG	mutagenesis/STF insertion
JPS67_PIPB2_STF_REV ¹	CAG CTA CTA TTC AGT AGC AGA TTG TTA TTC TTA CAT TGC TTT TAT TTC AG CATATGAATATCCTCCTTAG	mutagenesis/STF insertion
JPS68_SSPH2_STF_FWD ¹	TTGTGGAGGAGATGCTGGGGAGCTATCTGAACGTTTCAGTG GCGTCGTAAC GGCGGCTGGTCACACCCGCAGTTTG	mutagenesis/STF insertion
JPS69_SSPH2_STF_REV ¹	TCC GTA CTG TCT GAT GTT GTT CGT CCG GGA ATA TCT TTG TCG CAC CGC AC CATATGAATATCCTCCTTAG	mutagenesis/STF insertion
JPS70_SOPD2_STF_FWD ¹	ATAACACTTTTATTAAGTGAAAGTCGAGTTGTGCGCAATA TGCTTATA GGCGGCTGGTCACACCCGCAGTTTG	mutagenesis/STF insertion
JPS71_SOPD2_STF_REV ¹	ACT GAA ATT ACG CCA TAA AAA GCG TAC AAA AAA GGC TCC ATA TCA GTG GG CATATGAATATCCTCCTTAG	mutagenesis/STF insertion

JPS72_PIPB_STF_FWD ¹	CTCCACTCCCGGATTACAATGATAGAAGCTCTTTTCCCCCATC CGATATTT GGCGGCTGGTCACACCCGCAGTTTG	mutagenesis/STF insertion
JPS73_PIPB_STF_REV ¹	GTT TAT TTA ATA AAA CAA GGG GGC CTC TGT TTG AAT ACT TCT TGT TTA TA CATATGAATATCCTCCTTAG	mutagenesis/STF insertion
JPS74_SPVB_STF_FWD ¹	CTGACACAAACAGGATAAAAAGAATAATAAACATGAGGGTA CTCAACTCA GGCGGCTGGTCACACCCGCAGTTTG	mutagenesis/STF insertion
JPS75_SPVB_STF_REV ¹	GGT TCC GGA GTA TAA CCC CTT ATA GAG CTA GGC CGC TCA TAC CAC TTC TG CATATGAATATCCTCCTTAG	mutagenesis/STF insertion
JPS76_SSEL_STF_FWD ¹	CACTATTTAACACCCAAACCCGGCGGCAATATATGAATACA GTCTCCAG GGCGGCTGGTCACACCCGCAGTTTG	mutagenesis/STF insertion
JPS77_SSEL_STF_REV ¹	TAT AAA TTC TTC GCA GAG CAT CAT TTC AGG ATA AGA GCC TAA TGG GAT AG CATATGAATATCCTCCTTAG	mutagenesis/STF insertion
JPS78_SPVC_COLONY_FWD ¹	GGT TAT TTC AGG ACA GTG TCC	Diagnostic PCR/STF validation
JPS79_SPVC_COLONY_REV ¹	GCG GAC ATA TCA ATA TGC ATG A	Diagnostic PCR/STF validation
JPS80_STEC_COLONY_FWD ¹	TTAAAGCGGGCCGAGACCG	Diagnostic PCR/STF validation
JPS81_STEC_COLONY_REV ¹	GGC ATT TCA CCC ACT ATG GCA	Diagnostic PCR/STF validation
JPS82_SSPH1_COLONY_FWD ¹	GTACCGGAAGCTGTATGACG	Diagnostic PCR/STF validation
JPS83_SSPH1_COLONY_REV ¹	GGT CCA GTA CTT CCA TCA ACT	Diagnostic PCR/STF validation
JPS84_SSEI_COLONY_FWD ¹	AGCAGCTAATGCCTATGATGC	Diagnostic PCR/STF validation
JPS85_SSEI_COLONY_REV ¹	GCG CCT GTA TCC AGT CGT A	Diagnostic PCR/STF validation
JPS86_PIPB2_COLONY_FWD ¹	GCA AAC CTG CGA AAG GCG AG	Diagnostic PCR/STF validation
JPS87_PIPB2_COLONY_REV ¹	CGA GCT GAC AAC GCA CGA AC	Diagnostic PCR/STF validation
JPS88_SSPH2_COLONY_FWD ¹	ATG AGG AAA CGT ACC GGA TGC	Diagnostic PCR/STF validation
JPS89_SSPH2_COLONY_REV ¹	TGC CGT TAA TCG CGG AGC GA	Diagnostic PCR/STF validation
JPS90_SOPD2_COLONY_FWD ¹	CTGCTACAAGCATATAAACCG	Diagnostic PCR/STF validation
JPS91_SOPD2_COLONY_REV ¹	CCA TCC GTG TAT CTG GTT AC	Diagnostic PCR/STF validation
JPS92_PIPB_COLONY_FWD ¹	CGCTGCAATTCTATTCGGC	Diagnostic PCR/STF validation
JPS93_PIPB_COLONY_REV ¹	GTT AAT GTG CCA CAT ACA GGT	Diagnostic PCR/STF validation
JPS94_SPVB_COLONY_FWD ¹	AAGGGAGAGGCAGAGATGC	Diagnostic PCR/STF validation
JPS95_SPVB_COLONY_REV ¹	GGT CCG TTC CGA GCA GAA A	Diagnostic PCR/STF validation
JPS96_SSEL_COLONY_FWD ¹	GGA CAA AAC GAT CCT GCT ACC	Diagnostic PCR/STF validation
JPS97_SSEL_COLONY_REV ¹	CGT TGG CTT AAT GGC GAG GA	Diagnostic PCR/STF validation
JPS98_STEC_COLONY_FWD ¹	CAGGTGATTACAGTAGTTAC	Diagnostic PCR/STF validation
JPS99_STEC_COLONY_REV ¹	AACTCTCAATAATTGATCGG	Diagnostic PCR/STF validation
JPS104_SLRP_STF_FWD ¹	ATATATTGCTGAAAAAGAGGTGAGCTCGCTCATGAGCGCC TACTGGCGAGGCGGCTGGTCACACCCGCAGTTTG	mutagenesis/STF insertion
JPS105_SLRP_STF_REV ¹	CGCTTATCAGAAGCCTGTTTACACCGAAGGGTAAACAGGCT CTCTCCCTCCATATGAATATCCTCCTTAG	mutagenesis/STF insertion
JPS106_STEA_STF_FWD ¹	AATGGGCGGCCGACATAAAAAGCTCGCTACCATAACTATTTG GACAATTATGGCGGCTGGTCACACCCGCAGTTTG	mutagenesis/STF insertion
JPS107_STEA_STF_REV ¹	CGGCGTGTTAAATTTTTAACGCCGGCTCAGCGAGTCTGAT TTCTAACAACATATGAATATCCTCCTTAG	mutagenesis/STF insertion
JPS108_STEB_STF_FWD ¹	GGTTTGGCCTGAAACATCTGCTAACCTGTCACTCAAATGGT AATGTCAGAGGCGGCTGGTCACACCCGCAGTTTG	mutagenesis/STF insertion

Dissecting the host-pathogen interface during *Salmonella* infection

JPS109_STEB_STF_REV ¹	AGGAAAGAACTGAGCGCCCATATCTGTAGGCTGTGGAATAG CAATGCCGGGCATATGAATATCCTCCTTAG	mutagenesis/STF insertion
JPS110_SIFB_STF_FWD ¹	ATTTATCTTCACTCGTTGAAACAACAAAAATGAGGCTCATC ACCAGAGTGGCGGCTGGTCACACCCGCAGTTTG	mutagenesis/STF insertion
JPS111_SIFB_STF_REV ¹	TTTAAAGTTATTGTATTAGATGGTTTTGGTATTGCCAGGGGA TTGTAATCATATGAATATCCTCCTTAG	mutagenesis/STF insertion
JPS112_SRGE_STF_FWD ¹	TATTAGAAAAACACCCGTATCGCTTTTGTATGGGGCATATA AAAAGAAAGGCGGCTGGTCACACCCGCAGTTTG	mutagenesis/STF insertion
JPS113_SRGE_STF_REV ¹	CTTTACGACAATTGCTTCAAAAATCAATGCCAGACTTC CGCTACCACATATGAATATCCTCCTTAG	mutagenesis/STF insertion
JPS114_SSEF_STF_FWD ¹	AGCGCTCTGTCAATCTGCTACTACACCTGCATTAATGGACA GTTCTGATGGCGGCTGGTCACACCCGCAGTTTG	mutagenesis/STF insertion
JPS115_SSEF_STF_REV ¹	TTAACAGGACGTGCCCTCTACCTGAGCATTTGGGCTAAC AGGTTTCATATGAATATCCTCCTTAG	mutagenesis/STF insertion
JPS116_SSEG_STF_FWD ¹	CATTATATCGTTTGTGGCTCAGGTAACGCCAGAACAACGT GCGCCGGAGGGCGGCTGGTCACACCCGCAGTTTG	mutagenesis/STF insertion
JPS117_SSEG_STF_REV ¹	CATCGTAAGGATACTGGCAACATAGCAAAATTTAGAAAGCA ATGAACATCCATATGAATATCCTCCTTAG	mutagenesis/STF insertion
JPS118_SSEK2_STF_FWD ¹	ATGAACATATTTTATGGATACCAGCAGTTTACTATCAGCT CCTGGAGAGGGCGGCTGGTCACACCCGCAGTTTG	mutagenesis/STF insertion
JPS119_SSEK2_STF_REV ¹	AGTATGGTCTTTACGTTTAGCTTTGCCGAAACATTGCTCGCG TTTATATCCATATGAATATCCTCCTTAG	mutagenesis/STF insertion
JPS120_SLRP_COLONY_FWD ¹	GAGGTACAGATGGATGCAG	Diagnostic PCR/STF validation
JPS121_SLRP_COLONY_REV ¹	TTGGGTTAAGCCGTTTAC	Diagnostic PCR/STF validation
JPS122_STEA_COLONY_FWD ¹	AGCATATAATGCCTTACC	Diagnostic PCR/STF validation
JPS123_STEA_COLONY_REV ¹	GAGGTACGTGGAATTTTGG	Diagnostic PCR/STF validation
JPS124_STEB_COLONY_FWD ¹	CAGTCTGGATAATAGCGG	Diagnostic PCR/STF validation
JPS125_STEB_COLONY_REV ¹	TCTGGTAAAAGTCAGGC	Diagnostic PCR/STF validation
JPS126_SIFB_COLONY_FWD ¹	GAGATACTAATGAATATGC	Diagnostic PCR/STF validation
JPS127_SIFB_COLONY_REV ¹	ACTTATACTCAGTATGTC	Diagnostic PCR/STF validation
JPS128_SRGE_COLONY_FWD ¹	TCAGCAGCAGCAACGGG	Diagnostic PCR/STF validation
JPS129_SRGE_COLONY_REV ¹	TCGGGGAATCAGCGGAAG	Diagnostic PCR/STF validation
JPS130_SSEF_COLONY_FWD ¹	GGATTATTGCCTTGCCCG	Diagnostic PCR/STF validation
JPS131_SSEF_COLONY_REV ¹	AATACCCGCTCTTTCC	Diagnostic PCR/STF validation
JPS132_SSEG_COLONY_FWD ¹	TTTGGGACTACAGCCTC	Diagnostic PCR/STF validation
JPS133_SSEG_COLONY_REV ¹	CTGGCCTGCCTGGTGCGC	Diagnostic PCR/STF validation
JPS134_SSEK2_COLONY_FWD ¹	GTAACCTTATGGCGATCC	Diagnostic PCR/STF validation
JPS135_SSEK2_COLONY_REV ¹	ATGAGTGATTTTACCAC	Diagnostic PCR/STF validation
JPS188_SOPB_STF_FWD ¹	ATGAAAATATTTGGCAGTCAGTAAAAGGCATTTCTTCATTA TCACATCTGGCGGCTGGTCACACCCGCAGTTTG	mutagenesis/STF insertion
JPS189_SOPB_STF_REV ¹	GGC GCA TCC AGG CCT AAC GCG TCA TAT AAA CGA TTT AAT AGA CTT TCC AT CATATGAATATCCTCCTTAG	mutagenesis/STF insertion
JPS192_SIPA_STF_FWD ¹	CTGGCGTGGATCGGGTTACTACTACCGTTGATGGCTTGAC ATGCAGCGTGGCGGCTGGTCACACCCGCAGTTTG	mutagenesis/STF insertion
JPS193_SIPA_STF_REV ¹	ATA CAA GAG GTG ATC ACT TTT TTG ACT CTT GCT TCA ATA TCC ATA TTC AT CATATGAATATCCTCCTTAG	mutagenesis/STF insertion
JPS194_SPTP_STF_FWD ¹	TTGTACAACAAAAGCAATGCAAGCCAGTTGCTTATGACG ACGGCAAGC GGCGGCTGGTCACACCCGCAGTTTG	mutagenesis/STF insertion
JPS195_SPTP_STF_REV ¹	CGG CAA ACA AAT AAT TAT ACA GAA ATA GCT TAC TTT CAG ATA GTT CTA AA CATATGAATATCCTCCTTAG	mutagenesis/STF insertion

Dissecting the host-pathogen interface during *Salmonella* infection

JPS196_SSEB_STF_FWD ¹	AGCGCCGCTGGGGCGGGTTCCTGCGCGATTTTAAACAGAA CCGCATCATC GGCGGCTGGTCACACCCGCAGTTTG	mutagenesis/STF insertion
JPS197_SSEB_STF_REV ¹	TCC CGT AAC GCT CAA CGT CCA GAG CAG GTA AGC CAG GAG GCC GCC CTG TT CATATGAATATCCTCCTTAG	mutagenesis/STF insertion
JPS200_SOPB_COLONY_FWD ¹	ACTGAATAGCGGTAACCTGGA	Diagnostic PCR/STF validation
JPS201_SOPB_COLONY_REV ¹	CGC TGG TGT AGT TCA GAC GTA	Diagnostic PCR/STF validation
JPS202_SIPA_COLONY_FWD ¹	GGCTGACCAGGCTAAAAGG	Diagnostic PCR/STF validation
JPS203_SIPA_COLONY_REV ¹	GCA ACT AAT GTC AAA CTC CTC	Diagnostic PCR/STF validation
JPS204_SPTP_COLONY_FWD ¹	GGA AGA ACC GGA ACG ATG GC	Diagnostic PCR/STF validation
JPS205_SPTP_COLONY_REV ¹	CGT CGC CGA AAC GAT CGG AT	Diagnostic PCR/STF validation
JPS206_SSEB_COLONY_FWD ¹	TTC ACG CAG CGG GCA ATG TGG C	Diagnostic PCR/STF validation
JPS207_SSEB_COLONY_REV ¹	GCC AGC GGT GCT GCC GTG AT	Diagnostic PCR/STF validation
JSP228_AVRA_STF_FWD	ACAAAAAGAATGAACGCTTTATGAGCGATTTCGATAACAATGC CGTTATGC GGCTGGTCACACCCGCAGTTTG	mutagenesis/STF insertion
JSP229_AVRA_STF_REV	TACGGTTTAAGTAAAGACTTATATTCAGCTATCCTTTTTTTAT GAGCGGA CATATGAATATCCTCCTTAG	mutagenesis/STF insertion
JSP230_AVRA_COLONY_FWD	GAATATGTGGAGGCCAATCC	Diagnostic PCR/STF validation
JSP231_AVRA_COLONY_REV	AATCGTACCAGAGGCGCAAG	Diagnostic PCR/STF validation
JSP232_GTGE_STF_FWD	AGCCAAAACCTTTACTACTCCTCCTCCTGGAAAGACTGGTGT ACCATTTTA GGCTGGTCACACCCGCAGTTTG	mutagenesis/STF insertion
JSP233_GTGE_STF_REV	GAGAGGATTTGAACCTCCGCCCCCATGTTGGCGGTAGC CTGAATAATT CATATGAATATCCTCCTTAG	mutagenesis/STF insertion
JSP234_GTGE_COLONY_FWD	TGGTCTTTACTATGACGGTG	Diagnostic PCR/STF validation
JSP235_GTGE_COLONY_REV	CTCAATTTCTACGGGGAAG	Diagnostic PCR/STF validation
JSP236_SIPB_STF_FWD	TACAGCAAAATGCGGATGCTTCGCGTTTTATTCTGCGCCAG AGTCGCGCA GGCTGGTCACACCCGCAGTTTG	mutagenesis/STF insertion
JSP237_SIPB_STF_REV	TTAAATAAGCGGGGATTTATTCACACTACTAATTAACA TATTTTC CATATGAATATCCTCCTTAG	mutagenesis/STF insertion
JSP238_SIPB_COLONY_FWD	CCATGGATCAGATTCCAGCAG	Diagnostic PCR/STF validation
JSP239_SIPB_COLONY_REV	GATTATTTAAATAAGCGGCG	Diagnostic PCR/STF validation
JSP240_SIPC_STF_FWD	ACCAGTCGAAAGCATCCGCACTCGCTGCTATCGCAGGCAAT ATTCGCGCT GGCTGGTCACACCCGCAGTTTG	mutagenesis/STF insertion
JSP241_SIPC_STF_REV	AATATCCCAGTTCGCCATCAGGAGCGGATTAATCACAC CCATGATGG CATATGAATATCCTCCTTAG	mutagenesis/STF insertion
JSP242_SIPC_COLONY_FWD	GAAAGTTCACGTAATCGAC	Diagnostic PCR/STF validation
JSP243_SIPC_COLONY_REV	GAGTCTGCGGCCGTTCCGCA	Diagnostic PCR/STF validation
JSP244_SOPA_STF_FWD	GAAAATATTTCCCGAGTGTCTGTGCATCCATCCTGCCACTG GCCTGGGCG GGCTGGTCACACCCGCAGTTTG	mutagenesis/STF insertion
JSP245_SOPA_STF_REV	GACTAAAACGGGTCTATGTACAGAGGGACACAACGCTGTGT CCCTTAATT CATATGAATATCCTCCTTAG	mutagenesis/STF insertion
JSP246_SOPA_COLONY_FWD	AGCTGTCTCCGGCGATATTC	Diagnostic PCR/STF validation
JSP247_SOPA_COLONY_REV	GCAATCTGGCCGGGATCTCA	Diagnostic PCR/STF validation
JSP248_SOPD_STF_FWD	GTTCTTTGCACATTGGTAAAGATGGGTGCAGTCGTAATATAT TACTGACA GGCTGGTCACACCCGCAGTTTG	mutagenesis/STF insertion
JSP249_SOPD_STF_REV	GATTATACTTGCTGCTATGAAAAATCCGGCAGGCAGCCGGA TTTTAAATT CATATGAATATCCTCCTTAG	mutagenesis/STF insertion
JSP250_SOPD_COLONY_FWD	GAGTTTAAACCAACAAATTC	Diagnostic PCR/STF validation

Dissecting the host-pathogen interface during *Salmonella* infection

JSP251_SOPD_COLONY_REV	CGGGTATGGCGGAAGAAGAG	Diagnostic PCR/STF validation
JPS208_CIGR_STF_FWD	TCGCGCTCAGTACCGCGGTGGTCACGGCGATTATTAATGG CGTATTTGAT GGCTGGTCACACCCGCAGTTTG	mutagenesis/STF insertion
JPS209_CIGR_STF_REV	TACGCTCCGGTTTTTGGCGCGCTGTCCGTGTCCAAACTGGCT GCGCCAATA CATATGAATATCCTCCTTAG	mutagenesis/STF insertion
JPS210_CIGR_COLONY_FWD	CGCTACCGCCGGGAATCGCT	Diagnostic PCR/STF validation
JPS211_CIGR_COLONY_REV	GGCAGTGCTCGCCAAAACGC	Diagnostic PCR/STF validation
JPS212_GTGA_STF_FWD	AAGAGATGGGTACACATCACCACCAAGAATCGCCTACGAA TTTAGTAAT GGCTGGTCACACCCGCAGTTTG	mutagenesis/STF insertion
JPS213_GTGA_STF_REV	CTGTATTAGCTCAGACCTGAACTGGTTACTGTGTTGTAGCAT CGTGGGAT CATATGAATATCCTCCTTAG	mutagenesis/STF insertion
JPS214_GTGA_COLONY_FWD	GTTGACTCACCTTCAGGACA	Diagnostic PCR/STF validation
JPS215_GTGA_COLONY_REV	ATGTCCGAATCGATTCTGG	Diagnostic PCR/STF validation
JPS220_STED_STF_FWD	CCGGTTATATCGCTCAATACAGGCATTCTGCAGAGGTTTTTC CCGGATGAA GGCTGGTCACACCCGCAGTTTG	mutagenesis/STF insertion
JPS221_STED_STF_REV	ATCACACAATCCGGACTGAGTTCAATCAAAGTGATCTACTAT TCGGCGCA CATATGAATATCCTCCTTAG	mutagenesis/STF insertion
JPS222_STED_COLONY_FWD	GTTTCCCGGATGCTTTAAC	Diagnostic PCR/STF validation
JPS223_STED_COLONY_REV	CATCAGGCGTCGTTCCGGTAC	Diagnostic PCR/STF validation
JSP252_SOPE2_STF_FWD	TTCAGTTAACTATAGAAAATATTGCGAATAAGTATCTTCAGA ATGCCTCC GGCTGGTCACACCCGCAGTTTG	mutagenesis/STF insertion
JSP253_SOPE2_STF_REV	AACGAATATATAGTTTCAGAAAATCTGCTATTAATTCATATGG TTAATAG CATATGAATATCCTCCTTAG	mutagenesis/STF insertion
JSP254_SOPE2_COLONY_FWD	GTATTAATATCCGCATATG	Diagnostic PCR/STF validation
JSP255_SOPE2_COLONY_REV	CAGGTATTTAGAGTAATAAC	Diagnostic PCR/STF validation
JSP256_SPVD_STF_FWD	TCTCATCATCAGGGGAATTTTATGTCAGGGCTTATGATGAAA AACACGAT GGCTGGTCACACCCGCAGTTTG	mutagenesis/STF insertion
JSP257_SPVD_STF_REV	GGTTTACAGCGGATCTTCTAAGGCTCTCTATTAACCTACCA TTCATAAA CATATGAATATCCTCCTTAG	mutagenesis/STF insertion
JSP258_SPVD_COLONY_FWD	GAAAACATCCAACATACTTC	Diagnostic PCR/STF validation
JSP259_SPVD_COLONY_REV	TTGCCTGTAGCGCCGGTGGT	Diagnostic PCR/STF validation
JSP260_STEE_STF_FWD	CCGGACTATACCTTAGCGCAAATGGCATCAGAACCCGGCCA GCCTGGCCA GGCTGGTCACACCCGCAGTTTG	mutagenesis/STF insertion
JSP261_STEE_STF_REV	TCTGGACGATTAACACCCCGTGTATCGTCCGGAATTCGTCT TTCCCTAT CATATGAATATCCTCCTTAG	mutagenesis/STF insertion
JSP262_STEE_COLONY_FWD	GTAGTGGTGCGGCATATACT	Diagnostic PCR/STF validation
JSP263_STEE_COLONY_REV	CGTCAAAGACAATTGAATCG	Diagnostic PCR/STF validation
JPS208_CIGR_STF_FWD	TCGCGCTCAGTACCGCGGTGGTCACGGCGATTATTAATGG CGTATTTGAT GGCTGGTCACACCCGCAGTTTG	mutagenesis/STF insertion
JPS209_CIGR_STF_REV	TACGCTCCGGTTTTTGGCGCGCTGTCCGTGTCCAAACTGGCT GCGCCAATA CATATGAATATCCTCCTTAG	mutagenesis/STF insertion
JPS210_CIGR_SEQ_FWD	CGCTACCGCCGGGAATCGCT	Diagnostic PCR/STF validation
JPS211_CIGR_SEQ_REV	GGCAGTGCTCGCCAAAACGC	Diagnostic PCR/STF validation
JPS212_GTGA_STF_FWD	AAGAGATGGGTACACATCACCACCAAGAATCGCCTACGAA TTTAGTAAT GGCTGGTCACACCCGCAGTTTG	mutagenesis/STF insertion
JPS213_GTGA_STF_REV	CTGTATTAGCTCAGACCTGAACTGGTTACTGTGTTGTAGCAT CGTGGGAT CATATGAATATCCTCCTTAG	mutagenesis/STF insertion
JPS214_GTGA_SEQ_FWD	GTTGACTCACCTTCAGGACA	Diagnostic PCR/STF validation
JPS215_GTGA_SEQ_REV	ATGTCCGAATCGATTCTGG	Diagnostic PCR/STF validation

Dissecting the host-pathogen interface during *Salmonella* infection

JPS216_SSEK3_STF_FWD	ATGAACATATTTTTATGGATACCAGCAGTTTGACTATCAGCT CCTGGAGA GGCTGGTCACACCCGCAGTTTG	mutagenesis/STF insertion
JPS217_SSEK3_STF_REV	CGTCAGTATGGTCTTTACGTTTAGCTTTGCCGAAACATTGCT CGCGTTTA CATATGAATATCCTCCTTAG	mutagenesis/STF insertion
JPS218_SSEK3_SEQ_FWD	CGATCCATACATTGATGGTG	Diagnostic PCR/STF validation
JPS219_SSEK3_SEQ_REV	GAGTTAACCGGATGAGTGAT	Diagnostic PCR/STF validation
JPS220_STEE_STF_FWD	CCGGTTATATCGCTCAATACAGGCATTCTGCAGAGGTTTTTC CCGGATGAA GGCTGGTCACACCCGCAGTTTG	mutagenesis/STF insertion
JPS221_STEE_STF_REV	ATCACACAATCCGGACTGAGTTCAATCAAAGTGATCTACTAT TCGGCGCA CATATGAATATCCTCCTTAG	mutagenesis/STF insertion
JPS222_STEE_SEQ_FWD	GTTTCCCCGGATGCTTTAAC	Diagnostic PCR/STF validation
JPS223_STEE_SEQ_REV	CATCAGGCGTCGTTTCGGTAC	Diagnostic PCR/STF validation
JPS224_YEBF_STF_FWD	ATCAGGTCATCGTTGATTGCAAAGCCGGCAAGGCGGAATAT AAGCCCCGCG GGCTGGTCACACCCGCAGTTTG	mutagenesis/STF insertion
JPS225_YEBF_STF_REV	TAATGGTCAAGCGTACCTGAGGGGATGTCAGGAATTGTCTG TTCCGGCAA CATATGAATATCCTCCTTAG	mutagenesis/STF insertion
JPS226_YEBF_COLONY_FWD	GCAGGCTGACCCGGTCCGCT	Diagnostic PCR/STF validation
JPS227_YEBF_COLONY_REV	CCAGCAGTTTATTTAACCC	Diagnostic PCR/STF validation
JPS228_AVRA_STF_FWD	ACAAAAAGAATGAACGCTTTATGAGCGATTGATAACAATGC CGTTATGC GGCTGGTCACACCCGCAGTTTG	mutagenesis/STF insertion
JPS229_AVRA_STF_REV	TACGGTTTAAGTAAAGACTTATATTCAGCTATCCTTTTTTAT GAGCGGA CATATGAATATCCTCCTTAG	mutagenesis/STF insertion
JPS230_AVRA_COLONY_FWD	GAATATGTGGAGGCCAATCC	Diagnostic PCR/STF validation
JPS231_AVRA_COLONY_REV	AATCGTACCAGAGGCGCAAG	Diagnostic PCR/STF validation
JPS232_GTGE_STF_FWD	AGCCAAAACCTTTACTCTCCTCCTCGGAAAGACTGGTGT ACCATTTTA GGCTGGTCACACCCGCAGTTTG	mutagenesis/STF insertion
JPS233_GTGE_STF_REV	GAGAGGATTTGAACCTCCGCCCCCATGTTGGCGGTAGC CTGAATAATT CATATGAATATCCTCCTTAG	mutagenesis/STF insertion
JPS234_GTGE_COLONY_FWD	TGGTCTTTACTATGACGGTG	Diagnostic PCR/STF validation
JPS235_GTGE_COLONY_REV	CTCAATTTCTACGGGGAAG	Diagnostic PCR/STF validation
JPS236_SIPB_STF_FWD	TACAGCAAAATGCGGATGCTTCGCGTTTTATTCTGCGCCAG AGTCGCGCA GGCTGGTCACACCCGCAGTTTG	mutagenesis/STF insertion
JPS237_SIPB_STF_REV	TTAAATAAGCGCGGGGATTATCCCACATTACTAATTAACA TATTTTTTC CATATGAATATCCTCCTTAG	mutagenesis/STF insertion
JPS238_SIPB_COLONY_FWD	CCATGGATCAGATTCAGCAG	Diagnostic PCR/STF validation
JPS239_SIPB_COLONY_REV	GATTATTTAATAAGCGGCG	Diagnostic PCR/STF validation
JPS240_SIPC_STF_FWD	ACCAGTCGAAAGCATCCGCACTCGCTGCTATCGCAGGCAAT ATTTCGCGCT GGCTGGTCACACCCGCAGTTTG	mutagenesis/STF insertion
JPS241_SIPC_STF_REV	AATATCCCCAGTTCCGCATCAGGAGCGGATTAATCACAC CCATGATGG CATATGAATATCCTCCTTAG	mutagenesis/STF insertion
JPS242_SIPC_COLONY_FWD	GAAAGTTCACGTAATCGAC	Diagnostic PCR/STF validation
JPS243_SIPC_COLONY_REV	GAGTCTGCGGCCGTTCCGGCA	Diagnostic PCR/STF validation
JPS244_SOPA_STF_FWD	GAAAATATTTCCGAGTGTTCTGTCCATCCATCCTGCCACTG GCCTGGGCG GGCTGGTCACACCCGCAGTTTG	mutagenesis/STF insertion
JPS245_SOPA_STF_REV	GACTAAAACGGGTCTATGTACAGAGGGACACAACGCTGTGT CCCTTAATT CATATGAATATCCTCCTTAG	mutagenesis/STF insertion
JPS246_SOPA_COLONY_FWD	AGCTGTCTCCGGCGATATTC	Diagnostic PCR/STF validation
JPS247_SOPA_COLONY_REV	GCAATCTGGCCGGGATCTCA	Diagnostic PCR/STF validation
JPS248_SOPD_STF_FWD	GTTCTTTGCACATTGGTAAAGATGGGTGCAGTCGTAATATAT TACTGACA GGCTGGTCACACCCGCAGTTTG	mutagenesis/STF insertion

Dissecting the host-pathogen interface during *Salmonella* infection

JPS249_SOPD_STF_REV	GATTATACTTGCTGCTATGAAAAATCCGGCAGGCAGCCGGA TTTTAAATT CATATGAATATCCTCCTTAG	mutagenesis/STF insertion
JPS250_SOPD_COLONY_FWD	GAGTTTAAACCAACAAATTC	Diagnostic PCR/STF validation
JPS251_SOPD_COLONY_REV	CGGGTATGGCGGAAGAAGAG	Diagnostic PCR/STF validation
JPS252_SOPE2_STF_FWD	TTCAGTTAACTATAGAAAAATTGCGAATAAGTATCTTCAGA ATGCCTCC GGCTGGTCACACCCGCAGTTTG	mutagenesis/STF insertion
JPS253_SOPE2_STF_REV	AACGAATATATAGTTTCAGAAAACTGCTATTAATTCATATGG TTAATAG CATATGAATATCCTCCTTAG	mutagenesis/STF insertion
JPS254_SOPE2_COLONY_FWD	GTATTAATATCCGCATATG	Diagnostic PCR/STF validation
JPS255_SOPE2_COLONY_REV	CAGGTATTTAGAGTAATAAC	Diagnostic PCR/STF validation
JPS256_SPVD_STF_FWD	TCTCATCATCAGGGGAATTTATGTCAGGGCTTATGATGAAA AACACGAT GGCTGGTCACACCCGCAGTTTG	mutagenesis/STF insertion
JPS257_SPVD_STF_REV	GGTTTACAGCGGATCTTCTAAGGCTCTCTATTAACCTACCA TTCATAAA CATATGAATATCCTCCTTAG	mutagenesis/STF insertion
JPS258_SPVD_COLONY_FWD	GAAAACATCCAACATACTTC	Diagnostic PCR/STF validation
JPS259_SPVD_COLONY_REV	TTGCCTGTAGCGCCGGTGGT	Diagnostic PCR/STF validation
JPS260_STED_STF_FWD	CCGGACTATACCTTAGCGCAAATGGCATCAGAACCCGGCCA GCCTGGCCA GGCTGGTCACACCCGCAGTTTG	mutagenesis/STF insertion
JPS261_STED_STF_REV	TCTGGACGATTAACACCCCGTGTATCGTCGGAATTCGCTCT TTCCCTAT CATATGAATATCCTCCTTAG	mutagenesis/STF insertion
JPS262_STED_COLONY_FWD	GTAGTGGTGCGGCATATACT	Diagnostic PCR/STF validation
JPS263_STED_COLONY_REV	CGTCAAAGACAATTGAATCG	Diagnostic PCR/STF validation
JPS264_SRFJ_STF_FWD	CGCTGCCGCCGTCAGCGGCCAGTACGTTGCTATGGCGGCA GGAGTCGATC GGCTGGTCACACCCGCAGTTTG	mutagenesis/STF insertion
JPS265_SRFJ_STF_REV	AGCGTGGAGTTTCGCATACAGGTCGCTTCATTAATCCAG CTTCATCAT CATATGAATATCCTCCTTAG	mutagenesis/STF insertion
JPS266_SRFJ_COLONY_FWD	CACTCCTGGTATGGTATTGG	Diagnostic PCR/STF validation
JPS267_SRFJ_COLONY_REV	CGCTTAACGTATGTTTCTGC	Diagnostic PCR/STF validation
JPS268_SSAV_STF_FWD	TGGTAGAAAGTATTGACCTTAGCGAAGAGGAGTTGGCGGAC AATGAAGAA GGCTGGTCACACCCGCAGTTTG	mutagenesis/STF insertion
JPS269_SSAV_STF_REV	TCGGGGGGCGGATATTTACGCTCAGACGTTGCATCAATTC ATTCTTCAT CATATGAATATCCTCCTTAG	mutagenesis/STF insertion
JPS270_SSAV_COLONY_FWD	CAGACGGCAATGGGGACCTA	Diagnostic PCR/STF validation
JPS271_SSAV_COLONY_REV	CCCACGACTTCAGCAAGTTC	Diagnostic PCR/STF validation
JPS272_SPIC_STF_FWD	TTTTAAAAATGTAATACGCAATCACCATAAACTTTATTCGG GTGGGGTA GGCTGGTCACACCCGCAGTTTG	mutagenesis/STF insertion
JPS273_SPIC_STF_REV	GTATTGAGTATAAATAGTAAATTAAGATTAACGTTTATTTA CTACCAT CATATGAATATCCTCCTTAG	mutagenesis/STF insertion
JPS274_SPIC_COLONY_FWD	CGGATGGGGGATGGTTAAAC	Diagnostic PCR/STF validation
JPS275_SPIC_COLONY_REV	GTTATCAATGGGCTAATAGT	Diagnostic PCR/STF validation
PW137_STM14_3767_STF_FWD	CCAATTTTCGGCAGCAACTTAGAGTAGATGCAAAAAAATG CATCTGATTGGCTGGTCACACCCGCAGTTTG	mutagenesis/STF insertion
PW138_STM14_3767_STF_REV	GACTCATGATGTTTATATTTAGGGATGCTACATTAATAAATA GCATTAACATATGAATATCCTCCTTAG	mutagenesis/STF insertion
PW139_STM14_3767_SEQ_FWD	GCGAATGATACGATTTCTCG	Diagnostic PCR/STF validation
PW140_STM14_3767_SEQ_REV	CAAATATTAACGCTTTTCTG	Diagnostic PCR/STF validation
PW208_DSBA_FWD_1	GGATAAACCCAACCAGACTC	Diagnostic PCR/validation of deletion
PW209_DSBA_FWD_2	GGTTAACAGGGGAAGATTAC	Diagnostic PCR/validation of deletion

Dissecting the host-pathogen interface during *Salmonella* infection

PW210_PURD_FWD	GGTATTGCGATGATCTTCAC	Diagnostic PCR/validation of deletion
PW211_SSAP_FWD	AGGCGCAGAGCTTTTTGACG	Diagnostic PCR/validation of deletion
PW212_DSBA_REV_1	CATTAAACAGCCACAGAAAGC	Diagnostic PCR/validation of deletion
PW213_DSBA_REV_2	GAACGACAAAACATTCAAAC	Diagnostic PCR/validation of deletion
PW214_PURD_REV	GGTGATTCTGGCGGCACTGG	Diagnostic PCR/validation of deletion
PW215_SSAP_REV	ATCCACACCCTACCCAGCTC	Diagnostic PCR/validation of deletion
PW216_CYDC_FWD	AGTTGGAAGATCTCGCCGAC	Diagnostic PCR/validation of deletion
PW217_STM14_2242_1_FWD	GTTATTACTCTAAATACCTG	Diagnostic PCR/validation of deletion
PW218_AROK_FWD	GGTTTCAGTTCATGCTCTGC	Diagnostic PCR/validation of deletion
PW219_GLTK_FWD	CTGCCGGGCAACGTGGGGAG	Diagnostic PCR/validation of deletion
PW220_CYDC_REV	GTCGGGAAAGCTGAACCAGA	Diagnostic PCR/validation of deletion
PW221_STM14_2242_1_REV	CGAATTCACCATAGCGAG	Diagnostic PCR/validation of deletion
PW222_AROK_REV	CCTTAGTTACTTGTGCCGCG	Diagnostic PCR/validation of deletion
PW223_GLTK_REV	CAATCGGTCAGCACCTGAAA	Diagnostic PCR/validation of deletion
PW224_YFIC_FWD	CATCTGTTTGTATGGATATC	Diagnostic PCR/validation of deletion
PW225_LIVG_FWD	GCTGCCGATGACGCGTCCGC	Diagnostic PCR/validation of deletion
PW226_STM14_4558_FWD	CAACGAGGCTAATCTGGCCG	Diagnostic PCR/validation of deletion
PW227_TOLR_FWD	CTTACAACCGACTGAATCAG	Diagnostic PCR/validation of deletion
PW228_YFIC_REV	GATTATCCGCAACAAGTGGC	Diagnostic PCR/validation of deletion
PW229_LIVG_REV	ATGTGCAGACTGACGTCGTG	Diagnostic PCR/validation of deletion
PW230_STM14_4558_REV	GTCACTGAACTACTTAATG	Diagnostic PCR/validation of deletion
PW231_TOLR_REV	GCAAATAAGATGATATGCAG	Diagnostic PCR/validation of deletion
PW232_FDX_FWD	TGTTGACGCCATAGAACAAG	Diagnostic PCR/validation of deletion
PW233_STM14_3944_FWD	TGGTACGAGCCAGCAACCTG	Diagnostic PCR/validation of deletion
PW234_PYRC_FWD	GTGAAATCGTTATTCCTTTC	Diagnostic PCR/validation of deletion
PW235_HILA_FWD	CGTAGAATATGACATTAAGC	Diagnostic PCR/validation of deletion
PW236_FDX_REV	AGGATCGACATCAGGATATG	Diagnostic PCR/validation of deletion
PW237_STM14_3944_REV	CGCCTTTTATCGCCATCGTG	Diagnostic PCR/validation of deletion
PW238_PYRC_REV	GTTTTGGCTATAGTACTTC	Diagnostic PCR/validation of deletion
PW239_HILA_REV	CTAAGCAACCAGATTACGAT	Diagnostic PCR/validation of deletion
PW240_FLIN_FWD	CGACCGCATTATTGCTCATG	Diagnostic PCR/validation of deletion
PW241_ENVZ_FWD	CATCGACGTCCAGATCTCCC	Diagnostic PCR/validation of deletion
PW242_AMPE_FWD	GCTTATCGCTAGCTATCCGG	Diagnostic PCR/validation of deletion

Dissecting the host-pathogen interface during *Salmonella* infection

PW243_RLUD_FWD	CATGACGTTTTGACTTTCCT	Diagnostic PCR/validation of deletion
PW244_FLIN_REV	CGAATCCCATACGCTTAATC	Diagnostic PCR/validation of deletion
PW245_ENVZ_REV	CGAATCCCATACGCTTAATC	Diagnostic PCR/validation of deletion
PW246_AMPE_REV	CAGCCGATACGATCTAAGCC	Diagnostic PCR/validation of deletion
PW247_RLUD_REV	CAGATTCAGCGAGTCGTAAG	Diagnostic PCR/validation of deletion
PW248_STM14_0643_FWD	ACAATGATGCCATAATATC	Diagnostic PCR/validation of deletion
PW249_HOLD_FWD	CGATTATAGTAGTTTGATGG	Diagnostic PCR/validation of deletion
PW250_SLYX_FWD	CGAACACGCCCTATTATCAC	Diagnostic PCR/validation of deletion
PW251_FLGJ_FWD	CCAATCTGAACAGCGTAGTG	Diagnostic PCR/validation of deletion
PW252_STM14_0643_REV	GTTTCAGTAACTCAAGGCGAT	Diagnostic PCR/validation of deletion
PW253_HOLD_REV	CCACCTGTGTAATGGCAAAC	Diagnostic PCR/validation of deletion
PW254_SLYX_REV	GGTCATATAGTTATCTATGC	Diagnostic PCR/validation of deletion
PW255_FLGJ_REV	GATTAATCAAGCTGGACATG	Diagnostic PCR/validation of deletion
PW256_TRAB_FWD	GAAAATAAAATGCCGTCAGC	Diagnostic PCR/validation of deletion
PW257_YJEK_FWD	GTTTCACGAATTCACTGGAT	Diagnostic PCR/validation of deletion
PW258_STM14_5232_FWD	AGGCACAGAATCAGAATAGC	Diagnostic PCR/validation of deletion
PW259_STM14_5527_FWD	CTCTAATCAAGTTTATATGA	Diagnostic PCR/validation of deletion
PW260_TRAB_REV	AGAGCAGAATGACAACAATG	Diagnostic PCR/validation of deletion
PW261_YJEK_REV	CGAAGGTTAGTTTATCCTCG	Diagnostic PCR/validation of deletion
PW262_STM14_5232_REV	CTGGCTTACTACCGCGAGCA	Diagnostic PCR/validation of deletion
PW263_STM14_5527_REV	CGTAACCTGTGTTGGCGCAC	Diagnostic PCR/validation of deletion
PW264_INVH_FWD	GTTTTTTTTGCTAGCATTCC	Diagnostic PCR/validation of deletion
PW265_CYAA_FWD	CGGTATTAGATAAAAAATATG	Diagnostic PCR/validation of deletion
PW266_YADB_FWD	GAAAAACAGATGGCGGGTTA	Diagnostic PCR/validation of deletion
PW267_YBED_FWD	TGATTTTCGTCCCCATATAC	Diagnostic PCR/validation of deletion
PW268_INVH_REV	GTAAGAGACAAATGGCCAAC	Diagnostic PCR/validation of deletion
PW269_CYAA_REV	CCTGTAACCAATGCGGAG	Diagnostic PCR/validation of deletion
PW270_YADB_REV	CAACTTACTCTATGTCTTTC	Diagnostic PCR/validation of deletion
PW271_YBED_REV	CGTAGAGAATGAAAAAGAG	Diagnostic PCR/validation of deletion
PW272_GIDA_FWD	ACAGATCTCTAAATAAAAG	Diagnostic PCR/validation of deletion
PW273_PCNB_FWD	ATGATTAGCCGCTATTTTTG	Diagnostic PCR/validation of deletion
PW274_ALLR_FWD	GCTATTGGCCTTCTTGATA	Diagnostic PCR/validation of deletion
PW275_YCIT_FWD	CAGGTTAAAGACGGTATCTC	Diagnostic PCR/validation of deletion

Dissecting the host-pathogen interface during *Salmonella* infection

PW276_GIDA_REV	CTGTTAATAATCAAATGCCC	Diagnostic PCR/validation of deletion
PW277_PCNB_REV	GCGGCGGCGTGCGGTA AAC	Diagnostic PCR/validation of deletion
PW278_ALLR_REV	CTTCTTTTTCCAGCACATAC	Diagnostic PCR/validation of deletion
PW279_YCIT_REV	GTGATAGTCACTTCCTGTTA	Diagnostic PCR/validation of deletion
PW280_ARGE_FWD	CTTTATGCTCAACGTTAATG	Diagnostic PCR/validation of deletion
PW281_SPAP_FWD	CAGCTATTACTACTGCCGAC	Diagnostic PCR/validation of deletion
PW282_PROB_FWD	GTAATAAAATGGTCAAATTC	Diagnostic PCR/validation of deletion
PW283_YHEU_FWD	GTAGGATTTATCGGCGGTAC	Diagnostic PCR/validation of deletion
PW284_ARGE_REV	AATTCGCATCGTGCCAAATA	Diagnostic PCR/validation of deletion
PW285_SPAP_REV	CTACCAGGAGGCCGATAATC	Diagnostic PCR/validation of deletion
PW286_PROB_REV	GCTATTTTTCCAGCACGCG	Diagnostic PCR/validation of deletion
PW287_YHEU_REV	GAAACGCGAGGCTGGTGGTG	Diagnostic PCR/validation of deletion
PW292_SSEJ_SEQ_FWD	TAATTATTTGCTAAAGCGTG	Diagnostic PCR/validation of deletion
PW293_SSEJ_SEQ_REV	CACTATGATATTGAGCTGTG	Diagnostic PCR/validation of deletion
PW294_SIFA_SEQ_FWD	AATTATGTAGTCATTTTTAC	Diagnostic PCR/validation of deletion
PW295_SIFA_SEQ_REV	GTAGGCAAACAGGAAGTACG	Diagnostic PCR/validation of deletion
PW304_STEE_SEQ_FWD	GAGGTGTATTAATTGATAGG	Diagnostic PCR/validation of deletion
PW305_STEE_SEQ_REV	GGTGATTTGTGATTTTTGGC	Diagnostic PCR/validation of deletion
PW306_SIFB_SEQ_FWD	CAAACCGATGGGCAACATGG	Diagnostic PCR/validation of deletion
PW307_SIFB_SEQ_REV	GTAATCCATTATTCCTGG	Diagnostic PCR/validation of deletion
PW308_PIPB2_SEQ_FWD	CACTGTGTTGCTGTCTCTGG	Diagnostic PCR/validation of deletion
PW309_PIPB2_SEQ_REV	GCTTTTATTCAGATTTACG	Diagnostic PCR/validation of deletion
JB65_KANR_FWD ²	GATTGAACAAGATGGATTGCACGC	Diagnostic PCR/validation of deletion
JB66_KANR_REV ²	ACCATGATATTCGCAAGCAGG	Diagnostic PCR/validation of deletion

¹Designed by Dr. Joel Selkrig and Keith Fernandez

²Designed by Jacob Bobonis

3. List of stains and cell lines used in this work

The majority of strains and cell lines listed in Table VII.4 has been used in (Walch et al. 2020), and has been published there in Supplementary Table S12.

Table VII.4. All cell lines and bacterial strains used in this work. Identifier, genetic background and reference for the source are indicated for all used specimen.

Strains and cell lines	Genotype	Source or reference	Description
<i>E. coli</i>			
Rosetta(DE3) plysRare	host strain for recombinant protein expression,	Novagen	
<i>Salmonella enterica</i> serovar Typhimurium 14028s			
14028s	wild type <i>Salmonella enterica</i> serovar Typhimurium 14028s	¹	
NT13010	<i>gogB::STF-kan</i>	this study ²	STm 14028S carrying C-terminally (aa 497) STF-tagged STM14_3164
NT13012	<i>sseK1::STF-kan</i>	this study ²	STm 14028S carrying C-terminally (aa 336) STF-tagged STM14_4996
NT13016	<i>sseJ::STF-kan</i>	this study ²	STm 14028S carrying C-terminally (aa 408) STF-tagged STM14_1974
NT13032	Δ <i>ccdAB::Cm, sifA::STF</i>	this study ²	STm 14028S carrying internally (aa 136) STF-tagged STM14_1400
NT13066	<i>pipB::STF-kan</i>	this study ²	STm 14028S carrying C-terminally (aa 291) STF-tagged STM14_1233
NT13068	<i>pipB2::STF-kan</i>	this study ²	STm 14028S carrying C-terminally (aa 350) STF-tagged STM14_3350
NT13070	<i>sifB::STF-kan</i>	this study ²	STm 14028S carrying C-terminally (aa 316) STF-tagged STM14_1940
NT13072	<i>slrP::STF-kan</i>	this study ²	STm 14028S carrying C-terminally (aa 765) STF-tagged STM14_928
NT13074	<i>sopD2::STF-kan</i>	this study ²	STm 14028S carrying C-terminally (aa 319) STF-tagged STM14_1098
NT13076	<i>spvB::STF-kan</i>	this study ²	STm 14028S carrying C-terminally (aa 591) STF-tagged STM14_5562
NT13078	<i>spvC::STF-kan</i>	this study ²	STm 14028S carrying C-terminally (aa 241) STF-tagged STM14_5561
NT13080	<i>srgE::STF-kan</i>	this study ²	STm 14028S carrying C-terminally (aa 488) STF-tagged STM14_1877
NT13082	<i>sseF::STF-kan</i>	this study ²	STm 14028S carrying C-terminally (aa 260) STF-tagged STM14_1700
NT13084	<i>sseG::STF-kan</i>	this study ²	STm 14028S carrying C-terminally (aa 229) STF-tagged STM14_1701
NT13086	<i>sseI::STF-kan</i>	this study ²	STm 14028S carrying C-terminally (aa 322) STF-tagged STM14_1193
NT13088	<i>sipA::STF-kan</i>	this study ²	STm 14028S carrying C-terminally (aa 685) STF-tagged STM14_3481
NT13090	<i>sopB::STF-kan</i>	this study ²	STm 14028S carrying C-terminally (aa 561) STF-tagged STM14_1237
NT13092	<i>sseK2::STF-kan</i>	this study ²	STm 14028S carrying C-terminally (aa 335) STF-tagged STM14_2428
NT13094	<i>sseL::STF-kan</i>	this study ²	STm 14028S carrying C-terminally (aa 317) STF-tagged STM14_2824
NT13096	<i>sspH1::STF-kan</i>	this study ²	STm 14028S carrying C-terminally (aa 700) STF-tagged STM14_1483
NT13098	<i>sspH2::STF-kan</i>	this study ²	STm 14028S carrying C-terminally (aa 788) STF-tagged STM14_2769
NT13100	<i>steA::STF-kan</i>	this study ²	STm 14028S carrying C-terminally (aa 210) STF-tagged STM14_1912
NT13102	<i>steB::STF-kan</i>	this study ²	STm 14028S carrying C-terminally (aa 133) STF-tagged STM14_1970
NT13104	<i>steC::STF-kan</i>	this study ²	STm 14028S carrying C-terminally (aa 457) STF-tagged STM14_2050
NT13106	<i>sptP::STF-kan</i>	this study ²	STm 14028S carrying C-terminally (aa 543) STF-tagged STM14_3477
NT19006	<i>cigR::STF-kan</i>	this study	STm 14028S carrying C-terminally (aa 159) STF-tagged STM14_4534
NT19007	<i>yebF::STF-kan</i>	this study	STm 14028S carrying C-terminally (aa 117) STF-tagged STM14_2286
NT19008	<i>yebF::STF-kan</i>	this study	STm 14028S carrying C-terminally (aa 117) STF-tagged STM14_2286
NT19009	<i>steE::STF-kan</i>	this study	STm 14028S carrying C-terminally (aa 181) STF-tagged STM14_3166
NT19015	<i>avrA::STF-kan</i>	this study	STm 14028S carrying C-terminally (aa 278) STF-tagged STM14_3462
NT19016	<i>sipB::STF-kan</i>	this study	STm 14028S carrying C-terminally (aa 593) STF-tagged STM14_3484
NT19017	<i>sipC::STF-kan</i>	this study	STm 14028S carrying C-terminally (aa 409) STF-tagged STM14_3483
NT19018	<i>sopA::STF-kan</i>	this study	STm 14028S carrying C-terminally (aa 782) STF-tagged STM14_2557
NT19019	<i>steD::STF-kan</i>	this study	STm 14028S carrying C-terminally (aa 111) STF-tagged STM14_2638
NT13134	Δ <i>sseJ::</i>	this study ³	STm 14028S with <i>sseJ</i> gene deletion (FRT site scar)
NT13135	Δ <i>sseL::</i>	this study ³	STm 14028S with <i>sseL</i> gene deletion (FRT site scar)
NT13136	Δ <i>steC::</i>	this study ³	STm 14028S with <i>steC</i> gene deletion (FRT site scar)
NT13138	Δ <i>sseJ::kan</i>	¹	STm 14028S with <i>sseJ</i> gene replaced by kanamycin resistance
NT13139	Δ <i>sseL::kan</i>	¹	STm 14028S with <i>sseL</i> gene replaced by kanamycin resistance
NT13140	Δ <i>steC::kan</i>	¹	STm 14028S with <i>steC</i> gene replaced by kanamycin resistance
NT13152	Δ <i>sseJ::\Delta</i> <i>sseL::</i>	this study ³	STm 14028S with <i>sseJ</i> and <i>sseL</i> gene deletion (FRT site scar)
NT13108	Δ <i>ssaV::kan</i>	¹	STm 14028S with <i>ssaV</i> gene replaced by kanamycin resistance
NT13045	Δ <i>prgK::kan</i>	¹	STm 14028S with <i>prgK</i> gene replaced by kanamycin resistance

Dissecting the host-pathogen interface during *Salmonella* infection

NT13042	<i>ΔsifA::kan</i>	¹	STm 14028S with <i>sifA</i> gene replaced by kanamycin resistance
NT19031	WT pFCcGi	this study	STm 14028S WT expressing mCherry from pFCcGi
NT19032	<i>ΔsseJ::pFCcGi</i>	this study	STm 14028S <i>ΔsseJ::</i> expressing mCherry from pFCcGi
NT19033	<i>ΔsseL::pFCcGi</i>	this study	STm 14028S <i>ΔsseL::</i> expressing mCherry from pFCcGi
NT19034	<i>ΔsteC::pFCcGi</i>	this study	STm 14028S <i>ΔsteC::</i> expressing mCherry from pFCcGi
NT19035	<i>ΔyebF::pFCcGi</i>	this study	STm 14028S <i>ΔyebF::</i> expressing mCherry from pFCcGi
NT19036	<i>ΔsseJ::kan, pFCcGi</i>	this study	STm 14028S <i>ΔsseJ::Kan</i> expressing mCherry from pFCcGi
NT19037	<i>ΔsseJ::kan, pFCcGi</i>	this study	STm 14028S <i>ΔsseJ::Kan</i> expressing mCherry from pFCcGi
NT19038	<i>ΔsseL::kan, pFCcGi</i>	this study	STm 14028S <i>ΔsseL::Kan</i> expressing mCherry from pFCcGi
NT19039	<i>ΔsseL::kan, pFCcGi</i>	this study	STm 14028S <i>ΔsseL::Kan</i> expressing mCherry from pFCcGi
NT19040	<i>ΔsteC::kan, pFCcGi</i>	this study	STm 14028S <i>ΔsteC::Kan</i> expressing mCherry from pFCcGi
NT19041	<i>ΔsteC::kan, pFCcGi</i>	this study	STm 14028S <i>ΔsteC::Kan</i> expressing mCherry from pFCcGi
NT19042	<i>ΔyebF::kan, pFCcGi</i>	this study	STm 14028S <i>ΔyebF::Kan</i> expressing mCherry from pFCcGi
NT19043	<i>ΔsseJ::ΔsseL::, pFCcGi</i>	this study	STm 14028S <i>ΔsseJ::ΔsseL::</i> expressing mCherry from pFCcGi
NT19049	<i>ΔssaV::kan, pFCcGi</i>	this study	STm 14028S <i>ΔssaV::Kan</i> expressing mCherry from pFCcGi
NT19050	<i>ΔprgK::kan, pFCcGi</i>	this study	STm 14028S <i>ΔprgK::Kan</i> expressing mCherry from pFCcGi
NT19051	<i>ΔsifA::kan, pFCcGi</i>	this study	STm 14028S <i>ΔsifA::Kan</i> expressing mCherry from pFCcGi
NT19110	<i>Δalr::Kan</i>	this study	STm 14028S with <i>alr</i> gene replaced by kanamycin resistance
NT19111	<i>ΔhilA::Kan</i>	this study	STm 14028S with <i>hilA</i> gene replaced by kanamycin resistance
NT19113	<i>ΔSTM14_2242::Kan</i>	this study	STm 14028S with <i>STM14_2242</i> replaced by kanamycin resistance
NT19124	<i>ΔSTM14_3944::Kan</i>	this study	STm 14028S with <i>STM14_3944</i> replaced by kanamycin resistance
NT19125	<i>Δfdx::Kan</i>	this study	STm 14028S with <i>fdx</i> gene replaced by kanamycin resistance
NT19126	<i>Δalr::Kan pFCcGi</i>	this study	STm 14028S <i>Δalr::Kan</i> expressing mCherry from pFCcGi
NT19127	<i>ΔhilA::Kan pFCcGi</i>	this study	STm 14028S <i>ΔhilA::Kan</i> expressing mCherry from pFCcGi
NT19129	<i>ΔSTM14_2242::Kan pFCcGi</i>	this study	STm 14028S <i>ΔSTM14_2242::Kan</i> expressing mCherry from pFCcGi
NT19140	<i>ΔSTM14_3944::Kan pFCcGi</i>	this study	STm 14028S <i>ΔSTM14_3944::Kan</i> expressing mCherry from pFCcGi
NT19141	<i>Δfdx::Kan pFCcGi</i>	this study	STm 14028S <i>Δfdx::Kan</i> expressing mCherry from pFCcGi
NT19143	<i>ΔampE::Kan</i>	this study	STm 14028S with <i>ampE</i> gene replaced by kanamycin resistance
NT19147	<i>ΔpurD::Kan</i>	this study	STm 14028S with <i>purD</i> gene replaced by kanamycin resistance
NT19148	<i>ΔssaP::Kan</i>	this study	STm 14028S with <i>ssaP</i> gene replaced by kanamycin resistance
NT19149	<i>ΔSTM14_4558::Kan</i>	this study	STm 14028S with <i>STM14_4558</i> replaced by kanamycin resistance
NT19150	<i>ΔSTM14_0643::Kan</i>	this study	STm 14028S with <i>STM14_0643</i> replaced by kanamycin resistance
NT19158	<i>ΔyheU::Kan</i>	this study	STm 14028S with <i>yheU</i> gene replaced by kanamycin resistance
NT19159	<i>ΔSTM14_5232::Kan</i>	this study	STm 14028S with <i>STM14_5232</i> replaced by kanamycin resistance
NT19160	<i>ΔinvH::Kan</i>	this study	STm 14028S with <i>invH</i> gene replaced by kanamycin resistance
NT19162	<i>ΔspaP::Kan</i>	this study	STm 14028S with <i>spaP</i> gene replaced by kanamycin resistance
NT19175	<i>ΔampE::Kan pFCcGi</i>	this study	STm 14028S <i>ΔampE::Kan</i> expressing mCherry from pFCcGi
NT19179	<i>ΔpurD::Kan pFCcGi</i>	this study	STm 14028S <i>ΔpurD::Kan</i> expressing mCherry from pFCcGi
NT19180	<i>ΔssaP::Kan pFCcGi</i>	this study	STm 14028S <i>ΔssaP::Kan</i> expressing mCherry from pFCcGi
NT19181	<i>ΔSTM14_4558::Kan pFCcGi</i>	this study	STm 14028S <i>ΔSTM14_4558::Kan</i> expressing mCherry from pFCcGi
NT19182	<i>ΔSTM14_0643::Kan pFCcGi</i>	this study	STm 14028S <i>ΔSTM14_0643::Kan</i> expressing mCherry from pFCcGi
NT19190	<i>ΔyheU::Kan pFCcGi</i>	this study	STm 14028S <i>ΔyheU::Kan</i> expressing mCherry from pFCcGi
NT19191	<i>ΔSTM14_5232::Kan pFCcGi</i>	this study	STm 14028S <i>ΔSTM14_5232::Kan</i> expressing mCherry from pFCcGi
NT19192	<i>ΔinvH::Kan pFCcGi</i>	this study	STm 14028S <i>ΔinvH::Kan</i> expressing mCherry from pFCcGi
NT19194	<i>ΔspaP::Kan pFCcGi</i>	this study	STm 14028S <i>ΔspaP::Kan</i> expressing mCherry from pFCcGi
Mammalian cell lines			
HeLa	<i>Wildtype</i>	ATCC CCL-2	
HeLa	<i>NPC1-K.O.</i>	⁴	
RAW264.7	<i>Wildtype</i>	ATTC TIB-71	
3T3	<i>Wildtype</i>	⁵	
3T3	<i>FMNL2/3-K.O.</i>	⁵	
pBMDM	<i>Wildtype mice</i>	⁶	

¹ (Porwollik et al. 2014)

² Strains created by Dr. Joel Selkrig and Keith Fernandez

³ Strains created by Karoline Scholzen

⁴ provided by Dr. Willem Annaert (VIB, KU-Leuven)

⁵ provided by Prof. Dr. Klemens Rottner (TU Braunschweig, Helmholtz Centre for Infection Research, Braunschweig)

⁶ bone marrow provided by Prof. Dr. Wolf-Dietrich Hardt (ETH Zürich)

4. Bacterial growth conditions

Unless indicated otherwise, STm were grown on LB-agar plates or in LB Lennox liquid media (prepared by the EMBL media kitchen) at 37°C. If selection media was used, the appropriate antibiotic and its concentration are indicated. To store bacterial strains over a longer time, glycerol stocks (16% glycerol added to an overnight bacterial culture) were stored at -80°C. Prior to starting liquid cultures, all strains were streaked out from the glycerol stock on LB agar plates with the appropriate antibiotic. Strains on LB agar plates were stored at 4°C and never kept longer than two weeks.

5. Electroporation of bacterial strains

To generate electrocompetent bacteria, an overnight culture was diluted 1:100 in 25ml media in 50ml falcon tubes and incubated in a rolling incubator for 3 hours. Subsequent to that, the bacterial culture was centrifuged at 4000rpm, 4°C for 10 minutes and washed three times in pre-cooled distilled water, each time centrifuging the suspension at 4000rpm, 4°C for 10 minutes and discarding the supernatant. After the last wash, the bacterial pellet was resuspended in 300µl water and aliquoted in 6 Eppendorf tubes. Each of the aliquots was mixed with the donor DNA and kept on ice for 5 minutes.

Subsequently, the bacteria-DNA mixture was introduced into a pre-cooled electroporation cuvette (0.2 cm electrode gap, BioRad, cat. nr. 165-2086) using a glass Pasteur pipette and electroporated at 2.5 kV for 5ms in a BioRad GenePulser Xcell electroporator. Using the same Pasteur pipette, the bacterial suspension was pipetted into 1ml LB Lennox media and incubated at 37°C while rolling. After 1h, the culture was plated onto agar plates containing the appropriate selection antibiotic and grown overnight at 37°C.

6. P22 phage transduction

P22 phage transduction was used to introduce genomic alterations into WT STm 14028S in order to provide the same genetic background for all different mutant strains assessed in one experiment or to introduce a second mutation into a previously generated STm 14028S strain. To generate P22 lysate from a genetically modified donor strain, two donor colonies were cultured for 2 to 3 hours in 5ml LB Lennox until slight turbidity was reached. In one of the two tubes, two drops of WT STm 14028S lysate were added using a glass Pasteur pipette, the other one was left untouched and both cultures were grown overnight at 37°C while rolling.

The next day, bacterial lysis should be visible in the WT lysate treated vial, while the other culture should not display lysis. If this was the case, the lysate-treated culture was centrifuged at 4000rpm for 10 minutes. The supernatant was filtered through a 0.22µm sterile filter and subsequently, 200µl chloroform were added and the lysate was stored at 4°C until further use.

To transduce a recipient strain with donor lysate, a single colony of the recipient strain was used to inoculate a 5ml liquid culture (LB containing antibiotic where applicable) and incubated at 37°C for 2 to 3 hours while rolling until the culture turned slightly turbid. For transduction, the following conditions were assessed, using glass Pasteur pipettes for all steps:

- 100µl recipient strain (RS) culture + 2 drops of undiluted lysate
- 100µl RS culture + 2 drops of lysate diluted 1:10 in LB media
- 100µl RS culture + 2 drops of lysate diluted 1:100 in LB media

For each recipient strain or donor lysate, the following negative controls were set up:

- 100µl RS culture (recipient control)
- 100µl LB media + 2 drops of undiluted lysate (lysate control)

The transduction mixtures and negative controls were incubated at RT for 20 minutes and subsequently plated onto agar plates containing the appropriate selection antibiotic, as well as citrate. The plates were grown overnight and the following day, two colonies per donor-recipient combination were struck out on fresh agar plates containing citrate and the appropriate selection antibiotic, this was performed three times to eliminate residual phages.

7. Generation of STm tagged-effector library

To generate STm 14028S strains with 2xStrep-TEV-3xFLAG (STF) tagged effector proteins expressed from the endogenous locus, I used the donor plasmid pJPS1 (see Table VII.2). Cloning of the donor sequences into the plasmid backbone pGEM-T Easy (Promega, cat. nr. A1360) was conducted as described by the manufacturer, and was performed prior to this work by Dr. Joel Selkrig. Using primer-pairs with a 50-base pair overlap to the genomic sequence of the C-terminus of the given effector, as well as the downstream genomic region (see Table VII.3 for all primer sequences), the STF-sequence, as well as the kanamycin-resistance cassette, were amplified from purified pJPS1. This was done using Q5 Hot Start High-Fidelity DNA polymerase (New England BioLabs, cat. nr. M0493S)

The amplified fragment was then introduced into the genome by homologous recombination *via* λ -red recombinase (Datsenko and Wanner 2000; Uzzau et al. 2001). To do so, an STm strain carrying a plasmid encoding λ -red recombinase (pKD46) was electroporated (see section VII.5) with the donor-fragment and grown overnight at 30°C on selective agar (30µg/mL kanamycin). A subset of clones was verified by PCR and sequencing of the tagged C-terminal genomic region of the given effector.

In order to not disrupt the functionally relevant prenylation motif in the SPI-2 effector SifA, Dr. Joel Selkrig constructed an internally tagged strain (the STF-tag encoded between D136 and I137) prior to the start of this project. A detailed description of the strain generation is provided in (Walch et al. 2020). All other STF-tagged strains carry the affinity tag C-terminally. Table VII.4 lists all strains generated in this work.

8. STm gene deletion mutants

All single gene deletion mutants were struck out from a previously published collection of gene-deletion mutants (Porwollik et al. 2014). This library comprises almost 4000 STm strains, and in each one gene is replaced by a kanamycin-resistance cassette. All mutants that were used in this work were re-transduced into STm 14028S wildtype background using P22 phage transduction (as described in section VII.6) and subsequently PCR-validated. For the generation of double- and triple mutants, the kanamycin-resistance cassette replacing the gene of interest was excised in the recipient strain (i.e. deletion mutant of gene 1) using the FLP-FRT system, as previously described (Datsenko and Wanner 2000), and subsequently validated by PCR. Then, donor P22-phage lysate (obtained from gene deletion mutant 2) was used to introduce the second deletion. After phage transduction, the strains were selected on kanamycin-containing agar and validated by PCR.

9. Cell culture conditions

HeLa cells (ATCC CCL-2), RAW264.7 macrophages (ATCC TIB-71), NIH 3T3 murine fibroblasts (provided by our collaborator Dr. Klemens Rottner) and mutant versions of these cell lines were cultured as suggested by previous studies. In brief, all cells were cultured in DMEM (4.5 g/l glucose, 10% FBS, for 3T3 cells, 1mM sodium pyruvate, 1mM L-glutamine and non-essential amino acids (NEAA) were added) at 37°C, 5% CO₂. pBMDMs were differentiated in 10cm dishes in RPMI containing 10% FBS and 1µl/ml recombinant murine M-CSF (Pepro-Tech, cat. nr. 315-02) for five days and were directly used for infection. For cell lines, passage numbers were noted and cells were only used until passage 15. At 90% confluency, cells were passaged by aspirating the media, washing the cells in pre-warmed PBS and detaching in accutase (RAW264.7) or trypsin (HeLa, 3T3) for 3 minutes at 37°C. Detaching was stopped by addition of growth media and cells were counted in a BioRad TC20 using trypan blue. HEK293-T cells were passaged at 70% confluence by gently aspirating the media and detaching the cells by washing in fresh growth media. For infection, depending on the format, the following cell numbers were plated the day prior to the experiment:

seeding format	HeLa / 3T3 cells per well	RAW264.7 cells per well
96-well plate	7.5×10^3	3×10^4
6-well plate	2×10^5	9×10^5
15cm dish	3.5×10^6	15.4×10^6

For each replicate of the AP/QMS study, five 15cm dishes were seeded for each assessed effector. This corresponds to a total number of 7.5×10^7 cells for RAW264.7 cells and 1.75×10^7 cells for HeLa. Infection for all strains assessed in the same TMT-10plex was performed in parallel.

pBMDMs were only seeded for infection in 6-well plates, using a cell number of 1×10^6 cells per well. For detachment, the differentiation media was aspirated, cells were washed in pre-warmed PBS and 3ml PBS containing 2mM EDTA and 5% FBS was used for detachment in each 10cm dish. The cells were washed off the plate and centrifuged at 500 rpm for 5 minutes. Cells were resuspended in RPMI (supplemented with 10% FBS and 1 μ l/ml M-CSF), counted and seeded in 6-well plates in 1.5ml growth media.

If 96-well plates were used for infection, no cells were seeded in the outer rim (i.e. rows A and H, as well as columns 1 and 12). Instead, these wells were filled with 150 μ l PBS. Due to differences in oxygenation, the growth properties of host cells in the outer perimeter of a multiwell plate strongly differ from those in the inner wells. Therefore, a maximum of 60 wells was used in each 96-well plate and all unused wells were filled with 150 μ l PBS.

10. Infection and gentamicin protection assay

10.1. Infection of RAW264.7 macrophages and pBMDMs

After plating cells for infection, RAW264.7 cells were cultured in DMEM (4.5g/l glucose), BMDMs were cultured in supplemented RPMI at 37°C, 5% CO₂ overnight. STm strains used for infection were cultured in a rolling incubator at 37°C overnight in appropriate selection media (LB Lennox with or without antibiotics). Prior to infection, bacteria were washed once in pre-warmed PBS and OD-normalized to OD₅₇₈ = 1. The bacterial suspension was added to RAW264.7 cells or pBMDMs at an MOI of 100:1. If infection was carried out in a multiwell plate, the plate was centrifuged for 5 minutes at 170G to increase bacterial-host cell contact. Co-culture was maintained for 30 minutes to allow for invasion / uptake and subsequently, the media containing STm was aspirated and infected cells were washed in pre-warmed PBS. After washing, gentamicin-containing media was added for one hour (DMEM, 4.5 g/l glucose, 10% FBS, 100 μ g/ml gentamicin for RAW264.7; RPMI, 10% FBS, 50 μ g/ml gentamicin for pBMDMs) at 37°C, 5% CO₂. This is known as the gentamicin protection assay and serves to kill all remaining extracellular STm. After 1h, the selection media was replaced with 16 μ g/ml gentamicin media for the rest of the experiment. This marks time point zero for all time-course experiments (0 hpi).

10.2. Infection of HeLa and 3T3 cells

The day prior to the infection experiment, HeLa or 3T3 cells were plated as described in subchapter VII.9 and cultured overnight at 37°C, 5% CO₂ in DMEM (1 g/l glucose). STm used for infection were cultured overnight in a rolling incubator as described for RAW264.7 infection. Prior to infection, STm were subcultured (1:300, i.e. 300 μ l O.N. culture in 10 ml) in LB Lennox media under appropriate selective pressure in 100 ml Erlenmeyer flasks at 37°C, 45 rpm for 3.5 hours (Steele-Mortimer 2008). Infection at a MOI of 100:1 and gentamicin protection assay was performed as described in VII.10.1. As growth media, DMEM containing 1 g/l glucose was used.

11. Harvesting of protein lysates

11.1. Native harvest

Cells were harvested at the latest 20 hpi (for HeLa or RAW264.7) or 8 hpi (for 3T3 fibroblasts). At the appropriate time point, cells were washed in pre-warmed PBS and lysed in 1x PBS containing 0.1% Triton-X100 (Tx-100) and 1x cOmplete EDTA-free protease inhibitor (Roche, lysis buffer, 5ml per plate for 15cm dishes, 300µl per well in a 6-well plate) at 4°C for 30 minutes while rocking. Cells were subsequently scraped using a disposable cell lifter and washed off the plate by resuspending the supernatant (all at 4°C). To clear the lysate and separate Tx-100-soluble and -insoluble fractions, the lysate suspension was centrifuged at 20,000G, 4°C for 15 minutes. Of the cleared lysate, a small fraction was saved as “Total” fraction, the remaining lysate was subjected to immunoprecipitation (IP).

11.2. Harvest after crosslinking

Half of the samples in the AP/QMS study were subjected to crosslinking with the membrane permeable, reversible cross-linker dithiobis(succinimidyl-pyruvate) (DSP, ThermoFisher, cat. nr. 22585). To perform crosslinking, cells were washed twice in pre-warmed PBS and incubated in 1x PBS containing 1mM DSP (crosslinking buffer, 8ml per 15cm dish or 0.5ml for each well in a 6-well plate) for 2 hours at 4°C. The crosslinking reaction was quenched by washing twice in 20mM pH 7.5 Tris-HCl (quenching buffer) over 15 minutes at 4°C. Lysis buffer was added and lysis performed as described for native harvest.

12. Immunoprecipitation using anti-FLAG affinity gel

Immunoprecipitation of STF-tagged effectors was performed using anti-FLAG affinity gel (Sigma, A2220). For each sample, 50µl of the bead slurry were washed in pre-cooled PBS containing 0.1% Tx-100 (lysis buffer) and centrifuged at 5000rpm, 4°C for 1 minute. After the last washing step, the beads were resuspended in lysis buffer and added to the freshly harvested, cleared lysate. This mixture was incubated for 4 hours (native samples) or over-night (crosslinked samples) while tumbling at 4°C.

After this incubation, the suspension was centrifuged at 4000rpm, 4°C for 10 minutes. A small fraction of the supernatant was kept as “Unbound” fraction and the remaining supernatant was discarded. The FLAG-beads were washed in pre-cooled PBS containing 0.01% Tx-100 (wash buffer) and centrifuged at 5000rpm, 4°C for 1 minute. Four of these washing steps were performed. After the last washing step, the remaining wash buffer was discarded and 40µl PBS containing 0.05% RapiGest SF surfactant (Waters, cat. nr. 186001860) and 150µg/ml 3x FLAG peptide (Sigma, F4799) (elution buffer) were added to each sample.

The suspension was incubated for 1 hour at 4°C while tumbling and subsequently centrifuged at 8200rpm, 4°C for 1 minute. The supernatant (eluate) was kept on ice and 40µl elution buffer were added to each sample for a second elution for 1 hour at 4°C while tumbling. The suspensions were again centrifuged at 8200rpm, 4°C for 1

minute and the second elution was combined with the first to result in the “Elution” fraction. The beads were kept and 50µl 2x sodium dodecyl-sulfate (SDS)-loading buffer (Laemmli buffer, (Laemmli 1970)) containing 200mM dithiothreitol (DTT) were added (“Beads” fraction) for a 1x DTT concentration of 100mM.

13. SDS-PAGE and Immunoblotting

To assess the quality and efficiency of the immunoprecipitation, the different fractions (“Total”, “Unbound”, “Elution” and “Beads”) were loaded on a precast 4%-20% gradient polyacrylamide gel containing SDS (expedeon). 15µl of “Total”, “Unbound” and “Elution” fraction were mixed with 5µl 4x Laemmli buffer (Laemmli 1970) containing 400mM DTT and subsequently boiled at 95°C for 5 minutes. The entire “Beads” fraction was boiled alongside. After sample cooldown to room-temperature, all fractions were centrifuged for 10s at maximum speed and 20µl of each fraction were loaded into the pockets of the precast gel using a Hamilton syringe, alongside protein standard (Precision Plus Protein Dual Color Standards, BioRad cat. nr. 1610374 or Color Prestained Protein Standard, Broad Range, New England Biolabs, cat. nr. P7712S). SDS-polyacrylamide gel electrophoresis (SDS-PAGE) was performed in a BioRad gel cassette filled with 1x RunBlue running buffer (TEO-tricine, abcam, cat. nr. ab270468) for 1 hour with a constant voltage of 140V.

Subsequently, the gel was carefully taken out of the plastic holder and the top and bottom of the gel were removed. Western Blot was performed in a BioRad Mini Protean Tetra system using Immobilon-P PVDF and Whatman papers at a constant voltage of 100V for 90 minutes in Transfer buffer (25 mM Tris at pH 8.3, containing 192 mM glycine and 20% methanol). During blotting, the buffer was kept cold and a current of less than 400mA was maintained throughout the entire procedure.

Subsequently, membranes were placed in a tray and blocked using 10ml of 5% milk in Tris-buffered saline with Tween-20 (TBST) for 1 hour at room temperature while rocking. Primary antibody incubation was performed overnight at 4°C while rocking and the appropriate dilution in 5% milk in TBST (as indicated in Table VII.1) was used. Prior to secondary antibody incubation, membranes were washed three times in TBST for 5 minutes each time. Depending on the primary antibody used, the corresponding secondary antibody was chosen and diluted in 5% milk in TBST as suggested by the manufacturer (see Table VII.1 for details) and membranes were incubated for 1 hour at room temperature while rocking. Lastly, membranes were washed three times in TBST (5 minutes each) and incubated for 1 minute in Supersignal West Femto Max Sensitivity ECL or SuperSignal™ West Pico Plus chemiluminescent substrate (Thermo scientific), depending on the expected protein load on the membrane. In the dark, the membranes, as well as Lucent Blue X-Ray films (advansta) were placed in a light-sealed cassette and developed in a Kodak RP X-OMAT processor (Model M6B) to detect protein bands.

14. Mass spectrometry and data analysis

14.1. Preparation for TMT-labeling and Mass Spectrometry

In each TMT-10plex, elution fractions obtained from untagged (wildtype) control, alongside 9 STF-affinity-tagged STm effectors, were analyzed in parallel. 10-plexes were designed by effector protein translocation level, as discussed and experimentally assessed in sections II.3 and II.4.4. For each MS run (i.e. each multiplex), cell seeding, infection, harvesting and IP were carried out in parallel and a small fraction of the elution fraction was analyzed by Western Blot to confirm presence of bait protein. The following multiplexes were analyzed:

- RAW264.7 run 1 (high level of effector translocation): wildtype, PipB-STF, PipB2-STF, SifA-STF, SseJ-STF, SseL-STF, SspH1-STF, SteC-STF, SirP-STF, YebF-STF
- RAW264.7 run 2 (lower level of effector translocation): wildtype, AvrA-STF, GogB-STF, SipB-STF, SpvC-STF, SseI-STF, SseK1-STF, SspH2-STF, SteA-STF, SteE-STF
- HeLa run 1 (high level of effector translocation): wildtype, PipB-STF, PipB2-STF, SifA-STF, SseJ-STF, SseL-STF, SspH1-STF, SspH2-STF, SteC-STF, SirP-STF
- HeLa run 2 (low level of effector translocation): wildtype, AvrA-STF, GogB-STF, SifB-STF, SpvC-STF, SseF-STF, SseI-STF, SseK1-STF, SseK2-STF, SteA-STF)

In all other TMT-multiplexed runs, biological triplicates were combined within the same multiplex, alongside a biological triplicate of the untagged control. In this case, fold changes were calculated with respect to the untagged control or between effectors.

Prior to LC/MS sample preparation, total protein concentration in the elution fraction was determined by Micro BCA, using the commercially available kit by ThermoFischer (cat. nr. 23235) with respect to a previously prepared BSA protein standard. Each sample was adjusted to the following concentration and volume using elution buffer: 10µg of protein in 50µl volume for a concentration of 200µg/ml. Further sample preparation was conducted by Mandy Rettel in the EMBL Proteomics Core Facility, and the underlying procedure has been made publicly available (Walch et al. 2020).

In brief, the following steps were taken:

- reduction: using 10mM DTT in 50mM HEPES buffer (at pH 8.5) at 56°C for 30 minutes
- alkylation: in the dark using 20 mM 2-chloroacetamide in HEPES buffer at room temperature for 30 minutes
- SP3 preparation: according to (Hughes et al. 2019)
- trypsinization: at an enzyme-to-protein ratio of 1:50 using sequencing grade trypsin (Promega) at 37°C overnight
- recovery: in HEPES buffer, by collecting the supernatant after bead magnetization twice and combining the elution fractions.

Next, the recovered peptides were labeled using TMT10plex (Werner et al. 2014) Isobaric Label Reagent (ThermoFisher) as described by the manufacturer. In brief, a stock solution of 0.8mg TMT-reagent were dissolved in 42µl 100% acetonitrile and distributed across each sample in the 10-plex (4µl per sample). The sample-reagent mixture was incubated at room temperature for 1 hour and subsequently quenched for 15 minutes in 5% hydroxylamine. All samples were pooled and cleaned up using OASIS® HLB µElution Plate (Waters) and fractionated (high pH reverse phase fractionation) with 20 mM ammonium formate (at pH 10) in 100% acetonitrile as mobile phase (Reichel et al. 2016) on a Gemini C18 column (3µm, 100 x 1.0mm, 110 Å, Phenomenex) in an Agilent 1200 Infinity high-performance liquid chromatography system. Prior to LC/MS analysis, the first, as well as the last two fractions were discarded.

14.2. Mass Spectrometry Data acquisition

Data acquisition by LC/MS was performed and organized by Mandy Rettel and the workflow, including the parameters used in mass spectrometry has been published (Perez-Perri et al. 2018; Walch et al. 2020). In brief, the following components were used in mass spectrometry:

- liquid chromatography system: UltiMate 3000 RSLC nano LC system (Dionex)
- trapping cartridge: µ-Pre-column C18 PepMap 100 (5µm, 300 µm i.d. x 5 mm, 100 Å, ThermoScientific)
- analytical column: nanoEase™ M/Z HSS T3 (1.8 µm, 75 µm x 250 mm, 100 Å, Waters)

Trapping was performed using a constant flow (30µl per min for 6 minutes) of 0.1% formic acid in water. Samples were eluted via the analytical column using a constant flow rate of 0.3µl per minute and an increasing concentration of 0.1% formic acid in acetonitrile. The following gradient was used:

- first 4 minutes: increasing from 2% to 4%
- next 2 minutes: increasing from 4% to 8%
- next 96 minutes: increasing from 8% to 28%
- last 10 minutes: increasing from 28% to 40%

Subsequent mass spectrometry was carried out on a QExactive plus (Thermo) using the previously described parameters (Perez-Perri et al. 2018; Walch et al. 2020).

14.3. AP-QMS Data Analysis

The data analysis at the basis of the AP/QMS workflow has been published (Walch et al. 2020). Dr. Frank Stein conducted the protein query, quality control and statistical analysis in R, I set thresholds for hitcalling and performed all subsequent steps. In brief, the data acquired in LC/MS was processed using Mascot (v.2.2.07), as well as IsobarQuant (Franken et al. 2015). Within the two different host backgrounds, two distinct proteome databases were searched for protein identification (UP000000589 for *Mus musculus* (RAW264.7) and UP000005640 for *Homo sapiens* (HeLa)). In both

cases, the query was combined with the *Salmonella enterica* serovar Typhimurium strain 14028S database (UP000002695), as well as a database containing reverse sequences and common contaminants.

Due to the experimental workflow and labeling using TMT, several peptide modifications were included within the search. These comprise: TMT10 (lysine) and Carbamidomethyl (cysteine) as fixed modifications, as well as oxidation (methionine), acetyl (N-terminal) and TMT10 (N-terminal) as variable modifications. To increase the flexibility and maintain reliability of the peptide search, the following parameters were set:

- 10ppm mass error tolerance in the MS1 scan
- 0.02Da mass error tolerance in the MS2 spectrum
- $\text{fdr} < 0.01$ on the peptide and protein level
- peptide length > 7 amino acids
- 2 missed trypsin cleavages were allowed

Further analysis was conducted in R (ISBN 3-900051-07-0). The files obtained from IsobarQuant (Franken et al. 2015) were imported into R. Only proteins that were identified and quantified using at least two unique peptides and that were present in at least two of the three biological replicates were used in subsequent analysis steps.

After mapping the different effectors to their respective TMT10-labels, the median across all effectors was calculated for each protein in each replicate. The following steps were taken to improve comparability between the different replicate runs:

- batch-effect removal: the “removeBatchEffect” function, which is part of the limma package (Ritchie et al. 2015) was applied
- normalization: variance stabilization normalization (vsn, (Huber et al. 2002)) was used
- imputation: missing values (i.e. values detected in 2 out of 3 replicates) were imputed through application of the impute function in Msnbase (method = “knn”, (Gatto and Lilley 2012)). Proteins with imputed values were marked accordingly to track biases throughout the further analysis.

Lastly, differential expression was assessed by applying limma again to the cleaned-up data. Under the assumption that interactions are mostly effector-specific, enrichment was measured by assessment of fold changes (FC) with respect to the median value of a given protein across all conditions. To calculate alternative false discovery rates (fdr), the T-values obtained from limma were subjected to fdrtool (Strimmer 2008). In case where the standard deviation of T-values (limma) deviated from 1 so that there was no convergence of statistically significant hits, the q-values obtained from fdrtool were used. This is also discussed in section II.6.2.

All proteins surpassing the initial thresholds of $\text{FC} > 1.2$ and $\text{fdr} \leq 0.01$ were filtered and labeled as hits. The initial lists of hits (one for each cell line) were then further

refined as discussed and presented in large detail in section II.6.3. In brief, the following four additional steps were taken:

1. All PPIs passing the criterion $FC > 1.2$ in both conditions (i.e. native and cross-linked) were required to fulfill $fdr \leq 0.05$ (instead of $fdr \leq 0.01$)
2. For the PPIs of each effector, two rankings were established per cell line and condition: one with respect to fold change and one with respect to fdr .
3. All proteins identified in native *and* cross-linked IP, as well as the top 20 proteins within each ranking, were kept.
4. The lists were combined by cell line to yield four lists of hits (across two cell lines and two IP conditions).

15. Network building and GO-term analysis

To visualize the connectivity between the host proteins targeted by STm effectors, highlight enriched biological processes and assess the promiscuity of different effector proteins, I represented the hits for both native and cross-linked IP in interaction networks (one for each cell line). For construction, cytoscape (v3.7.2, (Shannon et al. 2003)) was used. Previously described interactions between host proteins (previous knowledge, functional and/or physical from genomic context, (conserved) co-expression and high-throughput experiments) and interactions between bacterial proteins (functional interactions) were imported using STRING DB protein query (version 11, (Szklarczyk et al. 2019)). The respective organism was searched and 0.7 was set as confidence cutoff. The entire list of functional interactions that were imported is published as Table S5 in (Walch et al. 2020). The network design was optimized for information display and visibility and exported to Inkscape (version 1.0.2) in which the final figure panels were created.

GO-term enrichment was performed using the ClueGO application (version 2.5.2) in cytoscape (Bindea et al. 2009). To accommodate the detectability of proteins in LC/MS, a list of all proteins detected in the AP/QMS workflow was established for each cell line. This background proteome was then used as a reference for the enrichment. To determine enriched GO-terms, a p-value cutoff (Benjamini-Hochberg corrected, (Benjamini and Hochberg 1995)) of 0.05 was set and GO-terms in hierarchy levels 4 and 5 were searched to avoid too general or too specific terms. At least 3 genes and 15% of genes per term were required. GO-term grouping, as well as fusion were enabled to reduce the number of redundant terms and groups were merged if at least 40% of terms and genes overlapped. To determine the leading term within each group, the GO-term with the largest number of genes was selected.

16. Reciprocal pulldown validation

To validate the interaction between a given host target and its associated STm effector, antibodies against the endogenous host target were purchased (they are summarized in Table VIII.3). To conduct the reciprocal pulldown, RAW264.7 or HeLa cells (depending on where the interaction occurred) were infected with the following STF-tagged STm strains: untagged control (WT), the interacting effector, a non-cognate

effector (i.e. an effector protein of comparable translocated amount which did not interact with the host target). For each condition, 3 wells in a 6-well plate were infected. To do so, the procedure described in section VII.10 was followed. To select the non-cognate effector, Figure II.3B (the translocation of tagged effectors into host cells) was considered. 20 hpi, the cell lysates were harvested in a total volume of 300 μ l (as described in section VII.11) and cleared to obtain the Tx-100 soluble fraction.

Prior to starting the reciprocal IP, the antibodies were loaded onto agarose beads coated in protein A (for antibodies produced in rabbit) or protein G (for antibodies produced in mouse). To do so, 50 μ l bead slurry per different lysate were washed in lysis buffer twice. After the second wash, the beads were aliquoted into different Eppendorf tubes at a volume of 100 μ l. Subsequent to that, 3.5 μ l of the antibody were added to each tube and the mixture was incubated at RT for 2h while tumbling. 250 μ l of the clear lysate were then added to the bead-antibody-mixture and the samples were incubated at 4°C overnight while tumbling. The remaining lysate was kept as “input” fraction.

The next day, the samples were centrifuged at 4°C, 5000 rpm for 1 minute and the supernatant was discarded. The beads were washed three times in pre-cooled wash buffer (PBS containing 0.01% Triton-X100) and after the final wash, 100 μ l 2x SDS-containing, reducing loading buffer were added to the beads. At the same time, SDS-loading buffer was added to the “input” samples to yield a final concentration of 1x. All samples were boiled for 10 minutes at 95°C and spun down to clear the supernatant. 20 μ l of each sample were loaded for PAGE and Western Blot (see section 13). For the immunoblot, anti-FLAG antibody as well as the antibody against the assessed host target were used at the adequate dilutions.

17. Sample preparation for microscopy

To image cells on a fluorescence microscope, cell seeding and infection was performed in 96-well glass bottom plates (CellContact) as described in subchapters VII.11 and VII.12. In order to avoid any differences in growth due to the well position on the plate, only the inner 60 wells (i.e. from B2 to B11 and G2 to G11) were used for experimentation. At the desired time point, the plates were washed twice with a multichannel pipette, using 150 μ l of pre-warmed PBS per well. Subsequently, 100 μ l 2.5% paraformaldehyde (PFA, Thermo Fisher, cat. nr. 28908) were added to each well and the plates were incubated at 37°C for 10 minutes. After fixation, cells were washed twice using 150 μ l PBS per well.

17.1. Staining of unesterified cholesterol with filipin

To track the distribution of unesterified cholesterol throughout the cell, filipin III from *Streptomyces filipinens* (Sigma, cat. nr. F4767) was used. A stock solution (1mg/ml) was diluted 1:200 and 100 μ l were added to each well. Subsequently, cells were washed twice in 150 μ l PBS.

As filipin emits fluorescence in a similar range as DAPI or Hoechst, another cell marker has to be used. In the experiments mentioned and discussed in this thesis, HCS CellMask Deep Red Stain (Thermo Fisher, cat. nr. H32721) was used for this purpose. A stock solution (10 mg/ml) was prepared in 25 μ l DMSO as described by the manufacturer. For staining, a dilution of 1:5000 in PBS was used and plates were incubated for 30 minutes and subsequently washed in 150 μ l PBS three times. As cell membranes are partly permeabilized by filipin, no additional permeabilization step was needed prior to CellMask staining.

17.2. Staining of F-actin with phalloidin

For experiments assessing actin bundling in 3T3 fibroblasts as well as all imaging to be quantified using CellProfiler, cells were co-stained with phalloidin-Atto-647N (Sigma, cat. nr. 65906) and Hoechst 33342, trihydrochloride, trihydrate (Invitrogen, cat. nr. H3570) after fixation. To do so, a stock solution of phalloidin-647N (kept at -30°C) was created by diluting lyophilized phalloidin (10nmol) in 500 μ l methanol (stock concentration: 20nmol/ml). Staining was performed at room temperature for 1 hour using a 1:1000 dilution for phalloidin and 1:5000 for Hoechst (kept at 4°C) in a volume of 100 μ l per well. After staining, all wells were washed three times in 150 μ l PBS and imaged immediately or stored for not more than 48 hours at 4°C.

17.3. Immunostaining for NPC1 or LAMP1

Prior to immunofluorescent staining with NPC1 or LAMP1, the fixed cells were blocked in PBS containing 0.2% saponin (Merck Millipore, cat. nr. 558255) and 10% goat serum (Merck, cat. nr. G9023) for 20 minutes and subsequently washed in PBS twice and PBS containing 0.1% saponin once. This is required as saponin permeabilization is reversible. Incubation with primary antibody was done at a dilution of 1:500 in PBS containing 0.2% saponin and 10% goat serum for NPC1 (Novus biologicals, cat. nr. NB400-148) and 1:500 dilution in PBS containing 1% BSA for LAMP1 (FITC-coupled, Abcam, cat. nr. ab24871). After 45 minutes at room temperature, cells were washed three times in PBS. For immunostaining of NPC1, incubation with a fluorescently labelled secondary antibody was necessary. To do so, cells were incubated in goat anti-rabbit antibody, coupled to Alexa-680 (abcam, cat. nr. ab175773) diluted 1:1000 in PBS containing 0.2% saponin and 10% goat serum. Subsequently, cells were washed three times in 150 μ l PBS and stored in the dark for a maximum of 48 hours.

18. Fluorescence microscopy

18.1. Widefield fluorescence microscopy

For widefield fluorescence microscopy imaging, a Nikon Eclipse Ti microscope, equipped with NIS Elements software (version 4.60) was used at a magnification of 10x or 20x. Automated image acquisition was set up to take evenly spaced images at predefined positions across the well (5 or 9 images in 10x objective acquisition and 12 or 16 images in 20x objective acquisition). To discern fluorescent staining, four different wavelength filters were used: DAPI (for Hoechst staining of nuclei or filipin staining),

FITC (for staining of Alexa-488 stained antibodies or GFP-expressing STm), Cy3 (for mCherry expressing STm), Cy5 (for phalloidin staining or CellMask).

18.2. Confocal fluorescence microscopy

To improve our understanding of subcellular localization and co-localization with host proteins, we used confocal microscopy on an Olympus confocal laser scanning microscope (FV3000) at 60x magnification using oil-immersion. The fixed cells were scanned in single image planes using the following laser wavelengths:

- 405 nm for Hoechst 33342 staining
- 488 nm for the Alexa-488-coupled secondary antibody (LAMP1)
- 594 nm for mCherry expressing STm
- 640 nm for the ATTO-680-coupled secondary antibody (NPC1)

19. Image analysis and quantification of infection rate and intracellular growth

To automatically analyze images and quantify cell entry and intracellular proliferation, the software CellProfiler (version 3.0.0) was used. As the initial step in cell segmentation, a nuclei mask was defined using the signal obtained in the DAPI channel. An object diameter preference of 30 to 60 pixels (in 10x magnification, doubled for 20x magnification) was set, and objects touching the image border were excluded. Thresholding was performed globally, using minimum cross entropy, a smoothing scale of 1.3488 and a correction factor of 1. Clumped objects were discerned and separated based on pixel intensity and smoothing filter size, and minimum distance between intensity maxima was calculated.

In a second step, the cell outline was defined by the phalloidin signal (Cy5 channel). The nuclei determined in the previous step were used as input (primary objects) and propagation was used to identify cell area (secondary objects). For thresholding, the same settings as in the first step were used, but the correction factor was set to 0.99 to avoid overdetection of background signal. A regularization factor of 0.05 was used and cells touching the border of the image were discarded to avoid artefacts.

Next, *Salmonella* were detected as primary objects, based on the signal from the Cy3- or (where applicable) FITC-channel. A diameter requirement of 1 to 50 pixels (for 10x magnification) was set and all objects outside these boundaries were excluded. A global, manually set threshold of 0.005 was used, but if this led to an overdetection of background signal, the manual threshold was increased to a maximum of 0.008. The threshold was kept identical within all conditions of one biological replicate. Clumped objects were treated as described for nuclei.

To connect the various objects identified in these steps, *Salmonella* were masked with cells, to exclude extracellular bacteria, and subsequently related as “children”, to maintain identification of infected cells. Lastly, *Salmonella* count and integrated intensity were calculated as measures of intracellular growth. All results were exported and subsequently analyzed manually. For calculation of the infection rate, all the

number of infected cells was divided by the total number of cells. For quantification of the intracellular proliferation, STm integrated intensity was the preferable measure and the distribution of the integrated intensity across all cells of one condition was compared to other conditions.

20. Colocalization quantification

Colocalization was quantified using an ImageJ (version 1.51n) macro, the code for which can be provided at request. Prior to submitting files to the pipeline, all images were manually assessed for imperfections, such as scratches on the plate or fibers in the sample which cause very strong fluorescence in one or more channels. In addition to that, fields of view that contained exceptionally few or exceptionally many cells, as well as cells with aberrant morphology were excluded. All remaining files were submitted to the macro.

In a first step, the background was subtracted, by using the “rolling background subtraction” command. The following settings were used: 10 pixel radius for phalloidin, 15 pixel radius for CellMask staining, 10 pixel radius for LAMP1 signal and 10 pixel radius for *Salmonella*. Then, a binary mask was generated for the cell surface (Otsu segmentation (Otsu 1979) for phalloidin, Huang segmentation (Huang and Wang 1995) for CellMask staining), the STm site (Otsu segmentation) and, where applicable, the LAMP1 signal (Otsu segmentation). Lastly, the binary masks for cell surface, where applicable the LAMP1 signal and the STm site, were combined through intersection, so that this new mask signified intracellular, LAMP1-positive STm sites.

In a next step, the binary masks for the cell surface and the combined mask were each applied to the original image to be quantified (depending on the assay this would be the NPC1-channel, the filipin channel or the actin channel). Lastly, the intensities of these images, as well as the surface of the masks, were quantified using the “measure” command.

The colocalization score was then calculated as follows:

First, the summed (integrated) intensity of each mask was divided by the size of the respective binary mask to normalize the signal to the size of the respective mask. The result thereof is the average intensity throughout the mask. Second, the average intensity within the combined mask (*Salmonella*, cell area and, where applicable, LAMP1) was divided by the average intensity of the cell mask. This was done the same way, irrespective of what was quantified (actin, NPC1 or filipin). Thereby, a colocalization score of 1 means a random distribution, and colocalization is indicated by a value >1 .

21. Protein purification and size exclusion chromatography

To assess the nature of the interaction between SteC and FMNL proteins in more detail, we expressed and purified recombinant SteC alongside a catalytically inactive version (SteC-K256H), as previously described (Poh et al. 2008). Subsequently, the

recombinantly expressed and purified proteins were subjected to overnight dialysis in 20 mM Tris-HCl (at pH 7.4) containing 200 mM NaCl at 4°C. Amicon centrifuge columns with a 3 kDa molecular weight cutoff (Ultra 15, UCF900324) were used to increase protein concentration by centrifugation at 4000 rpm for 15 minutes at 4°C. Next, glycerol was added to each sample for a final concentration of 10% and samples were frozen in liquid nitrogen and stored at -80°C until further usage.

As full-length FMNL proteins require specific expression conditions in insect cells, we expressed truncated, GST-tagged versions (FMNL1₁₋₃₈₅ and FMNL2₂₋₄₇₈) using a pGEX-4T1-tev expression system in Rosetta (DE3) pLysRare. To do so, cells were grown overnight in autoinduction media at 25°C while shaking at 250 rpm (Studier 2005). The next day, cells were collected and washed. Lysis buffer (50mM Tris-HCl (at pH 7.8) containing 500 mM NaCl, 100µg/ml lysozyme, 20% glycerol and protease inhibitor (cOmplete EDTA-free, Roche) was added and the cell suspension was sonicated to break the cell walls and harvest the expressed proteins. To enrich for GST-tagged proteins, pre-equilibrated Glutathione Sepharose 4B beads (Merck, cat. nr. GE17-0756-01) were added and the slurry was incubated overnight at 4°C. Subsequently, the beads were washed three times in 50mM Tris-HCl (at pH7.8), containing 100mM NaCl and 10% glycerol. To cleave the protein off the beads, biotinylated thrombin (Merck, cat. nr. 69672) was added according to the instruction by the manufacturer and incubated overnight at 4°C. The purified protein was then snap-frozen and stored at -80°C.

To determine the nature of the interaction between FMNL1 and SteC (or SteC-K256H), proteins were co-incubated and subsequently subjected to size-exclusion chromatography. Prior to protein loading, an Akta FPLC UPC-900 was equipped with a Superose 6 Increase 100/300 GL column (Merck) and equilibrated using 50mM Tris-HCl (at pH7.8), containing 100mM NaCl and 10% glycerol. Then, 500µg of the protein (or equimolar protein mixture) were incubated for 5 minutes on ice and loaded into the column. After injection, the optical density at 280nm was measured and quantified until the end of the experiment. To determine the precise sizes of each detected protein complex, a broad range (1.35 to 670 kDa) protein molecular mass standard (Bio-Rad, cat. nr. 1511901) was used. The acquired UV-traces across the retention times were exported and loaded into GraphPad Prism (version 7) for further analysis and display.

22. *In vitro* kinase assay using radiolabeled γ -³²P ATP

In order to understand whether the kinase SteC is capable of phosphorylating FMNL proteins in the absence of other host factors or bacterial proteins, an *in vitro* kinase assay was performed. To do so, 10µg of both purified, recombinantly expressed SteC, as well as the catalytically inactive mutant SteC-K256H were incubated in 5µl pre-activation buffer (50mM Tris-HCl (at pH 7.5), containing 50µM ATP, 2mM DTT and 10 mM MgCl₂) at 30°C for 5 minutes. 10µg of purified FMNL1 or FMNL2 were diluted in 14µl 50mM Tris-HCl (at pH 7.5), containing 2mM DTT to yield the substrate mix.

All subsequent steps were carried out in a radioactive lab under radiation monitoring and using the appropriate safety measures to avoid excessive exposure. 5µl of a 1:10 dilution of radioactively labelled [³²P]-γ-ATP were added to each substrate mix. To start the *in vitro* kinase assay, the substrate mixes containing radioactively labelled [³²P]-γ-ATP were added to the pre-activated kinase (or catalytically inactive variant). The reaction was carried out for 30 minutes at 30°C and subsequently stopped with 2x Laemmli buffer. All samples were boiled at 95°C for 5 minutes, cooled down and centrifuged for 10s at full speed. To visualize proteins and detect the presence of [³²P]-γ-ATP, the mixtures were separated by SDS-PAGE and immobilized on a PVDF membrane using semi-dry Western Blot for 7 minutes. Phosphorylated proteins were visualized by autoradiography and total protein amount was detected using Coomassie staining of the PVDF membrane.

23. *In vitro* kinase assay coupled with phosphoproteomics

The pre-activation of the kinase was performed as described in the previous section, but using 2µg of SteC or SteC-K256H. Similarly, 8µg of the substrate (FMNL1₁₋₃₈₅, FMNL2₂₋₄₇₈ or an equimolar mix of the two) were diluted in pre-activation buffer and added to the kinase mix. In the first replicate, 50µM ATP was used, in the second 5mM ATP. After incubation at 30°C for 30 minutes, all samples were frozen in liquid nitrogen and stored at -80°C until further processing. The following steps were conducted by Dr. Clément Potel and have been made publicly available (Walch et al. 2020).

For LC/MS preprocessing, the samples were thawed and HEPES buffer (at pH 8.5) to yield a final concentration of 100 mM was added. Then, the following steps were taken:

- reduction and alkylation: using Tris(2-carboxyethyl)phosphine hydrochloride (final concentration of 5mM) and 2-chloroacetamide (Sigma-Aldrich) (final concentration of 30mM).
- trypsinization: at an enzyme-to-substrate ratio of 1:25, trypsin (Sigma) was added and samples were incubated at room temperature overnight.
- desalting: on stage-tips (Rappsilber, Ishihama, and Mann 2003) that were prepared in-house. These were packed with 1mg C18 material (ReproSil-Pur 120 C18-AQ 5 µm, Dr. Maisch).
- resuspension: in 20 mM citric acid (Sigma) containing 1% formic acid (Sigma) prior to injection.

Liquid chromatography was performed as described in section VII.14.2, with two changes: First, the trapping was performed for 3 minutes (instead of 6 minutes) and second, a linear gradient from 8% to 32% for 45 minutes was used on the analytical column. MS analysis was performed on a Fusion Orbitrap Lumos mass spectrometer (Thermo Scientific) using the parameters published here: (Walch et al. 2020).

For data analysis, MaxQuant (version 1.6.2.3, (Cox and Mann 2008)) was used. First, the raw files were processed and searched against a manually curated database

containing the sequences for SteC, FMNL1, FMNL2, and common contaminants. The following parameters were set:

- maximum of 3 missed trypsin cleavages
- fixed modification: carbamidomethylation on cysteines
- variable modifications: oxidation on methionines, phosphorylation on serines, threonines, tyrosines, as well as acetylation of the N-terminus
- 4.5ppm mass tolerance in the MS1 scan
- 20ppm mass tolerance in the MS2 spectrum
- $fdr < 0.01$ on the peptide and protein level
- peptide length > 7 amino acids
- score cut-off for modified peptides >40
- match-between-runs option: retention time window of 2 minutes.

24. High-throughput infection of RAW264.7 cells and microscopy

To enable high-throughput screening in an infection context, a Biomek FX^P Laboratory Automation Workstation (Beckman Coulter), equipped with the manufacturer's software (version 3.3) was used. All replicates of HeLa cell infection were carried out by Dr. Bachir El Debs, and I performed one of the replicates in RAW264.7 cells.

On the day prior to infection, RAW264.7 cells were seeded in 384-well microscopy-suitable glass-bottom plates, using a Multidrop Combi automated cell seeder (Thermo) provided by the Advanced Light Microscopy facility at EMBL. To do so, a cell suspension of 20 million cells in 250 ml DMEM (1g/l glucose, supplemented with 10% FBS) was prepared and 50 μ l were seeded per well. The plates were then incubated at 37°C overnight. To prepare the liquid cultures of the knockout library required for infection, ten 384-well plates containing 60 μ l LB Miller supplemented with the appropriate selection antibiotic were inoculated from agar plates using a Singer Rotor colony picker. The plates were sealed with oxygen-permeable membranes and then incubated overnight at 37°C while shaking at 800 rpm.

Before infecting the cells, the plates containing the bacterial overnight cultures were centrifuged at 500rpm for 4 minutes at room temperature. Using the pre-set program on the Biomek, bacteria were washed once in PBS (by diluting the overnight culture 1:10) and 10 μ l were subsequently transferred to a prepared media-plate for opsonization in DMEM (dilution 1:10). Due to the incubation times, two time points (0 hpi and 8 hpi, or 4 hpi and 20 hpi) were run in the same experiment. Cells were infected by transferring 50 μ l of opsonized culture into the 384-plates containing RAW264.7. Infection and gentamicin protection assay were carried out as described in section VII.10.1, using preset programs for automated liquid transfer.

For cell fixation, 35 μ l fixation solution (5% PFA containing 0.2% Triton-X100) were added to each well. After an incubation of 45 minutes at room temperature, the fixation solution was removed, 50 μ l PBS were added and cells were stored at 4°C until staining and imaging. Automated image acquisition and plate loading was performed on a

Nikon eclipse Ti widefield microscope equipped with a Prior PLW20 automated plate loader and running the NIS Elements software (version 4.60).

25. Validation of a subset of mutants

We validated a subset of mutants from the STm single deletion library (Porwollik 2014) that were assessed in the genome-wide screen on a smaller scale. 14 mutants from representative pathways which had shown a phenotype in different timepoints and cell lines were selected, struck out under kanamycin selection, transduced to wildtype background using P22 phage, checked for validity using PCR, and transformed with pFCcGi. Phenotypes were assessed by high-throughput microscopy (after staining for DAPI (nuclei), mCherry (STm) and phalloidin-ATTO647N (actin)) at 0 hpi (cell entry) and 20 hpi (intracellular proliferation) in HeLa cells and macrophages using the Cell Profiler software (version 3.0.0). This was done in biological triplicate, each with technical duplicates. For the exact parameters used in CellProfiler, see section VII.19.

Mutants that displayed < 75% infection rate (at 0 hpi) compared to wildtype (across all replicates) were selected as having an invasion defect. Similarly, mutants that displayed < 75% integrated STm intensity (at 20 hpi) compared to wildtype (median across all replicates) were selected as having a proliferation defect. For determining whether true/false positives/negatives, we considered whether a defect in cell invasion or intracellular proliferation with a robust Z-score < -2 could be recapitulated in the small-scale validation using re-transduced and validated mutants.

26. Bibliography of this chapter

- Benjamini, Yoav, and Yocef Hochberg. 1995. "Controlling the False Discovery Rate: A Practical and Powerful Approach to Multiple Testing." *Journal of the Royal Statistical Society* 57 (1): 289–300.
- Bindea, Gabriela, Bernhard Mlecnik, Hubert Hackl, Pornpimol Charoentong, Marie Tosolini, Amos Kirilovsky, Wolf-Herman Fridman, Franck Pagès, Zlatko Trajanoski, and Jérôme Galon. 2009. "ClueGO: A Cytoscape Plug-in to Decipher Functionally Grouped Gene Ontology and Pathway Annotation Networks." *Bioinformatics* 25 (8): 1091–93.
- Cox, Jürgen, and Matthias Mann. 2008. "MaxQuant Enables High Peptide Identification Rates, Individualized P.p.b.-Range Mass Accuracies and Proteome-Wide Protein Quantification." *Nature Biotechnology* 26 (12): 1367–72.
- Datsenko, K. A., and B. L. Wanner. 2000. "One-Step Inactivation of Chromosomal Genes in *Escherichia Coli* K-12 Using PCR Products." *Proceedings of the National Academy of Sciences of the United States of America* 97 (12): 6640–45.
- Figueira, Rita, Kathryn G. Watson, David W. Holden, and Sophie Helaine. 2013. "Identification of *Salmonella* Pathogenicity Island-2 Type III Secretion System Effectors Involved in Intramacrophage Replication of *S. Enterica* Serovar Typhimurium: Implications for Rational Vaccine Design." *mBio* 4 (2): e00065.
- Franken, Holger, Toby Mathieson, Dorothee Childs, Gavain M. A. Sweetman, Thilo Werner, Ina Tögel, Carola Doce, et al. 2015. "Thermal Proteome Profiling for Unbiased Identification of Direct and Indirect Drug Targets Using Multiplexed Quantitative Mass Spectrometry." *Nature Protocols* 10 (10): 1567–93.
- Gatto, Laurent, and Kathryn S. Lilley. 2012. "MSnbase—an R/Bioconductor Package for Isobaric Tagged Mass Spectrometry Data Visualization, Processing and Quantitation." *Bioinformatics* 28 (2): 288–89.
- Huang, Liang-Kai, and Mao-Jiun J. Wang. 1995. "Image Thresholding by Minimizing the Measures of Fuzziness." *Pattern Recognition* 28 (1): 41–51.
- Huber, Wolfgang, Anja von Heydebreck, Holger Sültmann, Annemarie Poustka, and Martin Vingron. 2002. "Variance Stabilization Applied to Microarray Data Calibration and to the Quantification of Differential Expression." *Bioinformatics* 18 Suppl 1: S96–104.
- Hughes, Christopher S., Sophie Moggridge, Torsten Müller, Poul H. Sorensen, Gregg B. Morin, and Jeroen Krijgsveld. 2019. "Single-Pot, Solid-Phase-Enhanced Sample Preparation for Proteomics Experiments." *Nature Protocols* 14 (1): 68–85.
- Knodler, Leigh A., Vinod Nair, and Olivia Steele-Mortimer. 2014. "Quantitative Assessment of Cytosolic *Salmonella* in Epithelial Cells." *PloS One* 9 (1): e84681.

- Kolodziejek, Anna M., Melissa A. Altura, Junping Fan, Erik M. Petersen, Matthew Cook, Peter S. Brzovic, and Samuel I. Miller. 2019. "Salmonella Translocated Effectors Recruit OSBP1 to the Phagosome to Promote Vacuolar Membrane Integrity." *Cell Reports* 27 (7): 2147–56.e5.
- Laemmli, U. K. 1970. "Cleavage of Structural Proteins during the Assembly of the Head of Bacteriophage T4." *Nature* 227 (5259): 680–85.
- Otsu, Nobuyuki. 1979. "A Threshold Selection Method from Gray-Level Histograms." *IEEE Transactions on Systems, Man, and Cybernetics* 9 (1): 62–66.
- Perez-Perri, Joel I., Birgit Rogell, Thomas Schwarzl, Frank Stein, Yang Zhou, Mandy Rettel, Annika Brosig, and Matthias W. Hentze. 2018. "Discovery of RNA-Binding Proteins and Characterization of Their Dynamic Responses by Enhanced RNA Interactome Capture." *Nature Communications* 9 (1): 4408.
- Poh, John, Charlotte Odendall, Ad Spanos, Cliona Boyle, Mei Liu, Paul Freemont, and David W. Holden. 2008. "SteC Is a Salmonella Kinase Required for SPI-2-Dependent F-Actin Remodelling." *Cellular Microbiology* 10 (1): 20–30.
- Porwollik, Steffen, Carlos A. Santiviago, Pui Cheng, Fred Long, Prerak Desai, Jennifer Fredlund, Shabarinath Srikumar, et al. 2014. "Defined Single-Gene and Multi-Gene Deletion Mutant Collections in Salmonella Enterica Sv Typhimurium." *PLoS One* 9 (7): e99820.
- Rappsilber, Juri, Yasushi Ishihama, and Matthias Mann. 2003. "Stop and Go Extraction Tips for Matrix-Assisted Laser Desorption/ionization, Nano-electrospray, and LC/MS Sample Pretreatment in Proteomics." *Analytical Chemistry* 75 (3): 663–70.
- Reichel, Marlene, Yalin Liao, Mandy Rettel, Chikako Ragan, Maurits Evers, Anne-Marie Alleaume, Rastislav Horos, Matthias W. Hentze, Thomas Preiss, and Anthony A. Millar. 2016. "In Planta Determination of the mRNA-Binding Proteome of Arabidopsis Etiolated Seedlings." *The Plant Cell* 28 (10): 2435–52.
- Ritchie, Matthew E., Belinda Phipson, Di Wu, Yifang Hu, Charity W. Law, Wei Shi, and Gordon K. Smyth. 2015. "Limma Powers Differential Expression Analyses for RNA-Sequencing and Microarray Studies." *Nucleic Acids Research* 43 (7): e47.
- Shannon, Paul, Andrew Markiel, Owen Ozier, Nitin S. Baliga, Jonathan T. Wang, Daniel Ramage, Nada Amin, Benno Schwikowski, and Trey Ideker. 2003. "Cytoscape: A Software Environment for Integrated Models of Biomolecular Interaction Networks." *Genome Research* 13 (11): 2498–2504.
- Steele-Mortimer, Olivia. 2008. "Infection of Epithelial Cells with Salmonella Enterica." *Methods in Molecular Biology* 431: 201–11.
- Strimmer, Korbinian. 2008. "Fdrtool: A Versatile R Package for Estimating Local and Tail Area-Based False Discovery Rates." *Bioinformatics* 24 (12): 1461–62.
- Studier, F. William. 2005. "Protein Production by Auto-Induction in High Density Shaking Cultures." *Protein Expression and Purification* 41 (1): 207–34.

- Szklarczyk, Damian, Annika L. Gable, David Lyon, Alexander Junge, Stefan Wyder, Jaime Huerta-Cepas, Milan Simonovic, et al. 2019. "STRING v11: Protein-Protein Association Networks with Increased Coverage, Supporting Functional Discovery in Genome-Wide Experimental Datasets." *Nucleic Acids Research* 47 (D1): D607–13.
- Uzzau, S., N. Figueroa-Bossi, S. Rubino, and L. Bossi. 2001. "Epitope Tagging of Chromosomal Genes in *Salmonella*." *Proceedings of the National Academy of Sciences of the United States of America* 98 (26): 15264–69.
- Walch, Philipp, Joel Selkrig, Leigh A. Knodler, Mandy Rettel, Frank Stein, Keith Fernandez, Cristina Viéitez, et al. 2020. "Global Mapping of *Salmonella* Enterica-Host Protein-Protein Interactions during Infection." *bioRxiv*. <https://doi.org/10.1101/2020.05.04.075937>.
- Werner, Thilo, Gavain Sweetman, Maria Fälth Savitski, Toby Mathieson, Marcus Bantscheff, and Mikhail M. Savitski. 2014. "Ion Coalescence of Neutron Encoded TMT 10-Plex Reporter Ions." *Analytical Chemistry* 86 (7): 3594–3601.